Universitat Autònoma de Barcelona

How cognitive information drives movement in living organisms: A statistical physics approach from the individual to the collective

Javier Cristín

PhD Advisors: Dr. Daniel Campos and Dr. Vicenç Méndez

Thesis dissertation

How cognitive information drives movement in living organisms:

A statistical physics approach from the individual to the collective

Javier Cristín

July 12, 2021

Universitat Autonoma de Barcelona

"The laws of history are as absolute as the laws of physics, and if the probabilities of error are greater, it is only because history does not deal with as many humans as physics does atoms, so that individual variations count for more."

– Isaac Asimov, Foundation and Empire

Acknowledgments

Esta tesis nace los momentos que han tenido lugar durante los últimos años. Podría analizar cada uno de ellos por separado. Pero la realidad es que es de cómo se entrelazan de donde emergen las páginas que construyen este trabajo.

A mi parecer, la mejor (y más divertida) manera de investigar surge cuando interactuamos entre nosotros, dejando que crezcan ideas inesperadas. Por esto, esta tesis no sería la misma si no fuese por todas esas personas que han compartido su tiempo conmigo. Todas ellas, sin excepción, son parte fundamental de este trabajo. Para empezar, quiero agradecer a Daniel que me haya enseñado ese fascinante lugar en el que la física y la biología se funden. Por guiar nuestros pasos. Quiero agradecer a la gente del despacho C3/116 las discusiones eternas y su optimismo (creyendo siempre que nos iban a aceptar los artículos).

Quiero recordar también a los que han estado conmigo desde la carrera. A la gente del Palacio, por todos esos vermuts, escapadas e indispensables risas. A los Panellets, por los viajes por el mundo, que ayudan a recargar las pilas. A los amigos de la infancia, que han vivido todo este proceso a mi lado. No me olvido tampoco de la gente que me introdujo en la investigación: esta tesis es una continuación de lo que aprendí al lado de Joan, Carmen e Ignacio en la UB.

Finalmente, quiero agradecer a los que siempre han estado, están y estarán. Aquellos que me han apoyado desde el primer día, incluso cuando esta vida te lleva lejos del hogar: mi familia.

Para acabar, si estás leyendo esto y no has encontrado tu nombre, no te preocupes. No me cabíais todos. Gracias por tu aportación, grande o pequeña, porque de la suma de todas ellas nace este texto.

Javier

Publications list

The work in this thesis has been published in the following articles:

- Cristín, J., Méndez, V. and Campos, D. 'General scaling in bidirectional flows of self-avoiding agents'. In: *Sci Rep 9, 18488* (2019). https://doi.org/10.1038/s41598-019-54977-3

- Cristín, J., Bartumeus, F., Méndez, V. and Campos, D. 'Occupancy patterns in superorganisms: a spin-glass approach to ant exploration'. *R. Soc. open sci 7:201250* (2020). https://doi.org/10.1098/rsos.201250

- Cristín, J., Méndez, V. and Campos, D. 'Informational entropy refinement as a stochastic mechanism for sequential decision-making in humans'. *arXiv:2102.08802* (2021).

- Campos, D., Cristín, J. and Méndez, V. 'Minimization of spatial cover times for impaired self-avoiding random walks: the mirage effect'. *Journal of Stat. Mech.: Theory and Experiment 063404* (2021). https://doi.org/10.1088/1742-5468/ac02b8

Two more are in preparation, with the following tentative titles:

- Cristín, J., Méndez, V. and Campos, D. 'How information prospection facilitates spatial coverage of self-avoiding walks'.

- Cristín, J., Bartumeus, F., Méndez, V. and Campos, D. 'The exploitation-exploration trade off in ant foraging: the spin-glass method as a tool for *in silico* experiments'

Abstract

English:

Living organisms are characterized by their ability to adapt themselves to the circumstances. Bacteria, for example, are able to detect chemical signal gradients with the purpose of reorienting themselves. Ants in a colony organize themselves to distribute tasks, even to develop strategies that are unfeasible at an individual level. Even humans adapt continually our behavior to our dynamic context. This adaptation, based on the ability to incorporate and process information, represents the germ of intelligent behavior. In this thesis we have focused on providing a physical framework to describe some aspects of those mechanisms. More concretely, we have used tools from statistical physics to describe, in an effective way, the cognitive mechanisms that the organisms use to obtain and process information in the context of search or foraging processes. Our framework allows to analyze the impact of multiple cognitive layers over the organisms navigation during these processes.

The thesis has been divided into two parts. During the first one, we explore how the cognitive layers impact the search process efficiency in absence of interactions with other individuals. We illustrate how the cognitive memory and the prospection (the ability to sample the future) can represent fundamental ingredients to describe the behavior of living organisms. In addition, we provide experimental evidence that seemingly indicates that how humans quantify when the information of those layers is reliable enough (and then, to make a decision) can be effectively described by a simple mechanism based on concepts from information theory.

In the second part, we focus on the collective organization exhibited by a broad range of living organisms and how it emerges from the interactions between them. More concretely, we explore if the framework proposed for isolated individuals can be useful to describe these situations. We provide multiple evidence in this direction, putting our effort in two systems: pedestrian dynamics and ant foraging. For the first, we characterize how the balance between the basic ingredients of pedestrian motion may generate collective structures and how a description in a specific space (the time-to-collision space) can adequately capture these structures. For the second, it is known that ants cooperate while foraging to increase the colony survival. We explore how a better comprehension of the complexity of collective foraging strategies can be gained with the help of spin-glass frameworks.

In summary, this thesis illustrates how the understanding of the cognitive mechanisms of living beings can be approached through models based on statistical physics.

Castellano: Los seres vivos se caracterizan por su capacidad de adaptarse según las circunstancias. Las bacterias, por ejemplo, son capaces de detectar gradientes de señales químicas con el fin de reorientar su movimiento. Las hormigas de una colonia se distribuyen las tareas, para así desarrollar estrategias inviables a nivel individual. Incluso los humanos adaptamos continuamente nuestro comportamiento a nuestro contexto dinámico. Esta adaptación, basada en la capacidad de incorporar y procesar información, representa el germen del comportamiento inteligente. En esta tesis nos hemos centrado en proporcionar un marco físico para describir algunos aspectos de esos mecanismos. Más concretamente, hemos utilizado herramientas de la física estadística para describir, de forma efectiva, los mecanismos cognitivos que los organismos utilizan para obtener y procesar información en el contexto de procesos de búsqueda. Nuestro marco permite analizar el impacto de múltiples capas cognitivas sobre la navegación de los organismos durante estos procesos.

La tesis se ha dividido en dos partes. En la primera, exploramos cómo las capas cognitivas impactan en la eficiencia del proceso de búsqueda en ausencia de interacciones con otros individuos. Ilustramos cómo la memoria cognitiva y la prospección (la capacidad de simular el futuro) pueden representar ingredientes fundamentales para describir el comportamiento de los organismos vivos. Además, aportamos pruebas experimentales que parecen indicar que la forma en que los humanos cuantifican cuándo la información de esas capas es lo suficientemente fiable (para así tomar una decisión) puede describirse eficazmente mediante un mecanismo basado en conceptos de la teoría de la información.

En la segunda parte, nos centramos en la organización colectiva exhibida por una amplia gama de organismos, y en cómo esta surge de la interacción entre ellos. Más concretamente, exploramos si el marco propuesto para los individuos aislados puede ser útil para describir estas situaciones. Proporcionamos múltiples pruebas en este sentido, enfocándonos en dos sistemas: la dinámica de los peatones y la búsqueda de alimento de las hormigas. Para el primero, caracterizamos cómo el equilibrio entre los ingredientes básicos del movimiento de los peatones puede generar estructuras colectivas y cómo una descripción en un espacio específico (el espacio de los tiempos de colisión) puede capturar adecuadamente estas estructuras. En cuanto al segundo, se sabe que las hormigas cooperan mientras buscan comida para aumentar la supervivencia de la colonia. Exploramos cómo puede obtenerse una mejor comprensión de la complejidad de las estrategias colectivas de búsqueda con la ayuda del marco de los vidrios de espín.

En resumen, esta tesis ilustra cómo puede abordarse los mecanismos cognitivos de los seres vivos mediante modelos basados en la física estadística.

Català: Els éssers vius es caracteritzen per la seva capacitat d'adaptar-se d'acord amb les circumstàncies. Els bacteris, per exemple, són capaços de detectar gradients de senyals químics amb la finalitat de reorientar el seu moviment. Les formigues d'una colònia es distribueixen les tasques, per a així desenvolupar estratègies inviables a nivell individual. Fins i tot els humans adaptem contínuament el nostre comportament al nostre context dinàmic. Aquesta adaptació, basada en la capacitat d'incorporar i processar informació, representa el germen del comportament intel·ligent. En aquesta tesi ens hem centrat en proporcionar un marc físic per a descriure alguns aspectes d'aquests mecanismes. Més concretament, hem utilitzat eines de la física estadística per a descriure, de manera efectiva, els mecanismes cognitius que els organismes utilitzen per a obtenir i processar informació en el context de processos de cerca. El nostre marc permet analitzar l'impacte de múltiples capes cognitives sobre la navegació dels organismes durant aquests processos.

La tesi s'ha dividit en dues parts. En la primera, explorem com les capes cognitives impacten en l'eficiència del procés de cerca en absència d'interaccions amb altres individus. Il·lustrem com la memòria cognitiva i la prospecció (la capacitat de simular el futur) poden representar ingredients fonamentals per a descriure el comportament dels organismes vius. A més, aportem proves experimentals que semblen indicar que la forma en què els humans quantifiquen quan la informació d'aquestes capes és prou fiable (per a així prendre una decisió) pot descriure's eficaçment mitjançant un mecanisme basat en conceptes de la teoria de la informació.

En la segona part, ens centrem en l'organització col·lectiva exhibida per una àmplia gamma d'organismes, i en com aquesta sorgeix de la interacció entre ells. Més concretament, explorem si el marc proposat per als individus aïllats pot ser útil per a descriure aquestes situacions. Proporcionem múltiples proves en aquest sentit, enfocant-nos en dos sistemes: la dinàmica dels vianants i la cerca d'aliment de les formigues. Per al primer, caracteritzem com l'equilibri entre els ingredients bàsics del moviment dels vianants pot generar estructures col·lectives i com una descripció en un espai específic (l'espai dels temps de col·lisió) pot capturar adequadament aquestes estructures. En quant al segon, se sap que les formigues cooperen mentre busquen menjar per a augmentar la supervivència de la colònia. Explorem com pot obtenir-se una millor comprensió de la complexitat de les estratègies col·lectives de cerca amb l'ajuda del marc dels vidres d'espín.

En resum, aquesta tesi il·lustra com pot abordar-se els mecanismes cognitius dels éssers vius mitjançant models basats en la física estadística.

Contents

List of Figures

List of Tables

Preface

0.1 Physics for studying living organisms

Let me start this preface with an anecdote. It is related to the scope of the thesis, and it is very probable that if you have a background close to mine (statistical physics and complexity), you have experienced something similar.

Let's go back in time, looking to how physics was presented to me . When I was at secondary school, I learned how an atom was divided into protons, neutrons and electrons. When I was twenty I was in the middle of the Physics bachelor, so in college. At that point, I knew how an electron exhibits particle and wave properties simultaneously, which is called the wave-particle duality [1]. Two years after, when I was twenty-two, I obtained my Bachelor's tittle. By that moment, I had understood how, under some circumstances, the electrons could move without dissipation through a material, making emerge the astonishing phenomena of superconductivity [2].

Schrödinger's quote

...living matter, while not eluding the "laws of physics" as established up to date, is likely to involve "other laws of physics" hitherto unknown, which however, once they have been revealed, will form just as integral a part of science as the former.

I take this electrons' example because it describes very appropriately how the physical knowledge is usually like a pyramid, where new layers (new knowledge) are built on the previous ones.

Portrait of Erwin Schrödinger. Image taken from [3].

Electrons and their nature is not the unique topic I was taught: I was given many lessons about quantum physics, the framework that explains what happens to very small things. I also attended to some relativity lessons, where the framework to explain the phenomena at the cosmological scale was presented to me.

Maybe you are a bit concerned at this point, wondering why I am explaining all this. I assure you is not for the sake of reviewing how many topics I have explored during my formation. The underlying reason is much simpler. Where is the physics that can describe the fundamental features of our daily life? It is necessary to explore what is happening at the nano and cosmological scales, but I firmly believe that

the physics of **our scale** provides a deep list of incredibly interesting phenomena that needs to be explored. During the undergraduate formation, the study of this topic is almost residual. However, those very few moments where I was taught statistical mechanics or biophysics were my favorite ones. They made me wonder how interesting could be the study of a bacteria or the internet structure through the lens of physicists. Being coherent with my own past, I engaged this thesis project with the aim of extending and divulging the knowledge about these phenomena. My ultimate goal is then to provide a physical framework for the daily life scenarios, most of which are closely related with living organisms.

I'm sure that most of you have heard about black holes, worm holes or quantum coherence. However, how our brain works [4, 5], how the stock market evolves [6, 7] or how the animals forage [8] are also very awesome and relevant contexts where physics could play a key factor to obtain a better comprehension about why and how these phenomena occur.

If you are not familiar with these topics, it is probable that you are wondering how physics is related to the brain or the global economy. And that is a completely legit question. With the purpose of giving you an answer, let me make a brief aside. During the first decades of the XXth century, the science was built on different disciplines, such as biology or chemistry. And at some time they grew as isolated islands focusing into the phenomena that, by general agreement, belonged to that discipline.

However, there were great scientists, such as Niels Bohr or Erwin Schrödinger, that pioneered in bridging the gap between those islands [9, 10]. Their aim was to create a richer and deeper vision, where the knowledge of different disciplines could create a more complete description of our reality. That is why my previous quote *"...how our brain works, how the stock market evolves or how the animals forage..."* is not out of the scope of a physics project. Continuing with the idea of these brilliant scientists, in the recent years there have been many works that make the gap between disciplines more and more reduced, or combine the knowledge of multiple disciplines to explore a given phenomenon. And the gaps between physics and the rest of sciences is far from being an exception. So biological, social or psychological (broadly speaking, **our daily life** or **our scale**) phenomena are being addressed by physicists who are trying to develop mathematical frameworks to capture their essential behavior [11–13].

Let's focus on the case of how physics may be helpful to describe the features of living organisms. The scientists who live at the bridge (or the interface) between the well established disciplines of physics and life sciences study the living organisms, their behavior and their fundamental processes through the lens of fundamental laws or quantitative rules, with the aim of providing a mathematical or physical description [14–16].

During the recent years, there have been significant discoveries emerging from that kind of collaborating work. At the microscopic scale (but yet very distant from the quantum scale), the importance of the physical tensions in in cellular walls for the structure of organic tissues (morphogenesis) has been revealed [17, 18]. Statistical physics has also been used to describe the evolution of alleles frequencies and polygenic traits [19, 20]. It has been explored how the bacteria movement patterns could be understood through diffusive

(physically-based) and chemotactic models [21, 22]. And many other significant examples could be mentioned.

Nevertheless, not all the contributions are focused onto the microscopic features. Works such as [23] or [24] help us to understand with quantitative descriptions how the fruit flies or the ants colonies organize themselves at the individual level to improve the food intake. Some contributions have also been provided to understand physiological processes within humans. For example, a physical description is useful to understand how our cellular processes takes place [25], how the electric impulses between our neurons translates into our behavior [26], the metastasys dynamics that cancer causes [27, 28] or even how we interact with other people in the middle of a crowd or in social networks [29, 30], that could lead to provide improved responses to global challenges such as COVID-19 [31, 32].

0.2 Scope and organization of this thesis

My fundamental aim with this thesis has been to continue the path, helping to provide a physical description of behavior in living organisms. More concretely, I have spent the last four years exploring physicals framework that can describe the movement patterns of the living organisms in the light of the cognitive abilities that they exhibit as one goes higher and higher in the evolutionary scale. A complete mathematical description of such movement rules and/or generators is yet unknown. I have used concepts and tools coming from the statistical physics field, such as microscopic interactions or entropic considerations, as a way for developing that mathematical framework.

The writing of the thesis has been organized with the purpose of easing the reading and its understanding. There are two main parts, which correspond to the physical description of how living organisms move either when they are isolated or in a crowded media. For the sake of completeness, I provide here a very brief outline of these two parts of this thesis:

- **Part 1: Individual behavior**. This is dedicated to the development of a physical framework to describe the living organisms movement patterns. The framework tries to account for biological and psychological mechanisms, for which I try to reach an approximate physical description. I explore the resulting patterns of those mechanisms in the context of a search process. I also discuss how the organisms gather and process contextual information to readapt their movement to a given context.
- **Part 2: Collective behavior**. This is dedicated to the development of physical tools to describe the collective movement patterns. I provide different mechanisms coming from statistical physics to explore the self-organization of living organisms. I also explore experimentally if those collective patterns could represent a measure of intelligence (interpreted in a broad sense), where organisms collaborate to improve their overall performance.

Part I

Individual behavior

Introduction

The **movement of an organism**, defined as a change in the spatial location with time, is a fundamental biological trait, exhibited across multiple scales. All organisms move during their lives, with very different and significant implications for individuals, populations and even at the species level [33]. Through movement, organisms may locate food, mates, a place to live or may avoid predators [34, 35]. In general, the movement patterns of an organism plays a fundamental role in all its basic functions: reproduction [36, 37], nutrition [38, 39] and relation [40, 41].

Hawking's quote

Intelligence is the ability to adapt to change.

There is a vast variability of movement patterns featured by living organisms. One trait of those patterns is that they seem to be adapted to increase the organism efficiency, such as increasing the food intake or the energetic income [42, 43].

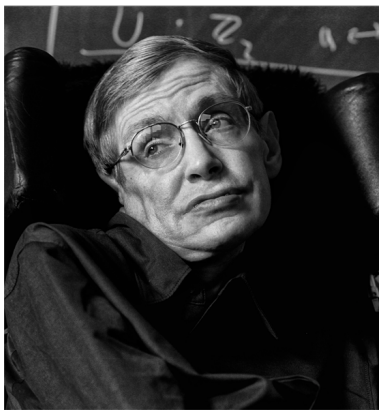

Portrait of Stephen Hawking. Image taken from [44].

This **adaptation** of the behavior according to the context has been proposed as a feature of **intelligence** [45, 46]. With that broad definition, one can consider bacteria or other microorganisms as intelligent species [47–50], as they have developed mechanisms to adapt to the specific context. To do this, the organisms need sensory detectors to obtain the relevant information from the current scenario. Bacteria, for example, are able to detect chemical signal gradients with the purpose of reorienting themselves [51–53]. That mechanism is known as chemotaxis [54–56]. Macroscopic organisms also use sensory inputs to adapt their behavior [57]. For instance, visual [58] or olfactory [59] mechanisms allow insects and animals to detect the relevant features of their habitats.

Also, the dynamic nature of some scenarios force the organisms to modify constantly their movement patterns. The less complex organisms adapt themselves through automatic responses to chemical signals. However, a complex processing of the sensory information is an exclusive trait of high level organisms. High level organisms are constantly facing challenging situations. A complex processing of that information helps to provide responses or make decisions about those situations more efficiently [60, 61].

Because movement is such a prevalent and important process, the development of a **physical framework** to provide a better comprehension of how organisms process and use the sensory information in this context is of great importance. For example, one can wonder if a movement pattern for an organism while foraging could be described on a set of rules. If these rules can capture the essence of the organism behavior, our understanding of the movements and its intrinsic mechanisms would be more profound.

From a physical perspective, those rules driving the movement patterns of living organisms can be condensed into **effective forces**. Thus, a physical description of the organisms dynamics would have to translate or map the cognitive or sensing mechanisms involved in such rule evaluation into such physical forces.

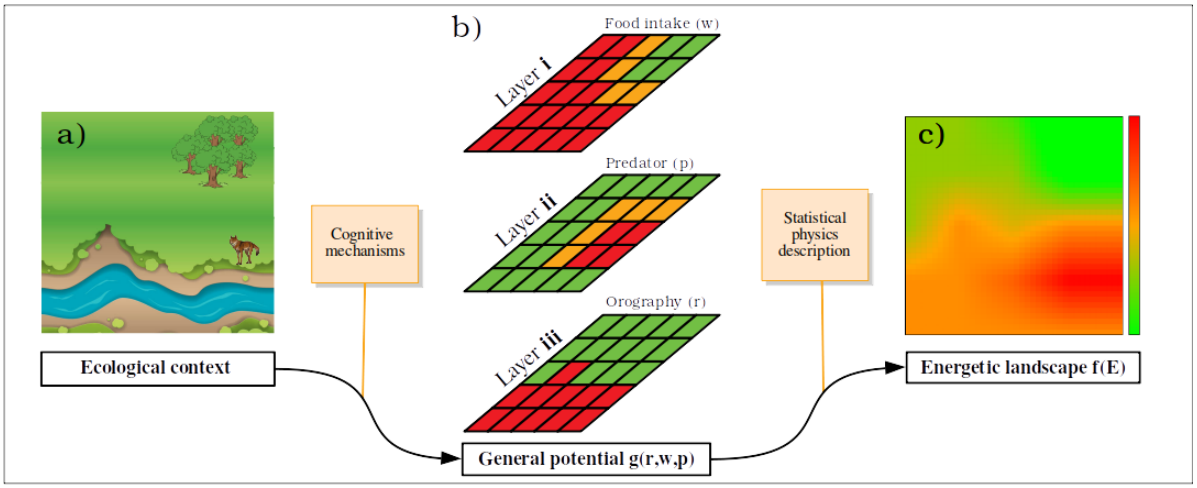

Figure 1.1: *Scheme of the physical description of the cognitive processing. The graph a) corresponds to a given ecological context. The graph b) corresponds to the cognitive processing of the ecological context by the organism. Each layer corresponds to the information of the food location (w), the predators positions (p) and the orography of the region (r) building the multidimensional potential $g(r, w, p)$. The graph c) corresponds to the physical description of the same given situation trough the mapping of the multivariable potential g into the one-dimensional energy landscape $f(E)$. The color code works as follows. Red regions are detrimental to the organism aims (high E), while green regions are beneficial to the organisms aims (low E).*

One can wonder how this mapping should be done. Let's start by establishing a general mathematical expression for the organisms dynamics $\frac{d^2x}{dt^2} = -\nabla g(r, w, p)$, where $x(t)$ corresponds to the individual position in the space and $g(r, w, p)$ is a general potential of a set of environmental variables $r, w, p, \ldots$ How the position evolves in time, and so how the organism adapts itself, should depend on the circumstances. Consequently, the potential g contains all the **contextual information**. For example, one can suppose that the orography of the region, characterized by a magnitude $r(x)$, is relevant for the dynamics. The same could apply to the food location $(w(x))$ or the presence of predators $(p(x))$, or any other relevant environmental trait.

Even so, the variables defined as fundamentals to adapt movement patterns may variate between situations or species. Statistical physics, which allows us to connect microscopic details of a system with overall measurable magnitudes, should provide tools to translate the information contained in $g(r, w, p, \ldots)$ into an effective statistical description. That

is why we propose to map the multi-dimensional potential $g(...)$, with all its variables, to a uni-dimensional **energetic landscape** $f(E)$, whose specific properties will obviously depend on the particular situation studied. One can identify that energy E as a macroscopic, or effective, representation of the cognitive processing done by the organisms. For a more visual explanation, see figure 1.1.

Using this analogy, we can connect the physical idea that systems tend to minimize energy, with the biological idea that organisms tend to maximize fitness (which is itself a function of the environmental variables $r, w, p, ...$).

So that, the physical framework for the living organisms trajectories would be effectively defined through $\frac{d^2x}{dt^2} = -\nabla f(E)$. The challenge is then how to construct realistic and insightful descriptions for $f(E)$ that could be helpful for the comprehension of organisms behavior and for predicting their patterns.

Search processes are a paradigmatic scenario where a high cognitive processing of the contextual information may adapt the movement patterns. In this thesis we intend to apply this kind of framework to explore movement patterns of living beings while engaged in search or foraging tasks. Living organisms are constantly searching for things. Food foraging [62, 63], the search for nest settlement [37] or a sexual mate [64] are examples of the ubiquity of search tasks. Previous studies have reported that mathematical exploration of optimal search strategies is a relevant tool to understand biological behavior. For instance, when a bird looks for the best suitable place to settle the nest or when a predator looks for preys [65, 66] (see figure 1.2 for visual examples of searches). An efficient movement pattern, or strategy, is defined as the one that minimizes the invested effort in comparison to the obtained reward. For a fixed reward quality, the optimal search trajectory is usually the one that finds the reward in a shorter time. Consequently, intelligent organisms adapt their movement to minimize the search effort (time) through the use of the contextual information.

Figure 1.2: *Foraging is a widespread search process across many different species. In this image, one can observe a bear and a seagull while searching. The images have been taken from [67].*

The foraging (food search) scenario is present at almost all scales, and while it is true that our social organization may have modified some of our search situations, the search processes keep being a constant feature in human daily life [68–71]. During the last years there has been a combined effort to develop a theoretical and computational framework for such processes, describing the relevant information that drives to an efficient performance [72, 73]. More specifically, search strategies (or algorithms, depending on the context) have

been proposed to optimize the search of targets under different circumstances, such as rescue protocols [74] or searching in databases [75, 76]. As noticed before, the optimal search strategy should give an answer to the dynamic situations that the individual faces during the process.

The following Chapters try to explore plausible landscapes $f(E)$ for different search contexts, and how this physical representation of the cognitive mechanisms of the organism may be able to recover some of the complex features of real movement patterns. By focusing on how the sensory information may be translated into the physical magnitudes, we analyze the emerging movement patterns and their corresponding search efficiency.

Movement models 1

1.1 The Random Walk model

One can wonder how an organism moves when it does not have any contextual information available or it is not able to process it. This organism could not adapt its movement patterns (it would not fit the criterion for an intelligent behavior provided in Chapter I). However, it can be illustrative to explore first the properties of those **non-informed** movement patterns. The analysis will serve as the starting point from which we can construct more complex scenarios, where the movement patterns are actually adapted to the context.

One can intuitively wonder whether a constant value $f = \text{ct}$ may represent the non-informed nature of the trajectory. However, such a landscape $f = \text{ct}$ corresponds to the organism being staked at the same position ($\frac{d^2x}{dt^2} = 0$). Instead, a more realistic proposal would be to represent the non-informed behavior with a random trajectory. Then, in absence of external forces, the velocity fluctuates randomly and $\frac{dx}{dt} = \eta$, where η corresponds merely to a noise term. Under these circumstances, the potential f does not incorporate contextual information and the trajectory of the individual is built up from random steps. For example, this would be the case of an entity of a very small (e.g. molecular) size, which is then lacking any adaptive mechanism characteristic of living beings, and so its movement is just a consequence of thermal noise.

In physical and mathematical literature, the properties of stochastic movements have been deeply explored [77, 78]. The mathematical approach to the random movement is provided by the **Random Walk model** (RW) [79–81]. In the following paragraphs, we review the basic properties of this classic model.

1.1.1 Definition and properties

A random walk is defined as a stochastic or random process that describes a path consisting on a succession of random steps on a given space [77]. The space, and so the steps through it, could be continuous or discrete. The analysis provided here focus on discrete spaces for the moment, but an extension to the continuous case is presented below.

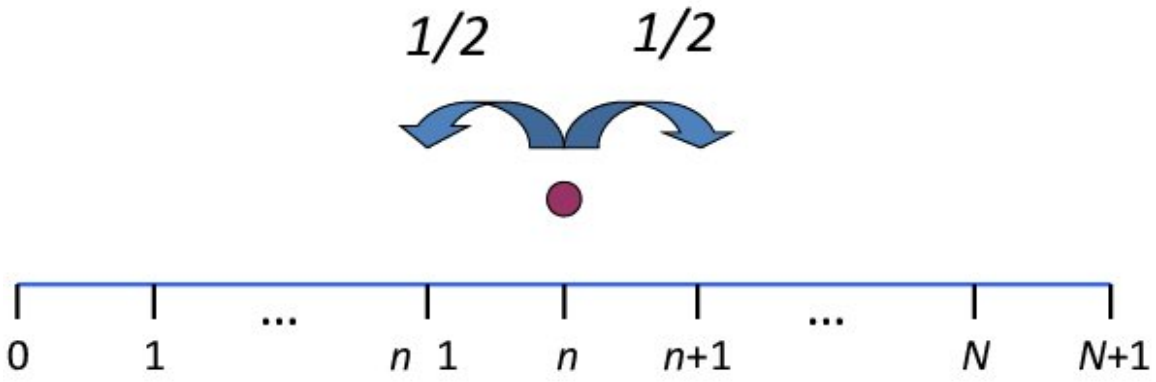

Figure 1.3: *Scheme of the random walk dynamics in a one-dimensional discrete space. The probability to move from the current site n to the anterior $(n-1)$ or the postterior $(n+1)$ sites are equivalent and fixed to $1/2$. The image is taken from [82].*

To comprehend how the RW works, let's use a straightforward example where a walker moves isotropically through a discrete one dimensional space (figure 1.4). We define n as the walker site within this discrete space. As the movement of the walker is assumed to be homogeneous, the probability to move to the site $n-1$ and to the site $n+1$ are the same. From a more general perspective, the probability of each option is $p_i = \frac{1}{k}$, k being the coordination number, which measures the number of first neighbours for each cell in the lattice. For the one-dimensional scenario studied here, the transition probabilities read as $p_{n-1} = p_{n+1} = \frac{1}{2}$. As the number of steps, or time, tends to infinity ($t \to \infty$), the number of forward and backward movements tends to be balanced. In consequence, the averaged position of the walker at that time t will be the same that the initial one (according to the figure 1.4, n).

Property I

The average walker's position after a given number of movements is equal to its initial position. Without loss of generality we consider an initial position $x_0 = 0$. According to that, the average position of the walker at time any time t reads

$$\langle x(t) \rangle = 0 \tag{1.1}$$

Due to the stochastic, or erratic, nature of the RW dynamics, predicting its exact position at a given time is impossible, and then the study of the distribution of positions must be carried out in order to capture the relevant features of the dynamics. Since the average position of the random walk, according to property I, provides only trivial information

about the properties of the movement the analysis of further moments of the positions distributions are of great interest to understand the RW dynamics. One can obtain the second moment trough the analysis of a trajectory until the step k. For the one dimensional case, the second moment reads

$$\langle x_k^2 \rangle = \langle (\Delta x_1 + \Delta x_2 + ... \Delta x_k)^2 \rangle, \tag{1.2}$$

where Δx_i corresponds to the transition at the step i (which can be, with equal probability, l or $-l$, where l is the distance between neighbor sites). If one defines $n_k = \sum_{i=1}^{k} \Delta x_i$, the expression can be rewritten as

$$\langle x_k^2 \rangle = \langle n_k^2 \rangle, \tag{1.3}$$

where the term n_k follows a Gaussian distribution whose standard deviation is $\sigma = k$ (this is only valid in the limit of large k). Then, the equation 1.3 can be rewritten as

$$\langle x_k^2 \rangle = l^2 \int_{-k}^{k} n^2 \frac{1}{\sqrt{2\pi}\sigma} \exp\left(-\frac{n_k^2}{2\sigma^2}\right) dn_k. \tag{1.4}$$

From this, one can derive then that the second moment after k steps reads

$$\langle x_k^2 \rangle = 2Dk, \tag{1.5}$$

where D is the diffusion coefficient and corresponds to $D = \frac{l^2}{2}$. The same procedure can be generalized to derive the second moments of the walker's position in higher dimensions.

Property II

The second moment of the position of the walker is defined as the **Mean Square Displacement** (MSD). According to that, the MSD at time t reads as follows, where n is the given dimension of the space.

$$\langle x^2(t) \rangle = 2nDt \tag{1.6}$$

The second moment provides information about the dispersion of the possible walker's position at time t. Despite being, in average, in the initial site, the distribution of possible positions broadens as the walker advances.

1.1.1.1 From the discrete to the continuous space

Until this point, the analysis of the RW model has been done for a walker moving through discrete spaces. However, the RW model can also describe the movement through **continuous** spaces, extending the notion of jumps between discrete sites to a fixed movement length l in a continuous space.

For the one-dimensional scenario, the dynamics of doing movements of fixed length l is equivalent to jump between sites of length l. In the two dimensional (rectangular) lattice, the walker can jump from the current site to a discrete number of sites, while in a continuous space, a movement of length l can be done in an infinite number of directions. From a general perspective, the properties I and II reported before for the discrete case are also valid are for the continuous case, with the diffusion coefficient being $D = \frac{l^2}{2}$.

We provide a comparison of the dynamics (trajectory and MSD) in both discrete and continuous spaces in figure 1.4, for the sake of completeness. The asymptotic behavior for the MSD provided by the Property II is clearly the same for both spaces, giving support to the claim of properties I and II remaining valid.

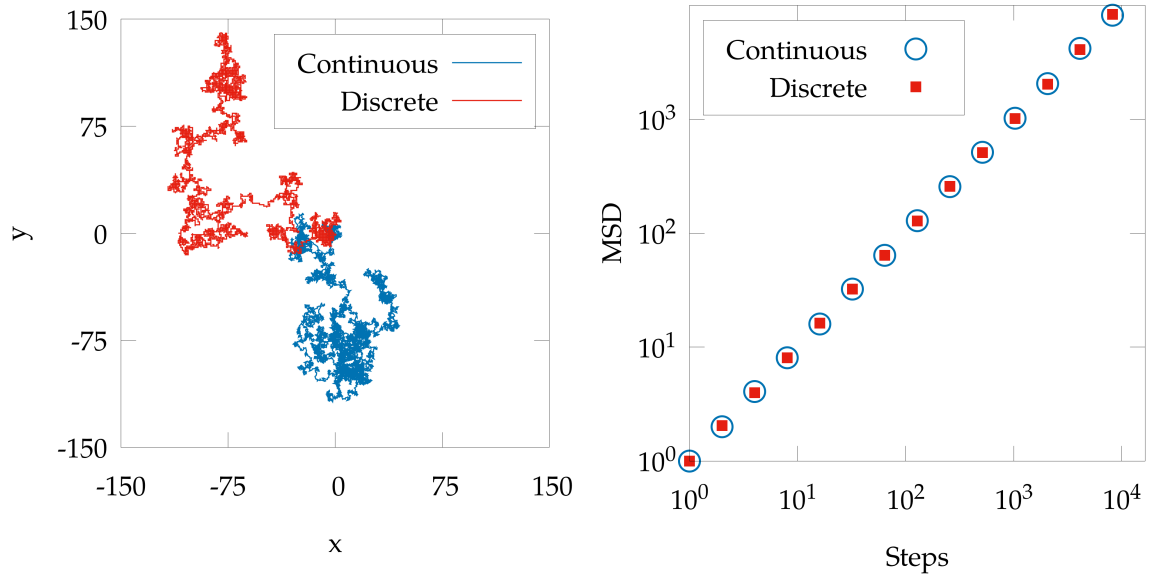

Figure 1.4: *Left: The trajectory of a random walker in a given set of* 10^4 *steps. Right: Mean square displacement of the walker. The results are provided for a continuous random walk (blue) and a discrete random walk (red) when moving trough a two dimensional space.*

Alternatively, the results above can be derived from a continuous formalism based on the well-known **diffusion equation**

$$\frac{\partial \rho(x,t)}{\partial t} = D\frac{\partial^2 \rho(x,t)}{\partial x^2}, \tag{1.7}$$

where $\rho(x,t)$ is the probability density to find the walker at position x at time t.

1.1.2 Target dynamics

Target dynamics refers to the process by which we measure the time the walker needs to reach a particular region of the spatial domain representing the position of one or multiple targets. The **search** for such targets may depend on a variety of different conditions. Targets may be sparse or hidden. The targets may be mobile or immobile. They may have a finite

life-time and vanish before they are detected. So to define a general estimator for how a random walker performs in those scenarios is far from trivial and depends strongly on the circumstances.

First, we focus on the case where the walker searches for a single immobile and non-vanishing target. Mathematically, this process is as follows. The trajectory $x(t)$ starts at a initial position $x(0) = x_0$. The target is defined as subdomain Z of the space domain. When the position $x(t)$ at a given time t pertains to the subdomain Z, the walker has found the target.

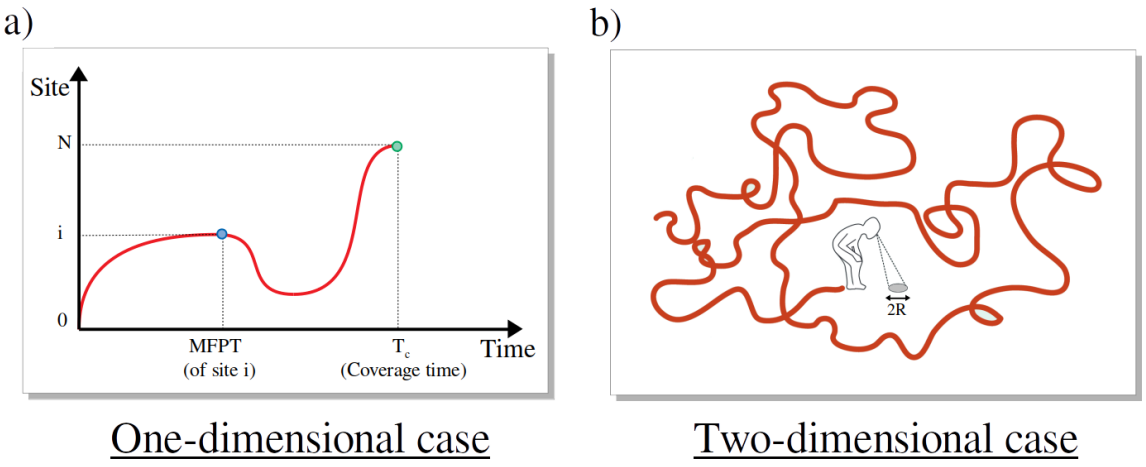

Figure 1.5: *Schematic representation of the target dynamics. a) Evolution of the walker's position as a function of time in a one-dimensional lattice. The two dots corresponds, respectively, to the MFPT of the site i (blue dot) and to the coverage time T_c, when all the N sites of the finite lattice have been covered (green dot) . b) Evolution of the walker's position in a two-dimensional lattice. To avoid the nule measure of the trajectory, one defines a region of radius R around the walker's position.*

Under those circumstances, one can propose different scenarios to characterize how efficiently the walker performs during the process. One possible estimator of search efficiency is the **survival probability** $S(t)$. It is defined as the probability that, after a time t since the beginning of the process, the walker has not reached the location of the target. When the survival probability goes to 0, it means that the walker has reached the target.

For the specific case of a walker satisfying the diffusion equation 1.7 in 1D, one can compute the survival probability by solving the equation in $(0, \infty)$ with a absorbing boundary condition at $x = 0$ (representing the target). The specific solution (see [83]) is

$$S(t) = \text{erf}\left(\frac{x_0}{\sqrt{4Dt}}\right), \tag{1.8}$$

which satisfies $S(\infty) = 0$, so the target will be reached with certainty.

From the survival probability, one can obtain the average time the walker needs to reach the target. The stochastic estimator of the number of steps to reach, on average, the target position starting at x_0 is called the **mean first passage time** (MFPT). For simple random-walk models, this time can be derived analytically [83, 84]. We illustrate here the

fundamentals of how that derivation is done for the simpler case of the classical random walk reviewed above (for more details, see [85]).

The diffusion equation 1.7 is known as the forward Fokker-Planck equation, which describes the evolution of $\rho(x,t)$ for fixed initial conditions (x_0, t_0). Now, instead, we use the backward Fokker-Planck equation, which describes the evolution of $\rho(x_0, t_0|x, t)$ back in time and space for fixed present conditions (x, t). We consider for simplicity a situation in which the walker moves across a one dimensional space $(0, L)$ with absorbing boundary conditions at $x = 0$ and $x = L$ (the absorbing boundaries stand for the presence of the target).

The survival probability after a moving time $\tau = t - t_0$ reads

$$S(\tau, x_0) = \int_0^L \rho(x, t|x_0, t_0)dx, \tag{1.9}$$

which now in finite media must satisfy $S(0, x_0) = 1$ and $S(\infty, x_0) = 0$. The first passage time distribution $f(\tau, x_0)$ can be connected to the survival probability through $f(\tau, x_0) = \frac{\partial S(\tau, x_0)}{\partial t}$, and the MFPT (T) can be computed as

$$T = \int_0^\infty \tau f(\tau, x_0)d\tau = \int_0^\infty S(\tau, x_0)d\tau. \tag{1.10}$$

According to the relation 1.9, one can introduce the survival probability into the backward Fokker-Planck equation. Now, it reads

$$\frac{\partial S(\tau, x_0)}{\partial t} = D\frac{\partial^2 S(\tau, x_0)}{\partial x_0^2}. \tag{1.11}$$

Now, after the integration in τ from 0 to ∞ it reads

$$-1 = D\frac{d^2 T(x_0)}{dx_0^2}, \tag{1.12}$$

from where we can obtain a closed expression for the MFPT. The solution of this ordinary differential equation leads finally to

$$T(x_0) = \frac{x_0(L - x_0)}{2D}. \tag{1.13}$$

A similar procedure can be done for multi-dimensional lattices [86]. However, for those cases the probability to reach a point target at $\vec{x} = \vec{x_c}$ has null measure. In consequence, one assigns to the walker a characteristic radius R to avoid the null measure problem.

Alternatively, an efficiency measure for scenarios where multiple targets cover homogeneously the whole spatial domain may require a different perspective, as the MFPT may not capture all the details of the process. Under these circumstances, to measure how fast

the walker covers the domain will provide a more suitable efficiency evaluation (as larger the covered region is, higher the probability to find all the targets).

One estimator to analyze how the walker covers the space is the **mean covered region** $V(t)$. It corresponds to the size of the region covered by the walker up to a time t, averaged over all possible realizations, and reads

$$V(t) = \int_R dr \int_0^t dt\, f(r,t), \tag{1.14}$$

where $f(r,t)$ is the first passage distribution to reach the point r for first time. One can find a detailed derivation of $V(t)$ in [87]. In the limit of large times, it can be obtained that $V(t) \sim \sqrt{2nDt}$, where n corresponds to the dimension of the space. One can observe that the analysis of the MSD also provided the same result (equation 1.3), so both measures coincide in the asymptotic limit.

Note that the volume covered by the random-walk grows indefinitely for infinite domains, while in the case of finite domains it will saturate for long times. For this reason, when the search region is finite, one alternative way to measure the efficiency at covering the domain is given by the mean **coverage time** T_c, which describes the average time a walker spends to cover an entire region [8, 88]. Coverage properties of random walks moving within regular lattices dimensions have been extensively explored over the last thirty years [89–92].

In the following, we illustrate how to derive the coverage time T_c of a walker in a one dimensional (cyclic) lattice of N sites with periodic boundary conditions. The entire derivation can be found in [89].

Let's define $T_c(N)$ as the time to cover the N sites of the domain. In order to cover N sites the walker should first cover $N-1$ sites and then proceed to cover the last one. The average time required to cover $N-1$ sites is identical to the coverage time for a ring (chain with periodic boundary conditions) of $N-1$ sites. So one can rewrite $T_c(N)$ as

$$T_c(N) = T_c(N-1) + \bar{t}, \tag{1.15}$$

where $\bar{t}$ is the average time required to cover the last site and it is identical to the MFPT through the site N of a walker that started from the site 1 on a ring of N sites, and corresponds to $\bar{t} = N-1$.

One can sequentially repeat the same process for the $N-1$ case ($T_c(N-1) = T_c(N-2) + \ldots$). That sequence leads to a final expression $T_c = \frac{N(N-1)}{2} \approx N^2$ for the periodic one-dimensional lattice.

In two-dimensional (or higher-dimensional) lattices, the mathematical analysis is more complicated. The number of paths to move from the initial site to the final one makes impossible to find a simple analytical expression to $\bar{t}$ in the same terms (see [86]). However, the same conjecture of the coverage process being governed by the last site reaching ($\bar{t}$) has

been proposed in [91, 93]. In there, the distribution of first passage times of that last site has been related with the lattice size N as

$$\frac{\bar{t}}{N\log^2(N)} \to \frac{\pi}{4}. \tag{1.16}$$

The scaling of the coverage time T_c, if governed by that last stage, will be equivalent to this scaling [94].

Property III

The averaged necessary time to cover all the sites of a finite space is called the coverage time T_c. The mathematical analysis of the random walk trajectories provide that the T_c for a given space scales with the number of sites N sites scales as

$$T_c \sim N^2 \tag{1.17}$$

when the space is one dimensional and as

$$T_c \sim N\log^2(N) \tag{1.18}$$

when the space is two dimensional (and higher dimensions).

In a finite and periodic lattice, one can define the general MFPT ($\langle T\rangle$), which corresponds to the MFPT to a given target site averaged over all starting sites. Within the last sites conjecture, there is a special subset of stochastic movements that permits a relation between the coverage time T_c and the general MFPT [95]. This subset corresponds to non compact (or non-recurrent) walks (which is not the case of the RW explored here). All the models that fit in that criterion show the same distribution of coverage times $P(T_c)$ of a N sites lattice when reescaled in terms of the general MFPT. The reescaling producing the collapse is $P(T_c) = \frac{T_c - \langle T\rangle \ln N}{\langle T\rangle}$.

1.1.3 The Persistent Random Walk

In the previous paragraphs we have explored the navigation properties without considering in any case correlations between subsequent steps. Living organisms usually tend to exhibit persistence, which means that they keep moving in the same direction at least for a given time.

The **Persistent Random Walk model** (PRW) provides a framework to include this feature in the walker's navigation [96, 97]. In the PRW, the jumping probabilities p_i are conditioned by the walker's previous step.

We use the one-dimensional case as an illustrative example. At each time step τ, the walker does a step keeping the previous direction with a probability $p = 1 - \alpha\tau$ (λ is the turning rate) or it changes the direction with probability $q = \lambda\tau$.

According to this probability definitions, one can derive the navigation properties of the walker as follows. Let $\rho(x,t)$ be the probability density of the walker being at position x at time t, and $\rho_-(x,t)$ and $\rho_+(x,t)$ the probability density that arrives to position x at time t from the left and and from the right, respectively. Hence

$$\rho(x,t) = \rho_+(x,t) + \rho_-(x,t). \tag{1.19}$$

The balance equations for $\rho_+(x,t)$ and $\rho_-(x,t)$ are

$$\rho_+(x,t+\tau) = p\rho_+(x-a,t) + q\rho_-(x-a,t) \tag{1.20}$$

$$\rho_-(x,t+\tau) = p\rho_-(x+a,t) + q\rho_+(x+a,t) \tag{1.21}$$

If one considers $a \to 0$, $\tau \to 0$ but requiring $\frac{a}{\tau} = \text{ct}$, one can arrive to the telegrapher's equation from the treatment of the balance equations. It reads

$$\frac{\tau}{2}\frac{\partial^2\rho}{\partial t^2} + \frac{\partial\rho}{\partial t} = D\frac{\partial^2\rho}{\partial x^2}. \tag{1.22}$$

From that equation, one can derive that $\langle x(t)\rangle = 0$. The persistence does not introduce any anisotropy in the system (the initial step of each trajectory is done randomly). The MSD calculation leads to the differential equation

$$\tau\frac{d^2\langle x^2(t)\rangle}{dt^2} + \frac{d\langle x^2(t)\rangle}{dt} = 2D. \tag{1.23}$$

This second order liner-differential equation can be solved under the initial conditions $\langle x^2(0)\rangle = 0$ and $(\frac{d\langle x^2(t)\rangle}{dt})_{t=0} = 0$. One obtains

$$\langle x^2(t)\rangle = 2D\tau\left[\frac{t}{\tau} + \exp\left(-\frac{t}{\tau}\right) - 1\right]. \tag{1.24}$$

The limits of this expression reads

$$\langle x^2(t)\rangle = D\tau t^2, t \ll \tau \text{ Ballistic regime} \tag{1.25}$$

$$\langle x^2(t)\rangle = 2Dt\ , t \gg \tau \text{ Diffusive regime} \tag{1.26}$$

Thus, the stochastic movement of a persistent walker does not yields a net movement. However, it introduces a **ballistic** regime where the walker moves in the same direction. It

means that there is a temporal correlation in the walker's velocity during a time τ. Note that $\tau \to \infty$ corresponds to an infinite ballistic regime, while $\tau = 0$ is analogous to the ordinary RW.

The MFPT can be computed as in Section 1.1.2. One obtains the expression

$$T(x_0) = \frac{x_0(L - x_0)}{2D} + \frac{L}{2v}, \tag{1.27}$$

where v corresponds to $\frac{a}{\tau} = \text{ct} = v$.

The coverage time T_c of the PRW is analogous to the results of the ordinary RW. The coverage is governed by the last visit process, and in the limit $t \gg \tau$, the walker's navigation is diffusive.

1.2 The Self-Avoiding Walk model

The framework $f(E)$ introduced in Chapter I translates the sensory information and its cognitive processing to a physical energetic landscape.

Focusing on search tasks, for instance, one can wonder how optimal search patterns may emerge from the efficient information processing. For example, to retain the knowledge of which regions have been explored during the task helps the individual to avoid exploring again those regions. A realistic $f(E)$ landscape could then add this **cognitive layer**.

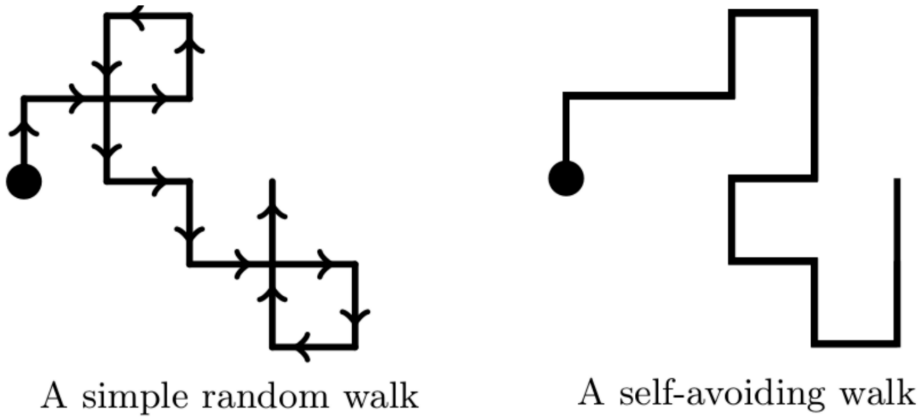

Figure 1.6: *A comparison between a pure random trajectory (left) and one self-avoiding trajectory (right). One can observe how the loops of the common random walk are deleted for the self-avoiding walk. Source: [98]*

Real biological organisms have developed mechanisms to incorporate that cognitive layer. At the microspic level, bacteria represent a paradigmatic exemple. Bacteria deposite chemical signals along their path. Through chemical detectors they can detect those signals to modify their direction of motion [51, 53, 99, 100]. At the macroscopic level, the capacity to retain information about olfactory, visual or hearing stimulus helps the organisms to avoid previous regions [101–104].

Self avoidance is defined as the mechanism of suppression of crossings or loops during a given trajectory with its own previous path (see figure 1.6). This idea where the organism avoids those revisits, can be introduced into the random walks framework through the Self-Avoiding Walk models (or SAW) [105, 106].

Despite its own mathematical interest and its relation with complex movement patterns, the SAW was first proposed to describe the structure of polymers [107, 108]. One polymer is defined as a set (or chain) of individual units, known as monomers. A polymer is built up from the concatenation of those units. Let's suppose all the monomers are identical, with a given size or length l. Since the number of units (n) present in the structure largely determines the functionality and many of the physical properties of the whole chain, it is particularly instructive to represent and analyze polymers in terms of the phase space of all the possible configurations that those units can adopt, assuming that they cannot overlap with others due to excluded volume reasons. From a SAW perspective, this is translated into a stochastic structure avoiding crossings or loops with itself. This idea is illustrated in figure 1.7.

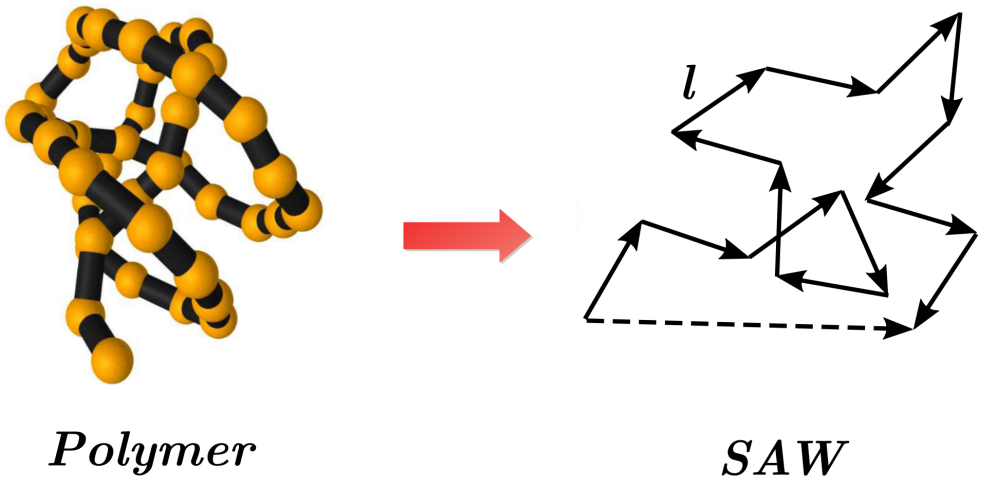

Figure 1.7: *The polymer structure can be modeled as a set of monomers of fixed length l, concatenated with random orientations. The unique requisite is the excluded volume, so the self-avoiding walks represent a very complete framework to study them. The image provides a three dimensional representation of the polymer, avoiding crossings. The two-dimensional nature may lead to a misinterpretation of the crossing of the random path.*

1.2.1 Definition and properties

The properties of SAWs on lattices have been extensively studied. An analytical treatment is complicated as the next step of the walk depends on the entire previous history of the walk (it is a example of non-Markovian dynamics). While some analytical results have been found [109, 110], most of what is known about self-avoiding walks comes from computer simulations [111].

Within the SAW framework, the trajectory of a walker in a discrete lattice consists of a set of random steps with a constraint: a given site cannot be visited more than once (it would

correspond to a crossing of the path with itself). Consequently, the probability to jump from the current site to a site i that has been visited during the previous trajectory is $p_i = 0$. As a result of this, the SAW presents a special feature. During a given trajectory, the walker may arrive to a situation in which all the possible sites available for jumping have been visited before, and then, all the probabilities of the sites to jump into are $p_i = 0$. In this situation, the walker will face a dead end and the SAW process is terminated. That situation can take place in any dimension, but as the dimensionality of the system becomes larger, the probability of facing a situation like this goes to zero (Polya's theorem [112]). The critical dimension of the SAW is $d = 2$ [113], and so the navigation through higher-dimensional spaces will provide analogous results to the RW ones. According to that definition, we explore in the following the properties of a SAW.

Despite the presence of self-avoidance, the nature of the motion keeps being isotropic. There is no a preferred direction. That fact leads to $\langle x(t)\rangle = 0$, as stated above. We illustrate this idea for one-dimensional case. Here, self-avoidance corresponds to move constantly towards one direction (a direction shift would lead to a crossing with the previous trajectory). Mathematically, the probability density $\rho(n, t)$ to be in a given site at a given time reads

$$\rho(n, t) = \frac{1}{2}\delta(n - t) + \frac{1}{2}\delta(n + t). \tag{1.28}$$

The walker will always be at sites n or $-n$, corresponding n to the number of steps of the trajectory (guessing the initial site is 0). The average of this distribution leads to $\langle x(t)\rangle = 0$.

When referring to the navigation through two-dimensional (or higher dimensional) lattices, a similar mathematical analysis is far from trivial. However, due to the isotropy of the system, one can derive that the averaged position reads analogously $\langle x(t)\rangle = 0$.

The suppression of crossings or loops may have an impact on how compact the walker trajectories are. One can characterize that feature trough the analysis of the MSD. For the one dimensional case, one can derive the MSD from equation 1.28. One obtains that $\langle x^2(t)\rangle = \int x^2\rho(x, t) \sim t^2$. These results report an analogous ballistic motion to the PRW with infinite persistence (Section 1.1.3). As stated before, for this case the walker does the first step of the trajectory randomly, but the subsequent steps are always in that direction.

For two and higher dimensions, random-walks become partially or completely non-recurrent due to the topological properties of the system. In consequence, one cannot expect ballistic motion. By using Renormalization Group techniques, one can derive that a walker moving trough a two-dimensional lattice exhibits a super-diffusive behavior, characterized by $\langle x^2(t)\rangle \sim t^{\frac{3}{2}}$ [114–116]. That corresponds to broader trajectories if compared to the common RW trajectories (where recurrence is not avoided). The probability to find a possible loop during the paths goes to zero as the dimension of the lattice grows. As a result, the statistical properties of the process become more and more similar to the diffusive case as the dimension increases.

Despite the non-Markovian nature of the process, some asymptotic limits have been proposed to characterize the coverage time T_c in the SAW. The derivation of T_c for a one

dimensional lattice is trivial. As stated before, the walker moves constantly in one specific direction. Thus, the number of steps to cover the entire structure is then equal to the lattice size ($T_c = N$).

Again, for two dimensional lattices, obviously the analysis is more complicated. The process is dominated by the search of the last site. However, that final stage depends on the entire previous trajectory and an analytical treatment is far from simple. Through the last site finding analysis it has been conjectured [117] and confirmed numerically [94] that the scaling properties depend on system size as $T_c(N) \sim N \log(N)$. That corresponds to a faster lattice covering if compared to the ordinary RW case. As stated before, $d = 2$ corresponds to the critical dimension of the SAW [113]. For higher dimensions, the scaling is analogous to the RW one.

1.3 The Partial Self-Avoiding Walk

Self-avoidance in general should rely either on the use of complex cognitive memory [118, 119] or the ability of the individual to leave scent cues (e.g. pheromones) to mark regions already visited, something that social insects and similar species have been proved to do [120].

However, the SAW algorithm does not represent a useful representation for self-avoidance in living organisms. In particular, the dead-end (or self-killing, as has been termed in [117]) effect described in the previous section lacks any meaning for biological trajectories.

To take into account these ideas, next, we introduce the concept of **partial** self-avoidance, according to which revisits are unlikely but still possible. To do so, we construct a probabilistic rule for self-avoidance, which which is governed by an energetic landscape $f(E)$ representing the cognitive layer containing the information about sites visited previously. This new scenario, where self-avoidance is partial, penalize the probability of the jumps that revisit a previously visited site. However, and differently from the SAW, this p_i will be different from 0.

As introduced in Section 1.1, the probability to jump from the given site to another site i is defined by p_i. These probabilities will be characterized by the following algorithm. Each site i, at the beginning of the trajectory, has an associated energy E_i. When the walker visits a site i during its path, the value for this site i is modified. Then, the visited nodes energy is different from the non-visited ones and minimization of the energy generates a tendency to move towards lower energy sites.

1.3.1 Maximal Entropy Principle

When introducing and energetic landscape $f(E)$ in the discrete walker's dynamics, one has to define exactly how that landscape modifies the probability to jump to a given site.

To do so, information theory provides a constructive criterion for setting up probability distributions on the basis of partial knowledge. It leads to a type of statistical inference which is called the **Maximum-Entropy Principle** (MEP) [121, 122]. It is the least biased estimate possible on the given information; the one that makes the fewest assumptions about the true distribution of data. In the following, we proceed to provide the origin of that criterion and how it can be adapted to compute the walker's next step probabilities p_i.

First, we introduce the **Shannon's entropy** (equation 1.29). It accounts for the level of uncertainty of a given discrete distribution. The expression corresponds to any general case, being then i the possible states of a given system and p_i their corresponding probabilities. When all p_i are equal, the Shannon's entropy S gets maximal, as it comes from an homogeneous (information-less) probability distribution.

$$S(p) = -\sum_i p_i \ln(p_i). \tag{1.29}$$

From any given distribution p_i, one can estimate an average value for the system for any magnitude. Let's define the estimator f, which depends on the state of the system. Then f_i corresponds to the function f evaluated in the state i. Assuming that

$$\sum_i p_i = 1 \text{ and } \langle f \rangle = \sum_i p_i f_i, \tag{1.30}$$

one can derive the maximal Shannon's entropy that fulfills those constraints by introducing the Lagrangian multipliers μ and λ.

That procedure leads to the equation

$$\frac{\partial S}{\partial p_i} = \frac{\partial}{\partial p_i}\left[-\sum_i p_i \ln p_i + \lambda(1 - \sum_i p_i) + \mu(\langle f \rangle - \sum_i p_i f_i)\right] = 0. \tag{1.31}$$

The solution to this equation reads

$$p_i = \frac{1}{Z(\mu)} \exp\left(-\lambda - \mu f_i\right), \tag{1.32}$$

where $Z(\mu)$ is a normalization factor that reads

$$Z(\mu) = \sum_i \exp\left(-\mu f_i\right). \tag{1.33}$$

The results may be rewritten as

$$\lambda = \ln Z(\mu) \tag{1.34}$$

and the averaged estimator value can be expressed as

$$\langle f \rangle = -\frac{\partial}{\partial \mu} \ln Z(\mu). \tag{1.35}$$

Redefining the estimator f as the energy E, the maximal entropy estimator leads to the Boltzmann factor

$$p_i = \frac{\exp(-\beta E_i)}{Z}, \tag{1.36}$$

where $Z = \sum_i \exp(-\beta E_i)$.

Back to our framework, the sites with lower E_i will have an associated higher probability (the walker tends to go to those sites) when compared with the higher E_i ones. The parameter β, which is known as the effective temperature in physics, modulates how strong the self-avoidance is. When $\beta = 0$, the energetic value of a site becomes irrelevant, and then the walker moves just as in the Random Walk model. When $\beta \to \infty$, when the walker has to choose between a visited and a non visited node, the walker will always move to the non-visited site. The tuning of β goes from a lack of self-avoidance to a perfect self-avoidance (but avoiding dead end situations).

1.3.2 The binary Self-avoiding Random Walk

One particular model for partial self-avoidance is provided by the framework of Self-Attracting Walks [123–125], of which the **binary self-avoiding random walk** (bSAW) represents a particular case.

As the 'binary' term indicates, the energy associated to a given site i can just take two values. The value for all sites is $E_i = 0$ when starting the trajectory. When the walker visits a site i during its trajectory, the value for this site i is switched to $E_i = 1$. Then, the visited nodes energy is equal to 1, and the energy of the non visited ones is equal to 0 (for the Self-Attracting Walks, one just replaces the visited value 1 by -1). The energetic landscape depends on just the first hitting to a given site i, meaning that posterior revisits does not modify energy E_i (see figure 1.8).

The probability to jump to any given site is defined by equation 1.36. In consequence, the walker will jump towards sites with an associated energy $E_i = 0$ more probably than to sites with an associated energy $E_i = 1$. The parameter β modulates how the energies E_i are translated to the probabilities p_i. When $\beta = 0$, the bSAW corresponds to the common RW, where the probability to jump to a given site is $p_i = \frac{1}{n}$, where n is the number of possible sites to jump.

In the following paragraphs, we explore the properties of the bSAW as a function of the parameter β.

To illustrate how the intensity of the self-avoidance impacts the walker's trajectory, we provide in figure 1.9 two paths corresponding to different β values. When $\beta = 0$, the

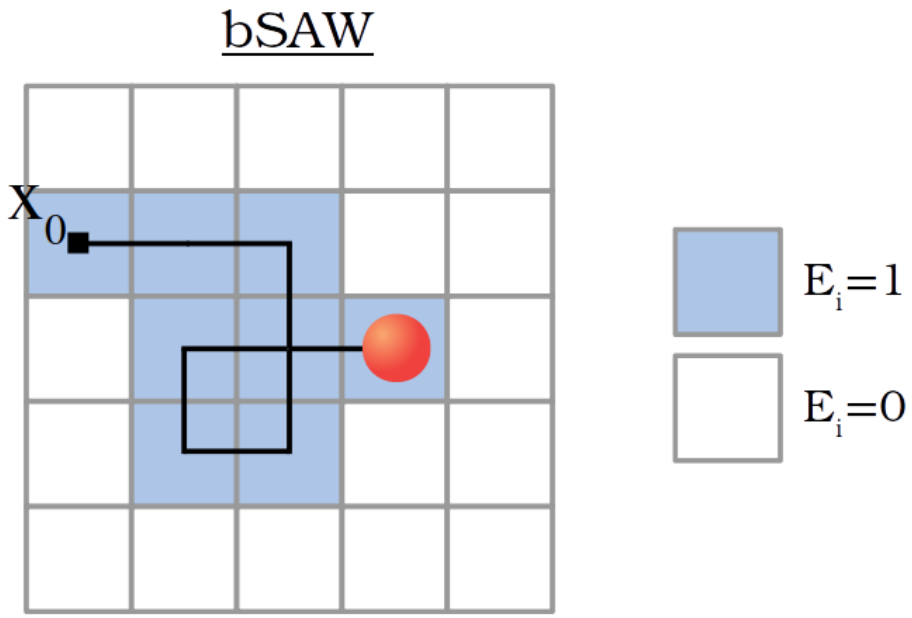

Figure 1.8: *Schematic trajectory and energetic landscape associated for a given walker path for the the bSAW model. he energetic landscape depends on just the first hitting to a given site i, meaning that posterior revisits does not modify energy E_i.*

walker's trajectory does not have any tendency to avoid overlaps. When the value of β becomes larger, the trajectory becomes broader, as overlaps become energetically less favorable. The isotropy preserves that $\langle x(t) \rangle = 0$.

The analysis comes from the study of the MSD and how the binary partial self-avoidance may impact the target dynamics. We illustrate in figure 1.9 the MSD in one and two dimensional lattices for different β values. For the one-dimensional case, one can observe the presence of two regimes for the MSD. Initially, the walker exhibits a ballistic behavior, but it asymptotically tends to a diffusive one (MSD $\sim t^{\frac{1}{2}}$). So the first part of the dynamics replicates the SAW's behavior (ballistic motion), while the asymptotic limit corresponds to a diffusive behavior due to the eventual periods in which the walker gets trapped within regions already visited whose size grows progressively with time. The intensity of the self-avoidance β modifies the size of that initial ballistic region. Note that this parameter can also be understood as the probability to misinterpret the energetic landscape. When β becomes larger (more intensity, less probability to take the "bad" choice), the size of the ballistic region gets increased. That switching between two different motion regimes makes it difficult to develop an analytic treatment to obtain the diffusive coefficient D.

For two dimensional lattices, the initial ballistic region seems to be almost suppressed as the walker has in general multiple paths available to avoid the overlap. So the bSAW seems to exhibit diffusive motion at all times for two or higher dimensions. Also the case where all the sites have been visited leads to a diffusive behavior (homogeneous energy landscape).

Next, we focus on the target dynamics by studying how the intensity β impacts the properties of the general MFPT and the coverage time T_c. The results derived from the

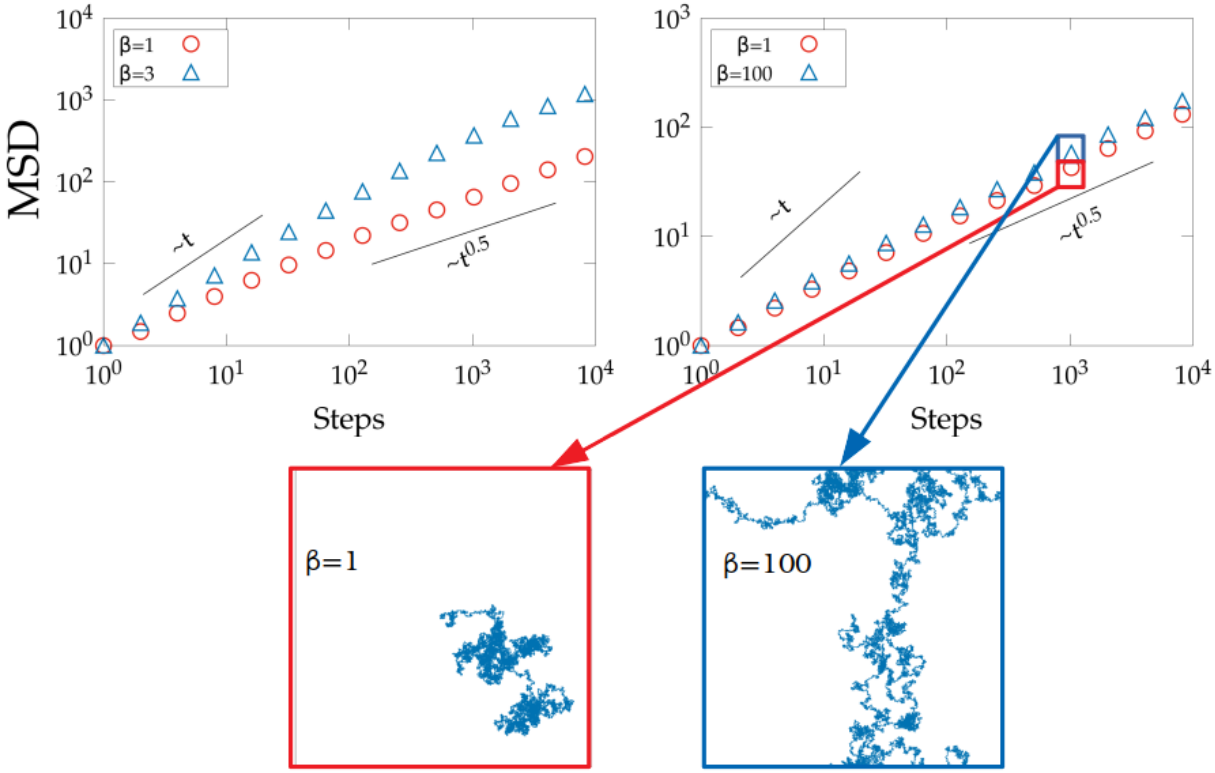

Figure 1.9: *Mean square displacement (MSD) as a function of the simulation time when the walker exhibits a binary self-avoidance. Left panel corresponds to a one dimensional lattice ($d = 1$, $N = 4096$) and the right panel, to a two dimensional lattice ($d = 2$, $N = 256 \times 256$). The insets correspond to a given trajectories of the walker.*

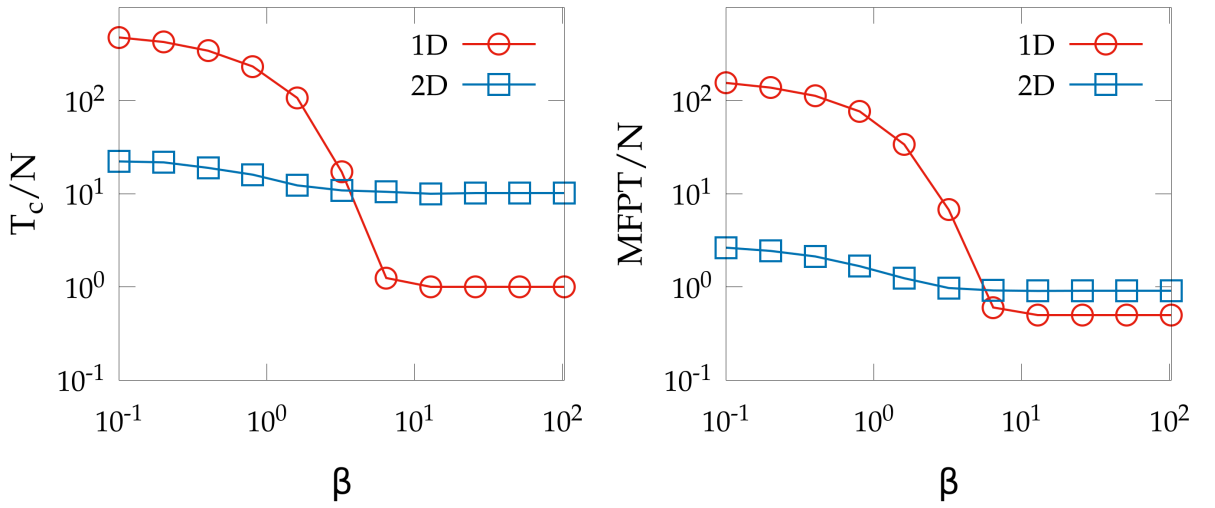

Figure 1.10: *Left: Coverage time T_c of the walker when the parameter β is modified and when the walker exhibits a binary self-avoidance. Right: General mean first passage time MFPT when the parameter β is modified. The space is divided into a* 1024 *and* 64×64 *lattices (for 1D and 2D spaces, correspondingly) with periodic boundary conditions.*

walker trajectories are reported in figure 1.10, being very similar for one and two dimensions. When β is increased, the broader trajectories done by the walker become more efficient when covering the entire space or when reaching a given position. From $\beta \sim 10$ to higher

values, the probability to jump to a visited site when there is another possibility is so small that the results do not get modified. As stated in Section 1.1, the statistics of the coverage is governed by the finding of the **last sites**. In the present model, this is still the case. However, a universal relation between the general MFPT and the coverage time T_c cannot be found as in [95] due to the strong memory effects present in the trajectory.

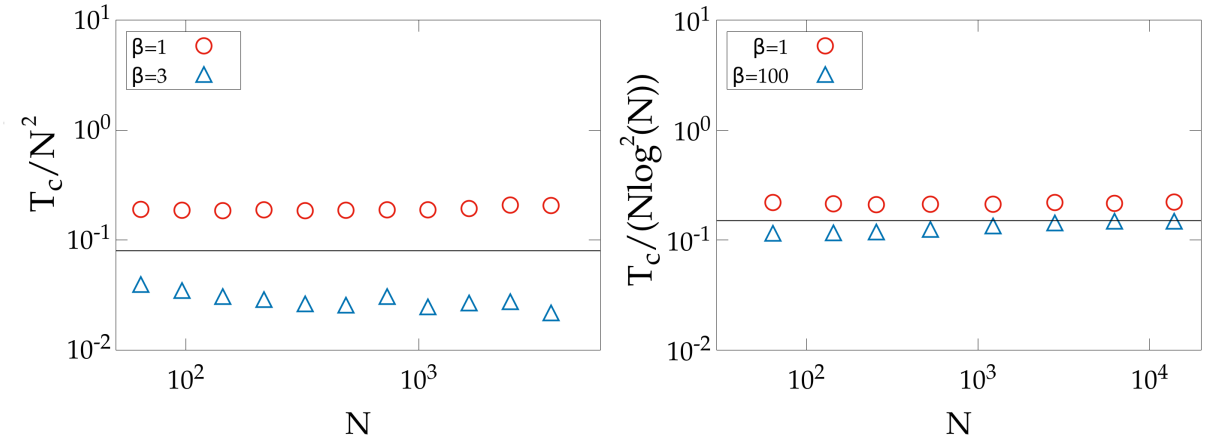

Figure 1.11: *Scaling for the coverage time T_c with the system size N when the walker exhibits a binary self-avoidance. Left panel corresponds to a one dimensional lattice ($d = 1$) and the right panel, to a two dimensional lattice ($d = 2$).*

We analyze how the coverage time T_c scales with the size of the finite lattice in figure 1.11. For a one-dimensional lattice, one can observe that scaling is $T_c \sim N^2$. For a two-dimensional lattice (and higher dimensional lattices), it scales as $T_c \sim N \log^2(N)$. Those results are equivalents to the reported scaling for a common Random Walk in Section 1.1.

1.3.3 The true self-avoiding random walk

The bSAW mechanism is built up from an energy that can just take two different values. However, one can wonder how cumulative effects during the trajectory may affect the walker's behavior. In this direction, a proposal that has attracted large interest is the **true self-avoiding random walk** (tSAW) [117, 126–128]. Here, the energy E_i is considered equal to the number of previous visits of the walker to site i. Then the energy of that site gets increased each time the walker visits this site. Using the idea that such energy landscape was a result of the chemical signal left by the walker as it advances, each revisit corresponds to a new signal deposition (see figure 1.12).

The tSAW model has been applied to describe animal exploration/foraging [129, 130], but also in search algorithms through the Internet [126, 131, 132], among other.

We proceed to analyze the tSAW properties when β becomes modified, as done for the bSAW. Again, the isotropy preserves that $\langle x(t) \rangle = 0$. The behavior of the MSD is presented at figure 1.13. For the one-dimensional case, one can observe that there is again an initial regime where the walker moves in a ballistic manner. However, the asymptotic region does not tend to a diffusive behavior; it tends to a super-diffusive behavior. It seems that the

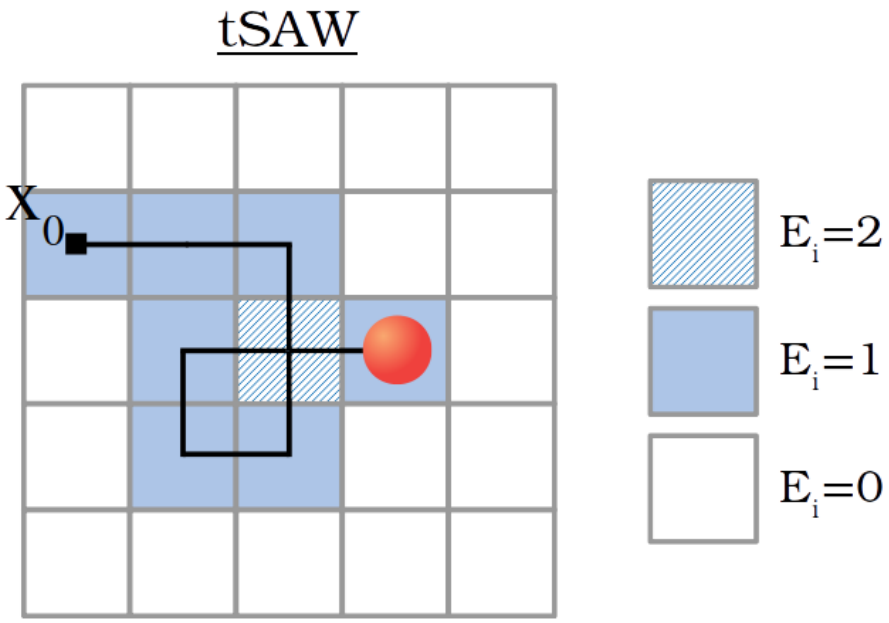

Figure 1.12: *Schematic trajectory and energetic landscape associated for a given walker path for the the tSAW model. The energy E_i is considered equal to the number of previous visits of the walker to the site i.*

ability to distinguish the number of visits enhances the dispersal capacity of the walker, so it now can escape in a reasonably short time from the signal left by its own trajectory.

For two-dimensional lattices, the tSAW exhibits diffusive behavior (figure 1.13). The navigation through higher-dimensional lattices should be asymptotically diffusive too, as the critical dimension of the tSAW is $d = 2$.

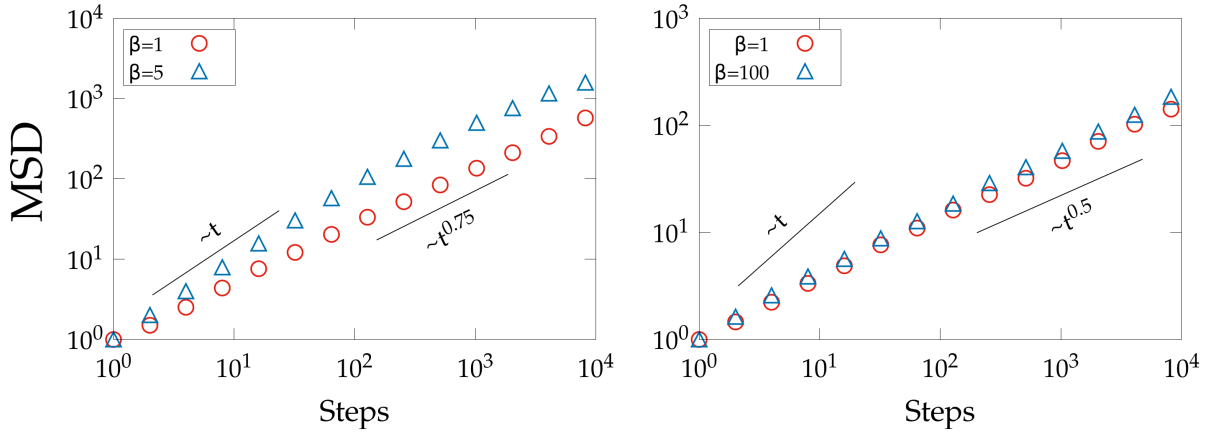

Figure 1.13: *Mean square displacement (MSD) respect of the simulation time when the walker exhibits a true self-avoidance. Left panel corresponds to a one dimensional lattice ($d = 1$, $N = 4096$) and the right panel, to a two dimensional lattice ($d = 2$, $N = 256 \times 256$).*

The analysis of the target dynamics reports very similar qualitative results when compared to the bSAW (see figure 1.14). When the self-avoidance strength β becomes larger, the general MFPT and the coverage time T_c get reduced. However, it seems again (as in the bSAW) that over $\beta \sim 10$, the self-avoidance is so intense that to increase its value does not translate into significant changes in the dynamics. The tSAW seems to cover faster the

lattice as the T_c is lower than the value found in the bSAW case for the same β and lattice size N. The effect comes from the ability to distinguish between the number of previous visits, which must be reckoned then as a helpful mechanism to avoid revisits that could come after the first visit.

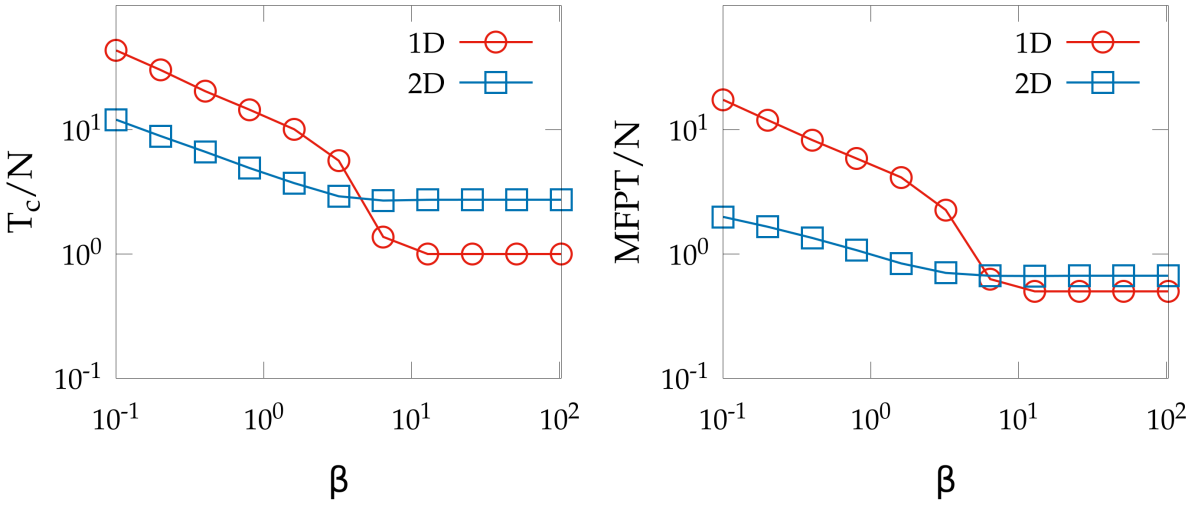

Figure 1.14: *Left: Coverage time T_c of the walker when the parameter β is modified when the walker exhibits a true self-avoidance. Right: General mean first passage time MFPT when the parameter β is modified. The space is divided into a* 1024 *and* 64×64 *lattices (for 1D and 2D spaces, correspondingly) with periodic boundary conditions.*

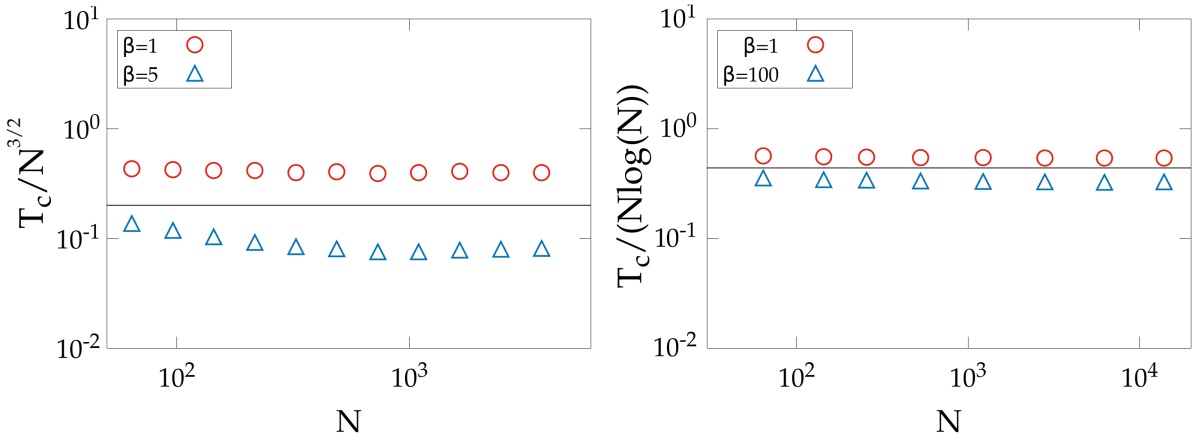

Figure 1.15: *Scaling for the coverage time T_c with the system size N when the walker exhibits a true self-avoidance. Left panel corresponds to a one dimensional lattice ($d = 1$) and the right panel, to a two dimensional lattice ($d = 2$).*

Next, we analyze the scaling of the coverage time T_c as the system size gets increased (figure 1.15). For a one-dimensional lattice, the coverage time scales as $T_c \sim N^{\frac{3}{2}}$. This scaling is in between those of the RW (or bSAW) case and the SAW case. For a two dimensional lattice, the coverage time scales as $T_c \sim N \log(N)$, which is equivalent to that reported for the SAW [94]. From that, one derives that a walker following the tSAW framework will cover faster a lattice if compared to a walker following the bSAW framework. This effect is increased as the lattice size becomes larger. For higher dimensions, as in the SAW model or in the ordinary RW, the coverage time scales as $T_c \sim N \log^2(N)$ for both models, and so differences there become largely reduced.

In summary, the dynamics of a walker that stores the number of visits (tSAW) instead of an all or nothing rule (bSAW) provides results that are closer to the SAW model. Its own nature favors the jumps to less visited regions, as the non-bounded E_i always permits to detect those differences. According to those features, one would certainly expect that its covering properties are similar to the SAW ones. In contrast, a large part the bSAW coverage is invested to move diffusively across an homogeneous landscape of visited sites. This is the reason why its properties are similar to the RW ones.

1.4 Impaired cognitive abilities

Cognitive processing of the contextual information is in general subject to fluctuations and errors. For example, many animal species are expected to recall roughly the regions already visited though they cannot retain particular details about all locations [133]. Chemical (as well as other internal/external) signals, on its side, are subject to physical or physiological processes that can reduce their effectiveness as a cue for driving the organism trajectory. For instance, chemicals can diffuse or evaporate, so the memory effect they generate will vanish progressively. As a whole, the physical or mental processes responsible for the self-avoiding mechanism are prone to become impaired with time. Continuing with the stochastic description we have used during the previous Sections, we incorporate into the partial self-avoidance a new level of detail in the **cognitive layer**, which corresponds to a **finite retaining memory** (or signal evaporation, depending of the example).

In this Section we explore how the impairment of a self-avoiding walker modify its movement patterns and, consequently, its efficiency during the search process.

The impairment will be described now as follows. The walker will forget (or miss-assign) part of its previous visits to some sites, using then an energy landscape during its movement that does not record and/or retain perfectly the trajectory information. Instead, when the walker arrives into a given site i, it stores the information only for a random time τ.

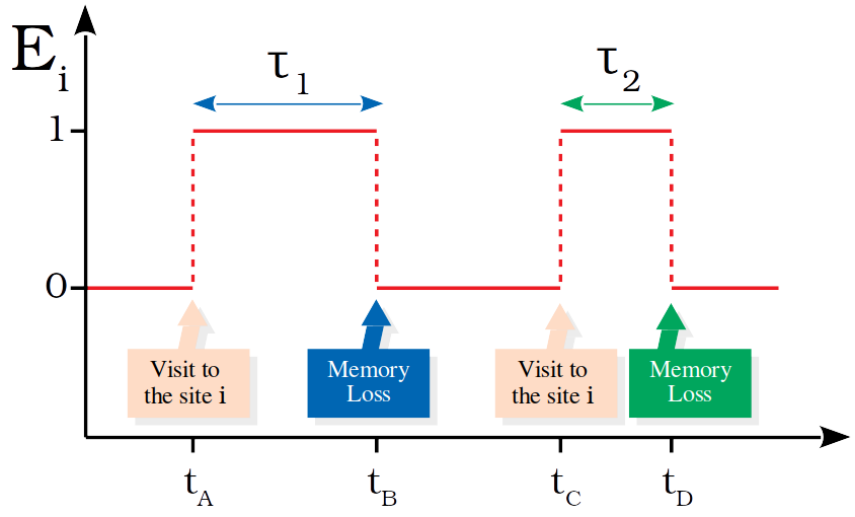

Figure 1.16: *Visual guide for the impairment process in the case of a bSAW model. After the walker first visit to the site i (corresponding to a time t_A), the cognitive map stores the information $E_i = 1$ during a span τ_1, obtained from $\rho(\tau)$. Then, the site i information is rewritten again as $E_i = 0$ at time $t_B = t_A + \tau_1$, the energy assigned to non-visited sites. A second process is also exemplified with a given different τ_2, visiting the site i at t_C and forgetting the information at $t_D = t_C + \tau_2$.*

In order to capture the properties of the random memory time, a characteristic memory/evaporation timescale τ_m is introduced, with $\rho(\tau)$ representing the probability distribution of that variable. For the sake of simplicity, here we use the exponential distribution $\rho(\tau) = \tau_m^{-1} e^{\tau/\tau_m}$. When $\tau_m = 0$, the walker is not able to store any information, as it forgets its previous trajectory instantaneously. Then, the walker understands each step as if it was in a totally unexplored region. Its movement becomes then equivalent to a ordinary Random Walk. When $\tau_m \to \infty$, the walker stores the information of the entire trajectory without any limitation. In that case, we recover the partial self-avoidance models presented in Section 1.3. For the sake of completeness, we have explored (not shown) that that a fixed $\tau = \tau_m$ would provide equivalent results to those obtained by choosing τ from the exponential distribution.

The cognitive map is defined as the information that is being stored by the walker. To facilitate the understanding of the cognitive map compared to the real information, we provide two visual graphs for the bSAW case. The figure 1.16 corresponds to the evolution of the energy values E_i associated to a given site i along the search process (so the evolution of the information of a given site i). In figure 1.17 one can compare the previous trajectory with the current cognitive map. As the memory time τ_m gets increased, the cognitive map gets closer and closer to the total trajectory information.

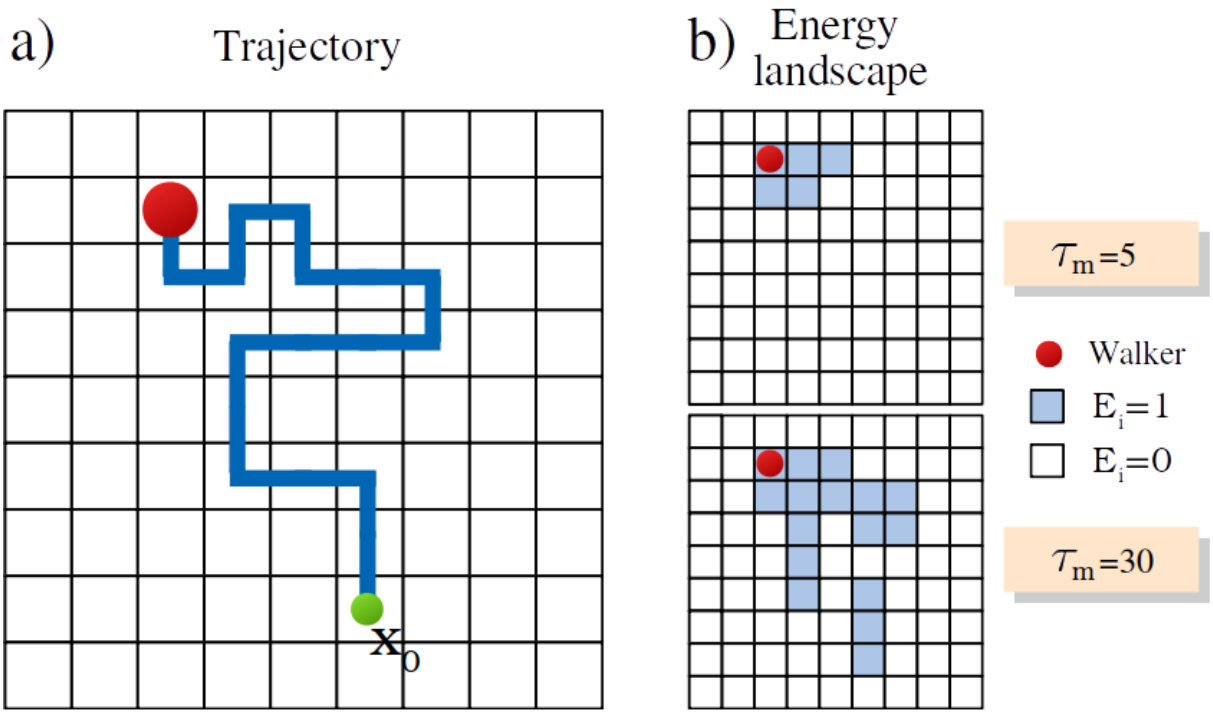

Figure 1.17: *a) The trajectory of a walker during a span of* 17 *time steps. The blue line is drawn to mark the sites that have been visited during the process. b) Energy landscapes (or cognitive maps) that store the information about the previous trajectories. Two memory times* τ_m *are shown.*

1.4.1 Impairment in the bSAW

As stated previously, self-avoiding dynamics leads the walker to promote movement in the current direction as a way to 'escape' from the regions that are left behind. However, further revisits to those regions are now possible, as the information of the cognitive map would probably be forgotten. That procedure reminds that of the Persistent Random Walk model (PRW) (see Section 1.1.3). One can expect a similar behavior for the impaired bSAW, and then one expects similar results in their properties. In agreement with that intuition, an initial

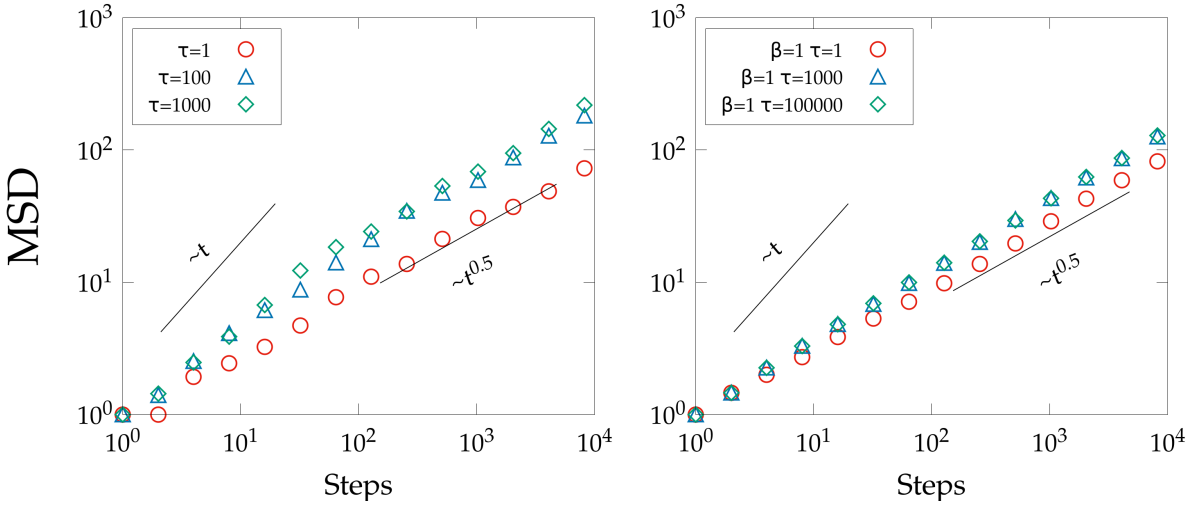

Figure 1.18: *Mean square displacement of the walker when the parameters β and τ are modified. The space is divided into a* 1024 *and* 64×64 *lattices (for 1D and 2D spaces, correspondingly) with periodic boundary conditions. The self-avoidance is introduced according to the binary model.*

ballistic region is observed when the MSD is plotted (figure 1.18), followed by an asymptotic diffusive region. Furthermore, the mean square displacement exhibits differences when τ_m is tuned. For larger memory times τ_m, the asymptotic diffusion coefficient D seems to be increased. As the cognitive map stores a larger part of the trajectory, the movement strategy gets closer to total self-avoidance, where the path avoids the overlap.

We focus now on how the retaining time τ_m modifies the target dynamics. The self-avoidance intensity is encoded in the parameter β (eq. 1.36), so the parameter space to be explored is given by all the possible combinations of τ_m and β. In the figure 1.19 we present a detailed exploration of the results as a function of β for a few memory times τ_m, and one can observe how the T_c and the general $MFPT$ qualitatively present the same behavior when β is tuned independently of τ_m (the stronger the self-avoidance mechanism is, the more efficient the search process becomes).

To fully characterize the parameters space, however, we provide in figure 1.20 a more detailed analysis of the effect of τ_m over T_c. Counterintuitively, this detailed study shows us that the relation between the retaining cognitive capacity and the search performance is far from trivial. Using a broad range of τ_m values shows us the existence of an **optimal** τ_m that minimizes the coverage time T_c. In addition, this feature seems to be robust as it appears for different self-avoidance intensities.

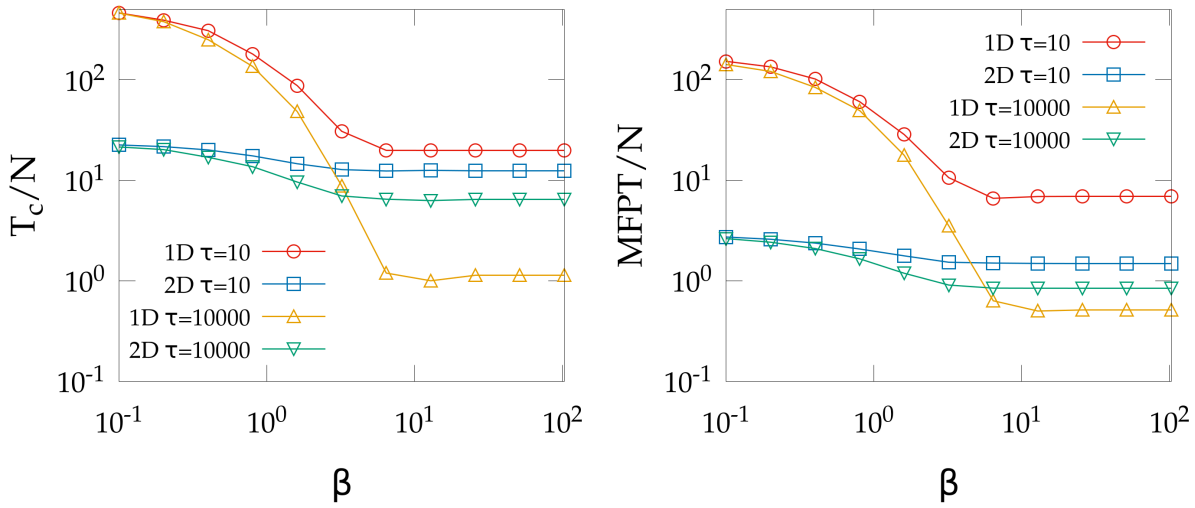

Figure 1.19: *Left: Coverage time T_c of the walker when the parameter β is modified. Different memory times τ_m are provided. Right: General mean first passage time MFPT when the parameter β is modified. The space is divided into a* 1024 *and* 64×64 *lattices (for 1D and 2D spaces, correspondingly) with periodic boundary conditions. The self-avoidance is introduced according to the bSAW.*

We explore in the following why to store just part of the path in the cognitive map could even be helpful and not detrimental for a more efficient coverage. Consider the case in which the cognitive map stores the entire trajectory ($\tau_m \to \infty$). In this scenario, one can divide the coverage process approximately into two phases. When the process starts, the walker performs a standard self-avoiding walk, where it avoids the immediately previous sites. That procedure is maintained until the walker lacks locally new sites to be visited. At this stage, the cognitive map is practically homogeneous, as the energy associated to the majority of sites is $E_i = 1$. When the walker faces situations like these where the energies of the available sites are identical, the next movement is chosen at random with the same probability between all the options. According to this, the movement generated by this cognitive map (despite it encodes the self-avoidance) produces a classical (diffusive) random walk dynamics. To find the last unvisited sites reduces then to a diffusive search through that homogeneous cognitive landscape. As stated in Section 1.1, the statistics of the coverage is largely governed by the process of finding of the last sites available in the lattice. In consequence, the final diffusive search for the remaining sites in the lattice will increase considerably the cover time T_c.

To understand why a finite τ_m can reduce the search time if compared to the $\tau_m \to \infty$ case, let's focus on the case where the information of the cognitive map could be partially forgotten. When the walkers forget part of their information, the cognitive map stores part of the visited nodes with an assigned energy $E_i = 0$ (miss-assignment). As a result, even when there are just a few sites to visit to complete the coverage process, the walker is always moving through a combination of seemingly explored and unexplored regions, and not through a homogeneous landscape. The possibility to move towards **seemingly unvisited** regions generates less recurrent trajectories (it is, a higher diffusion coefficient D), so enhancing the area explored and making search more efficient. We provide a visual guide of how those seemingly unvisited regions, that we could call **mirages**, can optimize

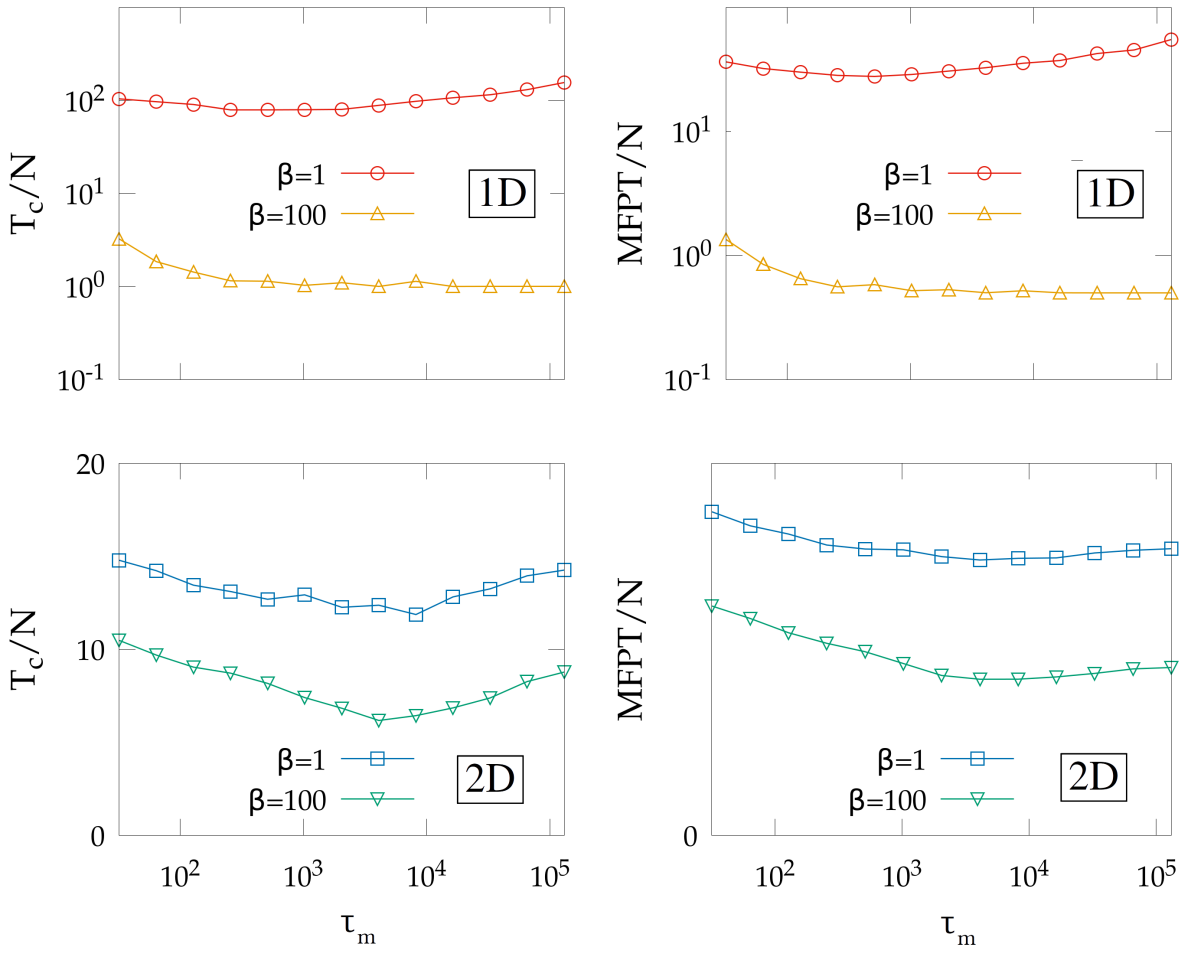

Figure 1.20: *Left: Coverage time T_c of the walker when the memory time τ_m is modified. Different values of the parameter β are provided. Right: General mean first passage time MFPT when the memory time τ_m is modified. The space is divided into a* 1024 *and* 64×64 *lattices (for 1D and 2D spaces, correspondingly) with periodic boundary conditions. The self-avoidance is introduced according to the binary model.*

the coverage in figure 1.21.

In short, this is the reason why to forget part of the previous path may become helpful. For the sake of completeness, we provide at figure 1.22 how the cognitive map changes with τ_m when the search process is in the final step. In a given search process, the white regions correspond to seemingly unexplored regions (or mirages), while the real trajectory has visited all sites but one.

1.4.2 Impairment in the tSAW

In the tSAW scenario, the energy site E_i corresponds to the previous number of visits to the site. Then, to obtain a homogeneous energetic landscape is almost impossible. Still, one can wonder if it is still possible in this situation to observe the presence of an optimal finite τ_m, as occurs for the bSAW.

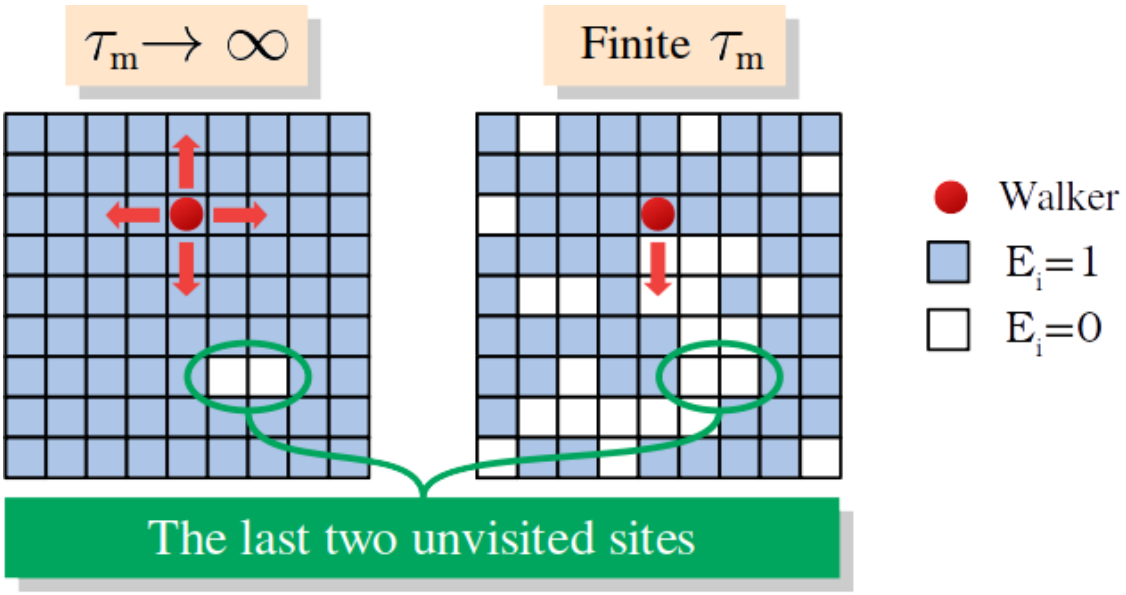

Figure 1.21: *Comparison between the cognitive maps generated by $\tau_m \rightarrow \infty$ and a finite τ_m when lacks just two sites to complete the coverage for the bSAW model. One can observe how the walker (red circle) will tend stochastically to move faster towards the unvisited region when the memory is finite, while for the other case the navigation will be diffusive with a lower D. That feature, called the mirage effect, helps the walker to reach faster the last targets when the retaining memory is finite.*

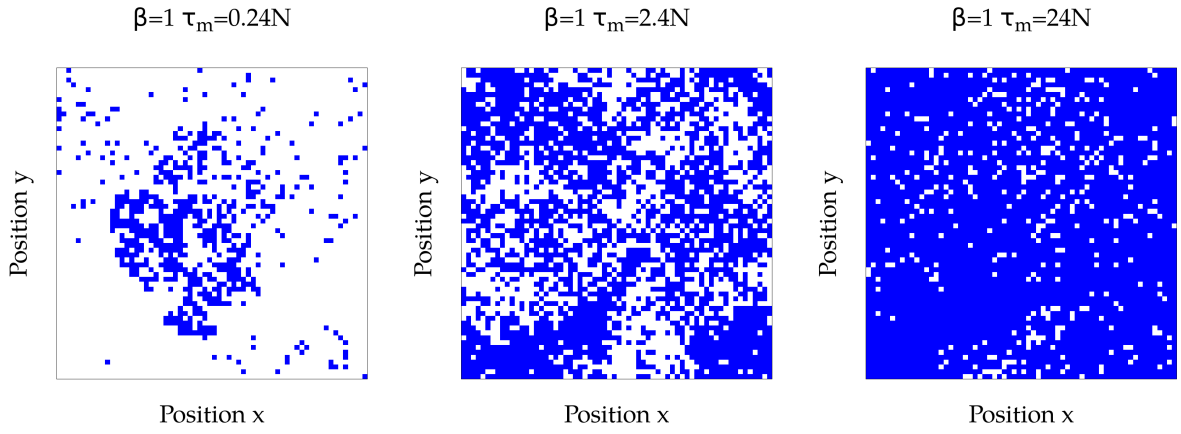

Figure 1.22: *The cognitive map of the walker when the coverage process is finished for the case of i) $\tau_m = 10^3$, ii) $\tau_m = 10^4$ and iii) $\tau_m = 10^5$. The space is divided into a 64×64 lattice. The white color corresponds to the sites considered as unvisited in the cognitive map, while the blue sites, to the considered as visited. The self-avoidance is introduced according to the binary model.*

In figure 1.23 one can see how the effect of β on T_c is very similar to what we have reported for the bSAW. To increase the self-avoidance intensity makes the coverage time decrease until the behavior saturates.

However, when exploring the τ_m space, it is found that the **mirage** effect no longer appears in this scenario (figure 1.24). One sees instead that the minimum T_c corresponds here to an infinite retaining capacity $\tau_m \rightarrow \infty$. As the cognitive map here is intrinsically heterogeneous, to forget part of the information does not destroy any homogeneity, and it is

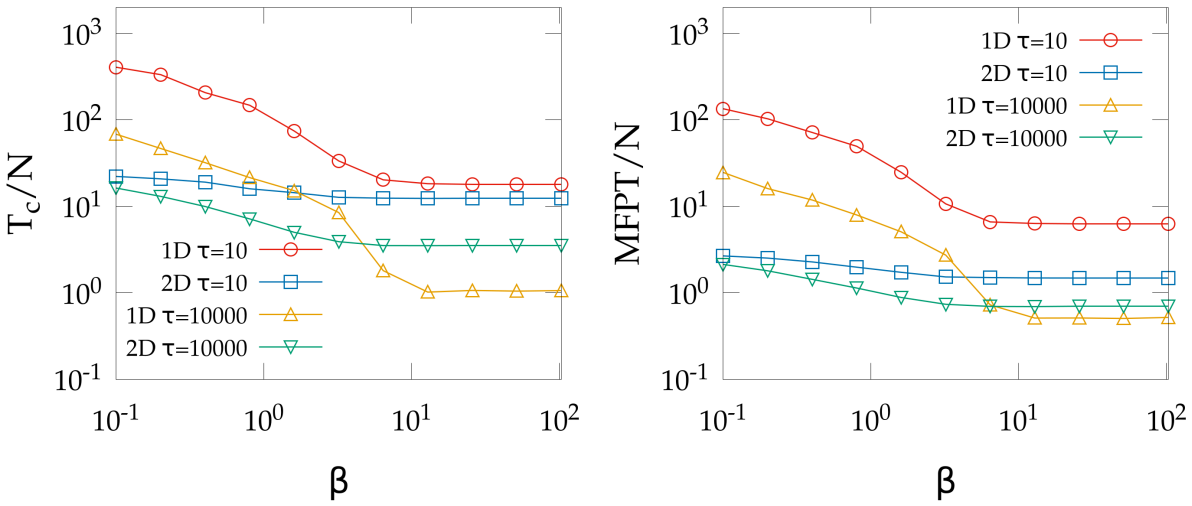

Figure 1.23: *Left: Coverage time T_c of the walker when the parameter β is modified. Different memory times τ_m are provided. Right: General mean first passage time MFPT when the parameter β is modified. The space is divided into a* 1024 *and* 64×64 *lattices (for 1D and 2D spaces, correspondingly) with periodic boundary conditions. The self-avoidance is introduced according to the tSAW model.*

always detrimental. The persistence is maintained even for **infinite retaining times** τ_m.

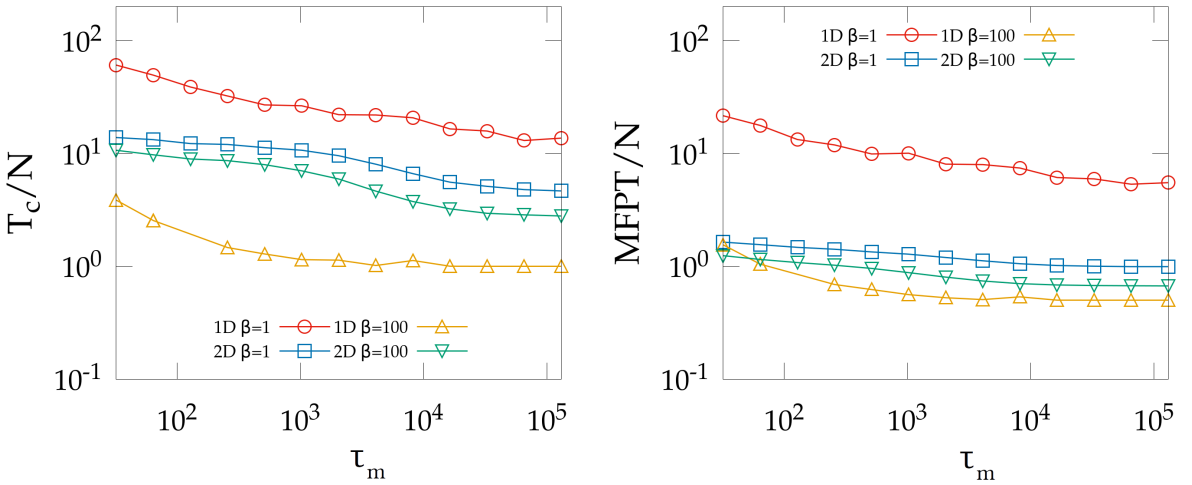

Figure 1.24: *Left: Coverage time T_c of the walker when the memory time τ_m is modified. Different values of the parameter β are provided. Right: General mean first passage time MFPT when the memory time τ_m is modified. The space is divided into a* 1024 *and* 64×64 *lattices (for 1D and 2D spaces, correspondingly) with periodic boundary conditions. The self-avoidance is introduced according to the tSAW model.*

1.5 Prospection or the ability to sample the future

While random-walk mechanisms explored up to now could be possibly implemented by primitive organisms able to leave a chemical signal across their trajectories, complex species, such as mammals, are recognized for their ability to process the contextual information at a

deep level and respond according to that processing. For deep level, we mean the capacity to evaluate the different options that are available and planning a response according to this, so breaking the classical stimulus-response paradigm which is prevalent in behavioral biology. For this, some organisms can evaluate the potential consequences of their choices into the future, computing mentally how the scenario will dynamically evolve if one option is chosen. This mechanism where the complex organisms evaluate the advantages and disadvantages of the different options by mixing sensory information and a projection of the situation into the future is called **prospection**. It involves gathering the relevant information from the scenario and projecting it into the future to evaluate its consequences.

Living organisms are constantly facing moments where the optimal answer to the given situation involves prospection. Animal foraging represents a significant example: an ideal performance should take into account (not just locally, but at a more global level) whether the organism has explored the region before or if one direction is better than other according to a given context. The idea of prospection has been extensively studied in cognition sciences [134–136]. In pedestrian dynamics, for instance, it has been observed that we avoid people by computing the time-to-collision and consequently choosing a new direction of motion that avoids such collision [137, 138]. More generally, it has been revealed that our ability to gather fundamental information impacts the efficiency of our decisions [139, 140]. Prospection does not only appear in human individuals, but also in animals [141, 142]. It has been reported that rodents can predict immediate future behavior during navigation [143] or that chimpanzees and orangutans override immediate drives in favor of future needs [144, 145].

1.5.1 Causal entropic forces

To include prospection in the physical framework, one has to include such mental projections into the future within the definition of the energetic landscape $f(E)$. One recent input in that direction is the framework provided by Wissner-Gross and Freer: the **Causal Entropic Forces** (CEF) [146]. In there, the authors develop a physical scheme to promote intelligent or adapted behavior emerging from a forecast of the future scenarios. Its fundamentals come from the notion of entropic forces. Entropic forces are commonly defined as those forces that drive the system towards its maximal entropy states [147, 148].

The classical physical framework constructs the forces to emerge from energetic gradients, as the systems tends naturally to minimal energy states. However, using common ideas from statistical mechanics we know that the Hemholtz free energy $E = U - TS$ involves two contributions: the internal energy U and the entropic term TS related to the microscopic disorder (where T corresponds to the temperature). Then, the entropic force is effectively defined as the one deriving from the gradient of the entropic term $F = T\nabla S$, making the system evolve towards maximal entropic configurations.

The novelty of the CEF framework comes from the statement that conscious or intelligent behavior derives from the evaluation of the entropy built over the possible future paths

available. The prospection is so included through the sampling of those future possible paths.

One can wonder if CEF breaks causality. As the force F emerges from a stochastic sampling of possible paths, the evaluated entropy is purely local in time, keeping causality unbroken. In general, the common definition for an entropic force F associated with a generic

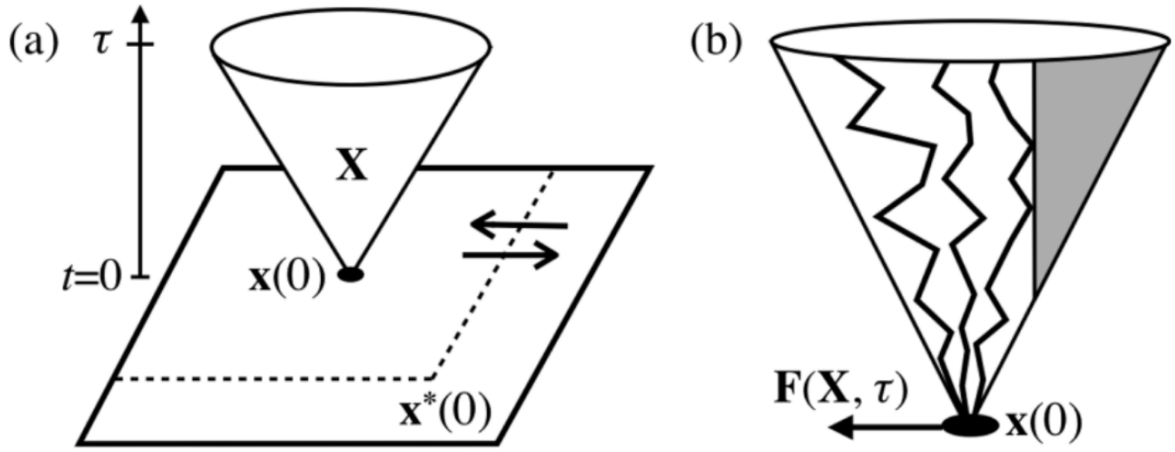

Figure 1.25: *Schematic depiction of a causal entropic force. (a) A causal macrostate X with horizon time τ, consisting of path microstates $x(t)$ (future possible paths) that share a common initial system state $x(0)$,in an open thermodynamic system with initial environment state $x^*(0)$. (b) Path microstates x belonging to a causal macrostate X,in which (for illustrative purposes) there is an environmentallyimposed excluded path-space volume that breaks translational symmetry, resulting in a causal entropic force F directed awayfrom the excluded volume. The image is taken from [146].*

macrostate partition, $\{X\}$, is given by

$$F(X_0) = T\nabla_X S(X)|_{X_0} \tag{1.37}$$

where T is a proportionality constant, $S(X)$ is the entropy associated with the macrostate X, X_0 is the current macrostate and ∇_X is the gradient in the X space.

Following the ideas provided in [149–151], Wissner-Gross and Freer generalize the idea of entropy force to a computation between the present and a future time horizon. More formally, they treat the phase-space paths taken by the system $x(t)$ over the time interval $0 \leq t \leq \tau$ as microstates and partition them into macrostates $\{X\}$. Two different microstates, or paths, $x_1(t)$ and $x_2(t)$ should start as the same state $x_1(0) = x_2(0)$, thereby identifying every macrostate X with a unique present system state $x(0)$, as schematically illustrated in figure 1.25. The CEF comes then from the sampling of possible paths starting from the current state $x(0)$ during the time horizon τ. The corresponding causal entropic force F can then be expressed as

$$F(X_0, \tau) = T_p \nabla_X S_p(X, \tau)|_{X_0} \tag{1.38}$$

where T_p is a proportionality constant that parametrizes the intensity of the system bias toward macrostates that maximize causal entropy. More concretely, T_p can be interpreted as

parametrizing the rate at which paths in a hypothetical dynamical ensemble of all possible fixed-duration paths transition into each other, in analogy to the transitions between configurational microstates of a classical physical system.

In their article, Wissner-Gross and Freer designed different "cognitive based" mechanical systems to validate the adaptive behavior of the CEF framework. They successfully proved that CEF can be used as a control mechanism to solve basical mechanical problems, such forcing a particle to a center of a box or solving a puzzle with isolated tools.

1.5.2 Prospection in the partial self-avoiding models

The CEF framework provides a beautiful mathematical framework to explore the idea of prospection as the ability to evaluate future options. When the self-avoidance and the impairment where studied in the partial SAW models (Sections 1.3 and 1.4), the walker's movement patterns were exclusively based on local sensory information and the external/cognitive limitations (retaining memory). However, if one intends to include the prospection as a general trait of the intelligent behavior of some organisms, it is necessary to consider the ability to introduce the **non-local information** to compute the different probabilities p_i driving the movement rules.

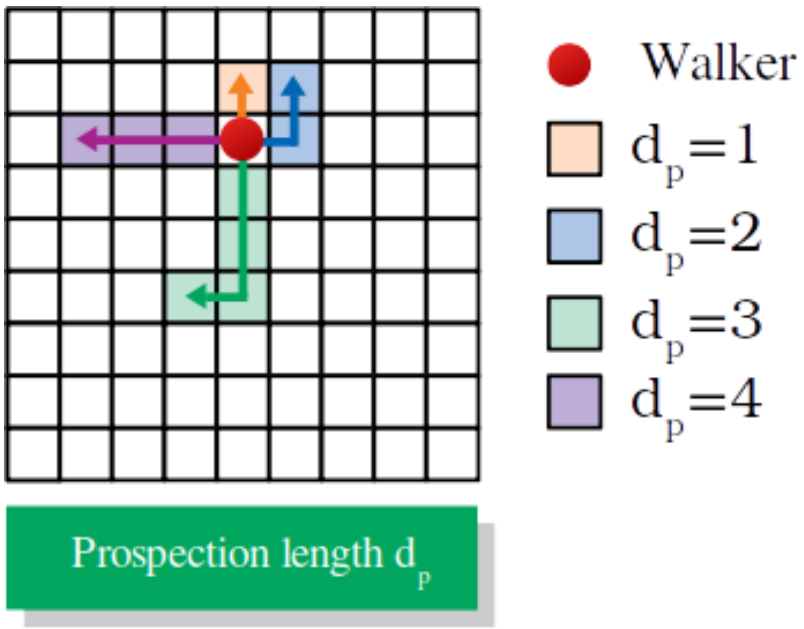

Figure 1.26: *Prospected/sampled paths with different d_p. The current position corresponds to the red circle. The color code corresponds to the paths virtually sampled when doing the prospection. The energy E associated to those paths corresponds to the average of E_i for all the sites i visited during the path.*

To incorporate this cognitive ability, we propose a mechanism inspired on the mathematical formulation of CEF. The walker will have the ability to sample (or forecast) future paths from the current position and incorporate the information of those paths to define the probabilities p_i (eq. 1.36). From a computational perspective, the sampling mechanism is described as follows. The walker samples all the possible paths of length d_p starting from the current position. The case of $d_p = 1$ will provide analogous results to Sections 1.3 and 1.4, in which the walker just uses the information of first-neighbour sites to build its

cognitive map. In figure 1.26, one can see from a visual scheme the meaning of the future d_p paths. Instead of using the information from first neighbors to assign the energy E_i to the neighbour site i, the walker now uses the information corresponding to those possible paths starting from that site i. The energy E_i corresponds to the average over all those possible paths, where the energy associated to each path is at the same time the average energy over the sites that it would visit.

One can observe that we have adapted the entropic formulation of the CEF to an energetic formulation. This has been done to keep the energetic criterion used in the previous Sections, based on the $f(E)$ framework.

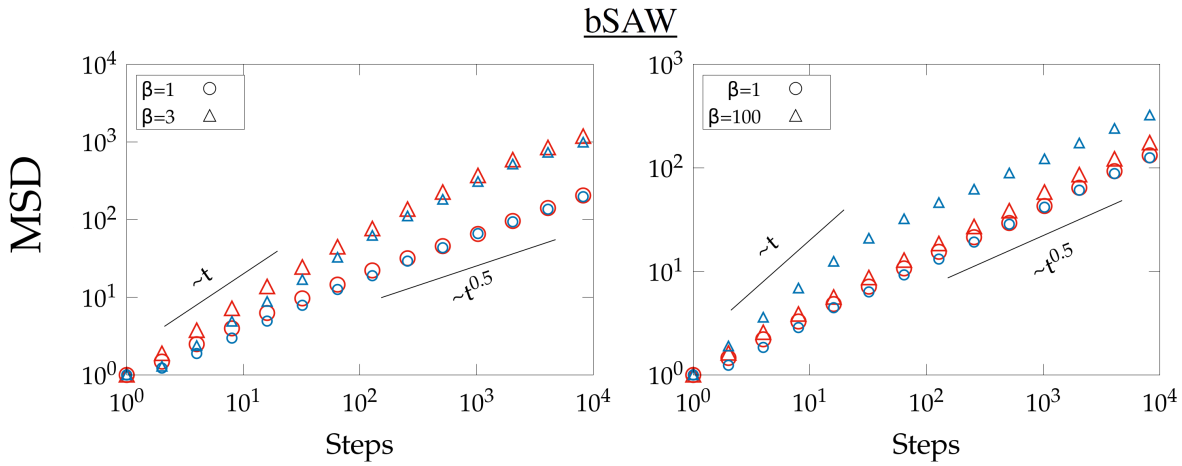

Figure 1.27: *Mean square displacement (MSD) respect of the simulation time when the cognitive map corresponds to the bSAW model. Left panel corresponds to a one dimensional lattice ($d = 1$, $N = 4096$) and the right panel, to a two dimensional lattice ($d = 2$, $N = 256 \times 256$). Red color corresponds to $d_p = 1$ and blue color, to $d_p = 5$.*

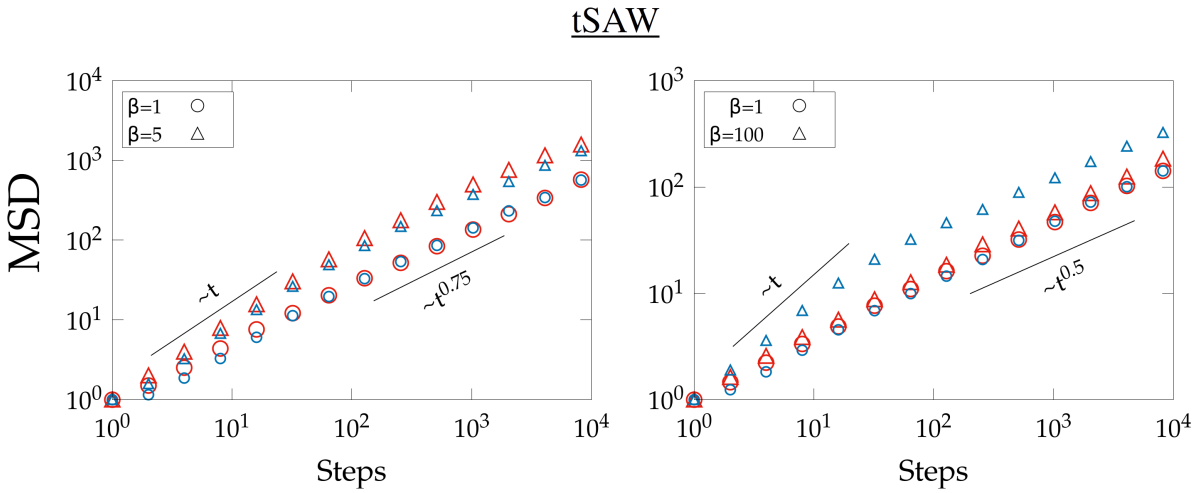

Figure 1.28: *Mean square displacement (MSD) respect of the simulation time when the cognitive map corresponds to the tSAW model. Left panel corresponds to a one dimensional lattice ($d = 1$, $N = 4096$) and the right panel, to a two dimensional lattice ($d = 2$, $N = 256 \times 256$). Red color corresponds to $d_p = 1$ and blue color, to $d_p = 5$.*

The introduction of a prospection length d_p has an impact over the evolution of the MSD (see figure 1.27 for the bSAW and figure 1.28 for the tSAW). One can observe in the left panel of both figures how the prospection length does not modify qualitatively the behavior of

one-dimensional walkers. However, the right panels show that the two dimensional case is different. The asymptotic walker's behavior is diffusive, and the prospection length d_p modifies significantly the diffusion coefficient D. The ability to prospect could promote persistent motion as the walker may detect the unexplored regions from larger distances. Apart from that, when self-avoidance is strong, the walker exhibits again an initial ballistic behavior, as found for the partial self-avoidance without prospection.

1.5.2.1 Target dynamics

We focus now on how the prospection ability modifies the efficient search strategy as a function of the prospection length d_p.

First, we study how the coverage time T_c depends on the prospection ability of the walker. One can observe in figure 1.29 that the one-dimensional and two-dimensional dynamics are here completely different. For the one-dimensional case, the prospection does not apparently affect the walker's performance (in agreement with the MSD results of figures 1.27 and 1.28). However, the results for 2d show a crossover (marked in the figure with a vertical line) in the efficiency of the search process between prospecting for further information ($d_p = 5$) or just for nearby information ($d_p = 1$) in two dimensional spaces.

Both mechanisms (the bSAW and the tSAW) provide similar results. In the computation of the probabilities associated to each option, the effective temperature β weights the information of the cognitive map. When the β value is low, the energetic differences between the sites in the cognitive map result in similar probabilities; actually, in the extreme case $\beta = 0$ all probabilities p_i are the same. As the prospection length is increased, many more paths are available for sampling, and by the Central Limit Theorem the corresponding energies of those paths tend to be centered around a mean value while avoiding extreme values, so the distribution of path energies becomes more peaked. As a result, the mean values associated to each option become more similar as d_p grows (the possible paths will become more similar even though the initial direction was different). In consequence, a low value of β will be ineffective in order to discriminate between better or worse choices, so increasing the probability of the walker to choose a suboptimal site. When β takes a higher value, instead, small energy differences still transform into significant probability differences. In that case the walker, roughly speaking, processes more accurately the gathered information. Thus, a longer prospection length d_p can provide significant information, and so it improves the coverage efficiency.

This suggests the importance of exploring in detail the parameter space given by β, τ_m and d_p. In figure 1.30, one can observe very clearly how the most efficient prospection strategy depends on β. For $\beta = 1$, the prospection length that optimizes the search process is $d_p = 1$. As d_p becomes larger, the coverage process becomes less and less efficient. The feature is present both for the bSAW and the tSAW cognitive maps.

The opposite occurs when $\beta = 100$. In that case, the larger the prospection length d_p is, the more effective the coverage process. There is monotonous relation between d_p and T_c. An optimal τ_m is still found for the bSAW case (the 'mirage' effect), though the existence of

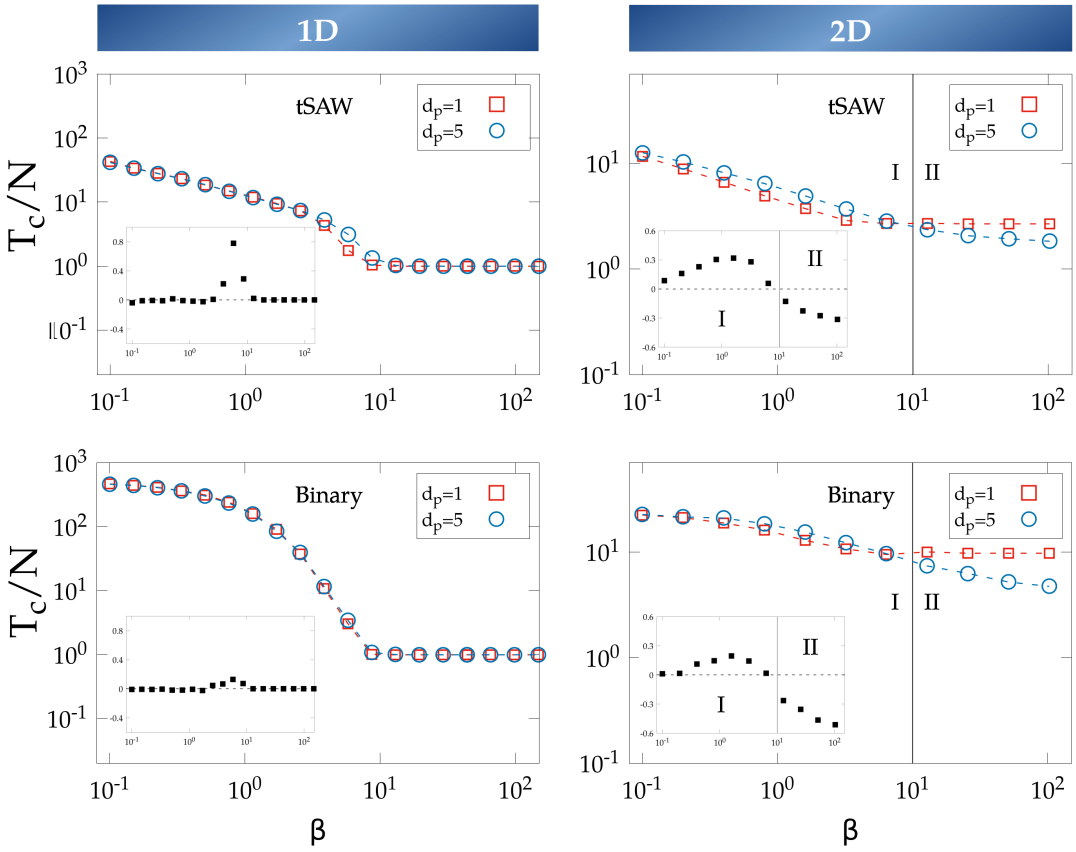

Figure 1.29: *Coverage time T_c according to the effective temperature β. The left panel corresponds to a one dimensional $N = 1024$ lattice while the right panel, to a $N = 64 \times 64$ two dimensional lattice. Red color corresponds to $d_p = 1$ and blue color, to $d_p = 5$. The inset is included to provide a visual guidance of the relative efficiency between $d_p = 1$ and $d_p = 5$.The y-axis of the inset corresponds to the magnitude $\alpha = (T_c^{d_p=5} - T_c^{d_p=1})/T_c^{d_p=1}$. The x-axis corresponds to β. We define the region I as the region where $\alpha > 0$, when the non-prospecting strategy ($d_p = 1$) is more efficient. We define the region II as the region where $\alpha < 0$, when the prospecting strategy ($d_p = 5$) is more efficient.*

such optimum seems to be less noticeable as long as d_p increases. The reason for this is that the ability to detect unvisited sites from larger distances reduces (but does not completely eliminate) the effect of the final diffusive phase emerging when only a few unvisited sites remain.

Finally, we study how the coverage time T_c scales with the system size of the space to explore. One can observe in figures 1.31 and 1.32 that the scaling reported in Section 1.3 is maintained despite modifying the prospection length d_p.

1.5.2.2 Variable prospection length

Real prospection strategies might vary between individuals. For example, different organisms of the same specie may not have equal cognivite capacities [152]. Even those capacities may evolve during the life of the individual [153, 154]. Even so, one can also consider that the cognitive effort putted by an individual may be variable during its performance in a given task. This, together with the intrinsic difficulty of gathering information from real environments leads to consider that a random and variable length d_p can be more realistic

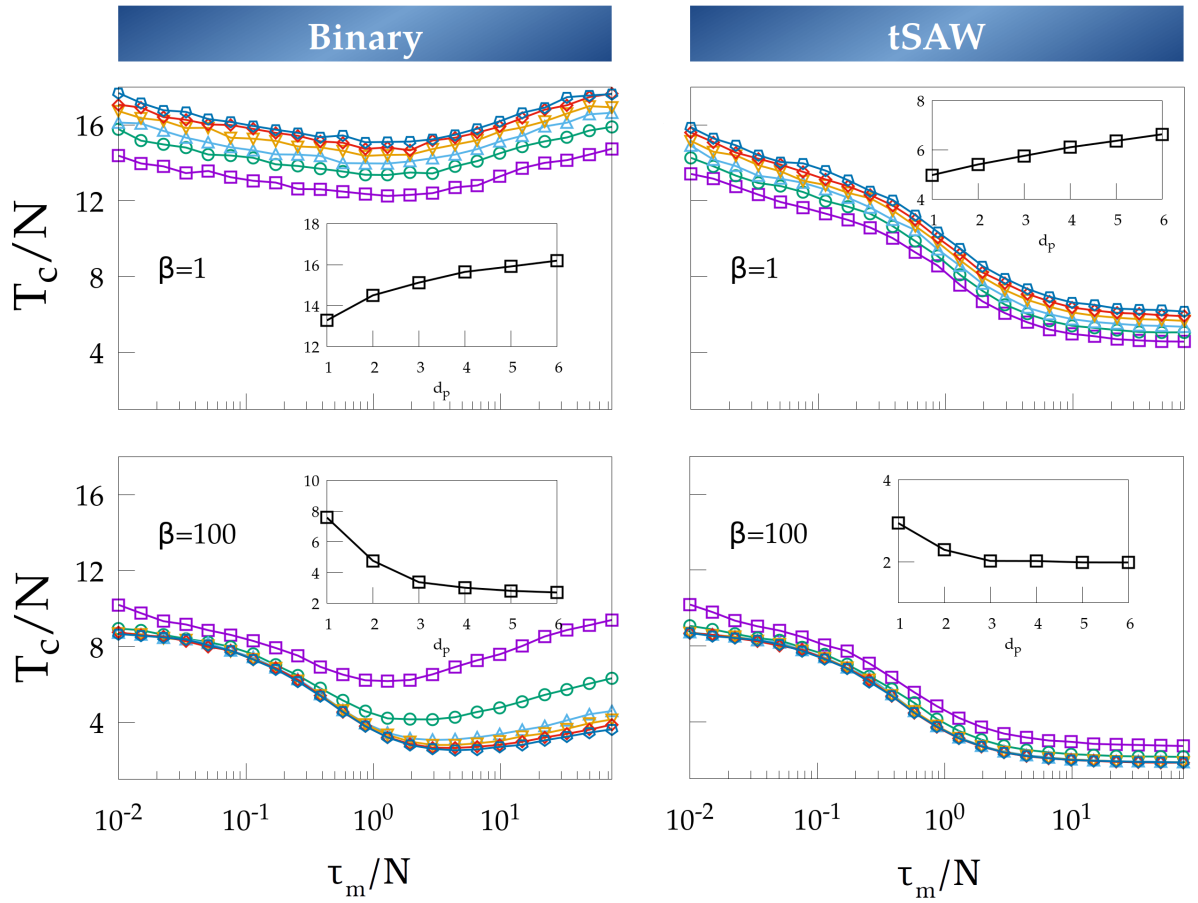

Figure 1.30: *Coverage time T_c as a function of the evaporation time τ for $\beta = 1$ and 100. Different prospections lengths d_p are provided. Left panel corresponds to the binary cognitive map and the right panel, to the tSAW cognitive map. The inset shows the T_c according to d_p for a $\tau = 10N$. Purple squares correspond to $d_p = 1$, green circles to $d_p = 2$, sky blue triangles to $d_p = 3$, yellow inverted triangles to $d_p = 4$, red diamonds to $d_p = 5$ and dark blue pentagons to $d_p = 6$.*

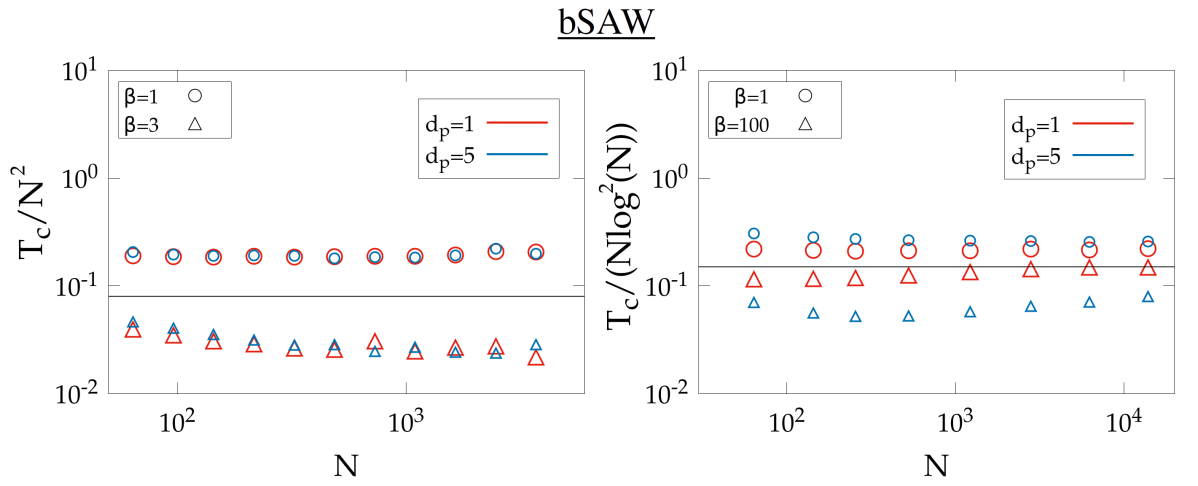

Figure 1.31: *Scaling for the coverage time T_c with the system size N when the cognitive map corresponds to the bSAW. Left panel corresponds to a one dimensional lattice ($d = 1$) and the right panel, to a two dimensional lattice ($d = 2$). Red color corresponds to $d_p = 1$ and blue color, to $d_p = 5$.*

than using a fixed value as done above. So, instead of fixing the prospection length, now we

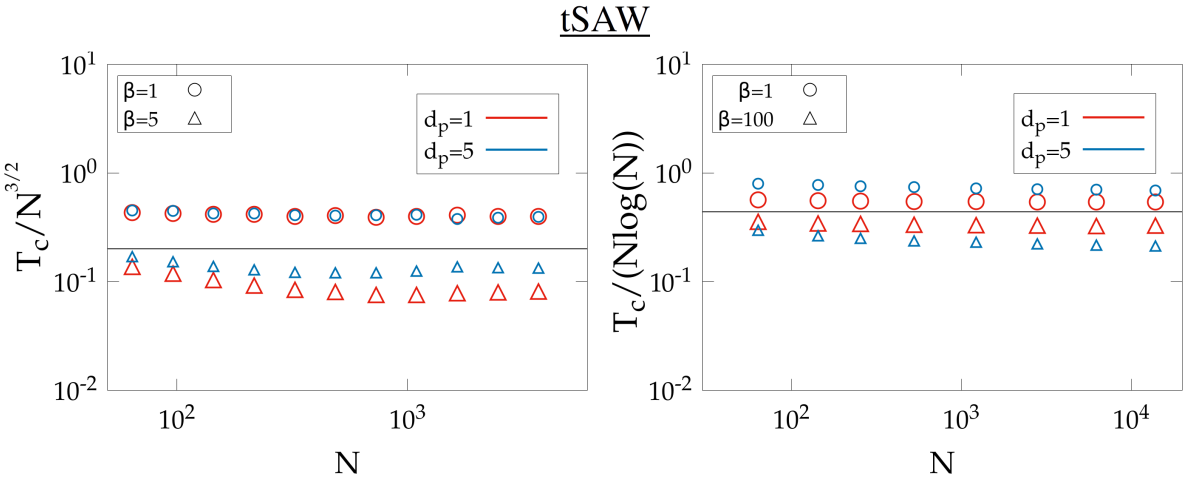

Figure 1.32: *Scaling for the coverage time T_c with the system size N when the cognitive map corresponds to the tSAW model. Left panel corresponds to a one dimensional lattice ($d = 1$) and the right panel, to a two dimensional lattice ($d = 2$). Red color corresponds to $d_p = 1$ and blue color, to $d_p = 5$.*

assume that d_p is taken from a certain **distribution** $\rho(d_p) \sim d_p^{-\alpha}$, with $\alpha > 0$ and $d_p \leq d_p^{max}$, so an upper boundary on d_p is used to take into account the finite prospection capacity of the walker. We have chosen arbitrarily $d_p^{max} = 6$ for our study. That mechanism allows the walker to incorporate non-local information but it still keeps the range of prospection very distant to the size of the system. It combines, then, the six different lengths d_p appearing in figure 1.30 during a given path. When $\alpha = 0$, all the prospection lengths are equiprobable. When $\alpha \gg 0$, the probability of gathering information from the neighboring sites is much larger than that from distant ones.

We reproduce the analysis done above where now the parameters space is defined by β, τ and α (instead of d_p). We find that when α is modified (Fig. 1.33), the walker dynamics looks qualitatively similar to the results obtained by modifying d_p (Fig. 1.30). For low β, the coverage time decreases as α grows (long prospecting paths are less probable), while for high β values, we find again that the most efficient mechanism includes as many long prospections as possible (so $\alpha \to 0$).

From these results, we observe that the coverage process remains almost equivalent when the walker prospects constantly with a given (large) d_p or when the walker prospects mainly for shorter paths but there is a small (but significant, meaning that at least the 1% of prospected paths corresponds to long ones) proportion of d_p paths. We stress that this feature is present both for the bSAW and for the tSAW models. We can quantify the effect for the particular case $\alpha = 2$. The probability of a prospected path of $d_p = 1$ is 36 times larger if compared to the probability of a $d_p = 6$ path ($P(d_p = 1)/P(d_p = 6) = 36$). Despite the small probability of $d_p = 6$ paths, the coverage properties are more similar to the output of a fixed $d_p = 6$ prospection length than to a fixed $d_p = 1$ prospection length for one for any β and τ.

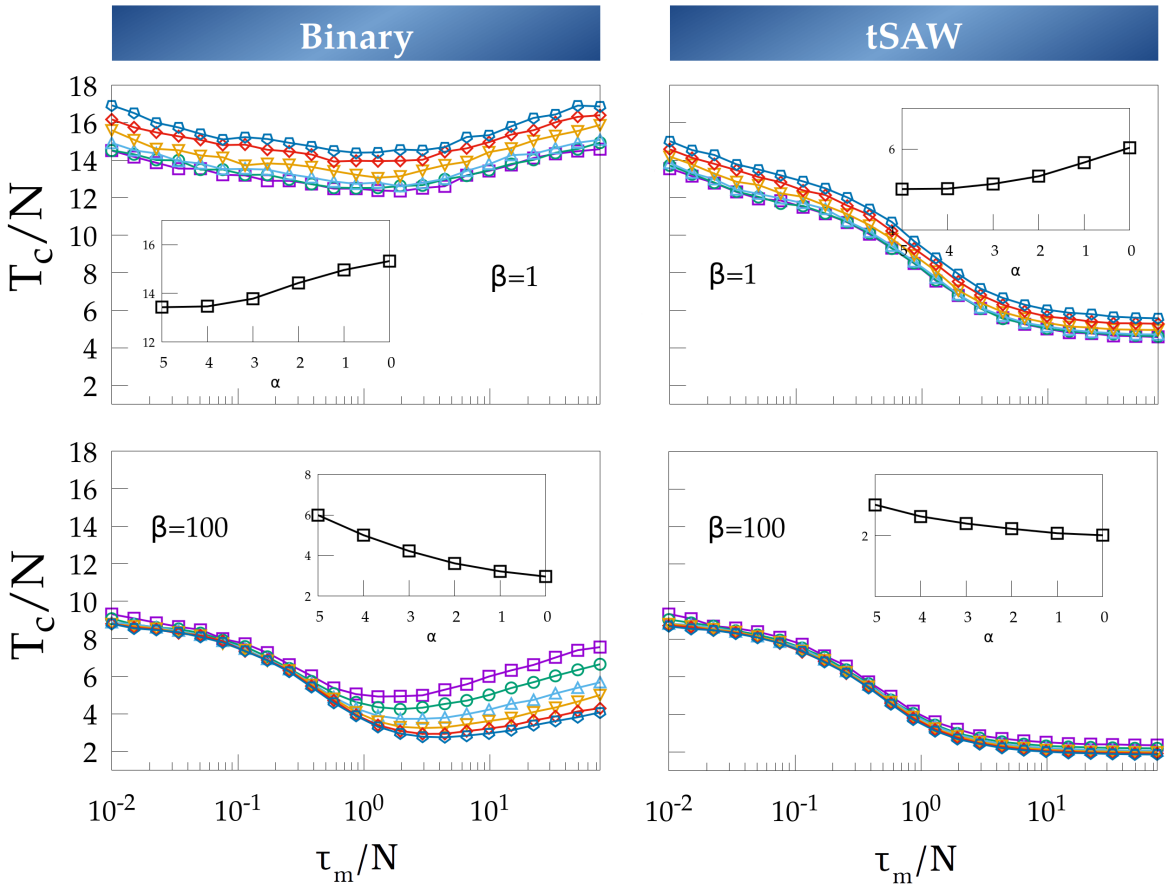

Figure 1.33: *Coverage time T_c as a function of the evaporation time τ for $\beta = 1$ (region I) and 100 (region II). Different prospections lengths distributions α are provided. Left panel corresponds to the bSAW and the right panel, to the tSAW cognitive map. The inset shows the T_c according to α for a $\tau = 10N$. Purple squares correspond to $\alpha = 5$, green circles to $\alpha = 4$, sky blue triangles to $\alpha = 3$, yellow inverted triangles to $\alpha = 2$, red diamonds to $\alpha = 1$ and dark blue pentagons to $\alpha = 0$.*

Concluding remarks

- The self-avoidance mechanism, generated through a cognitive map or signal deposition, increases the search efficiency of the random walk process. If the information processing associated to the self-avoidance is partial or imperfect, however, that efficiency can be drastically reduced. Interestingly, the combination of several of these cognitive drawbacks (such as partial self-avoidance and impairment) can lead to non-trivial optima in the search efficiency.
- Prospection stands for an efficient search strategy when the walker process accurately the obtained information. Otherwise, to prospect for non-local information may even increase the search time.

Decision making 2

Through adaptation, intelligent organisms develop more efficient responses to the task they face. As stated before in this thesis, the search process could be understood as a sequence of situations that require the individual to provide an answer to each. For example, deciding which one would be the next direction of movement or whether to revisit a previously explored region. The random walk framework studied during the previous Sections provides a perfect example to translate the movement pattern of the search process into a sequence of decisions. Within that context, each step of the walk could be understood as a **decision**, where the walker has to choose between different sites at which it can jump next. The cognitive mechanisms, through the evaluation of the information, are responsible for decoding which ones are the best options in each case. These mechanisms could range from the simple signal detection, leading to self-avoidance (as seen in Section 1.3), to a complex forecasting of the future consequences (as suggested in Section 1.5). The $f(E)$ framework, as explored before, provides an effective description of that process.

From those ideas, a clear connection exists between **efficient search** processes and **optimal decision making**. One could assume from this that to incorporate more and more information would lead to better decisions, but this is not necessarily the case. The living organisms need to provide fast and effective responses for their motor and mental tasks, so the time devoted to the search process and the information gathering shouldn't be too large. In addition, there might be some situations where more prospection does not provide necessarily more useful information. In general, prospection will be really useful as long as the quality of distant or non-local information is significantly higher than the local one.

During the Chapter 1, we haven't focused much on the specific dynamics of the cognitive mechanisms the individual uses to process the information. In our effective description, we have directly constructed the energetic landscape $f(E)$ (and then, probabilities) according to predetermined rules.

One can argue that these challenges lie within the field of psychology. Nevertheless, in the recent years there has been a growing interdisciplinary interest the quantitative study of decision-making. Neural correlates in decision-making tasks constitute at present an important source of information in cognitive and behavioral neuroscience [155–158]. The strategies to improve the efficiency of our decisions constitute an important subject in game theory and econophysics [159, 160] . Also, ideas from statistical physics and/or complex systems also have made its way; while most contributions to date focus on decision-making at the level of groups or collectives (see [161–165] for some reviews), tentative works suggesting physical principles that could be involved in individual decisions do also exist [166–170].

In this Chapter we will propose a possible mechanism to describe decisions carried out by humans within such contexts, and we will provide support for it based through an experimental sequential decision-making task carried out with human subjects on the computer screen.

2.1 The Drift-Diffusion model

Large efforts have been put in understanding the dynamics and the characteristics of **perceptual decisions**, it is, those where sensory information provides direct evidence for choosing between the options available, as in the famous random dot motion task [171, 172]. During this task, a subject is asked to look into a set of dots in a computer screen. Those dots are divided into two different groups, each moving in opposite directions (either right or left). The subject then has to decide in a minimum time whether the majority of the dots are moving to the left or to the right. The information is encoded in the screen, and the individual integrates it visually. A correspondence between such **sensory information** and the **neuronal responses** responsible for the evidence accumulation in the brain are assumed to be identifiable, providing a physical measure or correlate of the neural processes involved [173], captured by electroencephalography (EEG) techniques. A variation of this experiment is the color dot task. There, the subject looks into a set of dots, that can be either red or blue. Then, the subject is asked to identify the color that appears more often. Again, one can establish a correspondence between such sensory information and evidence accumulation.

There have been lots of efforts focused on developing a theoretical framework for those situations. Most of them lie within the so-called *accumulator* framework, in which **cognitive evidence** (described through some kind of stochastic process) is gained throughout the time until it reaches a given threshold, which then triggers the decision. The paradigmatic example of such approaches is the **Drift-Diffusion model** (DDM) [174]. The DDM was proposed as a model of the cognitive processes involved in simple two-choice decisions. Mathematically, the process of deciding between an option A and an option B is defined as follows (see figure 2.1). The individual accumulates information about each option (those accumulators represent the options payoffs and are labeled as E_A and E_B). A random variable $X = E_A - E_B$ denotes the relative evidence or the evidence accumulation between

the two possible options. X is assumed to be driven by the combination of a diffusion process (which introduces cognitive fluctuations or noise during the evidence accumulation), and a drift process that accounts effectively for the evidence accumulation. That accumulation drives X towards the correct answer gained through sensory information. The dynamic evolution of X is typically assumed to be described through the equation $X' = D + \eta$, where D corresponds to the drift towards the correct option and η corresponds to noise and/or fluctuations. Two thresholds, X_A and X_B are then defined. When X reaches one of these thresholds, it represents that the amount of evidence is enough to take the decision (A when X_A is reached first and B when X_B is reached first). In figure 2.1, a bi-optional decision corresponding to the color dot experiment mentioned above is characterized by the DDM. The gray line corresponds to X while the horizontal blue and red lines indicate the thresholds. If X reaches first the upper (blue) threshold, the subject decides that the number of blue dots is larger, and the opposite occurs if X reaches first the lower (red) threshold.

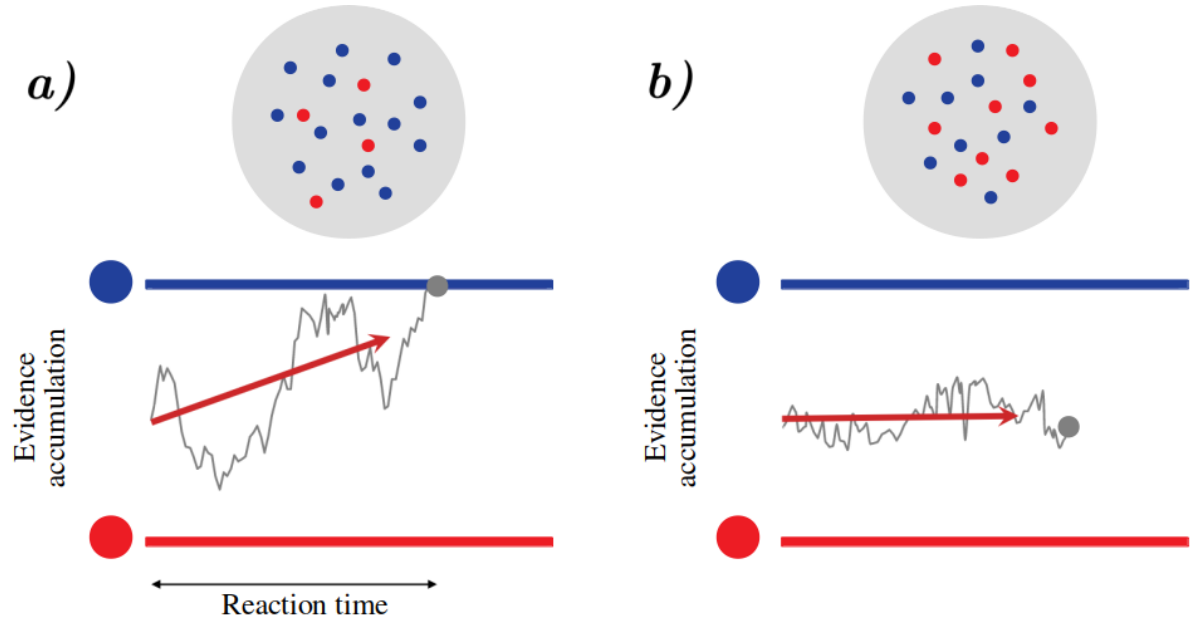

Figure 2.1: *Schematic representation of the DDM dynamics when deciding between two options in the color dots task. The gray line corresponds to X, while the horizontal blue and red lines corresponds to the thresholds of both options. In a), one option has to be taken between the red or blue dots being a majority. There is a clear majority of blue dots, so the drift D drives the evidence accumulator towards the superior (blue) threshold. In b), the drift D is close to zero due to the lack of a clear difference between red and blue numbers of dots. The noise η is a white noise where $\langle\eta\rangle = 0$ and $\eta(t)\eta(t_0) = \delta(t - t_0)$. The image is adapted from the Tajima et al article [175].*

The rate of accumulation of information, or drift rate D, is usually assumed to be related to the quality of the information extracted from the sensory stimulus. One can observe this idea when comparing the a) and b) panels of figure 2.1. For b) it is difficult to reach a decision as the number of points of each color are approximately the same (actually it is the same in the figure) so there is no a clear drift D in the evidence accumulation towards one decision or the other. Consequently, the dynamical process to reach one of the thresholds may take a longer time than for a) case.

This simple model has been widely used in psychology, neuroeconomics, and neuroscience to explain the observed patterns of choice and response times in a range of binary choice decision problems [176]. However, there are many cases where it requires modifications or extensions to be useful. Non-constant threhsolds have been introduced to recover realistic response times [177, 178]. The dynamic behavior could be introduced over different realizations of a given decision or even evolve temporarily across the evidence accumulation [179, 180]. Other studies have analyzed how dynamic changes of the drift D during the process or according to the current state of X may explain some experimental features [181–183]. Finally, other works have studied the role of the initial estimator of X [184] or have tried to extend the DDM to multi-optional choices [185].

2.1.1 Sequential Probability Ratio Test

Another tool that has been extensively used in decision-making theory is the Sequential Probability Ratio Test (SPRT), first introduced by Abraham Wald in 1946 [186]. The question it addresses is when the information processed by the individual is supposed to be good enough to make the decision. From a mathematical perspective, a quantitative criterion has to be established to identify when the subject has enough information in order to make the decision with some level of **accuracy**. Given two different options (A and B, each with its corresponding reliability), we define the probabilities (as they are estimated by the subject in terms of the information/evidence acquired) to take one of the options (A or B) as p_A and p_B (which are assumed to be mutually exclusive options, so $p_A + p_B = 1$). The SPRT is given in terms of the log-likelihood function

$$W = \ln\left(\frac{p_A}{p_B}\right) \tag{2.1}$$

and establishes that the decision should be taken as soon as the cumulative of $W(t)$ computed through evidence accumulation, $\sum_i W = \sum_i \ln(p_{A,i}) - \sum_i \ln(p_{B,i})$, exceeds (or falls below) a given threshold (W_{th}). Here, $p_{A,i}$ and $p_{B,i}$ are defined as the probabilities for each option (either A or B) when estimated through the accumulation of sensory evidence (assuming for convenience that such process can be divided into discrete samplings occuring sequentially, so the sum in the formula is carried out over all the samplings i carried out up to a given time). Consequently, the SPRT criterion above establishes a criterion to define the sufficient information to decide, and actually the DDM can be seen as a particular continuum implementation of this [187, 188].

The SPRT, in fact, also admits an interpretation in terms of information theory. If we redefine the probabilities of the options A and B as $p_A = 1 - p$ and $p_B = p$ then

$$W = \ln\left(\frac{1-p}{p}\right) = \frac{\partial S}{\partial p}, \tag{2.2}$$

where we have introduced in the last step the Shannon's entropy $S = -p\ln p - (1-p)\ln(1-p)$ (the extension from binary options to ternary, or more complex, decisions is straightforward).

So that, the SPRT criterion can be seen as a threshold in the **cumulative variation** of entropy with respect to variations in p during the process of evidence accumulation.

One can visualize in figure 2.2 (upper panel) how the SPRT criterion is used to describe a binary choice when the evidence accumulation provides sufficient evidence to make a decision (in analogy to the process shown for the DDM in figure 2.1). As stated above, the evidence accumulation is described in terms of E_A and E_B (figure 2.2 lower panel). If one defines canonically the probability for each option (as in equation 1.36), the SPRT criterion is then $W(t) = \ln(p_A/p_B) = -\beta(E_A - E_B)$, the traditional SPRT could be interpreted as a way to impose a threshold in the difference of the accumulators E_A and E_B computed through prospection.

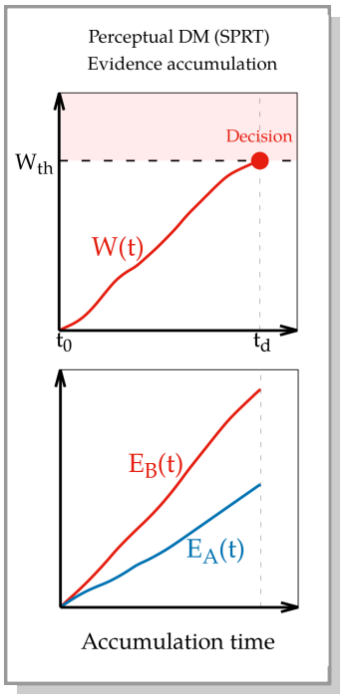

Figure 2.2: *Scheme for the accumulator mechanism. The lower graph corresponds to the evidence accumulation (E_A and E_B) for perceptual decision making, with the Wald's ratio W (derived from E_A and E_B) as quantifying magnitude (upper graph). The label t_d in the horizontal axis corresponds to the decision time, where the Wald's ratio W reaches a given threshold W_{th}.*

2.2 The entropic mechanism

Perceptual decisions, as in the random dot tasks, are based on a fast response to a given visual stimulus; for instance, in the random dot task responses/decisions typically span a few tenths of a second. Alternatively, one can introduce another class of decision-making processes in which reaching an answer is not trivial from sensory information alone because the task involves complex consecutive decisions that may even have an influence over the next ones. This obviously requires a higher cognitive capacity and a more reflective response by the subject in order to process the information. This is the typical case involved in tasks like playing board games as chess, or solving mazes or tasks presented in some intelligence tests. Note that all these decisions involve building a bunch of future possibilities, it is, carrying out a prospection of the possible situations that would occur after a single decision, in a tree-like fashion. This entails with the idea of prospection, as introduced before in

Chapter 1, that in general requires (and is actually coupled to) high memory and abstraction capacities [189–191]. Following some existing literature (see, e.g, [192, 193] and references there in), we will denote this kind of situations as **sequential decision-making**.

Stochastic mechanisms able to capture the dynamics of sequential, or more complex, decision making are scarce [194]. To contribute to the development of a physical framework, we adapt principles from statistical physics and information theory to show that human decision-making in such contexts may be described by a mechanism which involves the internal computation of **informational entropy** by the subject [5, 195].

During prospection, the individual carries out **mental simulations** which try to sample (at least partially) the future possible scenarios/outcomes of the decision [196–199]. As the number of samples grows, the amount of cognitive information processed by the subject increases. Previous studies have reported that subjects tend to use a mental shortcut based on selecting the first alternative they consider good enough rather than trying to evaluating perfectly all of the possible mental simulations [200, 201], so avoiding that decisions become arbitrarily lengthy. Such finite sampling strategies suggest the existence of a cognitive threshold that is used by humans to determine when the information prospected is enough in order to discriminate adequately between the options, and so going on with the sampling process can be probably unnecessary since it is unlikely that new significant information is added.

The mechanism we propose to understand sequential decision-making is that it would be the entropy itself, not its variations (as the SPRT mechanism implicitly considers through equation 2.2), the relevant magnitude for reaching a state at which the decision can be taken reliably. So that, we propose that one will take its decision once $S = -p \ln p - (1-p)\ln(1-p)$ has reached a given threshold S_{th}. Note that entropy cannot be *accumulated* (contrary to the case of evidence). Instead, our mechanism suggests that the initial state of the subject is characterized by maximum entropy (or maximum uncertainty), and the progressive information acquisition and prospection provides a better estimation of p_A and p_B, such that when the entropy decays below a threshold S_{th}, this means that one can discriminate well enough between the options available and so the decision will be taken. Accordingly, evidence accumulation typical of the SPRT would be replaced in our proposed mechanism by an **entropy refinement** process (Fig. 2.3).

To implement this mechanism we need to solve the problem of how the information processed by the subject may be translated into the probabilities $p_A = p$ and $p_B = 1 - p$ appearing in S.

If the information obtained during the prospection process results in a clear reward or payoff (we denote here these estimations as E_A and E_B for the options A and B), then the question reduces to find the mapping from the E's to the probabilities. At this point, we introduce the hypothesis that the prospection process is used by humans as a way to estimate (through $E_{A,B}$) the real mean value of the payoff (we denote it as $\mu_{A,B}$), that can be obtained from each choice (A and B). If that is the case, then a direct implementation of the Maximum Entropy Principle (MEP) (see Section 1.3 for details) from information

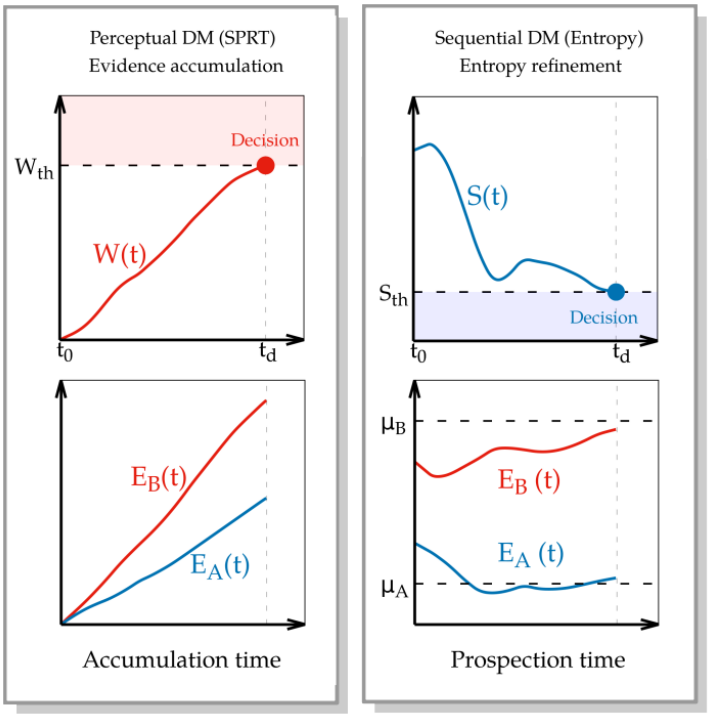

Figure 2.3: *Scheme for the accumulator and reliability mechanisms. The left column corresponds to the evidence accumulation for perceptual decision making (lower half), whit the Wald's ratio W as quantifying magnitude (upper half). The right column corresponds to the sequential decision making mechanism (lower half), with the Shannon's entropy S being the quantifying magnitude (upper half). The label t_d in the horizontal axis corresponds to the decision time.*

theory states that the most neutral (or unbiased) choice of probabilities that we can assign to each option i reads

$$p_i = \frac{\exp(-\beta E_i)}{Z}, \tag{2.3}$$

where β is a positive constant and Z a normalization factor.

One can observe that this p_i definition is analogous to the ones for the random-walk models in Chapter 1. From the energetic perspective, the entropic mechanism represents a estimator to describe when the individuals consider the landscape $f(E)$ provides sufficient reliability to make the decision.

2.2.1 The SPRT and the entropic mechanisms in a toy model

As an introduction to the entropic mechanism, it can be illustrative to explore some of its properties if compared to the classical SPRT criterion. This is a way to check whether they lead to qualitative differences that can be later used as a way to discriminate between models at an experimental level.

We propose the following toy model (a very simplified scenario) to compare both. As stated before, we denote the real associated payoffs for options A and B as μ_A and μ_B. Then we assume that, through the prospection process, successive estimates of E_A and E_B are obtained by the subject in such a way that each sample made during prospection leads to a set of estimates $E_i = \{E_i^1, E_i^2, ...\}$, with $i = A, B$. After successive samples, the value of E_i tends to the value of μ_i. Each estimate is taken from a Gaussian distribution of unit variance centered at $\mu_{A,B}$ (see figure 2.4).

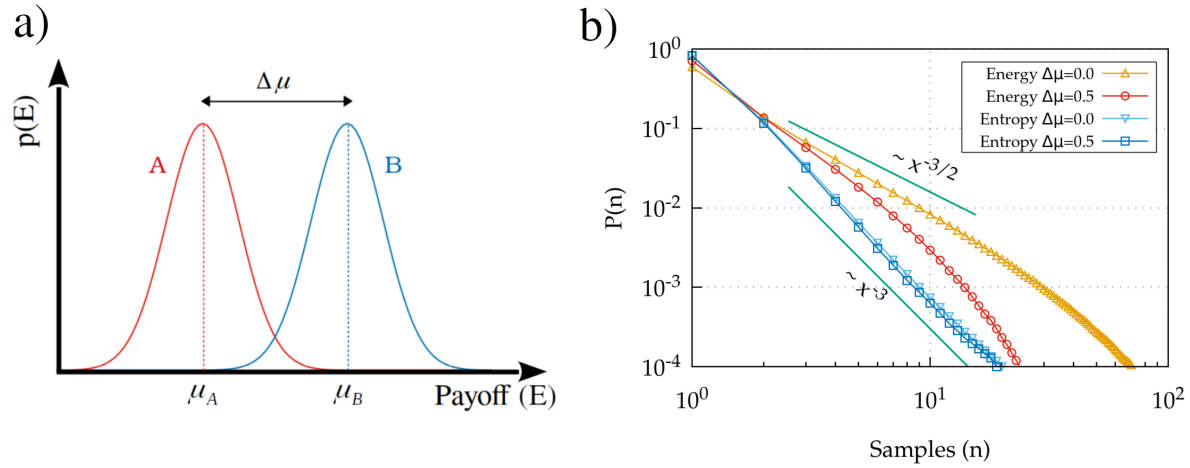

Figure 2.4: *a) Gaussian distributions corresponding to the possible payoffs that one can estimate for the A and B options. Each sample corresponds to a given value $E_{A,B}$ obtained from the red (A) and blue (B) distributions. The real mean payoffs of the distributions are represented by μ_A and μ_B, while the estimator after k samples corresponds to $\langle E_A \rangle$ and $\langle E_B \rangle$. b) Probability distribution for the number of of necessary samples (n) to reach the corresponding decision threshold both for the entropic and Wald's algorithms.*

The average estimated payoff $\langle E_i \rangle$ obtained after n subsequent samples reads

$$\langle E_i^n \rangle = \frac{1}{n} \sum_{j=1,n} E_i^j. \tag{2.4}$$

This estimator is used to compute the probabilities in equation 2.3. The fundamental question to answer is which is the number of samples n that are necessary to overpass (or fall below) a threshold, either in W (for the classical SPRT mechanism) or in S (for the entropic mechanism), as a way to decide between options A and B.

The SPRT case exhibits a distribution of the number of samples that depends strongly on the distance between the means $\Delta\mu \equiv \mu_A - \mu_B$ (figure 2.4). Instead, for the criterion of entropy refinement the distribution of necessary samples exhibits a **power law** behavior $P(n) \propto n^{-3}$, for a wide range of $\Delta\mu$ and S_{th}. The distance $\Delta\mu \equiv \mu_A - \mu_B$ is relevant for the SPRT criterion but it is not for the entropic mechanism.

At this point, we have demonstrated at least one fundamental difference emerges between using the SPRT or the entropy threshold, so we can use it as a criterion to discriminate between these two mechanisms.

2.3 Navigation task in humans

The mental processing of sequential decision making is in general deeply complex and hard to capture. Even with the help of brain activity monitoring, the information does not usually admit a direct interpretation. As a example, let's focus again on the case of perceptual decisions and the color dot experiment. When we observe the color of one of

these dots, the sensory information produces a signal in the brain activity corresponding to the visual sensory. But when planning a chess movement (sequential decision making), the assignment is far from trivial. So that, simple situations in which sensory information can be assumed to reflect somehow such complex mental processing would be helpful.

With this purpose, we have designed a particular **navigation task**. The participant in this task will have to move through a virtual maze with the goal of maximizing the number of different regions visited in it.

Efficient navigation strategies in a maze involve a prospection process through visual inspection of the possible paths available within the sight distance, so involving a gathering of non-local evidence. In order to capture this dynamics, we prepare the setup in such a way that we can estimate the paths prospected by the subjects with the help of eye-trackers.

2.3.1 Experimental setup

During the experiment, 18 clinically normal adults (11 women and 8 men) aged from 18 to 45 have participated. Anyway, the navigation task is done individually.

In the first part of the task, subjects are presented a discrete 7×7 regular lattice on the computer screen, representing a discrete set of 49 nodes. This one is the structure where the navigation process takes place (Fig 2.5, upper panel on the left). The nodes are linked through paths connecting them only to neighbor nodes (4 paths per node, except for the boundaries where paths are only 2 or 3). A fraction (20%) of the links between neighbour nodes have been removed in order to introduce some disorder in the structure. We have prevented isolated regions in the structure to be formed.

We asked the participants to visit the maximum amount of nodes of the resulting graph within 49 steps. In each task trial, the subject starts from the center of the structure. One step is defined as a transition between connected sites in the graph. They do this by clicking with the mouse over the site to which they want to move next (Fig 2.5, middle panels, show some realizations of the resulting trajectories). Heterogeneity of the graph then makes the process nontrivial (note that for a regular lattice the optimal strategy to cover the maximum number of nodes would be simply to perform a ladder-like trajectory). In our structure, they would have to process the information to decide the better paths to increase the number of visited nodes. Note that the navigation scenario described here is conceptually very similar to the search processes we have explored numerically during Chapter 1.

To assess the subjects performance under different levels of complexity, the nodes of the rectangular lattice are then reorganized in a circular way in two different ways. In the first case (Circular Ordered), we keep the order of the rows of the first rectangular graph (Fig 2.5 b)). For the third graph (Circular Disordered), we place the nodes following a circular structure but with the maximum visual disorder (Fig 2.5 c)). We remark that topologically the three structures are completely equivalent. However, intuitively we expect that growing difficulty will appear to gather information and prospecting as long as the visual distribution of nodes and paths gets disordered, resulting in a worse performance

(it is, a lower number of different sites visited during the task). Additionally, we rotated 90º, 180º and 270º the rectangular structure (with their corresponding Circular Ordered and Circular Disordered reorganizations) for randomizing the task (so 12 cases in total are presented to each subject) without changing the topology of the structure. The final dataset comprised 72 trajectories for each graph (Rectangular, Circular Ordered and Circular Disordered).

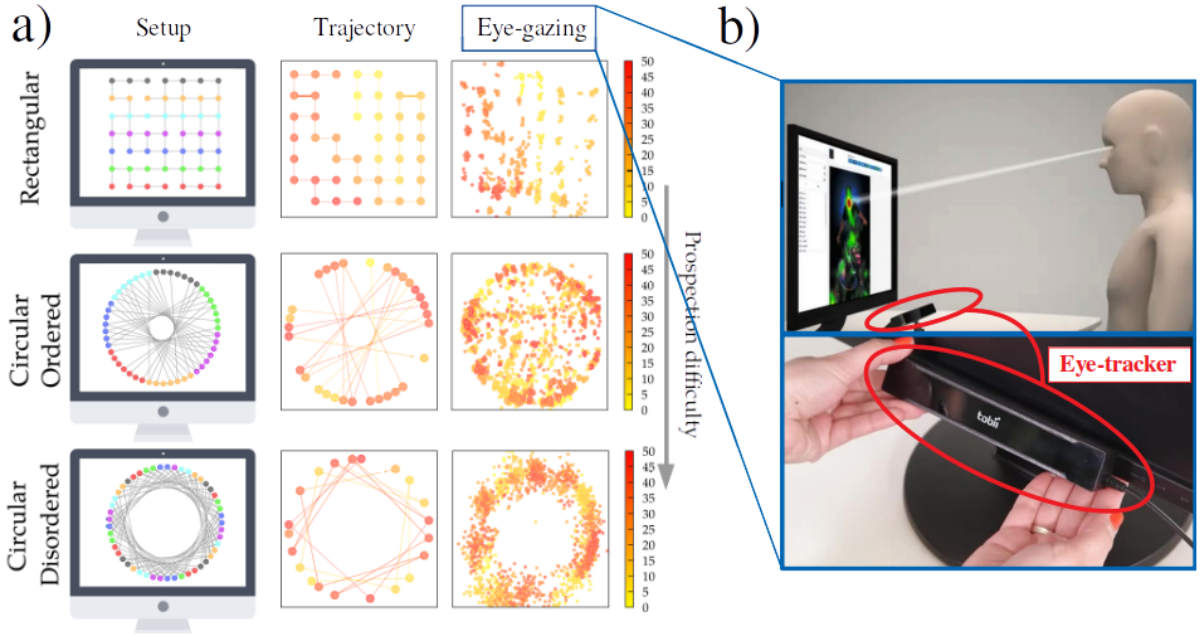

Figure 2.5: *a)Scheme of the experimental setup. The first column corresponds to the three 49 patch graphs. The paths correspond to the allowed movement between nodes (absence of them meaning the nodes aren't connected). The color of the nodes is introduced to facilitate the understanding of the spatial reorganization. The second column shows one individual trajectory within the structures (the color code corresponds to the current step of the 49 steps trajectory). The third column shows the locations where the individual has gazed into during the trajectory (the color code corresponds to the current step of the 49 steps trajectory). b) Scheme of how the eye-tracker works. It capture the locations of the screen where the participant is gazing during the task. The images were obtained from [202].*

During the task, one cannot infer directly the paths prospected by the subjects from their trajectory. We have used eye fixations measured through an eye-tracker (figure 2.5, right panels) to analyze (i) the number of nodes at which the subject gazes between consecutive steps/decisions, and (ii) the time it remains gazing at particular sites, as a way to infer how cognitive resources are being distributed throughout the prospection time. The eye fixations are the sensory input from which we try to decipher part of the relevant cognitive mechanisms driving the performance of the subjects in the task.

2.3.2 Quantifying prospection

With the obtained trajectories and associated datasets, one can analyze the participants performance. The global performance of the individuals in the three different levels of the graph is computed as the number of nodes that have been covered during the entire

trajectory (Fig. 5.13 a)). The efficiency of the navigation task is measured through the number of different sites covered during the trajectory.

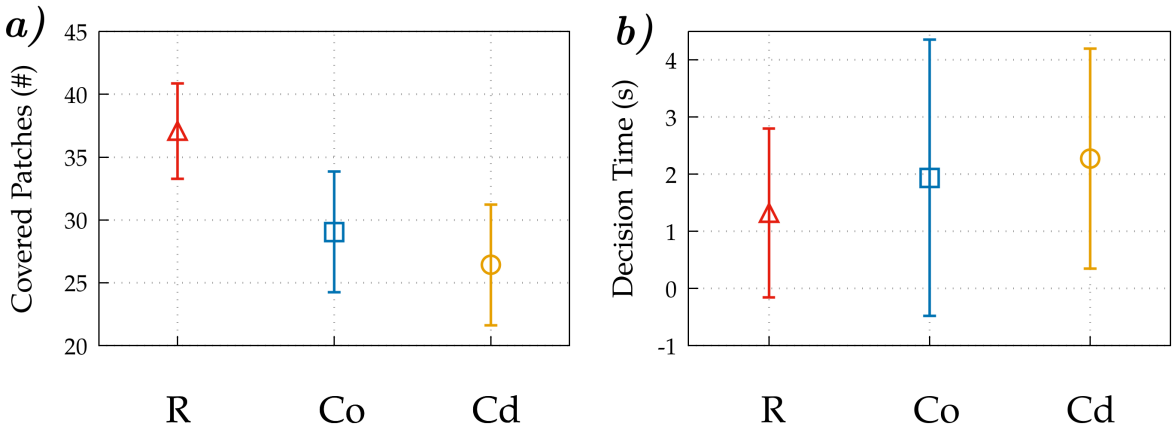

Figure 2.6: *a) Averaged number of covered nodes after the* 49 *steps trajectory for each one of the graphs. b) Averaged decision time accounting all the movement of the trajectory for each one of the graphs.*

For the Rectangular graph, the subjects visited in average 37.1 ± 3.8 nodes (this is, a $75,7\%$ of the total 49 sites). For the Circular Ordered graph, they covered 29.1 ± 4.8 nodes $(59,4\%)$ and for the Circular Disordered graph, 26.4 ± 4.8 nodes $(53,9\%)$. These results confirm that the difficulty of the task depends strongly on the visual organization of the nodes in the graph. Moreover, the averaged decision time shows us that the performance is not improved just by spending more time deciding (figure 5.13 b)) (where the decision time is considered to be equal to the time between two consecutive movements in the graph). This seems to confirm that the difficulty of the task is clearly the main element driving the subject efficiency.

The next step is to analyze the information gathered with the help of the eye-tracking data. We define the distance d_b as the minimum number of steps/bonds between the current patch and the one the individual is gazing at. The corresponding experimental distributions of d_b are found to be completely different for the three visual organizations considered (figure 2.7). The distance (in bonds) between any two nodes is exactly the same in all cases; then it is clear that the individuals do not prospect equally in these cases. While for the rectangular case a large amount of time is invested in gazing at nearby nodes, for the Circular cases (specially for the Disordered one) frequent gazes at distant sites are observed, which must be attributed either to (i) distractions caused by the presence of nodes which are close on the screen configuration (though they are not easily accessible from the current one), and (ii) the difficulty at identifying easily the nodes which are available in the next few steps. Intuitively, an efficient prospection should combine an intensive exploration of closer sites and a smaller (but not necessarily negligible) exploration of further ones. We illustrate that idea in the inset of figure 2.7, where the cumulative probability of being gazing at nearby nodes (defined as those with $d_b \leq 4$) is shown to decrease drastically as a function of the visual complexity of the task.

As a way to quantify and refine the ideas above, we propose to compare the subjects performance in our task to that of virtual subjects. As a virtual subject, we have used the

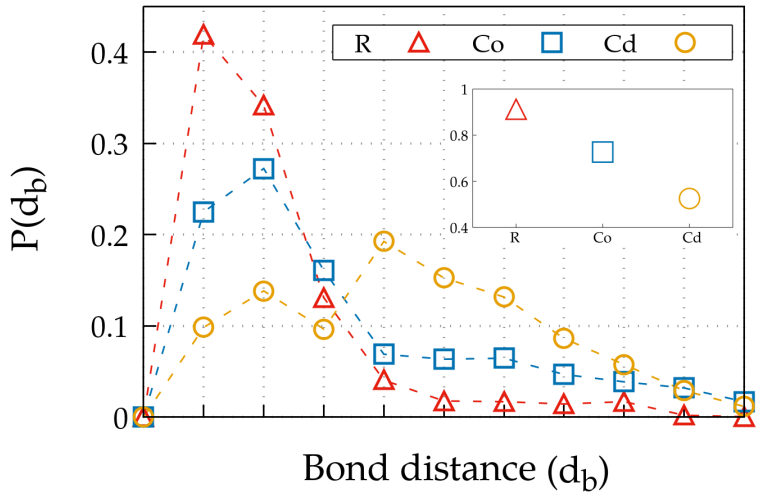

Figure 2.7: *Distribution of the bond distance d_b between the current patch and the nodes that have been gazed before doing a movement for each one of the graphs. The inset corresponds to the accumulated probability for gazing nodes at a distance $d_b \leq 4$.*

bSAW model with prospection described in Section 1.5. The differences with the analysis carried out in the Chapter reduce to the lattice (49 sites) being non-periodic and the suppression of part of the connections of the regular lattice.

The walker computes the probability to jump to a given site i again through equation 2.3. The length of the prospected path is characterized by the prospection length d_p. The previous visits to a site are kept in memory by the walker during a characteristic number of steps τ_m (according to the impairment mechanism, see Section 1.4). As a result, if a certain choice would imply moving to regions that, according to the prospection length and the memory capacity of the walker, are already visited, then the payoff associated to that option would be large. Instead, if a certain choice is seen to drive the walker to a region with a large number of non-covered sites, the corresponding payoff would be lower.

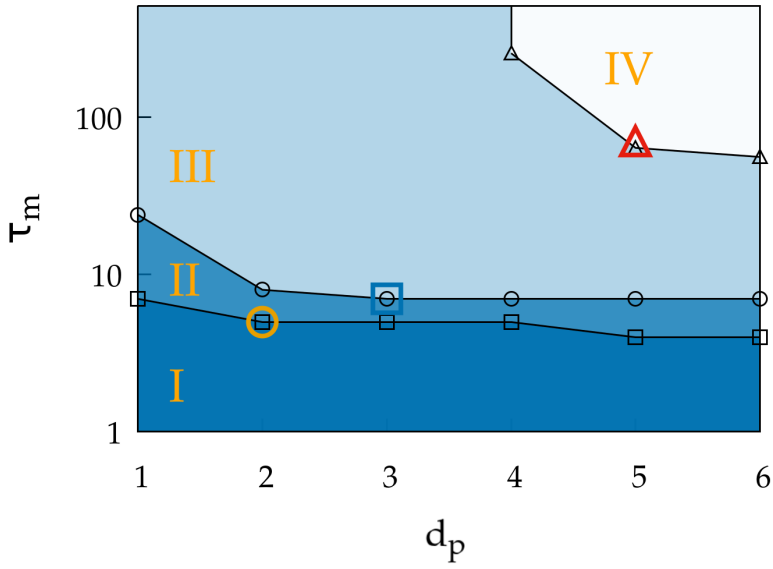

Figure 2.8: *Diagram for the walker covered nodes in comparison with experimental results. Regime I corresponds to a worse averaged performance than all geometries. Regime II corresponds to a better performance than in Circular Disordered. Regime III corresponds to a better performance than in Circular Ordered and Disordered. Regime IV corresponds to a better performance than in all geometries.*

The main adaptation of the walker mechanism to the scenario is that successive prospections of the paths available in each direction are carried out at random among all possible ones

of length d_p, and so values of the payoffs and the probabilities p_i are continuously updated. Here, the evaluation of the probabilities is done with the information given by a finite number of samples. Note that for a given value of d_p the number of paths that can be prospected is of the order of $\sim 4^{d_p}$ (if assuming that all links between neighbor sites are available). For large d_p, one cannot expect the subjects to explore all those possible paths. Conversely to the sampling mechanism explored in Chapter 1, the walker prospects here only a fraction of those paths.

The decision of when to move to the next patch is taken by the random walker according to the decision criterion described above in Section 2.2. After each single prospection of one path in each direction, the walker computes the corresponding Shannon's entropy $S = \sum_i -p_i \ln p_i$; if the computed value falls below a fixed threshold S_{th}, the walker makes the decision according to the probabilities p_i computed at that time (in case the option with the larger probability was always chosen by default, we have checked this would not change qualitatively the walker dynamics). On the contrary, if $S > S_{th}$ then the prospection process continues. However, we additionally introduce a rule such that the maximum number of prospections is limited to 100 to avoid (extremely unusual) situations in which S would never decay below S_{th} because all options available persistently exhibit very similar payoffs. We have carefully checked that this rule doesn't modify any of the results reported in a significant way. For the sake of simplicity, we fix here the parameter $\beta = 5$ during all the simulations.

The rules above generate self-avoiding trajectories of the random walker (more or less efficiently, in terms of the parameters d_p and τ_m) without explicitly requiring it to maximize the number of visited sites, as we do with the human subjects. As the performance of the algorithm is independent of the visual organization of the lattice (Rectangular, or Circular) we can use it as a reference model against which to compare the human performance in our experiment, so assessing the prospection mechanisms that are being presumably used by the human subjects.

By exploring the range of d_p and τ_m values in the computational model, we can divide the parameter phase space into four regions (figure 2.8). For region I the algorithm produces an averaged number of visited nodes lower than the individuals in any of the three versions of the experiment. The region II produces a performance which lies between the results obtained between Circular Ordered and Circular Disordered. The region III overcomes the results for the Circular Ordered performance but not for the Rectangular. The region IV, finally, outperforms all the experimental results (region IV).

Hence, we conclude that relatively large values both of τ_m and d_p are necessary to match or improve the efficiency reached by the human subjects in the Rectangular graph, suggesting that those subjects remember the visited sites and predict future outcomes efficiently in this case. According to this, the ability to prospect seems a necessary condition to justify the subjects performance in the experiments, at least for the Rectangular graph case, where $d_p \leq 4$ is necessary to reproduce the experimental results. For the Circular structures, instead, the individuals are probably not able to track the paths to distant nodes (there is no sufficient local gathering); in consequence, the value of d_p necessary to reproduce

their performance is lower than in the Rectangular case, and even the non-prospecting case ($d_p = 1$) seems to be enough as long as memory is large (but if memory is shorter, as is likely to be the case in our task, $d_p \geq 1$ seems to be necessary).

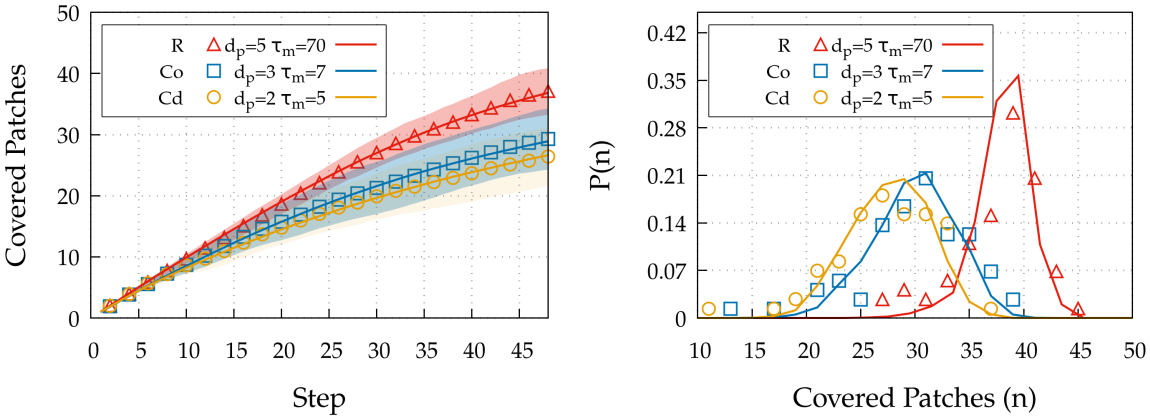

Figure 2.9: *a) Evolution of the averaged remaining non-visited nodes during the subject and walker performance. b) Distribution of final number of covered nodes obtained from the subject and walker performance. The dots correspond to the experimental data while the solid lines correspond to the walker mechanism.*

For certain values of d_p and τ_m the random walker actually reproduces the distribution of performances obtained from the experiments. In Fig. 2.9 we show results for the case (i) $d_p = 6$, $\tau_m^R = 70$, (ii) $d_p = 3$, $\tau_m^{CO} = 7$, and (iii) $d_p = 2$, $\tau_m^{CD} = 5$, which provide the best fits to the experimental data for each one of the three graphs, respectively. We also analyze the dynamical trends of the experimental trajectories and the trajectories of the fitted parameters (figure 2.9 left). The number of covered nodes presents in all cases a monotonic growth, which is reduced as the trajectory progresses and overlaps can appear in consequence. The experimental curves and those obtained from the algorithm with the parameters mentioned above agree almost perfectly. Then, the model reproduces in great detail the performance of human subjects throughout the experiment. Likewise, the distribution of the final performances so obtained is also in perfect agreement to experimental data (Fig. 2.9 right).

2.3.2.1 Coverage efficiency of the entropic mechanism

In analogy with Chapter 1, one can also explore how efficiently the random walkers above cover the whole lattice by computing the cover time instead of stopping the simulation after 49 steps. This provides an alternative measure of how efficient the walker is in terms of navigating the maze as a function of the memory and prospection parameters, τ_m and d_p. In particular, we focus again on the coverage time (T_c).

The main conclusion we can extract (as one can deduce from the results in Fig. 2.10) is that the ability to prospect future paths (so, having a large d_p) is useless unless the individual also has good memory skills (this is, a large τ_m value in our context). This makes clear sense, as when the walker cannot remember the previously visited sites (low values of τ_m), prospection would not be necessary or can be even detrimental; in that case the information

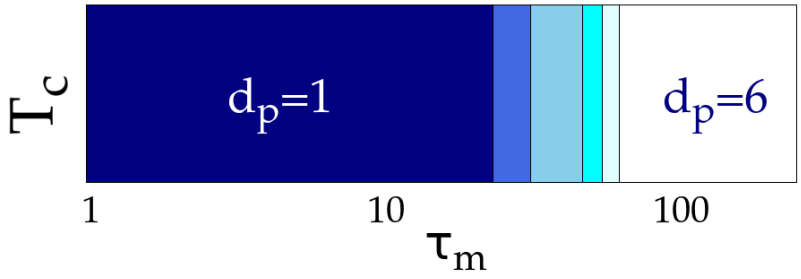

Figure 2.10: *Prospection length that minimizes the coverage time (T_c) of the walker as a function of memory time τ_m when the walker is placed in the same structure of the experimental design.*

provided by further nodes represents just useless noise as the walker always sees them as non-visited nodes. On the other side, for large τ_m the walker can correctly identify the previously visited nodes (large values of τ_m), so then progressively higher prospection lengths d_p are found to optimize the coverage of the structure and the search of a target.

2.3.3 Entropic mechanism validation

In Section 2.2 we have introduced a decision-making criterion based on the acquisition of sufficient decision reliability, based on a threshold for the informational entropy.

Once we have clear evidence that prospection is being used by the subjects during navigation through the maze (specially for the Rectangular case), we want to characterize decision-making dynamics within such context. For this we take now the eye-tracking data obtained from the experiments to analyse the distributions of: i) the times between decisions, ii) the times during which the subjects gaze at the same patch and iii) the number of different nodes gazed before making a decision (n).

Despite the different performances found for the three levels (Rectangular, Circular Ordered and Disordered) in previous Sections, the time distributions in all these cases exhibit extremely similar properties (Fig. 2.11). This suggests a common underlying mechanism for decision-making. What is more, all the distributions fit closely the **power-law** decay $P(t) \sim t^{-3}$ in agreement with the predictions from our information-theoretical criterion based on S (see figure 2.4). The only significant differences appear for smaller decision times, which seem to be scarce in the Circular Disordered case (as suggested from Fig. 2.11 b)).

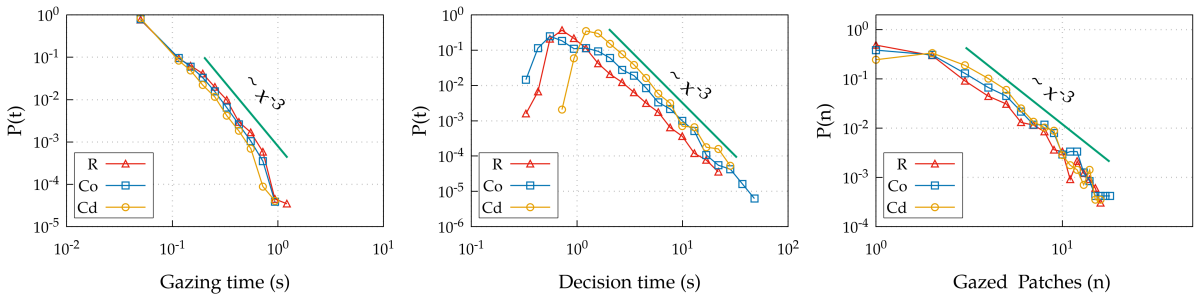

Figure 2.11: *a) Distribution of times the subject is staring to a certain patch. b) Distribution of decision times (consecutive movements). c) Distribution of the number of gathered nodes between consecutive movements. The results are shown for the three structures: the Rectangular (R), the Circulard Ordered (Co) and the Circular Disordered (Cd).*

Intuitively, the decision times may be understood as the sum of the times that the individual has been gazing at each individual patch. Then it could be that the power-law emerges either from (i) the distribution of times the subject keeps looking at a given patch, or (ii) the number of nodes that are gazed between decisions. Both cases would provide an explanation for the scale-free feature of the decision time distributions as a consequence of other distribution. However, we actually find that both distributions (for the number of nodes gazed and for the gazing times) present the same scale-free decay (Fig. 2.11, middle and right panels). So, the underlying mechanism yielding the power-law distribution for decision times is apparently a nontrivial combination of both.

We reproduce the same analysis of figure 2.4, where the number of samples n to reach the threshold S_{th} is explored. The results in figure 2.12 correspond again to the values t_m and d_p fitted from the experiments. We observe that exponent -3 is also exhibited by the walker dynamics.

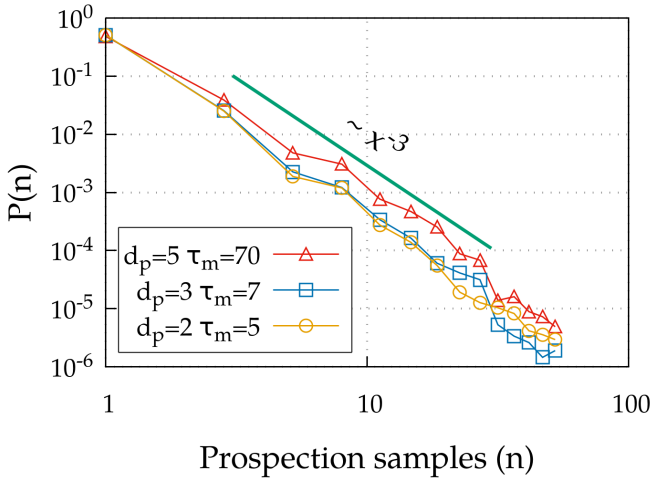

Figure 2.12: *Distribution of the number of prospections n performed by the walker to force the entropy S to fall below the threshold S_{th}.*

The robustness of the -3 exponent is further supported by additional evidence. First, in Fig. 2.13 left we show the explicit dependence of this behavior on the entropy threshold, and verify that the power-law behavior is kept as long as reasonable values of this parameter are chosen (extreme choices, with, $S_{th} \to 0$ for example, would modify the results, but this represents a rather unrealistic case). We fix $S_{th} > 0.5$, as reducing it may give problems with decisions with only two or three options. On the other side, we observe at Fig. 2.13 right that neither variations in d_p nor in τ_m values modify significantly the $\sim n^{-3}$ behavior as long as some significant level of memory and prospection is kept. This checks that the exponent remains as a robust feature of the algorithm, independent of the memory and prospection parameters, as well as the threshold S_{th} used in the algorithm.

We stress that the classical SPRT criterion, as well as other variations we have numerically explored, are unable to reproduce the -3 exponent and would lead to much smaller exponents and/or faster (exponential-like) decays in $P(n)$. This, together with the reliability analysis reported here, provides significant robustness to the entropy threshold criterion proposed here.

To provide even further evidence of the compatibility of the experimental results with

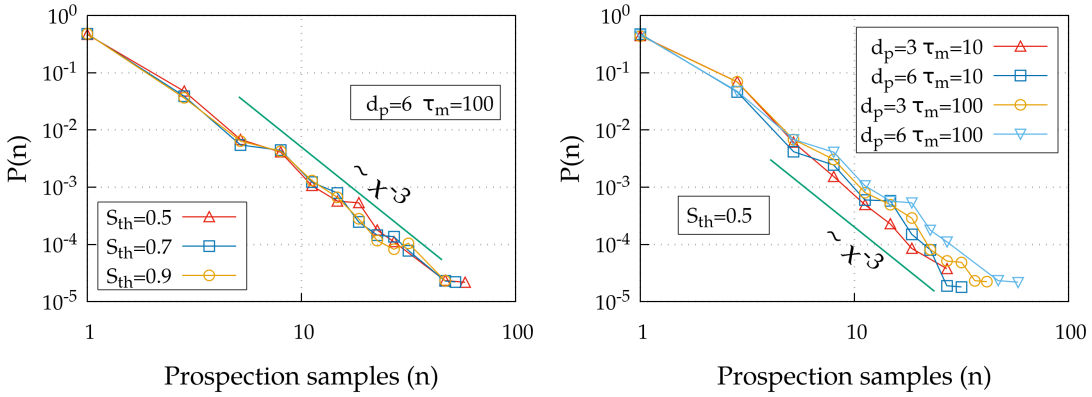

Figure 2.13: *a) Distribution of the number of prospections performed by the walker before making a movement for the fixed parameters $d_p = 6$ and $\tau_m = 100$ and a variable entropy threshold S_{th}. b) Distribution of the number of prospections performed by the walker before making a movement for a fixed entropy threshold $S_{th} = 0.5$ and different S and τ_m.*

our information-theoretical (entropy refinement) criterion, we quantify the payoffs E_i and the corresponding entropy S at the instant at which each decision is made by the subject in the experimental task (figure 2.14). We remind that the SPRT criterion for canonical probabilities (equation 2.3) is equivalent to impose that a threshold in the payoff difference ΔE triggers the decision (see Section 2.1.1), while for our criterion it is the entropy S which must reach a fixed threshold for the decision to be taken. For the experimental navigation task, we find that the difference ΔE (computed between the choices with lower and higher payoffs at the decision time) is a monotonically growing function of the decision time, so longer decisions require longer payoff accumulation (figure 2.14 a)). On the contrary, the informational entropy S remains approximately independent of the decision time, suggesting that this magnitude is really an invariant for all decisions and so supporting the view that a threshold in S may trigger the decision (figure 2.14 b)). This seems to be particularly robust for longer decisions, while shorter ones (< 2 seconds) may be probably induced by an automatic response, or simply taken at random without a proper amount of information gathering, so they probably do not follow the criterion above. Apart from such situations, however, it is clear that our results support the compatibility between experimental data and the **entropy refinement** mechanism for human choices under the navigation task used.

The analysis used here, based on comparing the navigation abilities of virtual subjects (or physical models) to those of human subjects, provides then an ideal way to reach a quantitative characterization of the cognitive memory and the prospection ability that should be required in sequential decision-making environments. Furthermore, the distribution of decision (or gazing) times together with the study of the final values for S reached at the moment of the decisions allows us to think that the criterion proposed here provides a good approximation to the real mechanisms of information processing employed by the subjects during the task. The fact that the power-law scaling scaling $P(t) \sim t^{-3}$ for decision times in our mechanism emerges in the binary toy model in Section 2.2.1 as well as in the virtual algorithms (where not binary but multiple choices are available) reflects also the robustness of the results. At this respect, it is important to note that traditionally

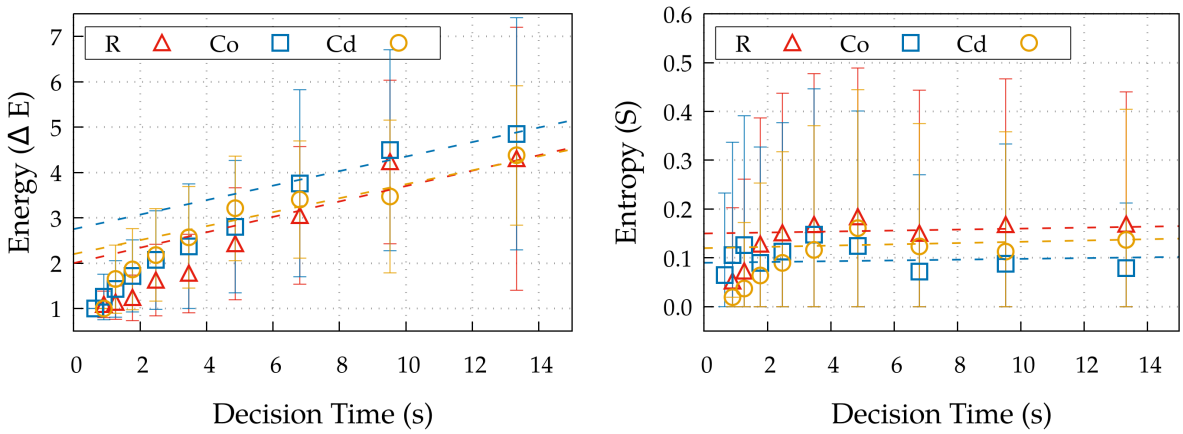

Figure 2.14: *a) Experimental payoffs difference ΔE between the options (directions) with more and less accumulated evidence when the decision is made. The x-axis groups the decisions by their corresponding decision time. The fitted curves are $f(x) = 0.17x + 2.02$ (Rectangular), $g(x) = 0.16x + 2.73$ (Circular Ordered) and $z(x) = 0.15x + 2.21$ (Circular Disordered). b) Experimental Shannon's entropy S according when the decision is made. The x-axis groups the decisions by their corresponding decision time. The fitted curves are $f(x) = 0.001x + 0.150$ (Rectangular), $g(x) = 0.000x + 0.096$ (Circular Ordered) and $z(x) = 0.001x + 0.122$ (Circular Disordered).*

mean times to decision, as well as the ratio of the times corresponding to choosing option A or B (for binary decisions) have been studied in detail by psychologists. On the contrary, decision time distributions are rarely computed in decision-making experiments. Our work has shown that such distributions can be used as a signature to discriminate between models.

Concluding remarks

- Memory and prospection are experimentally found to take part in the cognitive mechanisms that humans use for sequential decision making, as in navigation trough mazes. That conclusion can be obtained through eye-tracking data without a need for electroencephalographic (EEG) monitoring.
- Decision making dynamics used by humans in navigation tasks is compatible with a mechanism based on the computation of informational entropy to reach a given level of reliability.

Part II

Collective behavior

Introduction

In the previous Chapters of this thesis, we explored how isolated individuals may adapt their movement strategies for the sake of an efficient (intelligent) performance through a physical description of their cognitive mechanisms.

Nevertheless, in most realistic situations living organisms share their space and compete for resources with other organisms. This constant relation between individuals may altere their behavior [203], providing a broad range of scenarios where the **interactions** have consequences at very different levels.

M. Gell-Mann's Quote

You don't need something more to get something more. That's what emergence means.

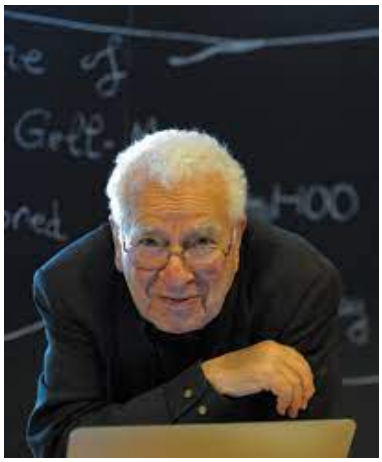

Portrait of Murray Gell-Mann. Image taken from [204].

For example, living in crowded ecosystems may affect the reproduction and the population of species [205, 206]. Or the competition for the food resources may drastically modify their evolution [207, 208], leading to species migrations or even extinctions.

However, not all the consequences of being part of a crowded space are detrimental. Organisms lacking complex cognitive capacities have been reported to interact with others to provide a **collective response** to a given situation [209–211]. Individuals join or combine their capacities, leading to a social cooperation [212]. That mechanism, that sums up the cognitive capacities of simple individuals, allows the individuals to process more contextual information (and more accurately) for the sake of a better adapted response. This collective ability corresponds then (loosely speaking) to an intelligent trait.

That **collective level of intelligence** can be observed at different scales (see figure 3.1). Bacteria use collective behavior to generate combat strategies [213, 214]. They also exhibit collective growing (fractal) patterns in culture growth [215, 216]. Cells coordinate their movement and their actin dynamics when migrating to shape tissues, to vascularize tissues, in wound healing and others processes [217, 218].

Ants in a colony organize themselves to distribute tasks, even to develop strategies that are unfeasible at an individual level [219, 220]. In aquatic ecosystems, one can observe how the fish form schools: through the coordination of their movement, the individuals respond more efficiently to stressful scenarios [221], such as predation risks [222, 223]. The collective behavior also appears in aerial ecosystems. Birds species form flocks, where they fly collectively [224], to increase the capacity to avoid predators or the food intake [225]. Humans also feature collective behavior in many scenarios [226–228]. The interactions between many individuals could provide collective patterns such as pandemic dynamics [229] or opinion contagion trough social media [230–232].

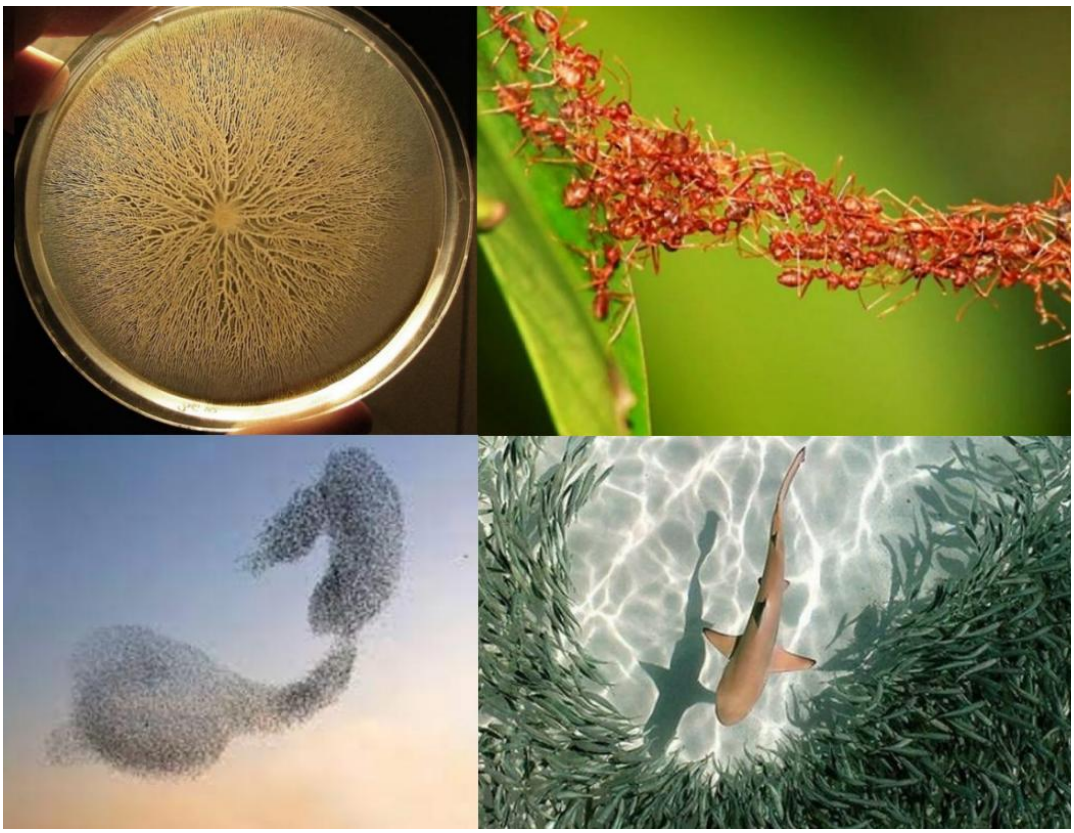

Figure 3.1: *Left upper image corresponds to the fractal structure created by bacterial growth. It is taken from [233]. Right upper image corresponds to cooperative ant colony which creates a bridge trough the interaction between multiple individuals. The image is taken from [234]. Left image corresponds to a fish school avoiding a predator. The image is taken from [235]. Left lower image corresponds to a bird flock, where the individuals fly showing cohesion. The image is taken from [236].*

Physics has been dealing with the concepts of **organization** and **synchronization**, which are the fundamental traits of collective behavior, for decades [237–239]. For example, many materials exhibit a broad set of collective features, where the interactions between atoms, molecules or colloids derive in collective movement patterns or spatial structures. The spatial self-organization of the graphene atoms promotes the appearance of stimulating physical properties, such as high termal and electric conductivities while keeping the structure resistent and light [240]. The spins (magnetic moments of the molecules) interact between them, yielding collective magnetic states in ferromagnetic materials [241]. Even the transition between a liquid phase and a solid phase in a glass of water is due to the collective organization of the molecules as a result of the underlying interactions

[242]. These features, among others, have promoted the development of experimental and theoretical studies to understand how interactions between the components of the system lead to the emergence of collective patterns.

However, the major part of the existing physics literature focuses on the case where systems are in equilibrium. The nature of living organisms keeps them far from equilibrium in most cases, as they are continually modifying their state. This trait of living organisms makes the development of complete theoretical frameworks difficult and enhances the role of the computational analysis.

The second part of the thesis is dedicated to exploring how the straightforward framework described previously for search patterns of isolated individuals can be extended to the multi-organism scenario. By focusing on how the individuals interact and how their internal mechanisms get affected by being part of crowded environments, we analyze the emerging movement patterns and their consequences over their targets under different circumstances. Combining experimental, theoretical and computational analysis, we address how the contextual information processing (including relating with others) is transformed into the physical energetic landscape $f(E)$ and how the collective patterns emerge from that mechanism.

From one to multiple random searchers

3

Nature is constructed mostly by very crowded environments, where the individuals are obliged to compete or socialize. The search process is not an exception to this, and the interactions with other organisms may condition the optimal movement strategies or even create new ones when referring to efficient searches. For example, it has been extensively reported that diverse species organize themselves at a social level to increase the food intake [243–245].

The aim of this Chapter is to extend the Random Walk scenario introduced in Chapter 1 to a **multi-walker** one, maintaining the complexity of the cognitive mechanisms and information processing used there. To be more concrete, we focus on how the presence of a variable number of walkers impacts the search efficiency, characterized by the coverage time T_c.

Let's start with the case of non-interacting walkers. For this case, the situation is reduced to a superposition of uncorrelated trajectories. Thus the coverage process is done at a rate that depends on the number of walkers (n). One can derive that the superposition of trajectories without any interaction (either direct or indirect) between them leads to the approximate expression $T_c(n) \sim \frac{T_c(1)}{n}$ when the walkers positions lack any correlation between them. In this case, $T_c(n)$ corresponds to the time where all the sites have been covered combining the n walker's trajectories.

However, the validity of this relation when the walkers interact between them, leading to correlated paths, is far from clear. One can introduce the social effect into the walkers dynamics in multiple ways. Here, we propose an **indirect interaction**, where all the walkers share the information contained within the cognitive map. Thus, the walker decision algorithm is equivalent to the one of the isolated case, but the energetic landscape is generated by the trajectories of all the walkers. That shared memory has been shown to be a fundamental part of insect navigation [246, 247]. It also represents a proxy for signal deposition (chemotaxis) in

bacterial or ants systems, where the individuals can detect the paths of other organisms.

We put the focus on the energy landscape generated by the bSAW model (Section 1.3). During the next paragraphs, we provide a detailed study of how the cognitive parameters, represented by the prospection length d_p, the evaporation time τ_m and the self-avoidance intensity β, coupled with the number of walkers n, modify the coverage time T_c. For the sake of clarity, we split the analysis in two Sections: one corresponding to the process in a one dimensional space and another one in a two dimensional space .

3.1 Searching through a one dimensional lattice

As a reminder of the bSAW model explored in Chapter 1, the space is discretized into sites. The sites that have been visited are assigned an energy $E_i = 1$, while the non-visited ones are assigned to an energy $E_i = 0$. The prospection length d_p allow the walkers to use the information of non-local sites to compute the next movement probabilities. The evaporation time τ_m corresponds the average time in which the energy of visited site is reset from $E_i = 1$ to $E_i = 0$ due to the impairment.

To start the analysis, we focus on the case where the evaporation time is infinite ($\tau_m \to \infty$). We provide the computational analysis of the coverage time T_c as a function of the number of walkers n for different values of the self-avoidance intensity β and the prospection length d_p in figure 3.2. There, one can observe that the prospection length d_p barely modifies the search efficiency. The effect of β, on the contrary, is more complex. When the self-avoidance is not very intense ($\beta \leq 1$), the addition of more walkers reduces the coverage time. That could be expected intuitively, as to add more walkers to cover a region of the same size should be beneficial. In the lower panels of figure 3.2, one can observe that for those β values, the coverage time asymptotically scales as $T_c(n) \sim \frac{T_c(1)}{n}$ with the number of walkers (the coverage time T_c in the figure was rescaled by n , showing a constant plateau). Thus, this case is equivalent to the non-interacting case, which implies that the indirect interaction plays a minor role under these circumstances.

However, as the self-avoiding intensity gets increased, the dependence of T_c when there are just a few walkers changes drastically (see figure 3.2). One can observe that the scenario that minimizes the coverage time when $\beta >> 1$ is $n = 1$. Unexpectedly, there is a **"more is less"** effect, where to add more walkers increases the coverage time. For $\beta = 5$ and $\beta = 100$ values (and for any d_p), one observes that the maximum T_c (the worst search efficiency) is produced when $n = 2$. Thus, the scaling with the number of walkers is far from trivial. It has to be noted that the non-interacting scaling $T_c(n) \sim n^{-1}$ also appears when the number of walkers is sufficiently large even for large β values. For this case, the probabilities p_i are strongly modified by the energetic landscape and the non-interacting feature should have a different origin when compared to the low β case. As stated in Chapter 1, the coverage time is governed by the finding of the last sites. When there is just one (or a few) site(s) to visit, the shared energetic landscape is homogeneous and the process corresponds to a superposition of diffusive trajectories (which is equivalent to the non-interacting case).

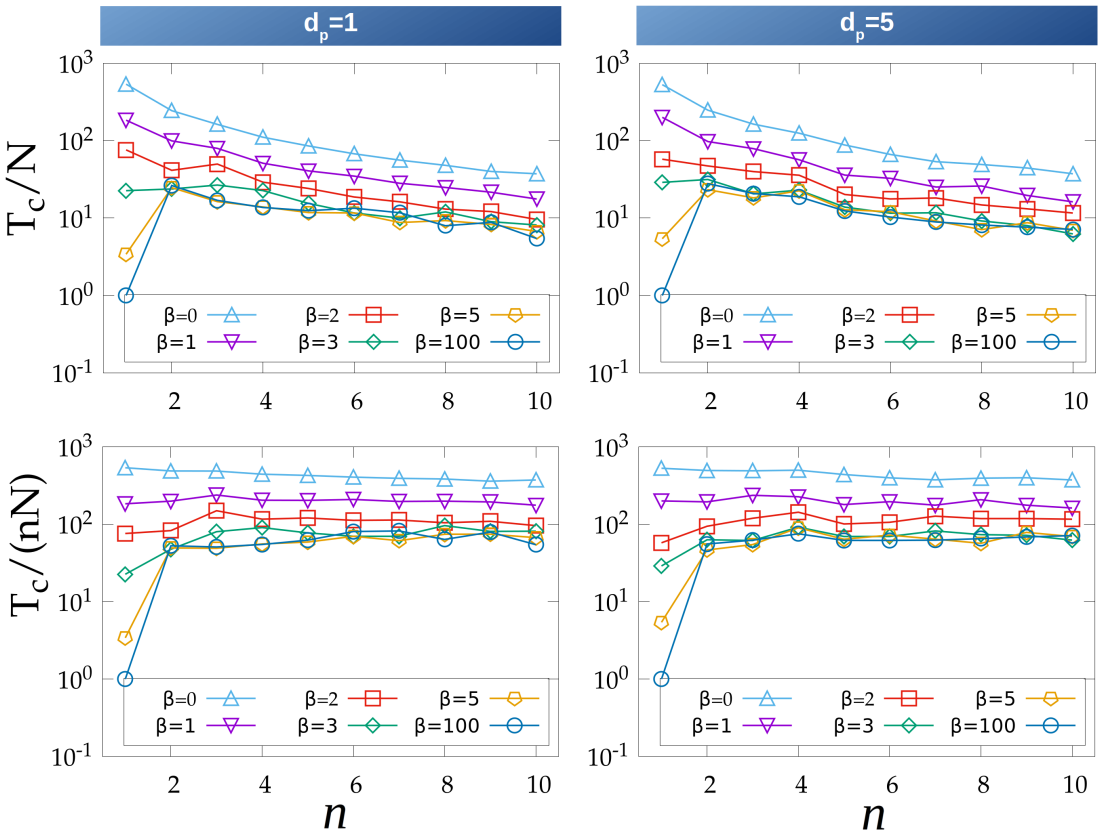

Figure 3.2: *Upper panel: Coverage time T_c as a function for of the number of walkers n for different β values (left image corresponds to $d_p = 1$ while the right image corresponds to $d_p = 5$). Lower panel: Scaled coverage time $\frac{T_c}{n}$ as a function for of the number of walkers n for different β values (left image corresponds to $d_p = 1$ while the right image corresponds to $d_p = 5$). All the results are obtained from a $N = 1024$ one dimensional lattice without impairment.*

One can wonder whether these results become modified if a evaporation time τ_m is introduced. We analyze how τ_m modifies the multi-walker dynamics. The information of a site i is forgotten or evaporated ($E_i = 1 \rightarrow E_i = 0$) after a random time τ starting from the last visit to that site. For simplicity, again we will consider that this time is obtained from an exponential distribution with characteristic time τ_m (as introduced in Chapter 1).

We provide the computational analysis of the coverage time T_c according to the number of walkers n when the evaporation time is tuned at figure 3.3. For an intermediate intensity of self-avoidance ($\beta = 3$, figure 3.3 upper panel), one can observe that the addition of more walkers reduces the coverage time (except for the case of two walkers with large evaporation time). The prospection length, again, does not seem to modify this dynamics.

However, for a very strong self-avoidance ($\beta = 100$), the computational results provide a quite different scenario. When the walkers cannot prospect ($d_p = 1$), the best strategy is to restrict the search to a one individual. But how it evolves with the number of walkers is strongly dependent on the evaporation time τ_m and the prospection length d_p. The presence of a finite optimal τ_m (explored in the first part of the thesis) seems to be maintained even when there are multiple walkers.

That optimal τ_m is approximately of the size of the region to be covered. In these circum-

stances, a larger prospection length is beneficial when the evaporation time is large, and detrimental when the evaporation rate is increased.

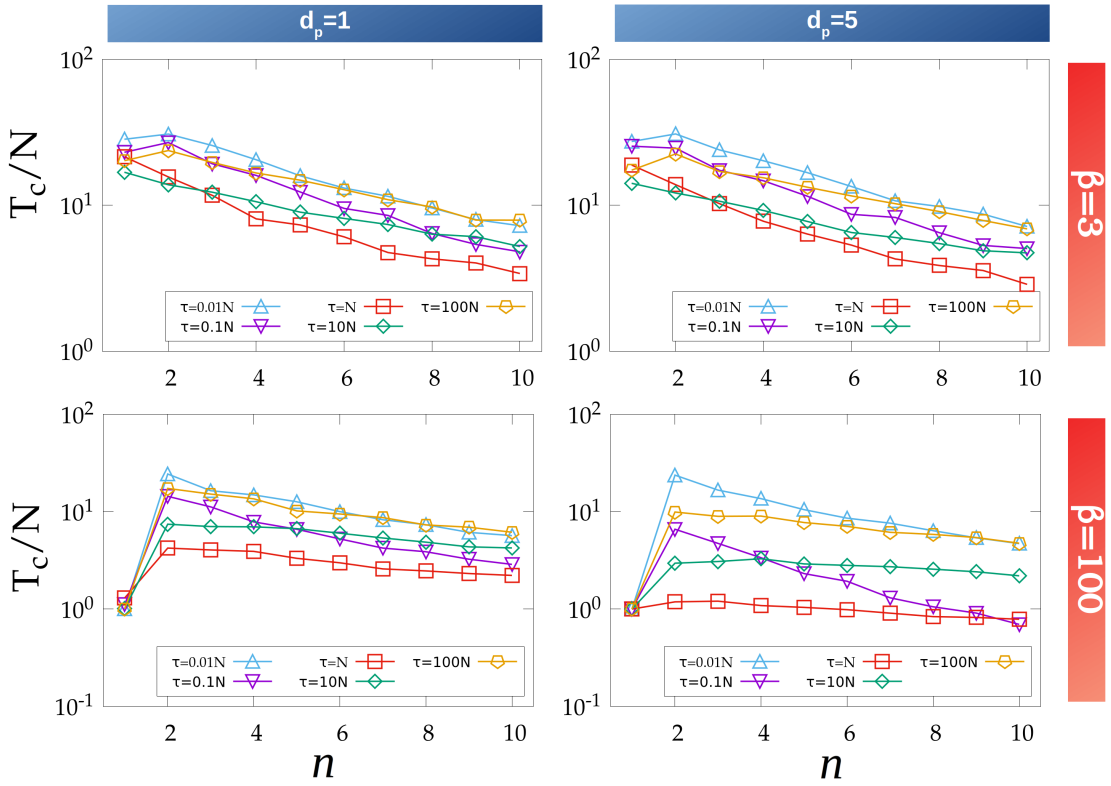

Figure 3.3: *Upper panel: Coverage time T_c as a function for of the number of walkers n for different τ_m values when $\beta = 3$ (left image corresponds to $d_p = 1$ while the right image corresponds to $d_p = 5$). Lower panel: Coverage time T_c as a function for of the number of walkers n for different τ_m values when $\beta = 100$ (left image corresponds to $d_p = 1$ while the right image corresponds to $d_p = 5$). All the results are obtained from a $N = 1024$ one dimensional lattice.*

3.1.1 The 2-walker scenario in one dimension

Given the unexpected feature that the addition of more walkers to the search can make the process slower, we explore in detail the dynamics for the two-walker scenario and why it can reduce or increase the coverage time of the one-walker search depending on the parameter values.

When the search process is commanded by two (or more) walkers, in the initial step each walker chooses randomly between the two possible directions available. However, the possibility of crossings with the previous trajectory of the other walker will affect significantly the subsequent dynamics of the coverage. The case when $\beta \to 0$ is again independent of the evaporation and prospection mechanisms, as both walkers moves diffusively and there are no energetic landscape effects. The scenario becomes more complicated when the self-avoidance gets important. A walker, in this case, tends to move ballistically as long as it does not find the region which has been visited by the other, but eventually it will interfere with the other walker's path. When this happens, one can split the corresponding situations into **two classes**.

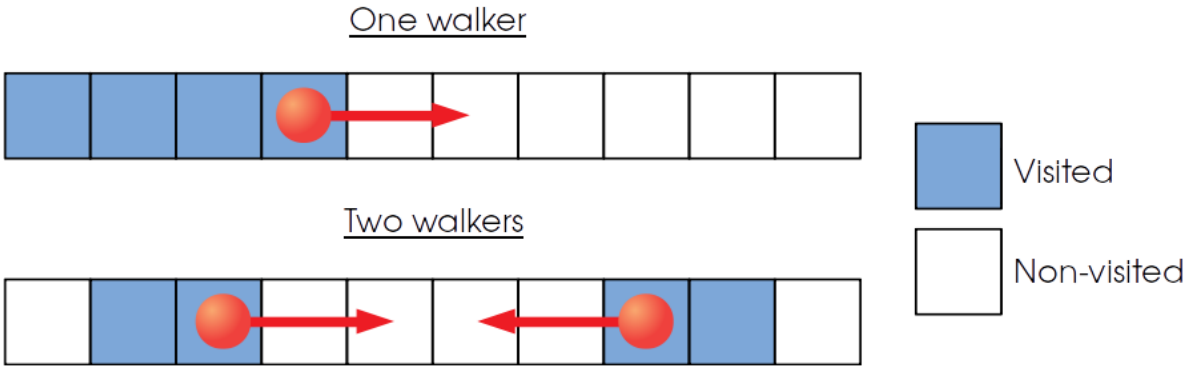

Figure 3.4: *Schematic representation of how the dynamics is modified between the one-walker and two-walkers scenarios. The blue squares corresponds to visited sites, while the white ones, to the unvisited sites. The two-walker version has been defined to exemplify the crossing or collision between walkers, creating the escape region.*

The first class corresponds to the situation where the two walkers are moving in the same direction. Initially, both perform a ballistic movement. When one walker (walker A) meets the path of the other one (walker B), the ballistic movement of the walker A is suppressed. However, due to the periodic boundary conditions of the lattice, the walker B keeps its ballistic movement until it reaches the path of the walker A. When that occurs, it means that the entire lattice has been explored, and then, the cover process is over. If the walkers can start the coverage process at any site of the lattice and with the consideration of periodic boundary conditions, the average distance between the walkers A and B at the initial step corresponds to $\Delta x = \frac{N}{4}$. So the walker A covers in average $\frac{N}{4}$ sites until its ballistic movement is suppressed. Simultaneously, the walker B can cover **ballisticaly** the $\frac{3N}{4}$ sites until it reaches the path of the walker A. The dynamics described above, under those initial circumstances, leads to an averaged coverage time $T_c(2) \approx \frac{3}{4}T_c(1) = \frac{3N}{4}$.

The second class corresponds to the case when the two walkers move in opposite directions at the initial step. Initially both walkers move ballistically again. However, there is a time step where the walkers necessarily cross their paths (see figure 3.4). If the initial distance between them is z, that process take $T = \frac{z}{2}$ steps.

Since both walkers have left a visited region behind them, they find themselves in the middle of a homogeneous energy landscape with sites with energy $E_i = 1$ (visited). For this reason, both will move **diffusively** until they escape from the joint visited region that they have created. The escaping time is

$$T \sim \frac{z^2}{8D} = \frac{z^2}{4}, \tag{3.1}$$

where $D = \frac{1}{2}$ (see Section 1.1). When z is large, this stage will be much larger than the previous one and it will govern the coverage time T_c.

The last part corresponds to the new ballistic span that the first escaping walker performs until the lattice is completely covered (we have dismissed the possibility of both walkers escaping at similar times). As z sites has been covered in the first stage, the escaping walker

needs $N - z$ steps to complete the coverage.

The two scenarios described above can appear with the same probability ($\frac{1}{2}$ each). According to all the initial positions where the walkers can start the process, one can derive an approximate estimator of the $T_c(2)$ that reads

$$T_c(2) \approx \frac{1}{2}\left\{\frac{3N}{4} + \frac{1}{N}\int_0^N \left(\frac{z}{2} + \frac{z^2}{4} + (N-z)\right) dz\right\}, \tag{3.2}$$

which leads to

$$T_c(2) \approx \frac{N^2}{24} + \frac{3N}{4}. \tag{3.3}$$

This expression is strongly dominated by the diffusive (quadratic) term when N is large.

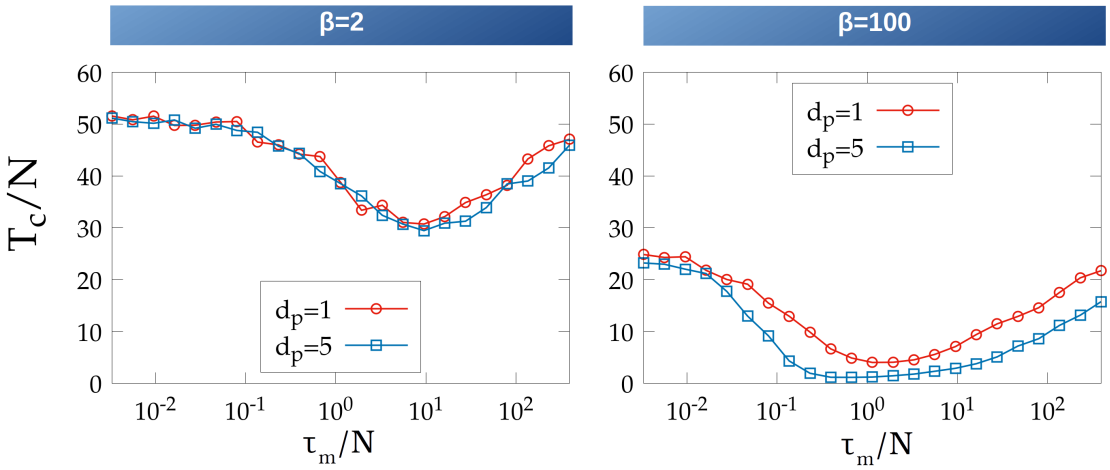

Figure 3.5: *Coverage time T_c as a function for of the evaporation time τ_m for two different prospection lengths and slef-avoidance intensities when the number of walkers is 2 (left image corresponds to $\beta = 2$ while the right image corresponds to $\beta = 100$). All the results are obtained from a $N = 1024$ one dimensional lattice.*

The same mathematical procedure can be applied to the case of multiple walkers. However, the straightforward analysis of the two walkers case provides a clear insight about why adding more searchers to the process may become detrimental to the coverage time when the self-avoidance is intense. The current analysis has been done for lattices with periodic boundary conditions, but one can expect for the case of reflective conditions a stronger effect since then the effect of trapping is produced also at the boundaries. On the contrary, this feature is not relevant for lower self-avoidance intensities, as there the two walkers do not necessarily move ballistically in the initial steps, but they get trapped into their own visited region most of the time, so the influence of the path followed by the other walker is relatively unimportant (it is generally diffusive from the beginning).

To complete the study of the two walkers scenario, we finally analyze how the combined effect of all the prospection length d_p, the self-avoidance intensity β and the evaporation time τ_m impact the coverage efficiency for this concrete case. One can observe at figure

3.5 how the optimal finite evaporation time already reported in Section 1.4, meaning that to forget part of the previous trajectory optimizes the process, appears for any β or d_p considered here. We have reported in Chapter 1 that modifying d_p does not modify the walker dynamics once the walker moves ballistically (high β values). However, for the case of two walkers, figure 3.5 reports that for large β values, a larger d_p seems to reduce T_c. The walkers can detect the end of the escape region from larger distances, and correspondingly, the coverage will be reduced as each trapping stage is reduced.

3.2 Searching through a two dimensional lattice

One can wonder if the effect of the crossings between walkers and its consequences over the search process would be different in a two dimensional space. According to the explanation given in the previous Section, such crossings will largely depend on the **topology** of the region to explore. In two dimensions, the walkers will more easily avoid the overlap with previously visited regions (see figure 3.6).

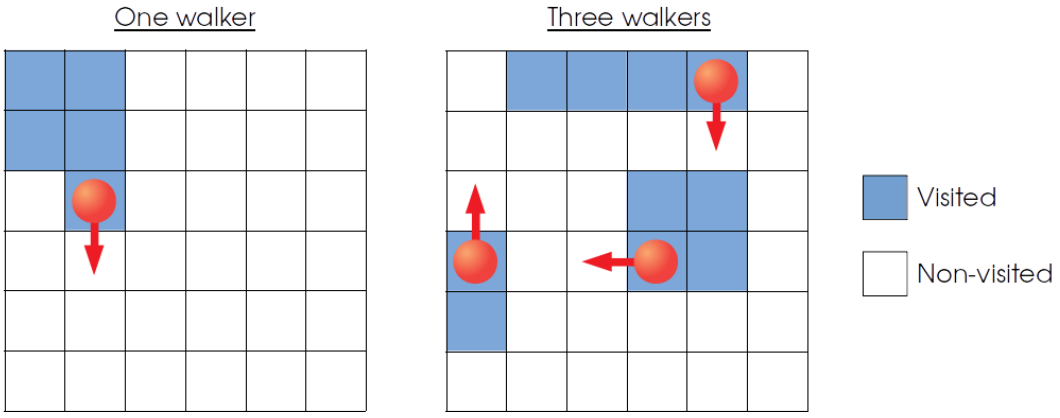

Figure 3.6: *Schematic representation of the dynamics when the number of walkers is $n = 1$ and $n = 3$ in a two dimensional lattice. The blue squares corresponds to visited sites, while the white ones, to the unvisited sites.*

In this Section, we explore how the self-avoidance intensity β, the evaporation time τ_m and the prospection length d_p combined with the presence of multiple walkers affect the search process and if the "more is less" effect will appear in these circumstances.

By sampling computationally the parameter space, one can observe at figure 3.7 that for the case without evaporation ($\tau_m \to \infty$), all studied cases reports the same results of a **non-interacting** system, where $T_c(n) \sim \frac{T_c(1)}{n}$.

If we explore the results as a function of the prospection length d_p, they seem to reproduce the same features of the one-walker case (reported in Chapter 1). When self-avoidance intensity is low, to prospect for non-local information is detrimental for the coverage efficiency. When the self-avoidance is sufficiently strong, to prospect for non-local information optimizes the coverage process. That feature seems to appear for any number of walkers (compare left and right panels in figure 3.7 for short and large d_p, respectively).

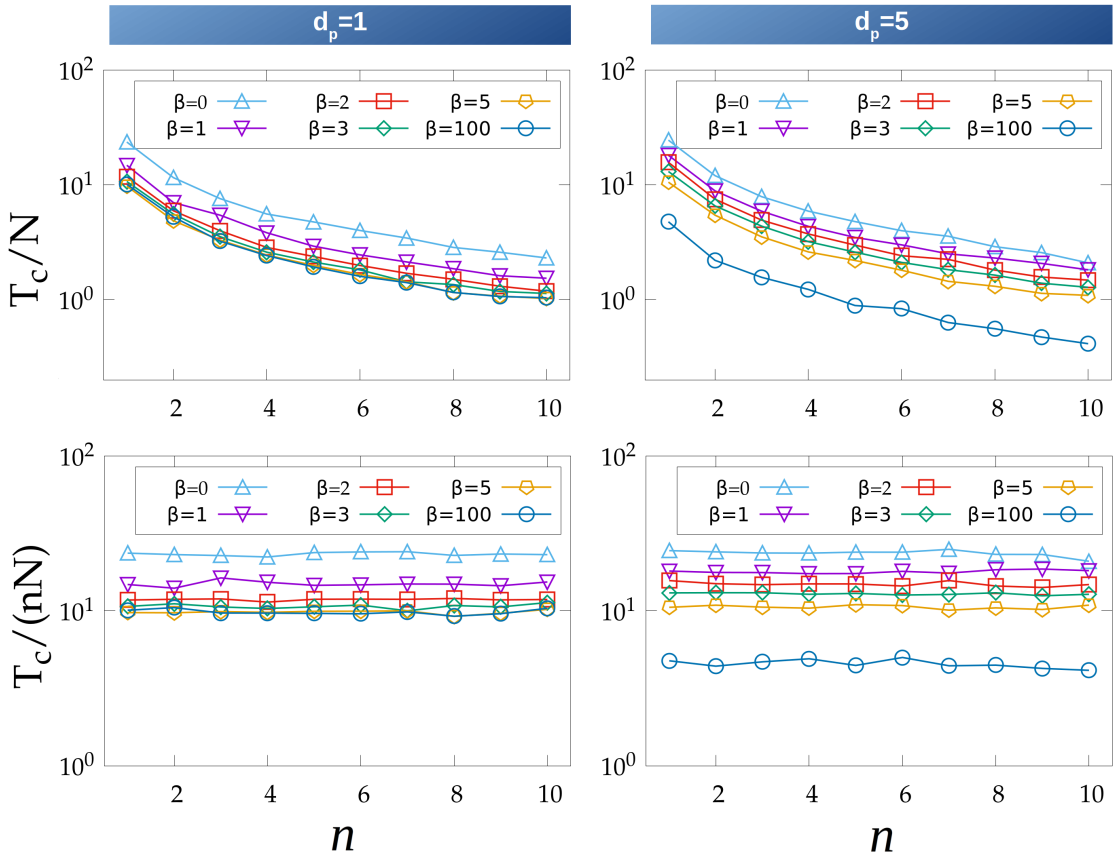

Figure 3.7: *Upper panel: Coverage time T_c as a function for of the number of walkers n for different β values (left image corresponds to $d_p = 1$ while the right image corresponds to $d_p = 5$). Lower panel: Scaled coverage time $\frac{T_c}{n}$ as a function for of the number of walkers n for different β values (left image corresponds to $d_p = 1$ while the right image corresponds to $d_p = 5$). All the results are obtained from a $N = 64 \cdot 64$ two dimensional lattice without impairment.*

When the impairment, or finite evaporation time τ_m, is introduced in the simulations, the results seems to remain unaltered. One can observe at the figure 3.8 that the coverage time T_c keeps scaling as $T_c(n) \sim n^{-1}$ when τ_m is modified for any β and d_p. In addition, it seems that the optimal evaporation time that has been shown for the one-walker case is also present in the multi-walker cases. One can observe that the lower curve (the more efficient coverage) always corresponds to finite evaporation times around $\tau_m \sim N$ (see figure 3.8).

We will not explore the behavior of the system for higher dimensions. Since $d = 2$ represents the critical dimension of a single self-avoiding random walk trajectory, the results for higher dimensions will be equivalent to those for regular random walks (including the scaling for $T_c(n)$), and so the effect of self-avoidance and impairment will be marginal there.

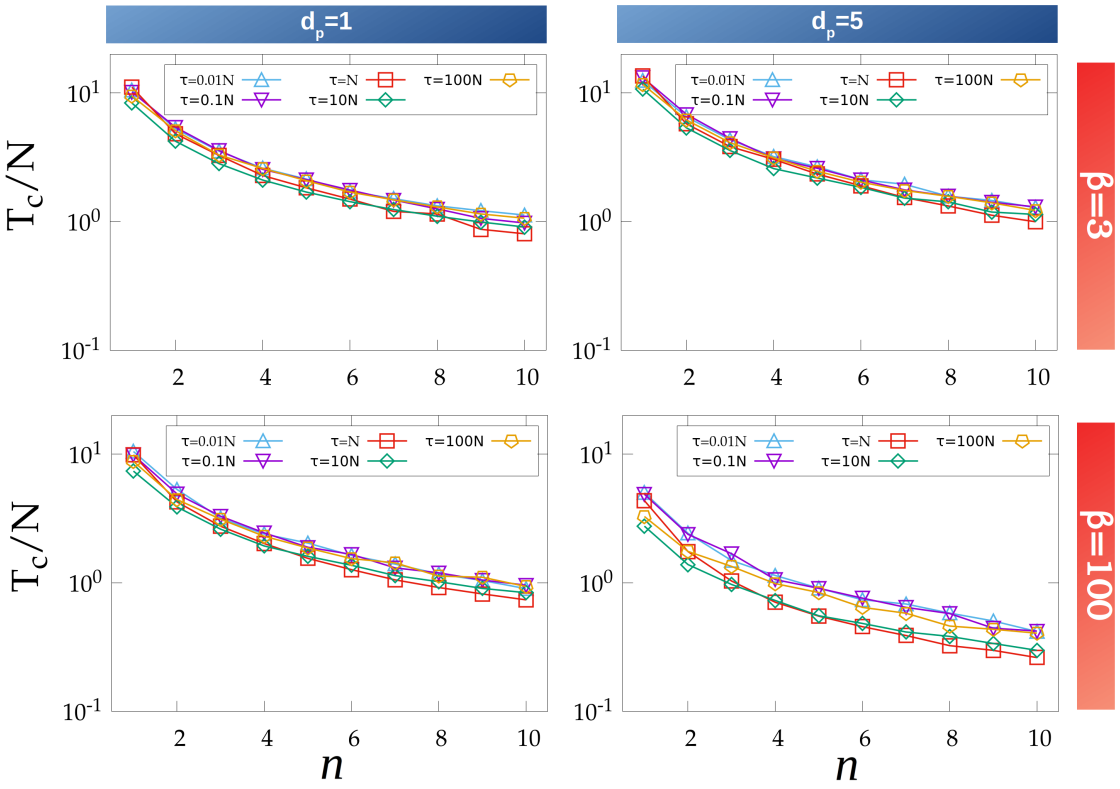

Figure 3.8: *Upper panel: Coverage time T_c as a function for of the number of walkers n for different τ_m values when $\beta = 3$ (left image corresponds to $d_p = 1$ while the right image corresponds to $d_p = 5$). Lower panel: Coverage time T_c as a function for of the number of walkers n for different τ_m values when $\beta = 100$ (left image corresponds to $d_p = 1$ while the right image corresponds to $d_p = 5$). All the results are obtained from a $N = 64 \cdot 64$ two dimensional lattice.*

Concluding remarks

- To add more individuals to a search process is not always beneficial. Under some circumstances, one can find the "less is more" effect, which is due to indirect interactions between the walkers, such that the signal left by one of them slows down the advance of the others.
- The topology of system largely determines the nature the indirect interactions, so it plays a fundamental role in the definition of an efficient search strategy.

A framework for pedestrian dynamics

4

Among all living organisms featuring collective behavior, the human beings probably exhibit the more variate set of examples [248]. Through interactions, we organize ourselves at many levels and we make collective patterns emerge, such as what occurs with epidemic processes [249] or population opinion evolution [165].

One subset of collective behavior in living organisms are the movement patterns appearing when they move within crowded environments. One example of **collective motion** patterns can be observed in crowds. In a crowd, the individuals may not be able to walk in their desired direction due to the collective (long-range) fluxes appearing as a result of the sum of interindividual (short-range) interactions. Another example can be observed when people get on the subway. When the density of pedestrians is high enough, people roll into a ball when trying to cross the doors. Thus, the individuals get stacked [250] altough this is detrimental for they aims. In both cases collective patterns govern the system dynamics, even if they go partially against individual tendencies or goals. However, through the interaction or communication between the individuals, efficient patterns can also be developed within crowds. **Lane formation** is a paradigmatic example. Pedestrians moving across a street can organize themselves onto the creation of two regions. The pedestrians moving towards the same direction of the street accumulate in one of those regions, easing the pedestrian flow, as it permits the individuals to move towards their targets with only little mishaps. When in a non-ordered crowd, a pedestrian dodges and faces constantly other pedestrians that come in the opposite direction. Even so, the self-emergence of those collective structures simplifies the cognitive complexity, easing the prospection for optimal paths and simplifying the response to possible collisions. Similar lane structures can be found in other systems, such ant colonies, which navigates trough those lines or trails to increase their foraging efficiency [251, 252].

A description of how pedestrian flows emerge from individual interactions represents a field of the greatest interest due to its direct impact on relevant issues of the daily life. For example, in urban planning, monitoring of public spaces or optimization of evacuation protocols, to name a few [253–255].

From a physical perspective, to implement the rules of ordering, alignment and self-avoidance (among other) between individuals is a great challenge. Thus, a significant effort has been put both in (i) understanding these interaction rules in order to recover the patterns observed in real scenarios [256, 257] and (ii) identifying the minimal models which are able to capture the essentials of such phenomena [258, 259].

4.1 How to model pedestrian dynamics

We explore in the next paragraphs the fundamentals of pedestrian modeling. In general, the description is done in terms of **agent-based models**, where each agent represents a pedestrian. Thus, the relevant work comes from the definition of the interactions and the study of how they can lead to complex patterns at the collective level.

4.1.1 The social force

In pedestrian modeling, the interaction between individuals should account for the contextual information coming from the other pedestrians or nearby obstacles. Traditional physical systems interact through forces coming from well-known energetic potentials, such as the electromagnetic or gravitational ones. The lack of an equivalent theoretical framework for pedestrians has instead led the scientists to explore context-based forces. Some examples can be found at [260, 261]. One approach that has been found to reproduce many of the crowd patterns is the **social force model** [262]. It is based on introducing a force composed by different terms, each describing a basic feature of the contextual processing of pedestrians.

The pedestrian dynamics is characterized by its velocity $\vec{v}$. The velocity $\vec{v}_k$ of the pedestrian k evolves according to

$$\frac{d\vec{v}_k}{dt} = \vec{F}_k + \eta(t) \tag{4.1}$$

where $\vec{F}_k$ corresponds to the social force and $\eta(t)$ corresponds to a white noise representing the fluctuations in the pedestrians dynamics. The social force is composed by three terms:

$$\vec{F}_k = \frac{1}{\tau_k}(\vec{v}^p - \vec{v}_k) + \sum_j -\nabla_{\vec{r}_{kj}} V_{kj}(||\vec{r}_{kj}||) + \sum_i -\nabla_{\vec{r}_{ki}} W_{ki}(||\vec{r}_{ki}||) \tag{4.2}$$

The pedestrian, when moving, does it to reach a given target (or direction). The first term forces the pedestrian to move in the direction of that target, which is defined by

the vector $\vec{e_k}(t)$. That will domain the pedestrian motion in the absence of obstacles or other pedestrians. However, the pedestrians do not accelerate constantly under these circumstances. To circumvent this, one uses the characteristic (or preferred) velocity $\vec{v}^p$, which is the velocity followed by the individual in the absence of obstacles or other pedestrians.

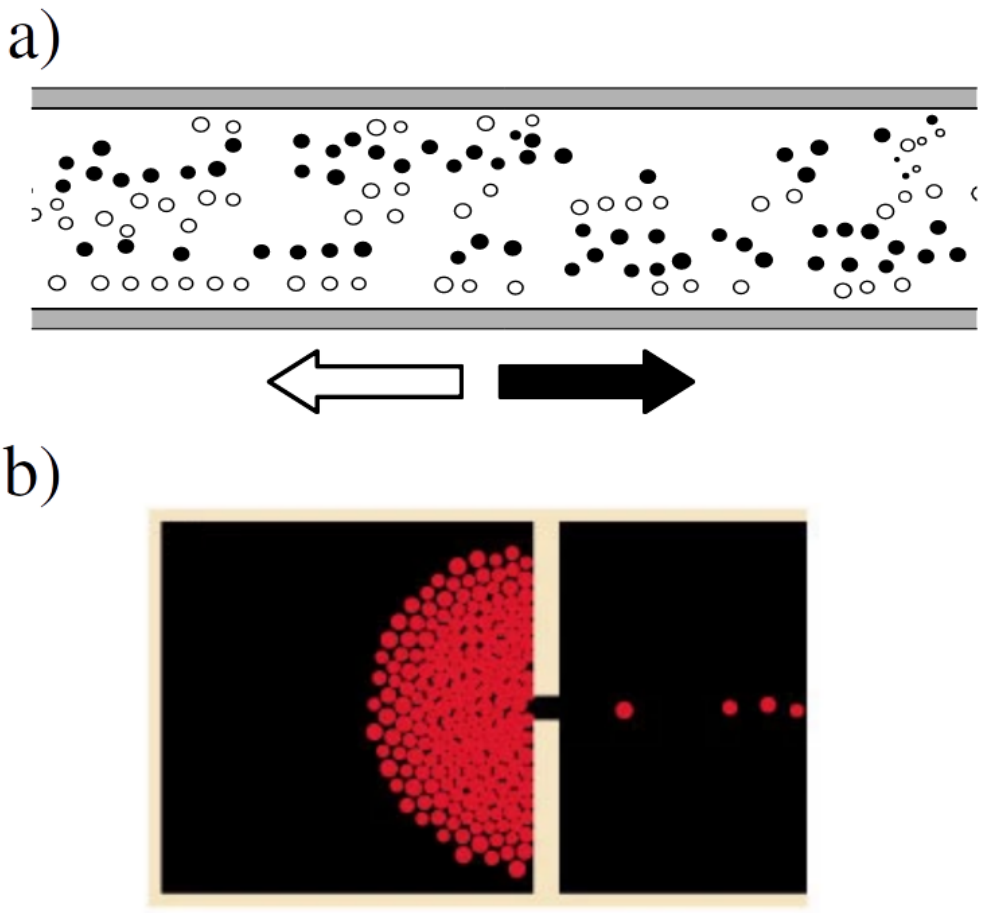

Figure 4.1: *a) Frame of a computational simulation where the pedestrians move across a corridor according to the social force model. With each half of the agents tending to go in one direction, the rest of the terms are enough to construct the collective lane pattern. The arrows correspond to the direction of the movement of the corresponding color agents. The image is taken from [262]. b) Frame of a computational simulation where the pedestrians try to escape from a room according to the social force model. The interactions lead to the collective to arrive to an undesired jammed state. The image is taken from [263].*

The second term accounts for the repulsion between pedestrians, which tends to avoid being too close to others. This effect is introduced as a repulsive force governed by the potential V_{kj}, which is supposed to decrease monotonically with the distance between the pedestrian k and the pedestrian j ($||\vec{r_{kj}}||$).

Pedestrians are sometimes attracted by other persons or objects These attractive effects contribute to the third and last term. Now, the potential W_{ki} monotonically grows with the distance between the pedestrian k and the pedestrian i ($||\vec{r_{ki}}||$), as it promotes attraction between the individuals. One expects the repulsive (second) term to dominate the pedestrians interaction when the individuals gets closer. However, the attraction (third term) may

dominate when pedestrians do not have to worry about immediate collisions.

To derive analytically the trajectory $\vec{r}_k(t)$ from the global expression for $\vec{F}_k$ is almost unfeasible. Nevertheless, one can run computer simulations to describe its behavior under convenient circumstances. The social force is sufficient to reproduce lane formation when the density of agents is high enough [262]. In figure 4.1 a), one can observe the self-organization of the system onto that state, where the pedestrians flow is maximized in comparison to a situation where the lanes are not formed. With the lanes structure, most collisions and reorientations are suppressed, allowing the pedestrians to move closer to their isolated ideal velocity. Other similar works have reported the clogging when the pedestrians are forced to go through doors or small channels and also movement waves that impacts into the collective dynamics (see figure 4.1 b)).

The social force framework is not the only way to describe pedestrian dynamics. It can also be done in terms of a cellular automata [264, 265]. In this case, the space is discretized and each pedestrian is assumed to occupy one single cell of the corresponding lattice. The interactions between individuals are thus introduced into the computation of the jump probabilities. As one can observe, this procedure is analogous to the one developed in Chapter 3.

4.1.2 Repulsive term proposals

The lane formation or the jamming patterns can be attributed in the case of humans to a complex decision-making based on visual information and subsequent prospection. However, simple rules have been proved to be sufficient to make those patterns emerge, as is the case of the Vicsek model for swarming dynamics [266, 267] or lattice-gas generalizations [268, 269].

Despite all this, the heterogeneity of models used nowadays to generate such flows/dynamics sometimes goes against the possibility of finding general and far-reaching conclusions. So, existing models/works can sometimes provide different or even contradictory conclusions [270]. Works aimed at providing unified frameworks and/or at revealing the common properties of these approaches are then convenient to promote understanding and theoretical research within the field [271].

Within this context, a valuable insight has been recently provided by Karamaouzas *et al* [272]. In their work, they have proposed an scheme to derive an inter-pedestrian force from experimental data. By analyzing 1500 trajectories of pedestrians in outdoor environments they found consistent evidence for an **effective potential** of interaction $V(\tau)$ between pairs, which was found to depend only on the **time-to-collision** τ between the individuals and not on the interparticle distance (as in the social force).

In addition, the time-to-collision concept is in line with the prospection of future outcomes as one of the main driving forces for intelligent agents, as happens with the Causal Entropic Forces [146, 273] discussed before in Section 1.5. Through cognitive mechanisms, the

pedestrian predicts the next collisions and respond accordingly (adapting its movement to avoid them).

In general, one can expect that bidirectional flows or lanes emerge from the tension between pair interactions and the existence of subpopulations that have preference for moving in opposite directions (representing the target or goals of the pedestrians). When the density of individuals ρ is large enough, the pedestrians freedom of movement gets reduced in a disordered medium due to collisions. The organization in lanes under these circumstances allows them to avoid a large part of those collisions and facilitates to move according to their targets.

In this Section, we explore numerically if the interaction mechanism by Karamouzas *et al* [272] based on the τ-space could represent a framework compatible with the large variety of inter-pedestrian interactions that can be found in the literature. More concretely, we explore if those inter-pedestrians interactions, which commonly depend on the distance between pedestrians and their velocity, can be mapped to a general interaction in the τ-space that is responsible of the pedestrians patterns.

We consider in the following an agent-based system where the dynamics of the agents is governed by a force

$$\vec{F} = \xi(\vec{v}^{\,p} - \vec{v}) + \vec{F}^{(sa)}. \tag{4.3}$$

Here, the first term accounts for the preference of each individual to maintain its preferred velocity $\vec{v}^{\,p}$ (denoting $\vec{v}$ as the actual velocity) with a certain intensity that we call the **stubbornness**, ξ. The value of ξ is strictly positive so that the first term acts as a restoring force to reach the preferred velocity (similar to the first term in equation 4.2). In order to generate bidirectional fluxes we assume two different subpopulations with the same number of agents each, whose preferred velocities are the same in modulus but have opposite directions. In particular, to avoid spurious effects in the simulations we sample for each agent a stochastic preferred speed from a Gaussian distribution with mean $\langle v^p \rangle = 1.3$ m/s and standard deviation $\sigma_v = 0.1$ m/s. These specific values are in agreement with those used in [272] and similar works on pedestrian dynamics [274, 275].

On the other hand, $\vec{F}^{(sa)}$ stands for the pair (self-avoiding) interaction between agents. For the sake of completeness, we propose to compare the results for three rules/mechanisms for $\vec{F}^{(sa)}$ based on completely different grounds. The goal, as exposed before, is to understand the origin of the interaction in the τ-space found in [272] and how universal such interaction might be.

i) Repulsive interaction The first proposal we will study consists of a more 'physical' pair repulsive interaction in the radial direction, $F^{(sa)}_{\vec{rep}} \sim r^{-k}$ (where r is the distance between

pairs of pedestrians), with $k > 0$. We introduce a repulsive pair energy which is a function of the distance r between the agents,

$$\vec{F}_{rep}^{(sa)} = -\frac{A}{r^k}\vec{e}_{ij}, \tag{4.4}$$

where $A > 0$, $\vec{e}_{ij}$ is a unit vector in the direction joining the pair of interacting agents, and the distance r is measured in units of the pedestrian's diameter, so $r = 1$ corresponds to the distance between two adjacent agents. The parameter k regulates the decay of the force, so implicitly it determines the range of scales where its effect is relevant, with the limit $k \to \infty$ reproducing hard-disk interactions with a characteristic disk size $A^{1/k}$. In this case the effect of $F_{rep}^{(sa)}$ is to pull all the individuals apart, regardless of the fact that they are moving forward to a collision or not.

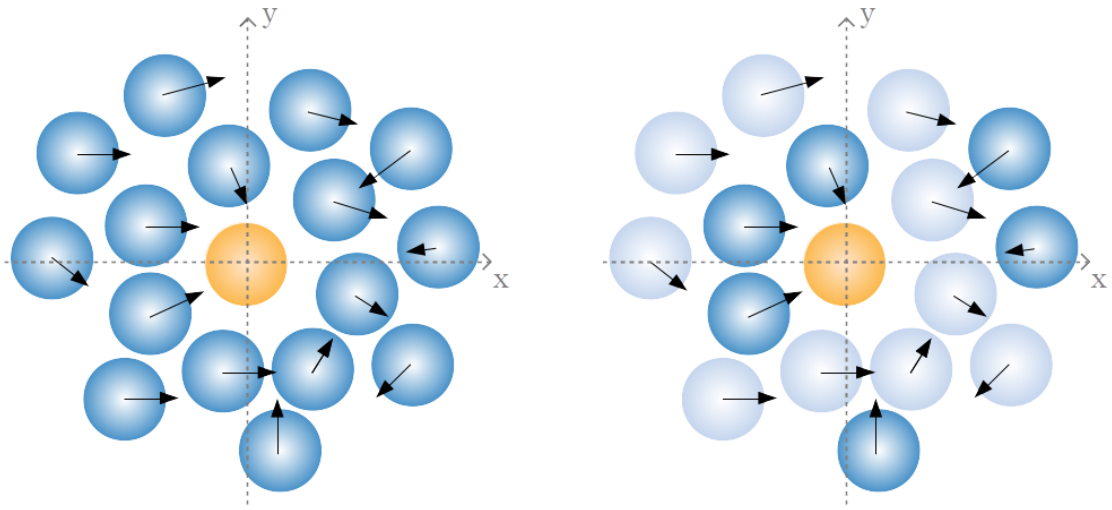

Figure 4.2: *Representation of the differences between the interactions based on the distance r (left) and those in the τ-space (right). The arrows represent the relative velocity of the agents respect to the orange agent at the origin. The individuals filled with solid blue are the only ones contributing to interactions with the orange one (it is, in the second case only those for which a finite and positive τ can be defined).*

ii) Time to collision interaction The second one corresponds to the effective potential empirically obtained in [272], this is, a repulsion in the time-to-collision (ttc) space, $F_{\mathbf{ttc}}^{(sa)} = -\nabla V_{\mathbf{ttc}}$, with $V_{\mathbf{ttc}} \sim \tau^{-2}$. This time τ can be explicitly defined in terms of the relative velocity $\vec{v}_r$ and the relative position $\mathbf{r}$ between two given particles,

$$\tau = \frac{-\vec{r}\vec{v}_r - \sqrt{(\vec{r}\vec{v}_r)^2 - |\vec{v}_r|^2(|\vec{r}|^2 - D^2)}}{|\vec{v}_r|^2}. \tag{4.5}$$

The rule reads then

$$\vec{F}_{tcc}^{(sa)} = -\nabla(k_\tau \tau^{-2} e^{-\frac{\tau}{\tau_0}}), \tag{4.6}$$

with $k_\tau > 0$, $\tau_0 > 0$, and D corresponding to the agent's diameter.

The potential so defined only applies to agents moving forward to a collision, such that τ for that pair can be defined and is positive. Then, pairs for which a positive value of τ cannot be found are considered as noninteracting agents. As a result, the set of agents interacting with a given one is a dynamic object which is updated continuously throughout the simulation (see figure 4.2). The exponential term is used as a cutoff to block the effect of outermost collisions, so introducing the idea that agents possess a characteristic radius of perception (τ_0, defined in the τ-space). This idea of a finite perception horizon has been explored before during this thesis: in Chapter 1, Chapter 2 and Chapter 3, the walkers could prospect up to a distance d_p. Both situations correspond to different manners of introducing those perception limit, either in the real space or in the τ-space.

iii) Heuristic rule Finally, as a third case, $F^{(sa)}_{\text{heu}}$, we consider a nonphysical (heuristic) rule which has been found to reproduce most features of collective behavior in pedestrians [276]. This rule is based on recomputing continually the direction of motion in order to maximize at each step the distance that the agent could travel without colliding with other agents. So, each agent samples its possible future trajectories by simulating internally (with a time horizon t_m) where it will reach by moving in a given direction (characterized by an angle α) for some fixed time, provided that the other agents are assumed to go on moving in their present direction. Again, a limit of perception is introduced to the algorithm through the parameter t_m. After sampling for a range of values of α (up to maximum α_{max}, to avoid sudden or extreme changes of direction) the agent will choose the one that maximizes the length covered d (assuming that all individuals maintain their current velocity and direction of movement). The minimization is done according to the following equation

$$d(\alpha) = d_{max}^2 + f(\alpha)^2 - 2d_{max} f(\alpha)\cos(\alpha_0 - \alpha), \tag{4.7}$$

where d_{max} corresponds to the maximum distance that would be covered without obstacles in the time horizon t_m and α_0 corresponds to the angle of the target. After the election, all the agents reorient synchronously and the internal simulation starts anew. A visual representation of the algorithm can be seen at figure 4.3. The mechanism again resembles the prospection mechanisms explored before.

There is a second rule, which determines the walking speed modulus after the reorientation. This is introduced in order to maintain a certain time to collision between the agent and the obstacle in the chosen walking direction [276]. For this, we define a minimum time τ_{min} such that times-to-collision are forced to stay always below τ_{min} by reducing adequately the speed of the agents. That speed is then computed at practice as $v(t) = \min[v, \frac{d_{obs}}{\tau_{min}}]$ where d_{obs} is the distance between the agent and the first obstacle in the desired direction α at that time step and v corresponds to the modulus of the current velocity.

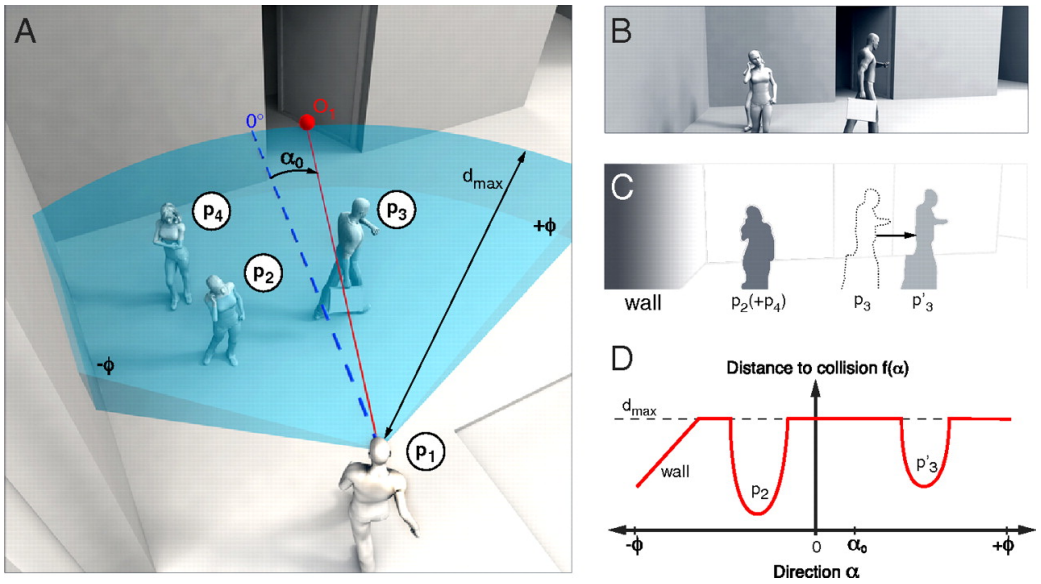

Figure 4.3: *a) Schematic guide of a pedestrian p_1 facing three other individuals and trying to reach the destination point O_1, which is marked in red. The blue dashed line corresponds to the perception limit. b) Illustration of the same situation, as seen by pedestrian p_1. c) Abstraction of the scene by a black and white visual field. Here, darker areas represent a shorter collision distance. d) Graphical representation of the function $f(\alpha)$ reflecting the distance to collision in direction α. The left-hand side of the vision field is limited by a wall. Pedestrian p_4 is hidden by pedestrian p_2 and, therefore, not visible. Pedestrian p_3 is moving away, so a collision would occur in position p_3', but only if p_1 moved toward the right-hand side. The image has been taken from the original article [276].*

4.1.2.1 Implementation and technical details

For the first two interactions, the number of agents is fixed to $N = 512$, while for the heuristic rule the number is fixed to $N = 128$ due to the computational cost of its simulations (different time steps Δt are also used in each case for the same reason, see below). The simulation time for the repulsive and time-to-collision mechanisms (it is, $F_{rep}^{(sa)}$ and $F_{ttc}^{(sa)}$) scales as $\propto N^2$, as they require to compute pair interactions. Instead, the heuristic rule prospects into the future the different α paths. This algorithm implies a scaling time $t \propto N^2 m_\alpha d_m$, where m_α is the number of explored directions α in each evaluation of the rule (fixed in our case to $m_\alpha = 50$), and $d_m = t_m/\Delta t$ is the number of time steps in the prospection. The agents are placed in a two-dimensional simulation box with density ρ using periodic boundary conditions. The pedestrians are considered as disks of diameter 1. The agent mass is settled as $m = 1$. The Verlet algorithm has been used to integrate the movement equations. The system is studied for different values of the density in the range $\rho = [0.05, 0.32]$, which is accomplished by fixing the number of individuals to a certain value N and changing the box size L, given $\rho = N/L^2$). The parameters used for the implementation of the self-avoidance mechanisms are as follows:

- The **repulsive interaction** (equation 4.4) is fixed to $k = 4$ (unless indicated otherwise), $A = 2.5$ and $\Delta t_{rep} = 0.001$.
- The **time-to-collision potential** (equation 4.6) is fixed to $k = 1.5$, $\tau_0 = 10$ and $\Delta t_{ttc} = 0.005$ according to [272]. The τ_0 value is chosen in such a way it will not affect the dynamics in the scaling region.

- The **heuristic rule** is fixed to $\tau_m = 0.5$ and $d_{max} = v_i t_m$, with $t_m = 5$, $\alpha_{max} = 75°$ and $\Delta t_{heu} = 0.05$, according to [276].

4.1.3 Pedestrians phase diagram

First, we simulate the dynamics of a large number of pedestrians as a function of the stubbornness to follow their goal or preferred direction of motion. Numerical implementation of the multi-agent system identifies, as expected, the existence of a phase transition for the three mechanisms i), ii) and iii) from a **disordered state to lane formation** as a function of the values of ρ and ξ. To characterize this transition we use the order parameter

$$\phi = \langle \cos(\theta) \rangle, \tag{4.8}$$

where θ is the angle between the actual and the preferred velocities (this is, between $\vec{v}$ and $\vec{v}^p$) and the average is carried out over all the agents in the system. So, $\phi \to 0$ corresponds to the disordered state in which individuals cannot follow its preferred direction and spend their time avoiding collisions in all directions, while $\phi \to 1$ represents the case where the agents are able to follow its desired direction of motion by adopting a collective pattern with alternate lanes in one direction and the other.

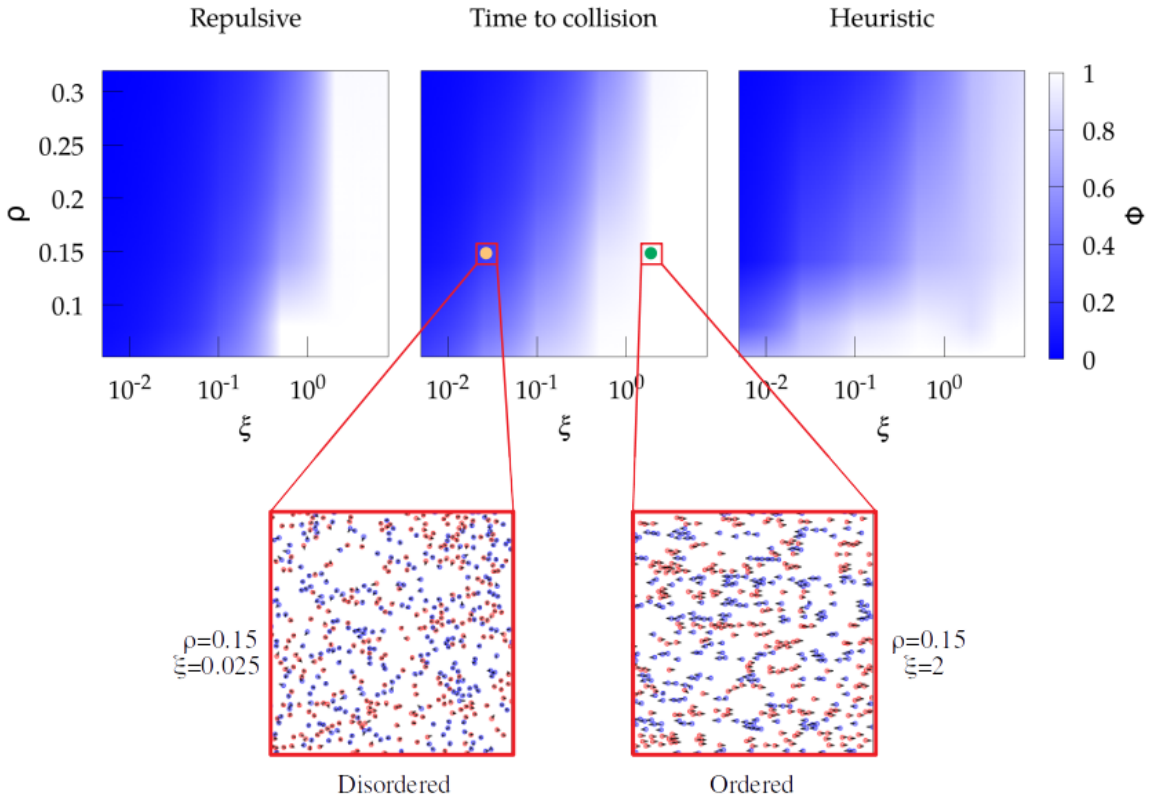

Figure 4.4: *Phase diagram of the order parameter ϕ for the three different mechanisms of self-avoidance as a function of the density of the system ρ and the stubbornness ξ. The repulsive interaction is fixed to $k = 4$. For the sake of clarity, a snapshot of the system is given both for the ordered and disordered states for the time-to-collision interaction.*

Figure 4.4 confirms that the three mechanisms of self-avoidance exhibit qualitatively a very similar behavior for the order parameter ϕ at the stationary state. Low stubbornness and high densities promote the disordered phase, while for high stubbornness and low densities the system self-organizes into bidirectional lanes. In the disordered state the difference between the actual direction of motion and the preferred one is relatively homogeneous in $(0, \pi)$. We can plot the probability distribution $p(\theta)$ of angle θ to visualize this (Fig. 4.5, left). For the case of lanes, on the contrary, most of the individuals move in their desired direction and then the probability distribution becomes clearly peaked at $\theta = 0$ (Fig. 4.5, right). Additionally, we observe how the heuristic mechanism exhibits a larger probability for large deviations in the lane state than the other interactions; this is due to the intrinsic properties of the algorithm, which allows larger reorientations provided they satisfy the maximization of the traveled distance, as explained above.

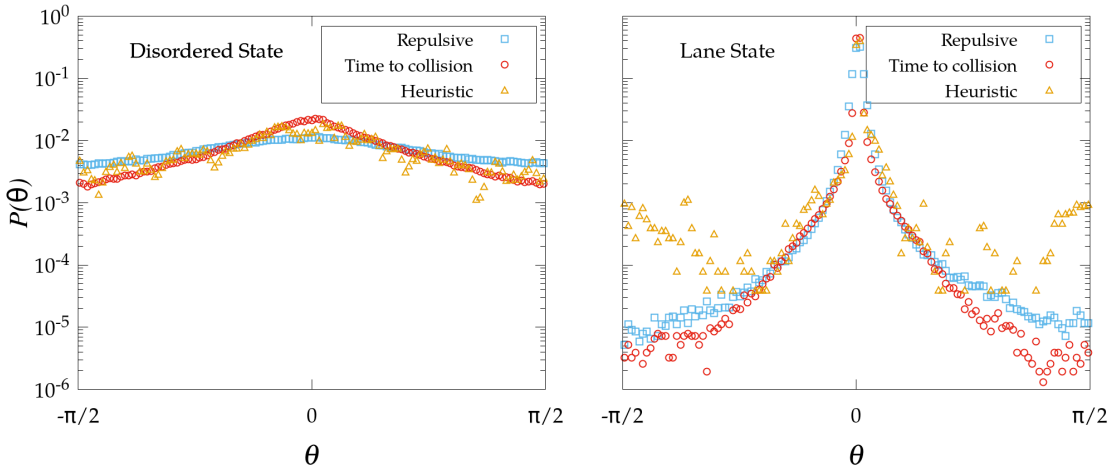

Figure 4.5: *Probability distribution of the relative angle θ. The left image corresponds to $\xi = 0.025$ and the right image for $\xi = 2$, with $\rho = 0.14$ in both cases. The blue squares correspond to the repulsive interaction ($k = 4$), the red circles correspond to the time to collision interaction, and the orange triangles correspond to the heuristic rule.*

4.2 Universal inter-pedestrian interaction

4.2.1 Structure analysis

To understand in greater detail the properties of these two phases, we next study the spatial distribution of the agents in stationary conditions through the **radial distribution function** $g(r)$ from the simulations using the three self-avoiding mechanisms mentioned. As in classical fluids, $g(r)$ here compares the density of interacting agents at a distance r with the density obtained for a non-interacting system, with $g(r) \to 1$ as $r \to \infty$. The corresponding results are presented in Fig. 4.6. Despite some qualitative differences found due to the different nature of the self-avoiding mechanisms, we observe that the results are relatively consistent with those from the classical Ornstein-Zernike (OZ) approximation for fluid systems [277], which predicts an asymptotic decay $G(r) \to r^{-0.5}$ (with $G(r) \equiv g(r) - 1$)

when the system is far from the critical region where the phase transition occurs. The oscillatory behavior observed in figure 4.6 is also characteristic from similar statistical analysis on fluids [278], caused by the underlying periodic structure of the system. All the points of the phase diagram that are far from the critical region satisfy approximately the OZ scaling while those close to the critical region (separating disorder from lane formation) exhibit a much slower asymptotic decay. In consequence, $g(r)$ cannot be easily used to discriminate the particular state (**disordered** vs **lanes**) in which the system is.

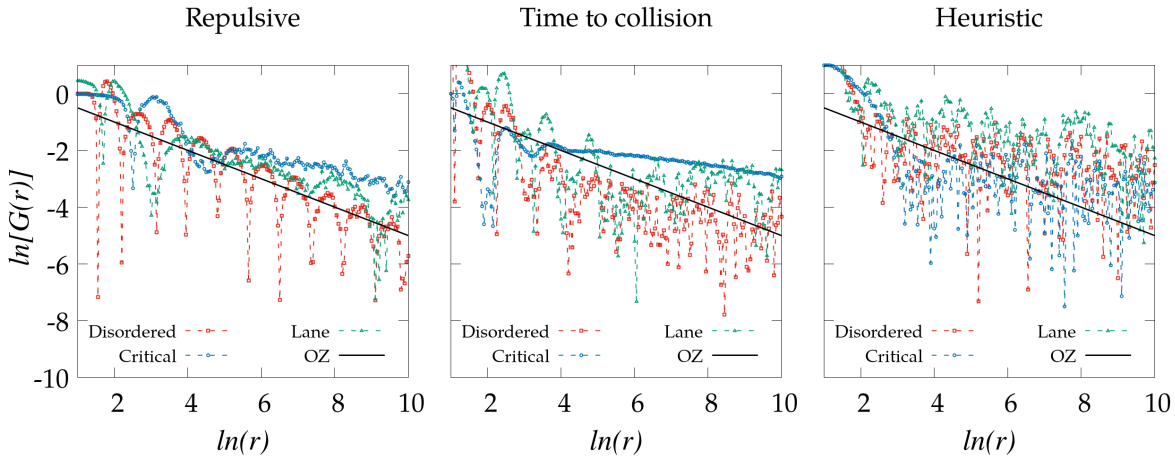

Figure 4.6: *Comparison between* $\ln[G(r)]$ *as a function of the radial distance* r *over the phase diagram. The black line corresponds to the OZ approximation (*$\sim \ln G(r) \sim -0.5 \ln r$*) which is introduced for visual comparison. The repulsive potential (*$k = 4$*) curves (left) correspond to a)* $\rho = 0.32$ *and* $\xi = 0.025$ *(disordered phase), b)* $\rho = 0.05$ *and* $\xi = 0.5$ *(critical region) and c)* $\rho = 0.14$ *and* $\xi = 2$ *(lanes phase). The time to collision curves (center) correspond to a)* $\rho = 0.32$ *and* $\xi = 0.025$ *(disordered phase), b)* $\rho = 0.32$ *and* $\xi = 0.1$ *(critical region) and c)* $\rho = 0.32$ *and* $\xi = 4$ *(lanes phase). The heuristic curves (right) correspond to a)* $\rho = 0.14$ *and* $\xi = 0.025$ *(disordered phase), b)* $\rho = 0.08$ *and* $\xi = 0.5$ *(critical region) and c)* $\rho = 0.14$ *and* $\xi = 4$ *(lanes phase).*

Going further, we reproduce the analysis in [272] by showing how $g(r)$ gets modified if the data is split into three parts according to the relative speed between pairs of individuals i and j, $v_r = |\vec{v}_i - \vec{v}_j|$. We find that individuals approaching each other with slow ($v_r < 1$), intermediate ($1 < v_r < 2$) or fast ($v_r > 2$) relative speeds exhibit very different behaviors in all cases (Fig. 4.7, left column).

The authors in [272] concluded that the differences observed in $g(r)$ for different values for v_r, reflect that such function is not a very appropriate descriptor for capturing the effective interactions within the crowd or, stated in different words, the collective statistics of the system does not apparently yield a consistent behavior in the physical r space of the distances between individuals. To explore here this idea we introduce a new magnitude $g^*(r)$, defined as the radial structure function but only for pairs of colliding agents, which are those for which τ is finite at that time step (see Fig. 4.2).

The splitting of $g^*(r)$ into different values of the relative velocities still shows that the results are strongly dependent on v_r (Fig. 4.7, middle column), albeit the differences get reduced for the mechanisms $F^{(sa)}_{\text{ttc}}$ and $F^{(sa)}_{\text{heu}}$ (since these two interaction rules only apply to particles which are about to collide). Instead, for the rule $F^{(sa)}_{\text{rep}}$, which applies to all pairs

of agents, the results found are almost the same as those for $g(r)$. So, still the statistical properties of the system are badly captured by the descriptor g^*.

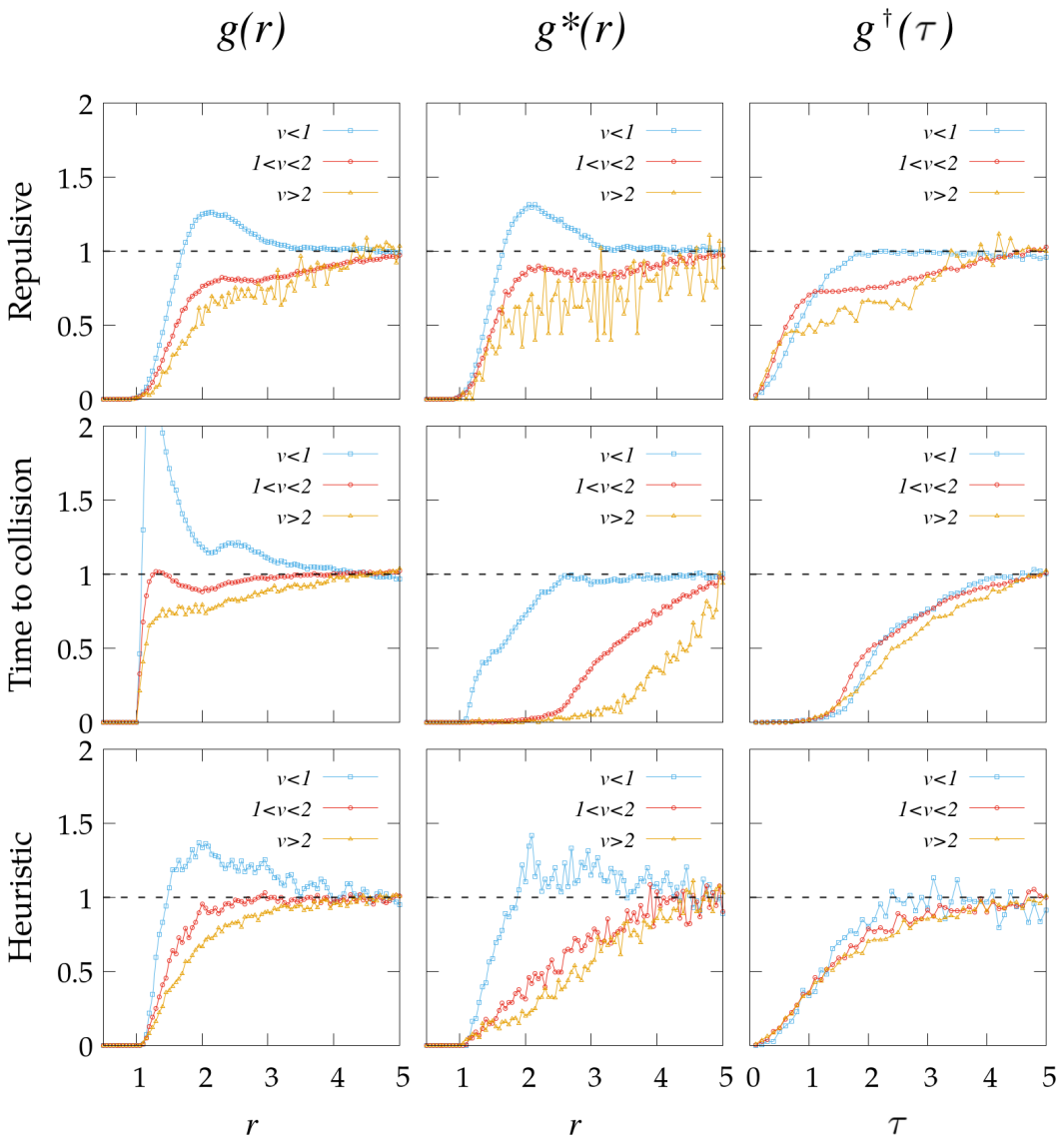

Figure 4.7: *Radial and partial distribution functions $g(r)$, $g^*(r)$ and $g^\dagger(\tau)$ when split into different regimes according to the relative speed between pairs v_r. Results are shown for $\rho = 0.14$ and $\xi = 0.1$, which corresponds to a disordered state. The repulsive interaction is fixed to $k = 4$.*

The intuition, however, gained from the results in [272] is that the dynamics of self-avoidance should rather translate into a robust behavior within the τ-space, as the events with low τ are the ones which must be avoided first. So, we finally introduce $g^\dagger(\tau)$, which is the equivalent to $g(r)$ but on τ-space, i.e. the density of agents found at a time-to-collision τ divided by the density we would find at the same τ for the case of non-interacting agents. The corresponding results are shown in Fig. 4.7 (right column). The idea that interactions should occur in the τ-space is of course introduced by hand in our rule $F^{(sa)}_{\text{ttc}}$, and also implicitly in the rule $F^{(sa)}_{\text{heu}}$, so when we explore the dynamics in the τ-space then we observe that the collapse between the three curves (for low, intermediate and high

relative speeds) is almost perfect. However, we unexpectedly find that the collapse between the curves is considerably improved for $F_{\text{rep}}^{(sa)}$ too, though in principle this self-avoiding rule has nothing to do with τ. This suggests the existence of an underlying phenomena enhancing the relevance (at least at the level of how collective structures emerge) of the τ-space whenever **self-avoidance** and **bidirectionality** effects drive the system dynamics. Note that the results in figure 4.7 do not necessarily mean that pair interaction occurs in the τ-space (which is not the case for our repulsive potential, actually) but that at a collective level this is the **effective** situation produced.

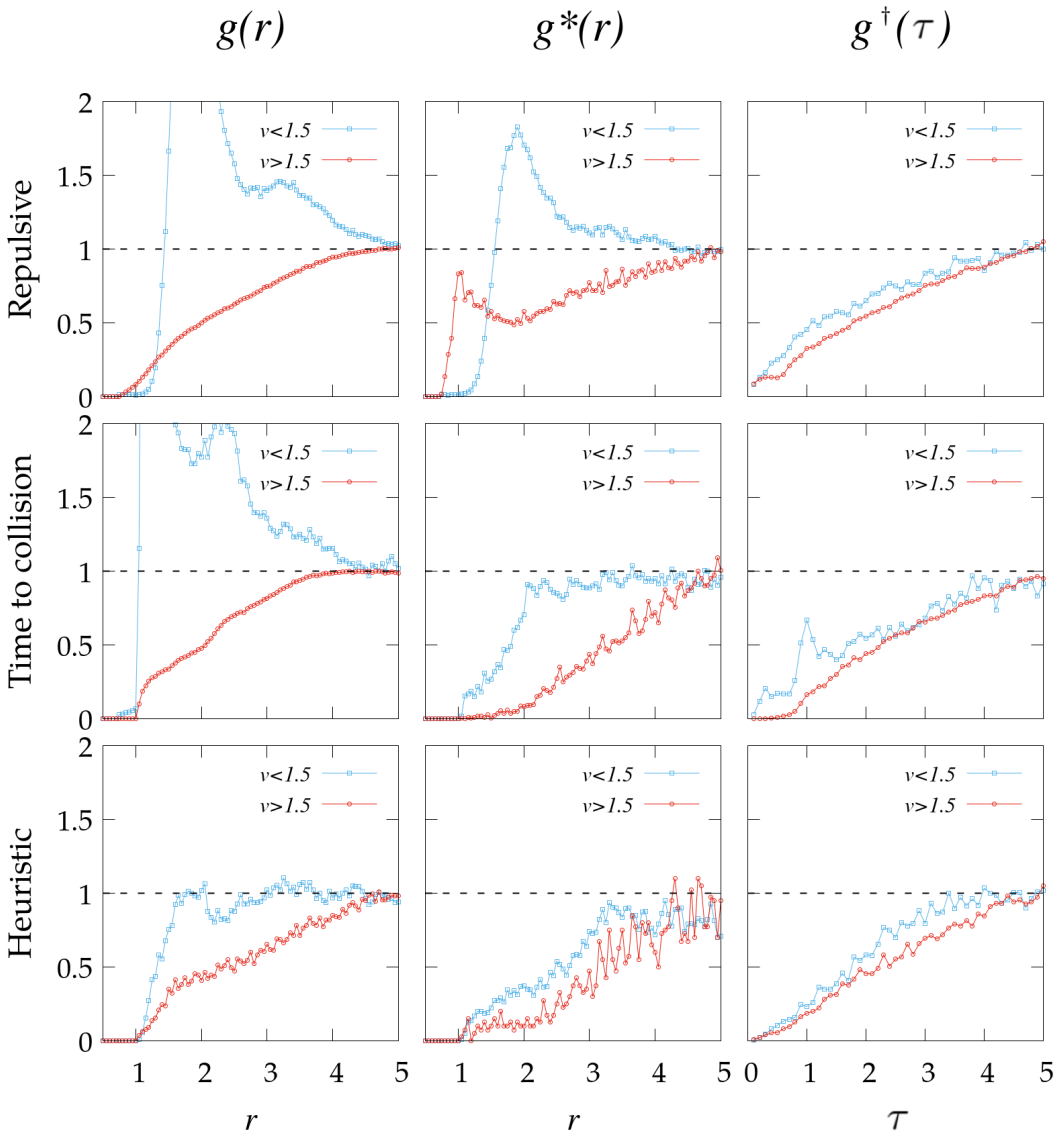

Figure 4.8: *Radial and partial distribution functions $g(r)$, $g^*(r)$ and $g^\dagger(\tau)$ when split into different regimes according to the relative speed between pairs v_r. Results are shown for $\rho = 0.14$ and $\xi = 4$, which corresponds to a lane state. The repulsive interaction is fixed to $k = 4$*

For the sake of completeness, we show in figure 4.8 the equivalent to the partial distribution analysis (Fig. 4.7) but now for the lanes state. The splitting in different ranges of v_r in this case has to be necessarily different to that for the disordered state due to the lack

of intermediate relative velocities when the lanes are formed. All agents will be moving either leftwards or rightwards (according to the preferred direction of each). Then relative velocities are either very low ($v_r < 1$, for agents in the same lane) or very large ($v_r > 2$, for agents in lanes with opposite directions). For this case, there is no statistics for intermediate regime $1 < v_r < 2$ used in figure 4.7, as the agents are either are flowing in one direction or another. Additionally, we often observe that particles persistently moving in the same lane and very close to each other (so, with $\tau \to 0$) artificially dominate the statistics, so these have been removed when computing $g^{\dagger}(\tau)$ in Fig. 4.8.

The collapse observed in the distribution $g^{\dagger}(\tau)$ for different v_r intervals confirms the behavior already reported for the disordered phase (note that now even the repulsive case satisfies the collapse to a great extent). This further supports the existence of an underlying phenomena enhancing the prominence of the τ-space whenever self-avoidance and bidirectionality effects drive the system dynamics.

4.2.2 Effective interaction in the τ-space

Next step is to derive an **effective potential** of interaction between agents in the τ-space. For the classical theory of fluids, the **reversible work theorem** [279] in the r space links the radial distribution function $g(r)$ with interaction energy between pairs in the form $V(r) \propto \ln[g(r)]$. Using an analogy with this classical result, the τ-space also admits an equivalent derivation. Here we provide a formal derivation of the relation between the distribution function $g^{\dagger}(\tau)$ and the effective potential $V(\tau)$. The derivation is a formal adaptation of the classical one to the case where the phase space is assumed to be defined by the times-to-collision between pairs of individuals, in agreement with the ideas stated throughout the previous paragraphs. Since the derivation works in the τ-space (not the real spatial space) then the concepts of force, work and potential must necessarily be interpreted in an effective (non-physical) way. The concept of thermal equilibrium is meaningless within this context. However, the idea of a canonical (Boltzmann-like) statistics is still attainable using an information-theory perspective in virtue of the Maximum Entropy principle (see Chapter 1). In particular, if one assumes that our knowledge about the system is reduced to the average of an effective potential $V(\tau)$ in the τ phase space then the MEP yields immediately such a Boltzmann-like statistics.

Within this context, the derivation works as follows. Consider a system of N particles where $V(\tau_{i,j})$ represents an effective pair interaction between individuals i and j, with $\tau_{i,j}$ the time-to-collision between them. The global effective potential in the system reads then $V_N = V_N(\tau_{1,2}, \tau_{1,3}, \ldots, \tau_{N-1,N}) = \sum_{i \neq j} V(\tau_{i,j})$. The corresponding phase space then consists of the $N(N-1)/2$ times-to-collision resulting from all possible pair interactions. We introduce now the magnitude $\nabla_{\tau_{1,2}} V_N$; for a classical conservative potential in the $\vec{r}$-space this would correspond to the force between particles 1 and 2, so one could be tempted to denote this magnitude as a generalized force. However, we will rather avoid such notation (i) to avoid misunderstandings coming from comparing our derivation to the classical one, and (ii) because that magnitude does not have dimensions of force, actually.

If one averages this magnitude in the Boltzmann-like statistics over the rest of coordinates of the phase space (this is, all except $\tau_{1,2}$) one has

$$\left\langle \nabla_{\tau_{1,2}} V_N \right\rangle = \frac{\int \left(\nabla_{\tau_{1,2}} V_N\right) e^{-\beta V_N} d\tau_{1,3} d\tau_{1,4} \dots d\tau_{N-1,N}}{\int e^{-\beta V_N} d\tau_{1,3} d\tau_{1,4} \dots d\tau_{N-1,N}}. \tag{4.9}$$

This can be rewritten as

$$-\left\langle \nabla_{\tau_{1,2}} V_N \right\rangle = \frac{1}{\beta} \nabla_{\tau_{1,2}} \left(\ln \int e^{-\beta V_N} d\tau_{1,2} d\tau_{1,3} \dots d\tau_{N-1,N} \right). \tag{4.10}$$

Next, if we define the distribution function $g^{\dagger}(\tau)$ as the probability that the individuals 1 and 2 will be found to have a particular value $\tau_{1,2} = \tau$ then we expect within our Boltzmann-like scheme that

$$g^{\dagger}(\tau) \sim \int e^{-\beta V_N} d\tau_{1,3} d\tau_{1,4} \dots d\tau_{N-1,N} \tag{4.11}$$

is satisfied. Accordingly, we can write

$$-\left\langle \nabla_{\tau_{1,2}} V_N \right\rangle = \frac{1}{\beta} \nabla_{\tau_{1,2}} \left[\ln \left(g^{\dagger}(\tau) \right) \right], \tag{4.12}$$

which is valid independently of the specific value of the normalization constant implicit in (4.11), since that constant is independent of $\tau_{1,2}$. Next, we observe that an effective pair potential $V(\tau)$ between particles 1 and 2 can be introduced as

$$V(\tau) \equiv \int_{\tau}^{0} \left\langle \nabla_{\tau_{1,2}} V \right\rangle d\tau_{1,2} \tag{4.13}$$

Putting this expression together with (4.12) one obtains

$$V_{\tau} = -\frac{1}{\beta} \ln \left(g^{\dagger}(\tau) \right) \tag{4.14}$$

after replacing the integration limits, and considering $V(\tau = 0) = 0$ to ensure that the behavior of the effective potential is meaningful in the τ-space.

We warn that the derivation we have presented holds in a non-standard phase space and by using Boltzmann statistics from an information-theory perspective, without introducing any reference to thermal equilibrium in the classical sense. So that, the effective potential considered must really be interpreted as an effective magnitude describing how statistics work in the τ-space, and therefore one is not allowed to interpret the spatial gradient of $V(\tau)$ as a real physical force between particles.

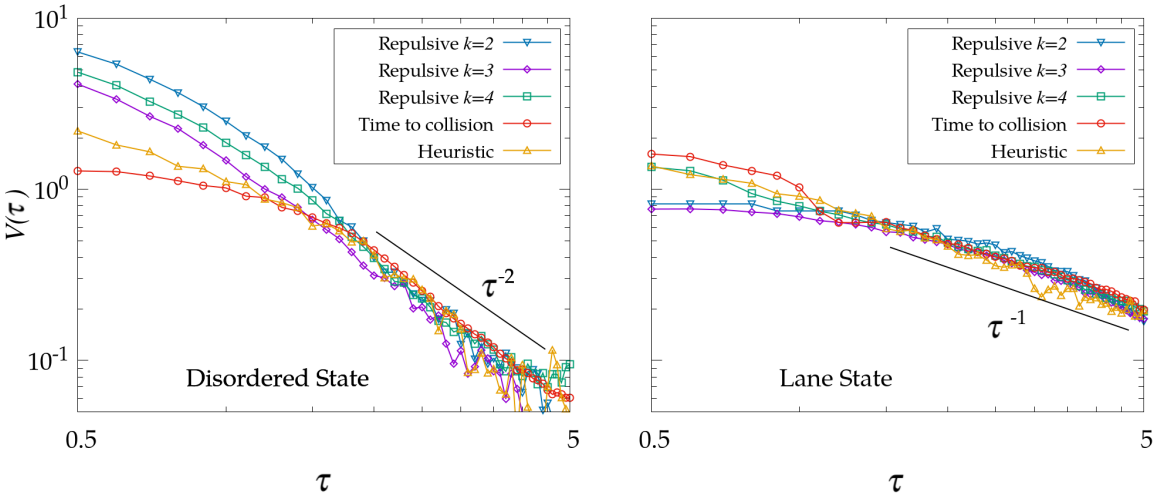

Figure 4.9: *Effective interaction $V(\tau)$ obtained from $g^{\dagger}(\tau)$ (see Eq. (4.14)) for $\rho = 0.14$ in the different states of the phase space (the top image for $\xi = 0.025$ and the bottom image for $\xi = 2$).*

The effective potential $V(\tau)$ obtained from the model is presented in Fig. 4.9. Surprisingly, we find that the three self avoiding mechanisms collapse for intermediate times-to collision (which is the significant region where most of the pair-pair interactions occur) into a common power-law relationship $V(\tau) \propto \tau^{-\gamma}$, with $\gamma \approx 2$ for the disordered state and $\gamma \approx 1$ for the state with lanes (in Table 4.1 we show the results obtained from fitting the curves presented in Fig. 4.9). This common scaling is then apparently independent of the self-avoiding mechanism, and would be a direct consequence of the bidirectional nature of the flow considered. Note also that, contrary to what happened for the radial distribution $g(r)$ (Fig. 4.6), the $g^{\dagger}(\tau)$ and the corresponding $V(\tau)$ show a different decay for the disordered phase and the case with lanes, so $g^{\dagger}(\tau)$ can be effectively used to discriminate statistically between these two states.

According to Fig. 4.5 (left panel), in the disordered state collisions can be produced in any orientation and the events corresponding to large τ are supressed by the shielding of closer events. The decay exponent γ takes then a value of 2, in agreement with the power-law proposed for pedestrians in [272]. While this is to be expected in the time-to-collision interaction $F^{(sa)}_{\text{ttc}}$ by definition, there is no apparent reason to justify why the same behavior emerges for $F^{(sa)}_{\text{rep}}$ and $F^{(sa)}_{\text{heu}}$. On the other side, the effective potential in the lane state exhibits a completely different behavior. The homogeneity in θ is there completely broken (Fig. 4.5, right panel) due to the two preferred directions of movement and most of the collisions are produced in the frontiers between opposite lanes. There is not shielding effect in this case and, as a consequence, the system is driven by a slower interaction decay, with $\gamma \approx 1$. For the moment it has not been possible, however, to find an analytical justification for the specific values of γ emerging in each state; this remains an open question.

From the findings in figure 4.9 we obtain that the same effective potential, if computed through Eq. (4.14) as done here, could emerge from a very wide range of interactions between the agents. This suggests that the result $V(\tau) \sim \tau^{-2}$ experimentally reported in

	γ (disordered)	γ (lanes)
Repulsive $k = 2$	2.2 ± 0.3	1.03 ± 0.06
Repulsive $k = 3$	2.13 ± 0.09	1.01 ± 0.04
Repulsive $k = 4$	2.07 ± 0.09	0.99 ± 0.05
Time to coll	2.09 ± 0.12	1.08 ± 0.07
Heuristic	1.97 ± 0.09	1.04 ± 0.06

Table 4.1: *Fit for the power law effective interaction $V(\tau)$ obtained from $g^{\dagger}(\tau)$ (see Eq. (4.14)) for $\rho = 0.14$ in the different states of the phase space (the left column for $\xi = 0.025$ and the right column for $\xi = 2$).*

[272] is not necessarily determining the actual rule of interaction (or self-avoidance) used by pedestrians, but it could rather be the manifestation of an **overall dynamics** exhibited by a wide range of systems combining self-avoidance and bidirectionality. In particular, the results in figure 4.9 confirm that it is not possible to discern whether pedestrians use a time-to-colision potential (as in [272]) or a heuristic rule of path maximization (as in [276]) only from examining the shape of the distribution function $g(\tau)$, but additional analysis would be required. Still, the scaling $V(\tau) \sim \tau^{-\gamma}$ will presumably work as a **useful effective rule** in bidirectional flows for different situations of interest. Such effective rule could be of great utility in order to simulate bidirectional fluxes without caring too much about the fine details of the interactions, and so it can be used as a toy approximation to computational or analytical works in the field of pedestrian dynamics.

Concluding remarks

- The interplay between individual preferences and the tendency to avoid collisions seems to be an important driver of collective organization for pedestrians. That translates into the formation of lanes (for strong directionality and low densities of pedestrians) independently of the nature of interactions between individuals.
- Alternative mechanisms of interaction collapse into an universal effective behavior in space of time-to-collisions. That effective description allows to discriminate between different levels of organization (lanes versus disorder).

Collective organization in ant foraging

5

Among all living organisms, insects exhibit a broad set of collective patterns [280]. Locusts [281] or crickets [282] synchronize their movement, creating polarized swarms or trails, respectively. Through this **social organization**, the individuals can improve their performance in many different tasks, such as food intake or nest allocation [283, 284].

Ants represents a paradigmatic example for both social organization and collective movement patterns. Ants have been shown to perform collectively many tasks, such as collecting, processing and distributing resources, or finding, building and defending their nests [285, 286]. Either through pheromone deposition or antennae contacts ant colonies can adjust: (i) the recruitment efforts on different tasks according to environmental fluctuations [287–289], (ii) the structure and intensity of foraging trails according to different types and quantity of resources [252, 290], and/or (iii) the amount of cooperative transport required [291]. These collective strategies meets the needs of the collective (colony) rather than individual ones. A **superorganism** is defined as a coordinated and coherent type of collective behavior performed by cognitively-limited interactive agents that ensures the survival as a whole over the individual level [292, 293]. Through this strategy, cognitive-limited organisms can provide an adapted (intelligent) response to the contextual circumstances, which fits perfectly the ants performance.

So far many studies of collective motion have focused on informed-naive or leader-follower relative positions and behavioural relationships [294]. The multi-walker and pedestrians scenarios are explored in Chapter 3 and Chapter 4 according to this idea. In a superorganism, the interactions between individuals should satisfy selection pressures and adaptability at the collective level rather than at the individual level.

Within this context, statistical physics provides powerful toolsets to ecologists to understand the theoretical foundations of emerging phenomena [85, 295]. However, the

characterization of the space occupancy dynamics has been far less studied. This lack of knowledge is particularly relevant when trying to assess the concept of superorganism. How coordinated groups/superorganisms move across the different regions of the space, for example to explore for and exploit food spots or nests, is a fundamental question to be answered.

The hypothesis we will pursue here is that collective and social organization within groups (and superorganisms, in particular) should translate into a non-trivial spatial use and, as a result, in **complex space occupancy** patterns. Then using spatial sites (not organisms) as the main units of interest and applying statistical physics tools at that level would represent a meaningful way to elucidate the existence of such complexity.

5.1 The Spin-Glass approach

5.1.1 State-based modeling

In the previous Chapters, we have described the collective dynamics in systems with multiple individuals in terms of the interactions between those individuals. In Chapter 3, the walkers interact through a shared energetic landscape. In Chapter 4, pedestrians interact between them through effective forces, making emerge non-trivial patterns such as lane formation. This modeling method is commonly called **agent-based modeling** [296, 297]. However, multi-individual systems can be described in alternative ways. Some of them even put away the notion of individual and put the focus on a more statistical or effective description [298, 299].

One proposal in that direction came from the **field-based models**. In there, the individuals are subsituted by an effective field. The field represents an averaged density, where the individual dynamics is substituted by this averaged treatment [300, 301]. Among a broad range of examples, the field models have been used to describe the evolution of bacterial growth [302], the prey-predator populations [303, 304] or the role of the morphogenesis in the brain development [305].

Despite both methodologies presented above represent the two typical approaches to describe collective behavior, one can find other mechanisms that can be useful to characterize multi-individual systems (see figure 5.1 for a comparison between the different methodologies).

State-based modeling represents a paradigmatic approach which is gaining attraction in the recent years. There, one focus on the possible configurations (states) that the system can take, known as the phase space. Based on this, one builds again an energy landscape, associating an energy E for each one of those states. The system evolution can then be modeled as a unique agent moving through that energy landscape, as in the $f(E)$ framework.

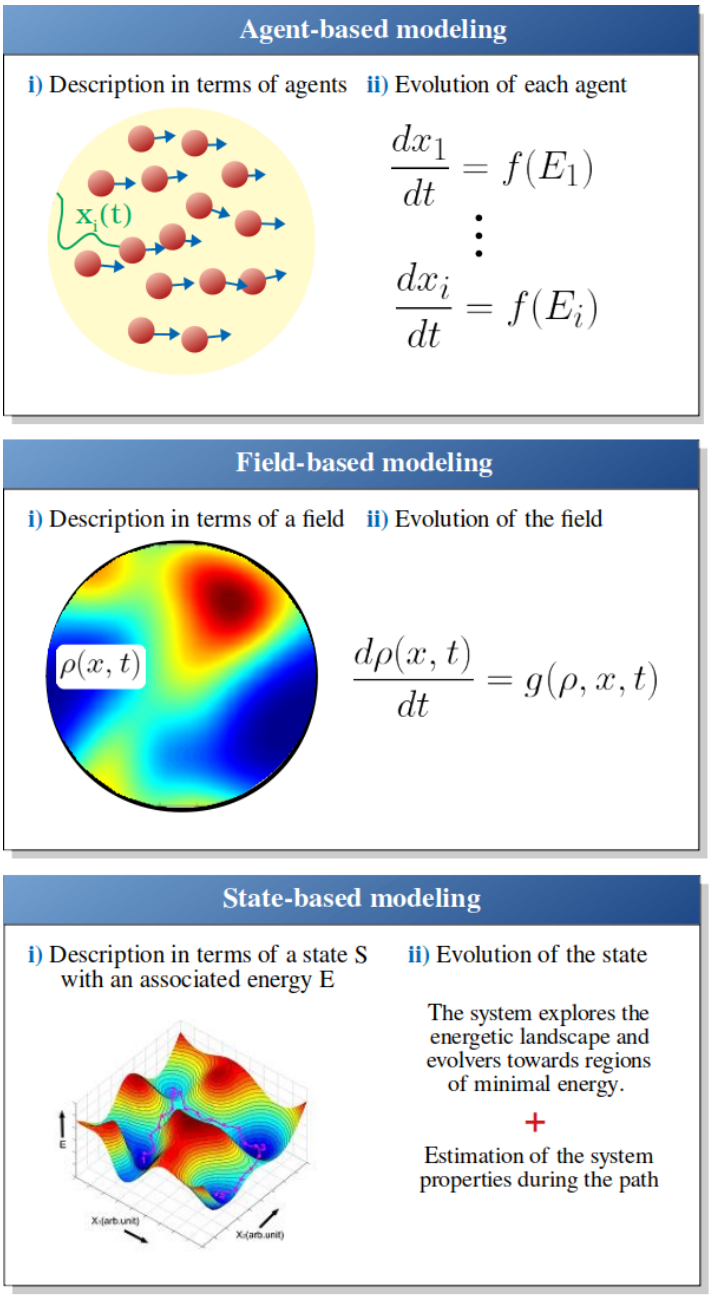

Figure 5.1: *Schematic depicting of agent-based (left), field-based (middle) and state-based modeling (right). state based modeling. The individual dynamics are substituted by the dynamics of a global agent (each position of this agent representing a collective state of the system) trough a given energetic landscape.*

The exploration of that energy landscape provides estimators of the different properties of the system and localizes the more stable (minimal energy) states the system will tend to move to. State based models have been shown to capture fundamental patterns of collective phenomena such as neural self-organization [306], human communication [307] or insect foraging strategies [308].

In the following Sections, we will use a state-based model to describe the collective foraging patterns of ant colonies.

5.1.2 The network representation

Networks have been widely used in biology [309, 310] at many different levels: prey-predator interactions [311], extinction dynamics in food webs [312] or hierarchical organization in social animals [313, 314] are just a few examples. For these, the network nodes can be identified as the different species inside the same ecosystem (this can be useful to study species or population survival and functioning within ecosystems), or as the individuals within a given group (when the aim is to understand connections in a hierarchical group).

Within the approach we will present here, however, nodes represent biologically meaningful spatial regions. In Fig. 5.2 a) and b) we illustrate the idea that even for the case of relatively homogeneous landscapes, the environment can be always properly discretized or partitioned according to some case-specific criterion. We stress that such kind of discretization is convenient in many biological studies, and can be exploited at different levels. This happens for example when using the concept of **patches** in fragmented habitats [315], but also in metapopulation theory (where a population is fragmented in several groups) [316, 317], in the context of polydomy (where a colony is established across multiple nest sites) [318], or in theoretical approaches as cellular automatas [319], to name a few.

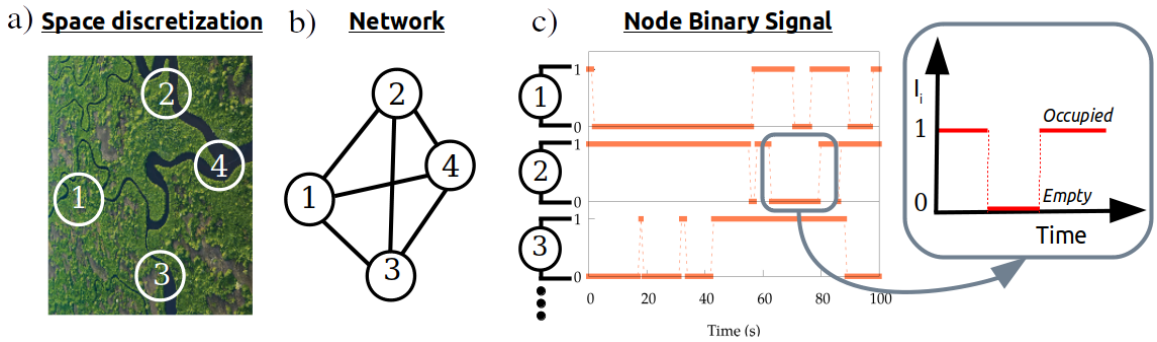

Figure 5.2: *Illustrative scheme of our approach to collective space use. (a) The biologically relevant regions of the space are considered as (b) nodes of a network structure. (c) The presence or absence of individuals at node i for a given time t is then understood as a binary signal $I_i(t)$ representing occupancy of that region (with $I_i(t) = 1$ if occupied, and $I_i(t) = 0$ if empty).*

In order to characterize occupancy at each node of the spatial network we will assume that a time-discrete **occupancy signal** $\mathbf{I}(t) = I_1(t), I_2(t), I_3(t), ..., I_N(t)$ is available experimentally. Here, $I_i(t)$ (with $i = 1, 2, ..., N$) will be taken for simplicity as a **binary** variable that tells us simply if the node i is occupied ($I_i(t) = 1$) at time step t or not ($I_i(t) = 0$), with N the total number of nodes in the spatial network. We note that more complicated versions of the approach could be proposed by relaxing this two-state (empty/occupied) hypothesis, while here we will focus on this case to keep the notation and analysis simple.

The overall signal $\mathbf{I}(t)$ (Fig 5.2 c) then carries the information about the occupancy patterns for a group of organisms. If the individuals within that group behave independently, then occupancy patterns at each site, or node, will be independent of each other. On the contrary, one should expect that in a superorganism-like system (that is, for strongly

organized groups exploring space according to some interaction rules and a global strategy) correlations between sites will emerge. Accordingly, a minimal model capturing such possible correlations would be a valuable tool. Furthermore, for predictive purposes and subsequent testing, such approach should be able not just to identify the statistical properties of occupancy signals $\mathbf{I}(t)$, but also to (i) generate new artificial realizations of those occupancy patterns and (ii) be flexible and meaningful enough to allow for introducing variations in the model as a way to inquire or predict its behavior under alternative conditions.

5.1.3 The Spin-Glass Hamiltonian and its construction

Spin glass models can be seen as a generalized version of the ubiquitous Ising model from statistical physics. While the Ising model was originally aimed at deriving macroscopic properties of magnetic systems from elementary pairwise interactions, it has been subsequently extended in many different ways. In particular, introducing randomly distributed intensities for pairwise interactions has become a paradigm for frustrated systems, spin glasses being a recurrent example. This idea has also pervaded many other areas of research, including biology, up to the point that recent works [320] sustain that the physical foundations for the origin of complexity (and so, collective behavior) in biology can be outlined within that framework of frustrated systems and spin glasses.

Following the usual formulation of Ising-like systems, we will consider N interacting units or **spins** (which in our context correspond to the sites within the spatial network structure) whose individual dynamics is described by a binary signal $s_i(t)$, with $s_i(t) = \pm 1$, so the overall state $\mathbf{S}$ of the system is characterized by a specific realization of each, it is $\mathbf{S} = \{s_1, ..., s_i, ..., s_N\}$. The spins are assumed to interact through pairwise (both short-range and long-range) interactions with intensities J_{ij}, and are subject to external fields of intensity h_i, such that the resulting Hamiltonian for the spin glass reads

$$H(\mathbf{S}) = -\sum_{i=1}^{N} h_i s_i - \sum_{i<j} J_{ij} s_i s_j, \tag{5.1}$$

where the second sum extends over all possible pairs of spins in the system.

Under equilibrium conditions, the spin-glass system is expected to satisfy a Boltzmann distribution, so

$$P(\mathbf{S}) = \frac{1}{Z} e^{-\beta H(\mathbf{S})}, \tag{5.2}$$

must hold, where Z represents a normalization factor and $\beta = 1$ will be used from now on for the sake of simplicity.

This Hamiltonian also admits an interpretation from information-theoretic grounds (see [321] for a comprehensive discussion). In particular, it corresponds to the energy functional that minimizes redundancy (or, equivalently, maximizes informational entropy) for modeling the system, provided that the only information available are the time-averages of

the spins (it is, $\langle s_i(t) \rangle$) and their pairwise time correlations ($\langle s_i(t) s_j(t) \rangle$). For this reason, the spin-glass model is typically employed for assessing whether complex systems can be possibly characterized or not only through pairwise correlations. Those correlations C_{ij} between pairs read

$$C_{ij} = \frac{\sum_t (I_i(t) - \langle I_i \rangle_t)(I_j(t) - \langle I_j \rangle_t)}{\sqrt{\sum_t (I_i(t) - \langle I_i \rangle_t)^2 \sum_t (I_j(t) - \langle I_j \rangle_t)^2}}, \tag{5.3}$$

and they encode information about how the nodes are related between them.

This idea has been already used, for example, to study the spike dynamics of different kinds of neuron groups [306]. The spike/silent periods characteristic of these systems can be mapped into a binary signal representing the activity of each neuron, such that activity patterns of a group of neurons then provide information about their functional response and connection patterns. Furthermore, in the recent years there has been a growing interest in exploring the applicability of the spin-glass approach to different biological and social systems, including social human and animal connections [307, 322] or financial markets [323, 324].

To construct the Hamiltonian for the space use scenario one has to find the set of parameters h and J that provide the best fit to the statistical properties of the occupancy signal. This procedure is called an inverse problem, where one infers the model parameters from the data instead the common procedure of tuning manually the parameters to fit the data. More concretely, when one uses the Hamiltonian in equation5.1, the process is called the **inverse Ising problem**.

One can define the distribution of collective states $P_{exp}(\mathbf{S})$, where $\mathbf{S}$ corresponds to $\mathbf{S} = \{s_1, ..., s_i, ..., s_N\}$ and the label exp refers to the experimental data. The fitting procedure is then defined as the process of fitting the h and J parameters that produce a $P_{sim}(\mathbf{S}) \sim P_{exp}(\mathbf{S})$, where sim labels the distribution of states coming from sampling states from the Hamiltonian obtained through simulations.

At the heart of many methods to reconstruct the parameters of the Ising model is the **maximum likelihood framework**. It consists on estimating the parameters by maximizing a likelihood function, so that under the assumed statistical model the observed data is the most probable. One can demonstrate that this procedure is equivalent to finding the parameters that minimize the Kullback-Leibler divergence [325] between the two distributions $P_{sim}(\mathbf{S})$ and $P_{exp}(\mathbf{S})$.

For two general probability distributions Q and P, the Kullback-Leibler divergence (D_{KL}) reads

$$D_{KL}(P||Q) = \sum_i P(i) \ln \left(\frac{P(i)}{Q(i)} \right). \tag{5.4}$$

It is a non-negative quantity and when the two distributions are identical, the divergence is exactly $D_{KL} = 0$. To find the J and h parameters that minimize that divergence, one

commonly uses Monte Carlo simulations, where the divergence is progressively minimized trhough stochastic simulations [326, 327]. During the stochastic simulations, the procedure involves sampling the whole phase space of parameters. Note that the model contains N parameters of type h_i and $N(N-1)$ parameters of type J_{ij}, for a total of N^2 parameters in the system, where N is the number of nodes in the network. So that, the computational cost of generating a distribution $P_{sim}(\mathbf{S})$ for each point of the phase space also scales as $\sim N^2$ with the number of spins in the network. The cost of this method to reconstruct the parameters scales then as $\sim N^4$, making it unmanageable for large networks.

An alternative methodology to fit the experimental data comes from the maximum entropy principle. By using information theory and Lagrangian multipliers (see Chapter 1), the maximum-entropy estimate has been proposed as the most unbiased estimate of the unknown probability distribution compatible with the observed expectation values [121, 122] (see Chapter 1). If one does some assumptions, the MEP can provide semianalytical expressions for the h and J parameters as a function of the experimental data. The mean-field approach [328], the TAP reconstruction [329], the Plefka expansion [330, 331] or the Sassek-Monasson expansion [332] are examples of those pseudo-analytical derivations. Those expressions allow to derive the parameters instantaneously. In consequence, they have been largely used in substitution of the maximum likelihood estimator when its computational cost makes it unfeasible. On the other side, the assumptions one has to make to derive those expressions may not be appropriate for some data.

Given the scaling $\sim N^4$ of the computational time required for the maximum likelihood estimator, the system size becomes then the critical criterion to decide when to use that method or the one based on semi-analytical expressions. During the next Sections we will provide two examples where we infer the Hamiltonian parameters from the data coming from ant colony experiments. The reduced size of the network ($N = 8$) used to describe the first experiment (Section 5.2) will allow to use the maximum likelihood estimator to derive the Hamiltonian parameters for that case, while for the second experiment, in which $N = 620$ (Section 5.3), we will apply the semi-analytical method.

5.2 Foraging in a simple environment

To illustrate the application of the method presented in the previous Section to a real situation, first we carried out a simple experiment on ant foraging under laboratory conditions specifically designed to suit the spatial network approach in figure 5.2. We expect this experiment to provide a direct measure/evidence of superorganism-like behaviour in ants by a comparison between the spin-glass approach and the experimental occupancy signal exhibited by the colony.

5.2.1 Experimental method

We put a colony of around 100 workers of *Aphaenogaster senilis* (previously collected from the Campus of the Universitat Autònoma de Barcelona) in a plastic nest together with several eggs and larvae to keep them stimulated for working. The eggs and larvae were not renovated, but they were left to grow and become adult during the experiment; while this introduced some non-stationarity in experimental conditions, we note that the duration of the whole experiment (25 days) was relatively short compared with the time required for the ants to mature to the adult stage, so we expect that this bias had minimum effects on the results. The colony nest was connected to a tree structure (figure 5.3) by a plastic tube finalizing in eight different Petri dishes of 4 cm diameter. Each of these dishes (nodes) is then connected to a spiral plastic tube, whose end is used as the resource area where food for the ants is laid at the start of the experiment.

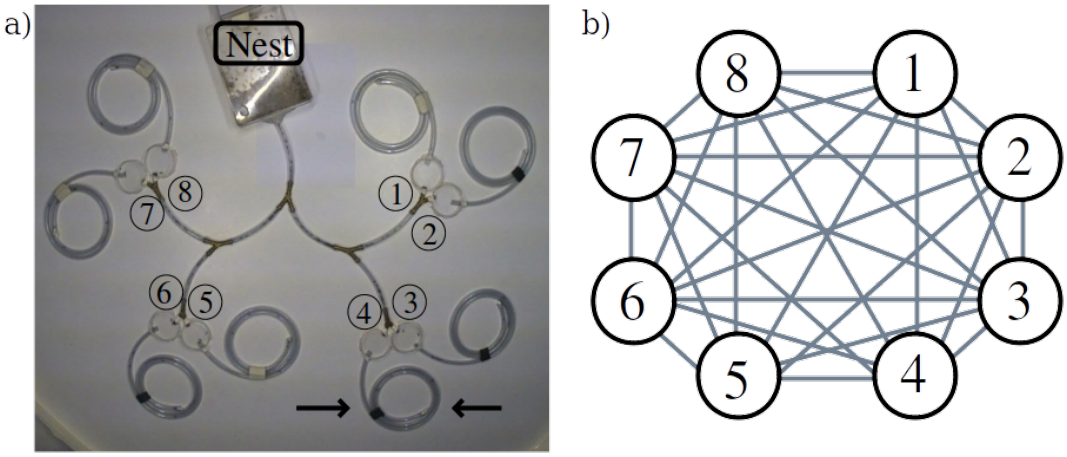

Figure 5.3: *a) Experimental set-up, labelling from 1 to 8 the nodes representing the endings of the tree structure. The black arrows indicate the plastic spirals where the food is laid. (b) Equivalent network representation of the experimental set-up, assuming every node can interact with any other.*

While such a ramified structure does not represent a very natural environment for foraging, it provides an ideal opportunity to explore how the ant colony distributes their exploration resources (scouts) in a discrete network environment. In particular, the eight Petri dishes in the structure (which have different topological distances between them) will represent from now on the eight 'nodes' (see figure 5.3 b)) in our network (see figure 5.2).

The experiment was carried out through daily trials of 90 min during 25 days (in June and July 2018), which were recorded using a time-lapse camera at a frame rate of 1 Hz. During the 90 min of the trial, ants were allowed to explore the structure starting from the nest. Before each trial, the food was placed at some of the resource areas (dead-end spiraling tubes) departing from the eight nodes. Food consisted of single small mealworm pieces, so recruitment through pheromone was so avoided (previous studies on the recruitment rules of *A. senilis* have shown that this species uses group recruitment only if the amount/density of food to be carried exceeds a critical value [333]). Foraging then was expected to rely on memory and landmarks solely. At the end of the 90 min trial, we removed the remaining food in case the ants had not collected it. The overall quantity of food received by the

colony according to this procedure (about three pieces of mealworm per day, in average) was enough to nourish the colony while still keeping it active for foraging.

The resource areas containing food at each trial were decided according to probability rules. They were used as a control variable in order to evaluate the response of the colony to induced resource heterogeneity. So that, for days 1–13 (that we will denote as **Regime A**), half of the nodes (nodes $1, 4, 5, 8$) had a high probability to contain food (50%), and the other half (nodes $2, 3, 6, 7$) had a lower probability (25%), while in days 14-25 (**Regime B**), the probabilities were inverted (nodes with 50% probability turned to have 25%, and vice versa). Figure 5.4 shows the 25 day profile of the nodes where food was laid before the experiment (white and yellow nodes), and when was the food collected by the ants (white nodes).

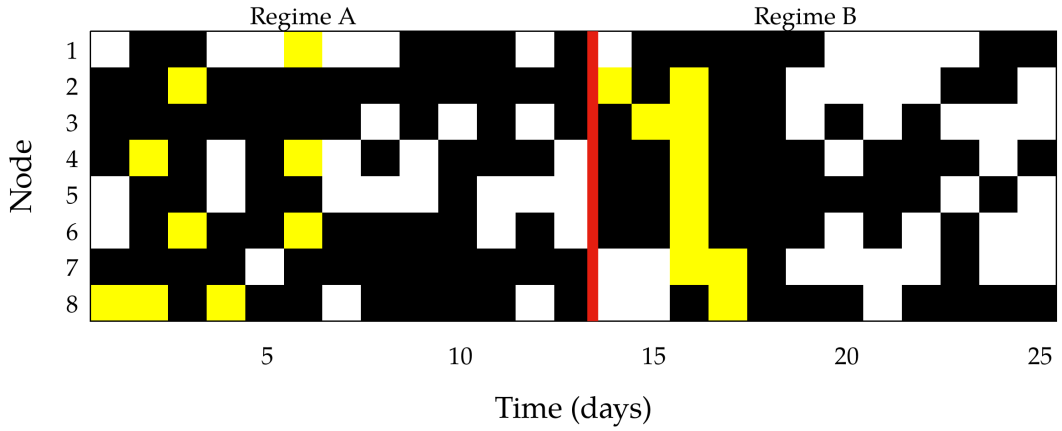

Figure 5.4: *Food dynamics in the network nodes during the 25 days of experiment. Black cells correspond to nodes where food was not present at that day, white regions correspond to nodes which contained food and it was picked up by the ants, and yellow cells correspond to nodes where the food was present but it was not picked up by the ants during the trial. The red line separates the regimes A and B used in our analysis.*

We expected to observe changes in the occupancy patterns of the network as a result of variations in the resource availability on the nodes from food regime A (days 1 to 13) to regime B (days 14 to 25). Though it was not possible from the experimental design to assign directly the changes observed in space occupancy pattern to the change in the resource distribution (due to a mixture of effects present in the system, including memory and/or habituation effects), we intended to check if variations in the external conditions driving foraging could reflect into a change in the collective occupancy patterns, which we could observe through our spin-glass approach. So, despite not controlling all the biological forces that may govern the behavior at both regimes (A and B), we decided for convenience to analyze them separately in order to quantify their differences.

5.2.1.1 Construction of the binary signal

For extracting the experimental data, we used our own video-analysis code (implemented in the open-source software *Scilab*) to determine the presence or absence of ants in each

one of the 8 nodes at each frame (as stated above, we considered a node i as occupied whenever one or more ants are detected at that node). After the processing of the videos, the complete dataset of 135000 frames was transformed into an occupancy binary signal $\mathbf{S}(t)$. So, every frame was characterized by a set of 8 binary variables, for a total set of $2^8 = 256$ possible states where the system can be found.

Without losing generality, in the following we will explore the statistics of occupancies $I_i(t)$ (which take values 0 or 1) from that of spins $s_i(t)$ (with values +1 and −1) by means of the mapping $s_i(t) = 2I_i(t) - 1$. So, given the experimental signal of node occupancies, we can then immediately find the corresponding states $\mathbf{S}$ and their probability distribution $P_{exp}(\mathbf{S})$.

We studied the daily profile of the average occupancy $\langle I \rangle_t$ (which corresponded to the occupancy at a given time averaged over the 8 nodes) during the 90 min of experiment (i.e. 5400 s). From this we found that, as expected, the dynamics during food regimes A and B were significantly different (see Fig. 5.5 a) and 5.5 b) and the corresponding captions). At the beginning of each daily trial, the ants were in the nest and it took some time (around 10 minutes) before the nodes were visited for the first time. Then the average occupancy during this transient period reads $\langle I \rangle_t = 0$. After that period, there was a tendency for $\langle I \rangle_t$ to grow until it reached saturation in 20 or 30 minutes. When we analyzed by separate those nodes where food had a higher (50%, orange line) or lower (25%, blue line) probability to be laid, we observe that for regime A the ants were clearly visiting the nodes with more food with a higher frequency (Fig. 5.5 a)). On its side, for regime B the ants performed a seemingly homogeneous exploration of the nodes independently of the presence of food (Fig. 5.5 b)).

For the sake of completeness, we can also show the daily average of the occupancy throughout the 25 days of the experiments, labeled as $\langle I \rangle_d$. From this analysis we reach again very similar conclusions as for the $\langle I \rangle_t$ (see figures 5.5 c) and 5.5 d)). For the regime A, the nodes with larger quantities of food showed higher occupancy, while for regime B the colony carried out a more homogeneous exploration, independent of the quantity of food. In any case, this daily average shows that the occupancy is highly fluctuating throughout the days.

One can wonder if a high/low probability node classification corresponds to an adequate splitting. With the purpose of answering this question, we analyze if the conclusions extracted from figure 5.5 become modified when a different node classification is considered. In this case, we group the nodes in terms of the actual presence (or absence) of food. One can observe in figure 5.6 that the new node classification leads qualitatively tot the same conclusions extracted from the high/low probability classification. According to those results, it sounds reasonable to keep using in the following the high/low node classification during the rest of the analysis.

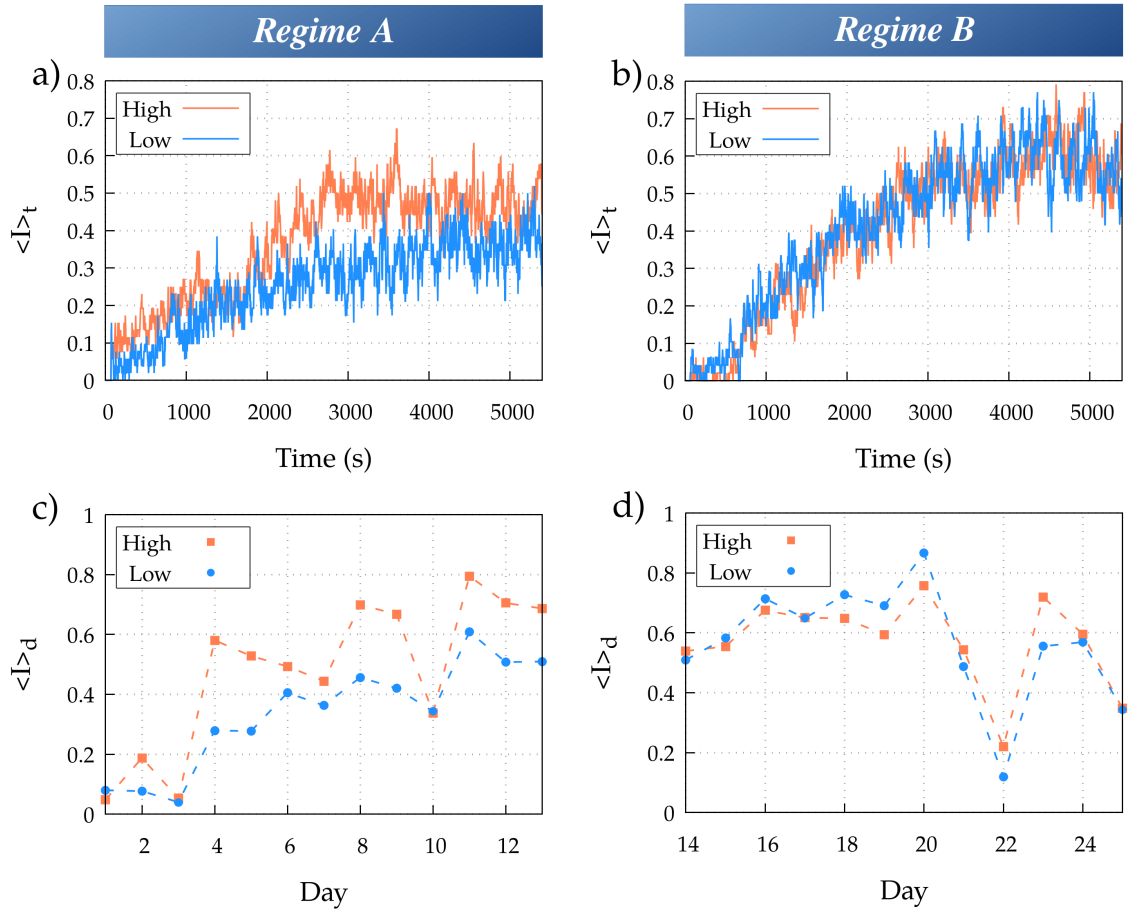

Figure 5.5: *Averaged daily occupancy $\langle I\rangle_t$ for a) regime A ($\langle I\rangle_t^h = 0.48$; $\sigma_I^2 = 0.012$ and $\langle I\rangle_t^l = 0.34$; $\sigma_I^2 = 0.004$) and b) regime B ($\langle I\rangle_t^h = 0.57$; $\sigma_I^2 = 0.004$ and $\langle I\rangle_t^l = 0.57$;$\sigma_I^2 = 0.006$). Averaged occupancy split into nodes with high or low probability of containing food during c) regime A and d) regime B. Differences between the two types of nodes are statistically significant ($T - Student$ test) for the regime A ($\langle I\rangle_d^h = 0.48$ and $\langle I\rangle_d^l = 0.34$; $|T_s| = 4.70 > T_{95\%} = 0.0002$) but not for the case B ($\langle I\rangle_d^h = 0.57$ and $\langle I\rangle_d^l = 0.57$;$|T_s| = 0.11 < T_{95\%} = 0.46$).*

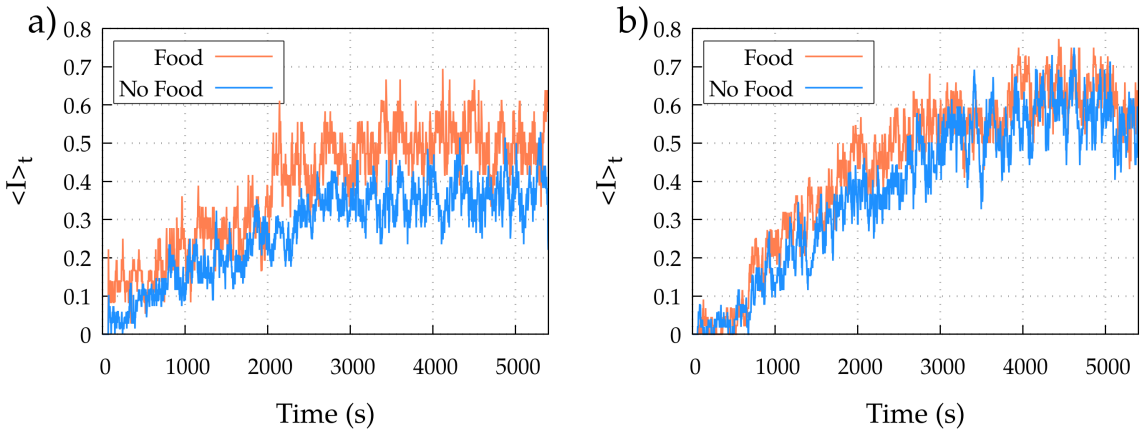

Figure 5.6: *Averaged daily occupancy $\langle I\rangle_t$ for those nodes where food is present (red) or not (blue), for a) regime A and b) regime B. Comparison of stationary (2700-5400 s period) values leads to ($\langle I\rangle_t^f = 0.50$ and $\langle I\rangle_t^{nf} = 0.34$) for the case in a), so showing significant departures, while for case in b) we find ($\langle I\rangle_t^f = 0.60$ and $\langle I\rangle_t^{nf} = 0.55$), so much less differences are obtained.*

5.2.2 Simulation and fitting details

As we mentioned previously, the spin glass approach we have proposed requires a learning or fitting process to determine the parameters h_i, J_{ij} based on the inverse Ising approach.

Since in the experiments occupancy signals present a transient period until exploration of the space is possible for the ant colony (Fig. 5.5 c) and 5.5 d)), only the stationary part of the signal (period $2700s - 5400s$) was used for the learning protocol. Learning or fitting procedures for the regimes A and B are carried out separately in order to see how the differences observed in the space-use dynamics between both reflect into the spin-glass approach.

As the number of nodes in the network is small, one can use the **maximum likelihood estimator** to fit the parameters. Given the experimental signal of node occupation, we can find the corresponding distribution of states $P_{exp}(\mathbf{S})$.

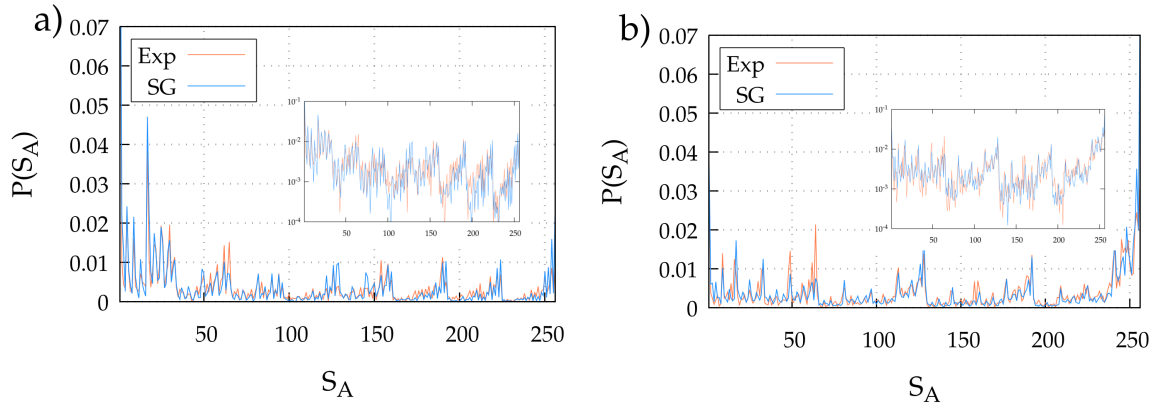

Figure 5.7: *Probability distribution of states (the x-axis contains the $2^8 = 256$ possible states) for the experimental data and the spin glass approach for a) regime A and b) regime B. The insets show the same probability distributions in logarithmic scale.*

The fitting procedure works as follows. First, one sets an initial (random) set of parameters h and J. Then, one runs a Monte Carlo simulation (MC) using acceptance rules in the spin-glass Hamiltonian to generate a distribution $P_{sim}(\mathbf{S})$. After this, one proposes a shift to a parameter J_{ij} or h_i (chosen randomly) to a new value J^*_{ij} or h^*_i and simulates again the spin-glass dynamics to obtain a new distribution $P^*_{sim}(\mathbf{S})$. At this point, one computes the $D_{KL}(P_{exp}(\mathbf{S})||P_{sim}(\mathbf{S}))$ and $D^*_{KL}(P_{exp}(\mathbf{S})||P^*_{sim}(\mathbf{S}))$ divergences. If $D^*_{KL} < D_{KL}$ (which means that the new Hamiltonian reproduces more accurately the experimental data), the shifted parameter J^*_{ij} or h^*_i is accepted and a new set of parameters is established. This procedure is repeated until the divergence D_{KL} between the simulated and experimental distribution falls below a fixed threshold. That methodology is often known as the gradient descent method.

Before we carry out any subsequent analysis we show that after the training process, the resulting spin-glass Hamiltonian is able to generate artificial occupancy signals (through new Monte Carlo simulations) whose probability distribution are almost in perfect agreement

with the experiments. Fig. 5.7 provides this comparison, and verifies that the agreement reached so is excellent for both regimes A and B.

5.2.3 Time dynamics comparison

Once the spin-glass has been proved to reproduce the experimental distribution of states, one can intend to compare the temporal evolution of the spin-glass and the experimental data. For this, one has to define a relation between the Monte Carlo time (number of steps) and the real time. By comparing the relaxation to the stationary state when starting from $\mathbf{I} = 0$, we conclude that a proper rescaling of the MC results consists of using the equivalence that 1 MC step corresponds to 50s.

We run simulations with the parameters J and h obtained through the learning algorithm above to compare the properties of the occupancy signals produced by the model with the experimental ones. The agreement found at the level of stationary probability distributions (see figure 5.7) is to be expected by default since this is the criterion used for fitting, but the spin-glass approach is not necessarily expected to reproduce the time dynamics of the experimental system beforehand. This is what we test in the following.

So, we first fix the initial state in the Monte Carlo simulations to $\mathbf{I} = 0$ (or, equivalently, $\mathbf{S} = -1$), corresponding to the case where the eight nodes of the system are empty, for reproducing the initial conditions of the experiments, and we study the behavior of the corresponding average occupancy $\langle I \rangle$ during the 90 min of the trial. On average the simulations recover almost completely the temporal signal of the experimental data for both regimes (see Fig. 5.8 a) and 5.8 b) and corresponding captions). Furthermore, we also find that the fluctuations around this average, measured through the corresponding standard deviation σ among the different trials, are also very similar in all cases (Fig. 5.8 c) and 5.8 d) and corresponding captions). The mean occupancy, when averaged over the whole time period of the trial for each node, also recovers reasonably well the experimental pattern observed (Fig. 5.8 e) and 5.8 f) and corresponding captions).

In order to expand on this idea we also measure the distribution of **persistence times** at single nodes, defined as the amount of time one node stays in the same state (either occupied or empty) before switching to the other. When looking at the corresponding distribution of persistence times $P(\tau)$ experimentally for the ants, one can find it follows a nontrivial behavior which corresponds to an intermediate decay between exponential and power-law functions (Fig. 5.9). Though it is not possible to derive an expression for that distribution from the analytical treatment of the Hamiltonian, we observe that the spin-glass approach yields again a very good agreement to the experimental data, both for regimes A (Fig. 5.9 a)) and B (Fig. 5.9 b)). Altogether, these results prove that the spin-glass approach is able to reproduce dynamical properties, as well as the stationary statistics, in the experimental conditions used.

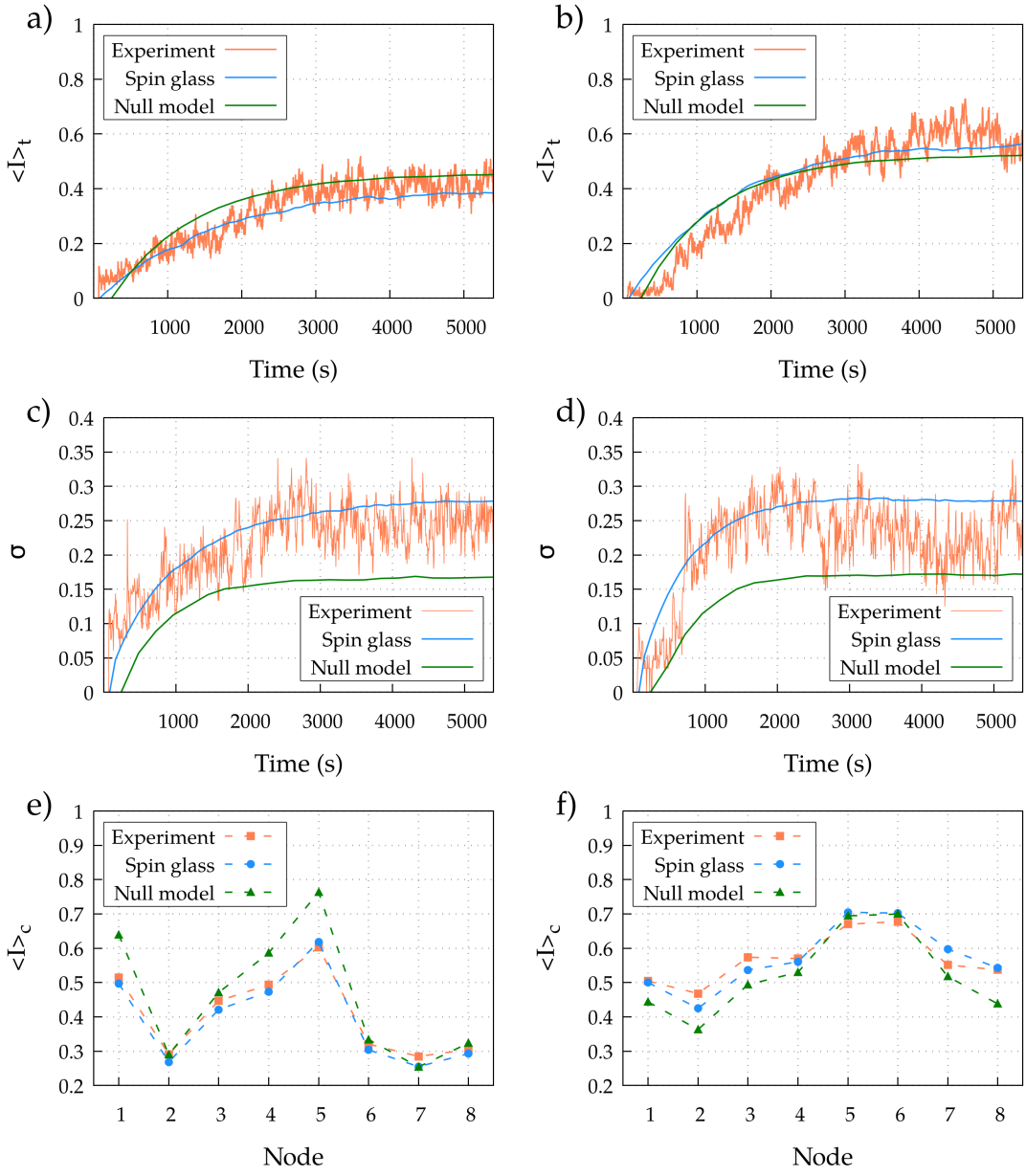

Figure 5.8: *Averaged daily occupancy dynamics $\langle I \rangle_t$ for the spin-glass approach (with and without pairwise interactions) and experimental data during a) regime A and b) regime B. The corresponding standard deviations are also shown for c) regime A and d) regime B. Averaged occupancy in the stationary regime $\langle I \rangle_c$ for the spin-glass approach and experimental data during e) regime A and f) regime B. The deviation of $\langle I \rangle_c$ obtained from the models to the experimental one is computed from the variance of the departures from one to the other: for panel e) we find ($\sigma^2_{SG} = 0.0004$ and $\sigma^2_{J=0} = 0.0065$), and for panel f) ($\sigma^2_{SG} = 0.0011$ and $\sigma^2_{J=0} = 0.0025$). In both regimes, the spin-glass model shows smaller departures from the experiment than the null model. Additionally, an ANOVA test with $\alpha = 0.05$ for null differences with the experimental data leads to $p - value = 0.80$ (spin-glass) and $p - value = 0.54$ (null model) for the regime A, and $p - value = 0.96$ (spin-glass) and $p - value = 0.37$ (null model) for regime B.*

5.2.4 Biological interpretation of the model parameters

It would be desirable that the parameters h_i and J_{ij}, obtained through statistical inference, also admit a **biological interpretation**. In some contexts, the parameters h_i and J_{ij} did not necessarily possess such experimental interpretation, since spins or units lived in

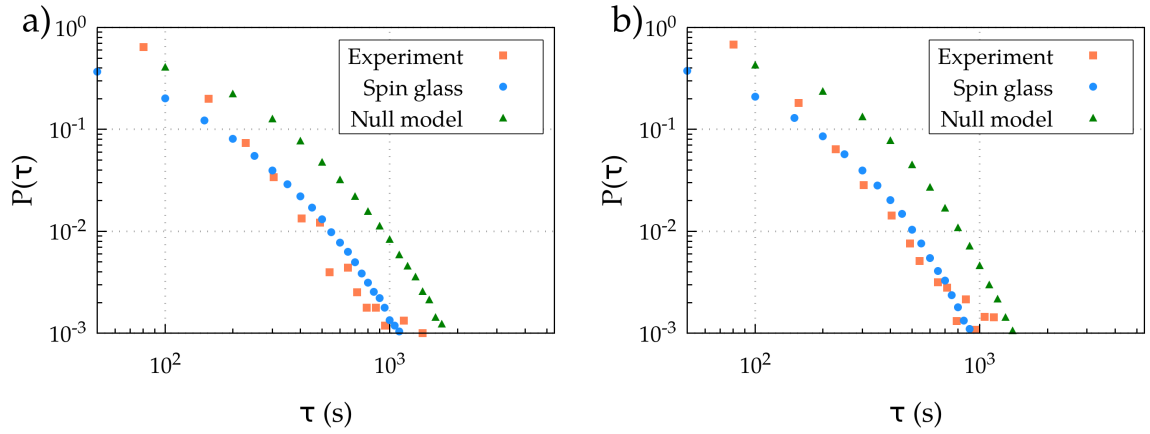

Figure 5.9: *Probability distribution of persistence times $P(\tau)$ during a) regime A and b) regime B. An ANOVA test with $\alpha = 0.05$ for null differences with the experimental data leads to $p - value = 0.86$ (spin-glass) and $p - value = 0.04$ (null model) for the regime A, and $p - value = 0.82$ (spin-glass) and $p - value = 0.09$ (null model) for regime B.*

an abstract phase space and could only be treated then as effective parameters. On the contrary, for the case of our experiment we find that a relation between the experimental data and these parameters comes straightforward (see figure 5.10). The external field h_i, for instance, should determine the propensity that organisms have to occupy the i node (i.e. the attraction towards node i) at an average level. Each term $-h_i s_i$ present in equation 5.1 drives the system in this direction. When h_i is large (small), provided that the other parameters remain unchanged, that node should have a tendency to be in average more (less) time occupied. Using a physical analogy, when the sign of the spin is aligned with the sign of the external field, the system's energy gets reduced. The external field parameter h_i should thus correlate with the average occupancy $\langle I_i \rangle$ of each node; this is confirmed by comparing the values of both magnitudes in both regimes considered (Fig. 5.11 a)).

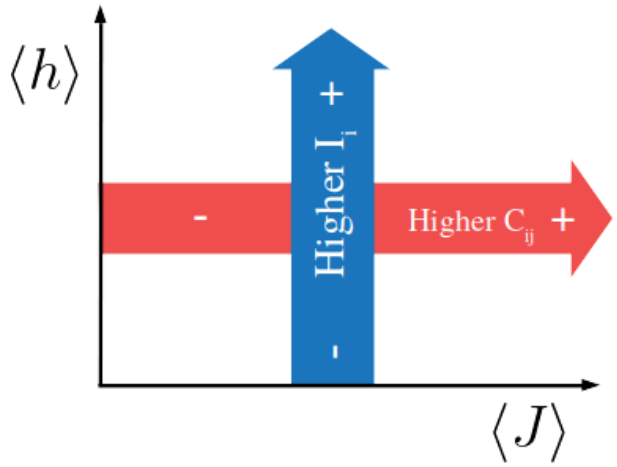

Figure 5.10: *Schematic representation of the biological meaning of the parameters $\langle h \rangle$ and $\langle J \rangle$. A larger external field h_i corresponds to a larger activity in the node i, while a larger pairwise interaction J_{ij} corresponds to a greater correlation between the nodes i and j.*

According to the previous result, the parameters h_i capture the average node-occupancy of the system; this should be good enough as long as one is not concerned about cooperation and collective effects. The role of the interaction parameters J_{ij}, however, is extremely relevant since they capture spatial correlations at a collective level (in particular, how likely it is that two separate nodes/spots are simultaneously occupied by the colony). To confirm this intuition we compare the J_{ij} parameters, obtained from the learning process, with

pairwise correlations (see equation 5.3) of the experimental occupancy signal $\langle I_i I_j \rangle \equiv C_{ij}$ (Fig. 5.11 b)). We again find a high correlation between both magnitudes, so confirming our intuitive interpretation.

The alignment between the model parameters h_i and J_{ij}, and the observables $\langle I_i \rangle$ and C_{ij} is still found if computing average values by separate for the nodes with high and low resource probability (Figure 5.12). Noteworthy, the average occupancy per node $\langle I_i \rangle$ and the spatial correlations C_{ij}, as well as the corresponding model parameters h_i and J_{ij}, are statistically different in nodes with high and low resources (food) only for the case of regime A, but it does not happen for regime B. This suggests either an habituation of the colony to the experimental setup, or a memory-delayed process in order for the colony to adjust the shift in high/low resourced nodes from regime A to regime B. Whatever the underlying biological process, in regime B the ant colony shows a more homogeneous activity, with no differences in attraction and correlation patterns based on the amount of resources in the nodes (Figure 5.12), something that the spin-glass approach adequately captures.

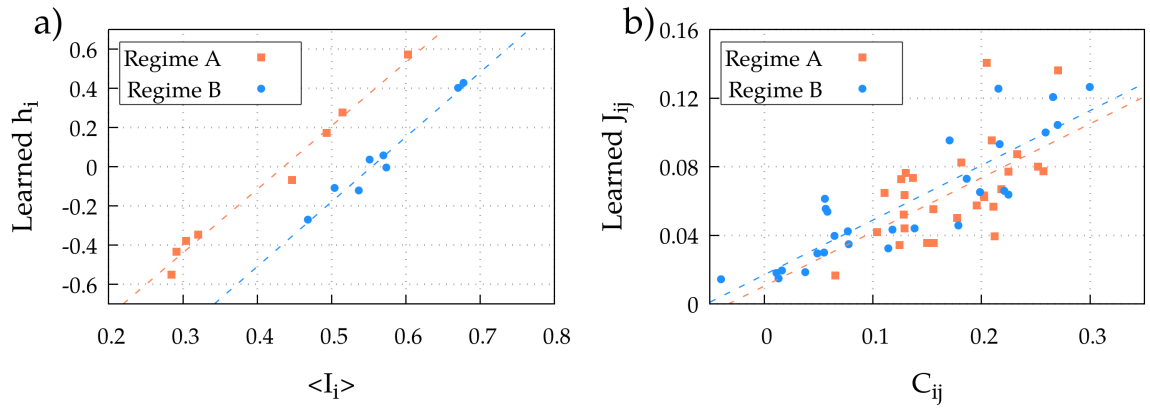

Figure 5.11: *a) Averaged experimental occupancy for each node $\langle I_i \rangle$ in comparison to the learned external field h_i. The correlation coefficients are $C = 0.991$ for the regime A dataset (orange) and $C = 0.982$ for the regime B dataset (blue). b) Experimental correlation between the nodes i and j, C_{ij}, in comparison to the learned pairwise interaction J_{ij}. The correlation coefficients are $C = 0.597$ for the regime A dataset (orange), and $C = 0.876$ for the regime B dataset days (blue).*

Finally, one can also wonder about the effect that real topological distance between nodes may have on the J_{ij} values, and whether there is an inverse correlation between both (so distant nodes show weaker interactions). The distance is measured as the number of tree bifurcations between the nodes (see left panel at figure 5.13). The results show that there is not a reliable correlation of this topological distance to the interactions between the nodes (Fig. 5.13). Then, in average, the distance doesn't have a strong effect in the J_{ij}. In summary, we find that the topological distance between nodes does not seem to be an adequate descriptor for the occupancy dynamics in the experiments.

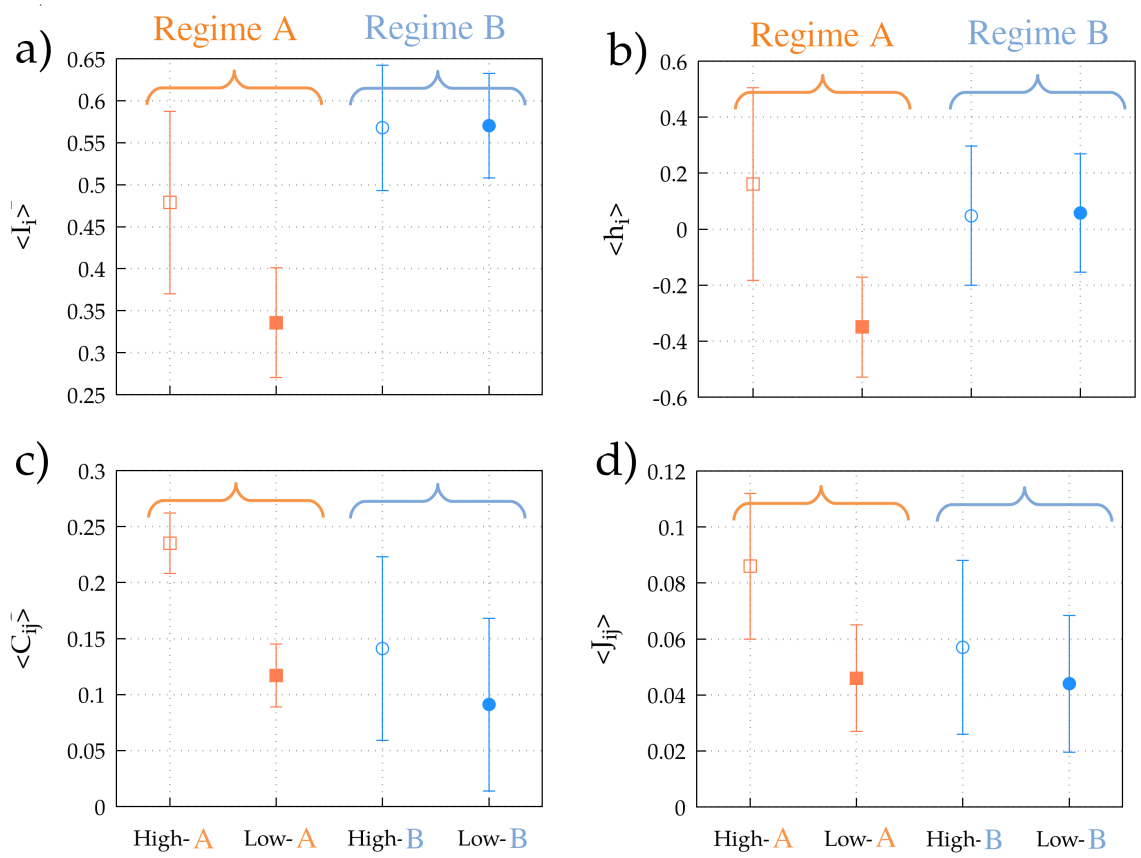

Figure 5.12: *a) Averaged experimental occupancy* $\langle I_i \rangle$ *for the different sets of nodes and experimental regimes A (*$T-Student$ *test:* $|T_s| = 2.21 > T_{95\%} = 0.06$*) and B (*$|T_s| = 0.23 < T_{95\%} = 0.41$*). b) Averaged field* $\langle h_i \rangle$ *for the different sets of nodes and experimental regimes A (*$|T_s| = 2.82 > T_{95\%} = 0.03$*) and B (*$|T_s| = 0.15 < T_{95\%} = 0.44$*). c) Averaged pairwise correlations* $\langle C_{ij} \rangle$ *between the nodes of the same set in the experimental regimes A (*$|T_s| = 8.71 > T_{95\%} = 0.00001$*) and B (*$|T_s| = 6.90 > T_{95\%} = 0.00001$*). d) Averaged pairwise interaction* $\langle J_{ij} \rangle$ *between the nodes of the same set in the experimental regimes A (*$|T_s| = 3.83 > T_{95\%} = 0.001$*) and B (*$|T_s| = 2.18 > T_{95\%} = 0.03$*). H corresponds to the set of nodes with high probability of food presence while L corresponds to the set of nodes with low probability. A corresponds to the experimental regimes from days 1 to 13 of experiment, while B corresponds to the days 14 to 25.*

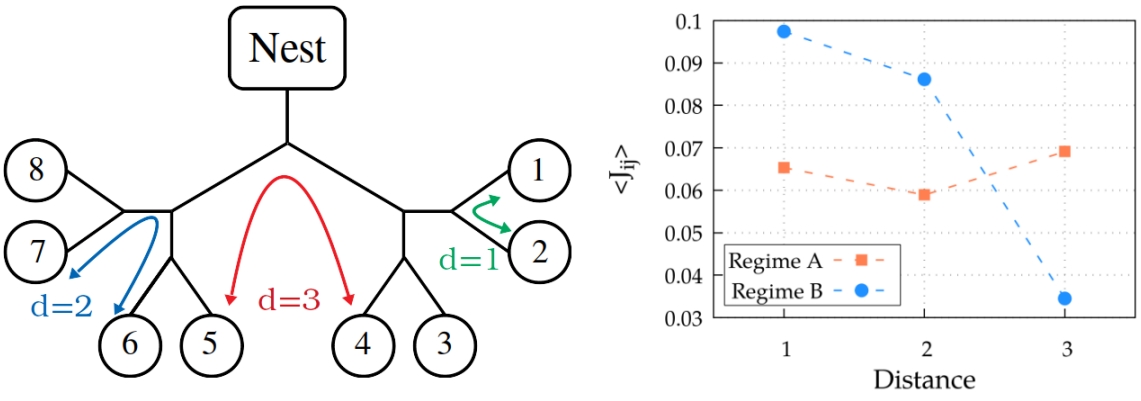

Figure 5.13: *Left panel: schematic representation of the distance between two nodes* i *and* j*. Right panel: averaged pairwise interactions* (J_{ij}) *between the nodes* i *and* j *by distance for regimes A and B.*

5.2.4.1 Relevance of pairwise correlations in the occupancy patterns

We come back finally to the initial idea of checking whether pairwise correlations between occupancies at different nodes are required in order to describe the overall occupancy dynamics. If so, then such correlations would indicate that some kind of global strategy is being used by the colony for exploring the arena and for distributing their foraging resources. On the contrary, if ants acted as individual foragers then such correlations would be almost negligible or they would not have any significant effect on the occupancy pattern observed.

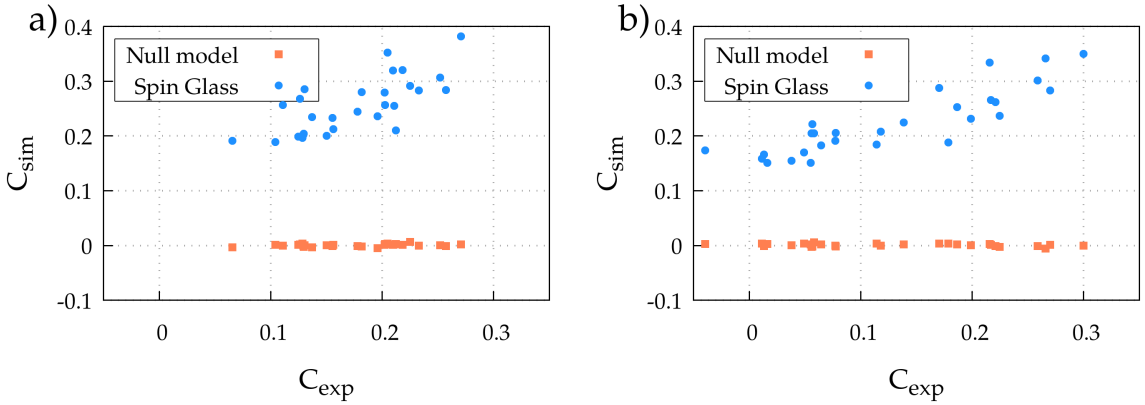

Figure 5.14: *Experimental correlation between the nodes i and j* $(C_{ij})_{exp}$ *in comparison to virtual correlations obtained from MC simulations* $(C_{ij})_{sim}$*, for a) regime A and b) regime B.*

The existence of non-zero correlations C_{ij} between nodes (Figure 5.11) tells us that some collective effects emerge in ant colony space use, but one may still wonder whether these correlations are key to reproduce the experimental data. In order to assess that idea we compare the results obtained from the spin-glass approach to a null model in which all pairwise interactions are set to zero, it is, $J_{ij} = 0$. After imposing such condition the fitting algorithm is run again and the values for h_i are determined anew. Also, in order to make the comparison fair we redefine the time step in the Monte Carlo simulations for comparing the artificial occupancy signal (obtained from the null model) to the experimental one; by doing so we find that when single time steps in the simulation correspond now to 140s. Then we obtain the best possible fit for the average global occupancy (Fig. 5.8 a) and b), green lines). However, even if such rescaling is used to force that the average occupancies of the null model fit the experimental ones, the other properties of the occupancy signal perform poorly in comparison to the general model. In particular, fluctuations in the overall occupancies (Fig. 5.8 c) and d), green lines), as well as characteristic switching times (Fig. 5.9, green dots) depart very much from those observed in the experiment, contrary to what happens for the general model (see Figure captions to find the statistical significance of these departures).

Additionally, it is evident that if $J_{ij} = 0$ is imposed in the null model, then experimental correlations C_{ij} (equation 5.3) found experimentally cannot be reproduced. The model

without interactions loses its capacity to reproduce the time correlations in the system, as is confirmed in figure 5.14.

All this together proves that the statistical patterns exhibited by the colony cannot be properly explained with the null model, so giving support to the superorganism-like hypothesis and to the idea that pairwise correlations present in the general spin-glass model are required to capture the system dynamics.

5.3 Foraging in a complex environment

In the previous Section, we have proved that the Spin-Glass approach could be a useful tool to characterize hierarchical or superorganism-like behavior under simple experimental conditions. Next we will try to test whether this can be extended to much more complex scenarios, where the number of nodes present in the spatial network is much higher.

In particular, we address the collective organization of *Alphaenogaster Senilis* ants when forced to find its food through large hexagonal mazes (see figure 5.15), where the food is located either at deterministic or random locations. These two food configurations will result in a larger or lower promotion of exploration through the domain, ginving us the opportunity to interpret the resulting behavior in terms of the well-known exploration-exploitation tradeoff [334, 335]. The **exploration-exploitation trade-off** states that the colony must locate adequately its resources between those invested in consuming known resources (exploitation) and those used in searching for new food sources (exploration), which is an ubiquitous dilemma at many relevant biological scales [336–338].

5.3.1 Experimental method

Two ants colonies of the species *Alphaenogaster Senilis* were collected independently (named colony A and colony B) with 100 individuals each, approximately. We hold the colonies isolated in independent plastic structures, with a darker region in it, as a nest.

A square PVC structure of 2 m of length and 2 cm of height was designed which represents the experimental arena. The square is subsequently divided into two rectangular regions (of $2x1$ square meters each), such that each region represents the foraging region for one of the colonies. Each of the regions contains an hexagonal lattice (figure 5.15) of channels within the PVC structure, such that we subsequently cover the whole structure with a semitransparent piece of cloth well stretched, so restricting the ants movements to the channels. The movement of all individuals can be recorded with a set of cameras placed 1 m above the structure. As a result of the hexagonal nature of the lattice used as an arena, the ants will experience continuous Y-intersections and so they will need to decide between following one path or another of the crossing. The lattice is constituted by 620 of these intersections, with channels of length 0.05 m separating the neighboring intersections.

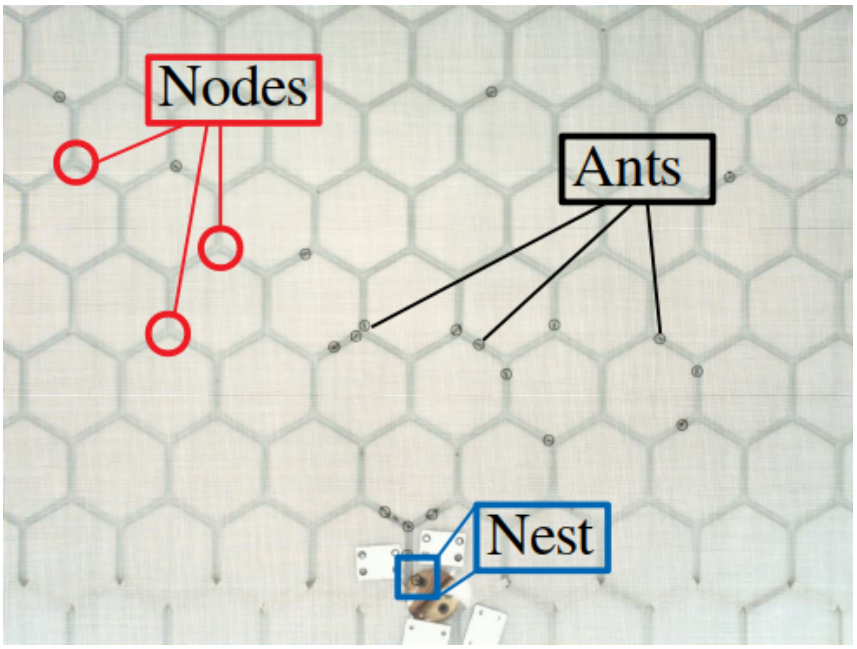

Figure 5.15: *Frame of the experimental set-up for one colony. The square PVC structure is constituted by a set oh hexagons. One can observe the connection between the nest and the structure, which represents the entrance to the channels. The ants moving through the channels have been rounded by a black circle for easing their localization in the frame. Three different nodes (of $r = 20$ mm) are shown rounded by red circles.*

The foraging experiments are carried out as follows. First, we introduce two pieces of food (small worm pieces), each in a given crossing. Then, the nest is connected to the main structure. From this point and for the successive 10800s, we capture a picture of the structure on grounds of two frames per second. During this span, the ants move freely within the structure while foraging.

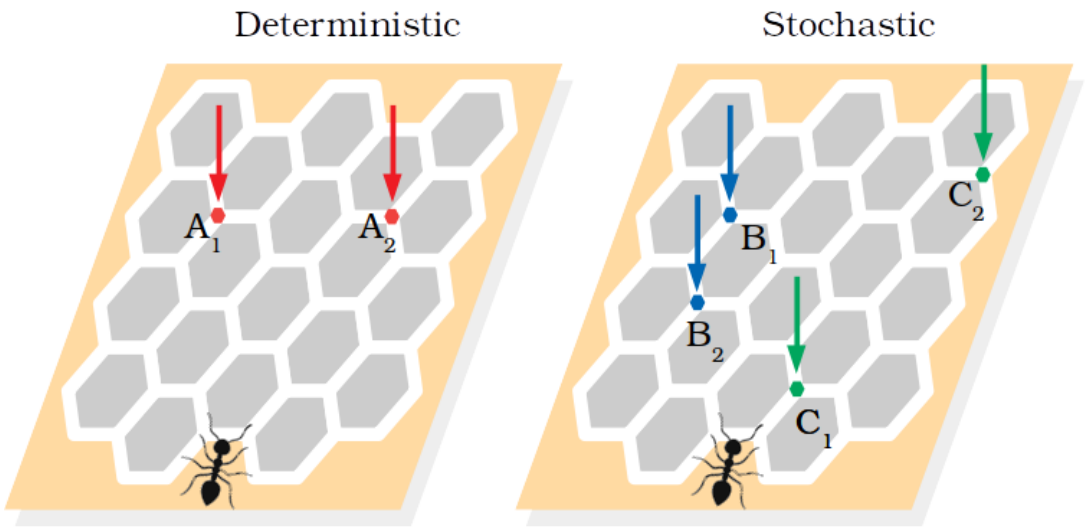

Figure 5.16: *Schematic representation of the resource location. In the left panel, we represent the scenario in which both worm pieces are placed in the same patches in each daily experiment (A_1 and A_2). We name this scenario as the condition D. In the right panel , we represent the scenario in which both worm pieces are placed in patches selected at random in each daily experiment. We name this scenario as the condition S. Blue dots corresponds to the resource location for a given daily trial i and the green ones, for the trial $i + 1$.*

We perform this experiment on a daily basis during a 14 days period for each one of the colonies, A and B. The environmental variability is introduced in the experiment through two scenarios, D and S, which differ in how the worm pieces are placed (see figure 5.16).

For the scenario D (**Deterministic** setting), the pieces are located in all daily trials in the same intersections. For the scenario S (**Stochastic** setting), each piece is located by choosing randomly one single intersection in the lattice. The structure is cleaned after each experimental realization to avoid any possible chemical marks. The first 7 days of experiments, the resources were placed accordingly to the scenario D for both colonies, which, according to our observations and the previous experience with similar foraging experiments [308, 339, 340] is a time large enough for the colony to get adapted to such conditions. Then, during 7 additional days food was located in the maze following the scenario S. While the colony A seems to explore more actively the structure than the colony B, both picked all the worm pieces during all the experimental trials.

5.3.1.1 Construction of the binary signal

As done for the previous experiment presented in Section 5.2, we assign a value 1 (occupied) to the i-node in the corresponding frame time if one or more ants are detected in there, and otherwise, the value is settled to 0 (empty). So we have transformed the videos to a binary signal of occupation for each node, with a framerate of 2 Hz.

Each intersection in the hexagonal lattice (figure 5.15) is defined as a node of the Spin-Glass lattice using the idea from figure 5.2. To assign an intersections as occupied, we define a radius r (which is approximately of the size of he intersection). When an ant is detected at a lower distance than r from the center of a certain i-node (intersection) in a given frame, we assign the ant to that i-node in that given frame. The value of r is related with the hexagonal structure and the characteristic distance between the nodes. We have used a value $r = 20$ mm. The total number of nodes of the resulting lattice is $N = 620$.

The large number of nodes in comparison to the colony population leads to the presence of empty nodes during large time spans. The interesting point of the Spin-Glass method relies on comparing and decoding why some nodes tend to be occupied or empty and how are related between them. So we have coarse-grained the temporal signal in sets of 50 frames to amplify the behavior. If one (or more) of the 50 frames within the group have a corresponding value 1 for the i-node, the new superframe or coarse-grained signal would be considered as a occupied state. In any other case, the new superframe would be settled as 'empty'. According this, 1 step in the coarse-grained signal corresponds to 25 s of experimental data.

5.3.2 Simulation and fitting details

The fitting procedure provided in Section 5.2 becomes extremely expensive from a computational perspective when N is large. Here, the structure considered fulfills $N = 620$, so the size of the parameter phase space is extremely large compared to the experiment in Section 5.2 ($N = 8$).

For those situations, approximated analytical expressions have been derived to obtain the parameters from the data-set, as stated before in Section 5.1.3. Here, we use the expression derived in [332]. That approach, named as the **Sassek-Monasson** approach (SM), comes from a second order variational approximation of the maximal entropy principle [121, 122]. The Sassek-Monasson expression describes the h and J parameters as a combination of the first two moments of the experimental data: the node occupation m_i and the correlation between pairs C_{ij}. The SM approach is a refinement of the Independent Pair approximation (IP), and the mathematical expressions corresponding to SM approach include the expressions of the IP approach. The IP approach is obtained from a first order expansion in the entropy potential between two spins [321]. The pairwise interaction in the IP approach reads

$$J_{ij}^{IP} = \frac{1}{4} \ln \frac{\left((1+m_i)(1+m_j)+C_{ij}\right)\left((1-m_i)(1-m_j)+C_{ij}\right)}{\left((1+m_i)(1-m_j)-C_{ij}\right))\left((1-m_i)(1+m_j)-C_{ij}\right)} \tag{5.5}$$

The SM method, as stated, extends the expression for J_{ij}^{IP} to the case of small correlations. Then, the expression for the external fields h_i and the J_{ij} in the SM approach are

$$h_i = 0.5 \ln \frac{1+m_i}{1-m_j} - \sum_j J_{ij}^{IP} - \sum_j 0.5 \ln \frac{(1-m_j-C_{i,j})(1-m_i)}{(1-m_j+C_{i,j})(1+m_i)} \tag{5.6}$$

$$J_{ij}^{SM} = J_{ij}^{IP} - (C^{-1})_{ij} - \frac{C_{ij}}{(1-m_i^2)(1-m_j 2)-C_{ij}^2} \tag{5.7}$$

where the sum in j extends over all the nodes that interact with the node i.

Once the parameters have been introduced, one can state that the corresponding spin-glass model so obtained represents an *in silico* replica of the ant colony at the level of its spatial distribution. To be more specific, we obtain from the fitting techniques four different replicas. They correspond to ant colonies A and B in the conditions D and S. We validate the method by comparing some of its predictions to the properties of the real experiments done in the lab. The exact procedure we use for this is as follows. As done in Section 5.2 with the simple environment experiment, we set the initial state of the spin-glass at $\mathbf{I} = 0$, which corresponds to all nodes empty , so there are no ants within the arena. The unique node settled as occupied is the one corresponding to the nest position. Then, the system is stochastically allowed to evolve in time according to a Monte Carlo dynamics with the Metropolis algorithm. According to this, new candidate states (with new occupied nodes) will be proposed and subsequently accepted (rejected) if the corresponding state approaches to (departs from) the most stable patterns (energy wells) of the spin-glass Hamiltonian.

As a result of this procedure, the average occupancy $\langle I \rangle$ in the spin-glass is defined as the average over the entire time window and the collective of nodes. From the figure 5.17, we observe that replicas of the colonies generated by the spin-glass method reproduce almost

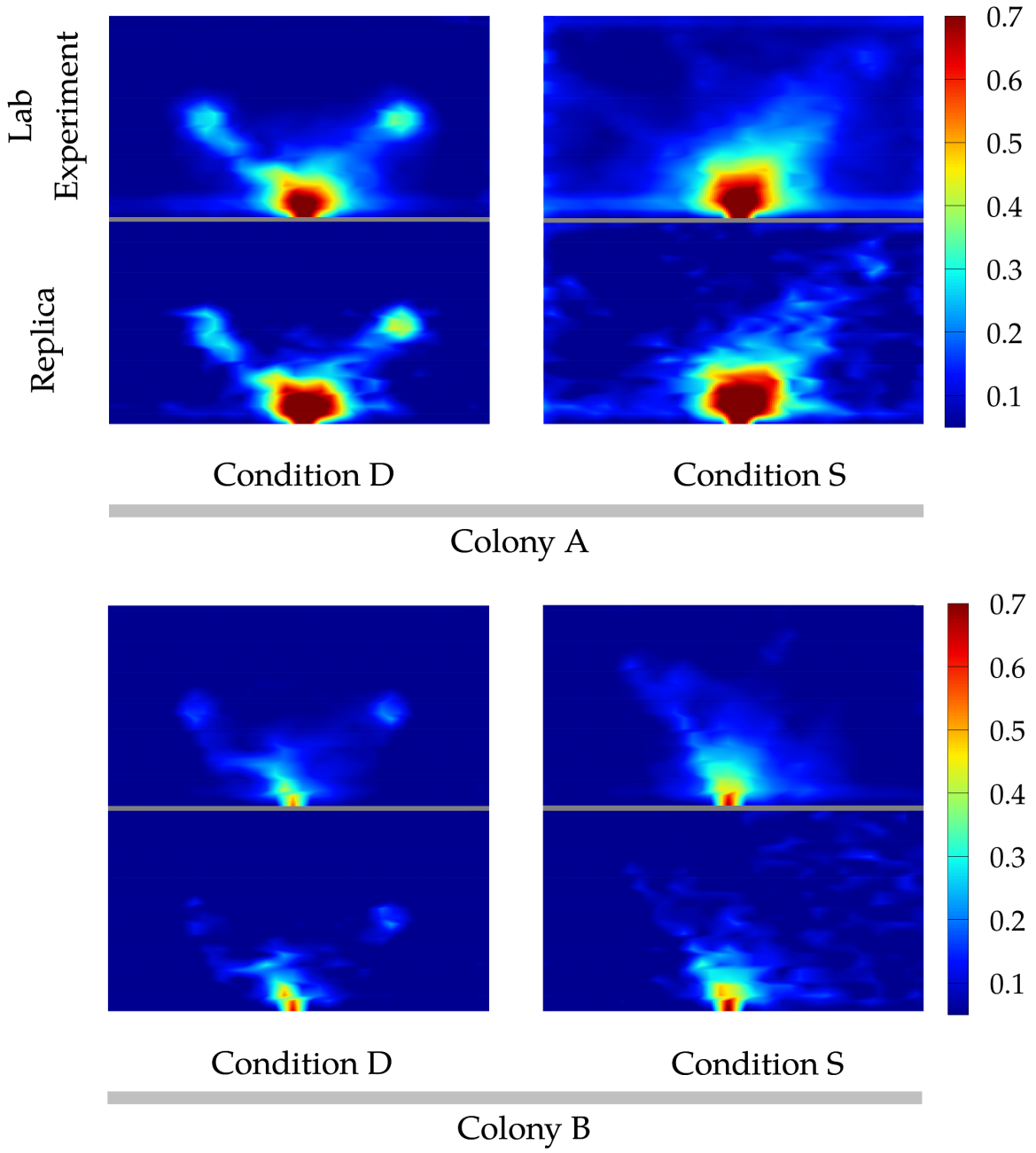

Figure 5.17: *Averaged occupation* $\langle I \rangle$ *in each node of the structure during the last* 5400*s of experiment of each daily trial. The upper panel of each figure corresponds to the experimental data, while the lower panel corresponds to the replica's data.*

perfectly the spatial patterns present in the experimental data. The colony A seems to explore more actively the structure than the colony B, producing a larger average occupancy $\langle I \rangle$. The computational replicas yield so consistent results for both colonies and for both resource conditions.

These occupation patterns also tell us that the foraging strategies seem to differ between the stochastic and the deterministic food conditions. For the stochastic (S) case, the spreading of the colony through the arena exhibits **radial** symmetry from the nest. So the ants explore

	General Parameters					
	Field			Pairwise		
	$\langle h \rangle$	$\langle h_f \rangle$	$\langle h_n \rangle$	$\langle J \rangle$	$\langle J_f \rangle$	$\langle J_n \rangle$
Colony A - Deterministic	-1.37±0.48	-0.43±0.03	-0.29 ±0.31	0.86±0.33	-0.03 ±0.11	0.02 ±0.08
Colony A - Stochastic	-1.04±0.40	-0.99±0.25	-0.09 ±0.18	0.22±0.46	0.09±0.10	0.01 ±0.05
Colony B - Deterministic	-1.85±0.53	-0.97±0.03	-0.88 ±0.36	3.13±0.99	-0.02±0.24	0.09 ±0.07
Colony B - Stochastic	-1.41±0.36	-1.34±0.27	-0.62 ±0.29	0.35±0.82	-0.01±0.15	0.05 ±0.05

Table 5.1: *Averaged external field and pairwise interaction for the entire structure ($\langle h \rangle$ and $\langle J \rangle$), for the patches that contain resources ($\langle h_f \rangle$ and $\langle J_f \rangle$) and for the region close to the nest ($\langle h_n \rangle$ and $\langle J_n \rangle$). The results are presented for both colonies and both experimental conditions.*

in average randomly the structure. On the contrary, we observe for the deterministic (D) condition that, in addition to the region close to the nest, there are two **hot spots**. They correspond to the location of the resources in the real experiment in the lab. The ants exploit the hot spots and spend significant times collecting the food therein. The computational replica, accordingly, exploits these regions too and discards the exploration of the rest of the structure. In summary, the average behavior of the colonies adapt its foraging strategy from a more exploratory pattern (for stochastic food conditions), where the ants invest more time exploring the entire structure, to an exploitation mechanism (for deterministic conditions), where the ants focus on the hot spots, as a function of the conditions found.

5.3.3 Time dynamics comparison

Since foraging in ants is obviously a non-stationary process which proceeds through several phases (recruitment, food gathering, ...), one can wonder whether the spin-glass results, obtained from the experimental occupancy patterns without explicitly considering such phases, are really meaningful. To check this we have compared the main properties of the set of h and J parameters obtained with (i) those that appear if only the first half of each trial (where searching and recruitment are dominant) is considered, and (ii) those obtained for the second half of the trial (where food gathering is dominant). Despite the biological differences between the two situations, we observe that the mean values of the spin-glass parameters ($\langle h \rangle$ and $\langle J \rangle$), and their corresponding dispersion, remains quite similar (see Tables 5.1, 5.2 and 5.3) . This means that the information captured through such parameters is not strongly dependent on the particular stage of the process, but mostly depends on the foraging activity of the colony and their tendency for exploration or exploitation.

We observe that Colony A clearly shows higher values of $\langle h \rangle$ (corresponding to higher foraging activity) than colony B. Also, we observe that $\langle J \rangle$ values are much higher for the D scenario than for the S scenario. All these results are detailed in Table 5.1. This corresponds to the case in which the whole spatial domain is analyzed. However, if we only explore those particular regions either in the vicinity of the nest or the vicinity of food, the correlations are expected to be relatively similar for both colonies and for both scenarios. Then mean values of J will show very similar values independent of the colony or the scenario; this is actually what we observe from our analysis (Table 5.1).

One can wonder if there is a dynamical evolution, or different regimes, for the colonies behavior during each trial. We split the experimental data in two regimes (I and II)

	Temporal evolution of h					
	Regime I (3600 − 7200 s)			Regime II (7200 − 10800 s)		
	$\langle h \rangle$	$\langle h_f \rangle$	$\langle h_n \rangle$	$\langle h \rangle$	$\langle h_f \rangle$	$\langle h_n \rangle$
Colony A - Deterministic	-1.15±0.42	-0.12±0.02	0.04 ±0.14	-1.46±0.42	-0.58 ±0.03	-0.36 ±0.30
Colony A - Stochastic	-0.86±0.31	-0.81±0.18	0.01 ±0.09	-1.06±0.26	-1.04±0.19	-0.14 ±0.21
Colony B - Deterministic	-1.74±0.51	-0.79±0.04	-0.84 ±0.38	-1.88±0.52	-1.03±0.06	-0.89 ±0.36
Colony B - Stochastic	-1.23±0.23	-1.05±0.18	-0.54 ±0.32	-1.57±0.20	-1.44±0.15	-0.63 ±0.30

Table 5.2: *Averaged external field for the entire structure ($\langle h \rangle$), for the patches that contain resources ($\langle h_f \rangle$) and the averaged field close to the nest ($\langle h_n \rangle$). The results are presented for both colonies and both experimental conditions. The values are divided into two regimes, each one of them coming from a part of the temporal signal of the experiments.*

	Temporal evolution of J					
	Regime I (3600 − 7200 s)			Regime II (7200 − 10800 s)		
	$\langle J \rangle$	$\langle J_f \rangle$	$\langle J_n \rangle$	$\langle J \rangle$	$\langle J_f \rangle$	$\langle J_n \rangle$
Colony A - Deterministic	0.70±0.33	-0.07±0.06	0.01 ±0.04	1.66±0.57	0.03 ±0.06	0.02 ±0.05
Colony A - Stochastic	0.22±0.32	0.06±0.21	0.01 ±0.04	0.23±0.43	0.11±0.20	0.01 ±0.03
Colony B - Deterministic	2.30±0.80	-0.15±0.06	0.08 ±0.07	3.81±1.30	0.14±0.12	0.07 ±0.07
Colony B - Stochastic	0.27±0.12	0.01±0.09	0.04 ±0.04	0.43±0.28	-0.01±0.06	0.05 ±0.04

Table 5.3: *Averaged pairwise interaction for the entire structure ($\langle J \rangle$), for the patches that contain resources ($\langle J_f \rangle$) and the averaged interaction and the averaged interaction close to the nest ($\langle J_n \rangle$). To do the average, only the interaction with patches located at a smaller distance of* $200mm$ *are taken. The results are presented for both colonies and both experimental conditions. The values are divided into two regimes, each one of them coming from a part of the temporal signal of the experiments.*

corresponding to the second (I) and third (II) thirds of the experimental signal (3600 − 7200 s and 7200 − 10800 s, respectively). We disregard the initial third to avoid the time region in which the ants have not yet gotten out of the nest. One can observe in Tables 5.2 and 5.3 that the parameters h and J seem to be robust for both regimes.

Next, the dynamical trends predicted by the computational replica of the colony can be compared to the patterns of the real colony, too, by measuring the distribution of persistence times (τ). As noted in Section 5.2, the persistence time is defined as the amount of time one node (or spin) stays in the same state (either occupied or empty) before switching to the other one.

When we look at the corresponding distribution of persistence times $P(\tau)$ experimentally for the ants, again it follows a non-trivial behavior which corresponds to an intermediate decay between exponential and power-law functions (figure 5.18). Although it is not possible to provide a simple fit for that distribution, we observe that the replicas yield a very good agreement to the experimental data. So, these results again confirm that the spin-glass method is able to reproduce dynamical properties, as well as the stationary statistics, in the experimental conditions used.

5.3.4 Biological interpretation of the model parameters

Figure 5.19 summarizes qualitatively the most relevant biological information that can be extracted from the spin-glass approach in the present context. Since the h_i parameters reflect the occupancy of each node i, then the mean $\langle h \rangle$, averaged over all nodes, provides a measure of the **foraging activity** of the colony. More interestingly, when foraging efforts are localized in small regions (exploitation) then we have both large regions unoccupied

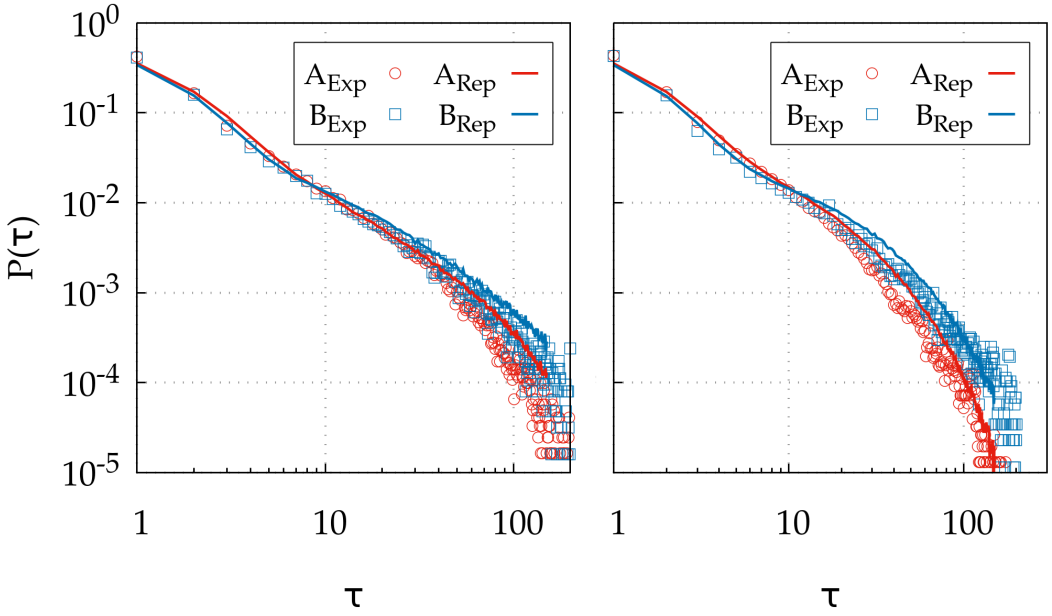

Figure 5.18: *Probability distribution of the persistence time $P(\tau)$. The results for the experimental data (points) and the replica simulations (solid lines) are provided. The left panel corresponds to the deterministic experimental condition D and the right one, to the stochastic condition S.*

(where J_{ij} between neighbour nodes will be large and positive, since occupancies follow the same pattern), and small regions with a high occupancy (so there correlations between neighbours are also large and positive).

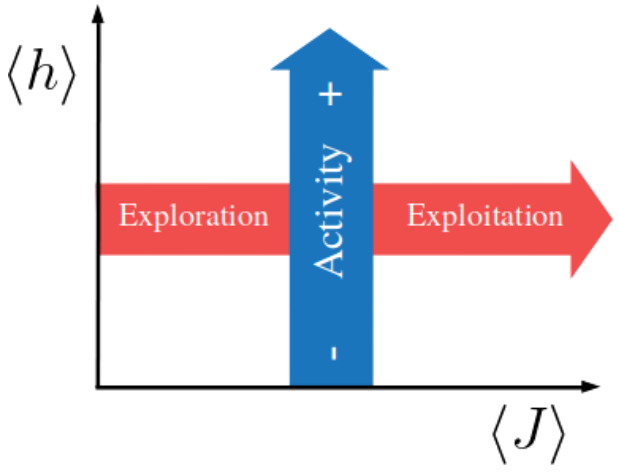

Figure 5.19: *Schematic representation of the biological meaning of the parameters $\langle h \rangle$ and $\langle J \rangle$. The obtained values from the experimental dataset represent a proxy for the strategies the ant colony develops during the foraging process.*

On the contrary, when foraging efforts are disperse the correlation between the occupancy patterns of neighbour nodes will be null or even negative (as occupied nodes will be in general surrounded by empty nodes). Then most J_{ij} values are expected to be negative. Accordingly, the mean $\langle J \rangle$ (averaged over neighbour nodes) provides a significant measure to compare the level of exploitation and exploration that is being employed by the colony. The intensity of the interactions can be well captured by the absolute value $|J_{ij}|$ (figure 5.20). As intuitively expected, the interaction is more intense between closer nodes and seems to decay without a characteristic scale length for short distances.

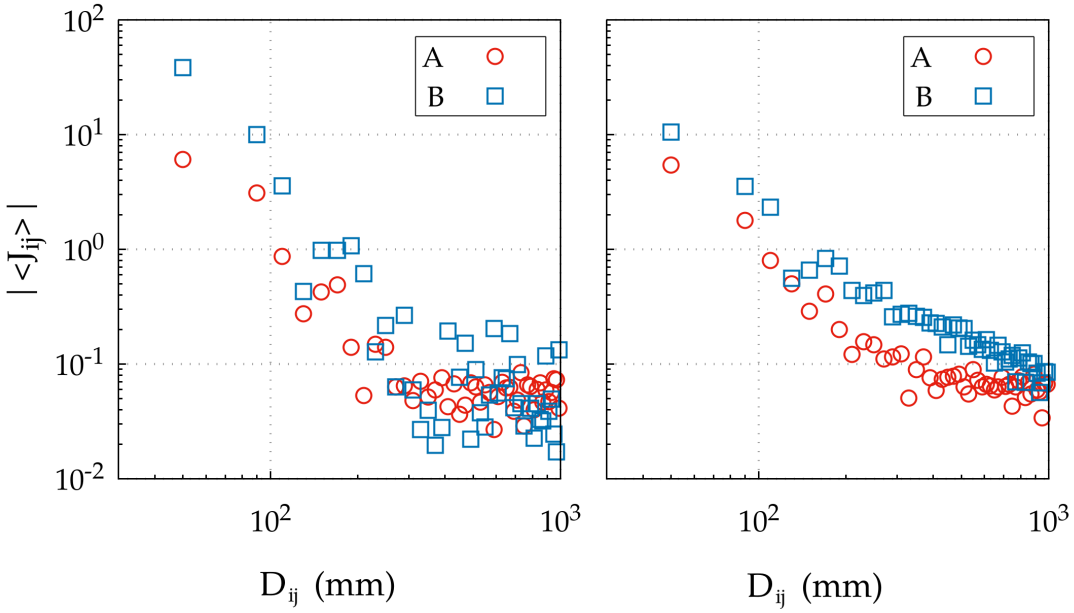

Figure 5.20: *Averaged pair interaction $\langle J_{ij} \rangle$ (in absolute value) between the nodes i and j according to the distance between them. The left panel corresponds to the deterministic condition D and the right one, to the stochastic condition S.*

5.3.5 Foraging strategies and the exploration-exploitation trade off

Besides the useful value of the previous results in order to understand the foraging patterns followed by the ant colonies in complex environments, one of the most interesting advantages of building computational (spin-glass) replicas of the colony patterns is to design ***in silico* experiments** for predicting their behavior under alternative scenarios. So, for example, the flexibility of the foraging patterns exhibited under the resource conditions S and D could be tested by analyzing its efficiency when alternatives food conditions are considered.

The foraging patterns adapted to changing (random) conditions S, where exploration is largely promoted in comparison to the condition D of deterministic food location, are expected to offer a more flexible response. While this idea is easy and intuitive, quantification of such effects is far from trivial under field or lab conditions, so in the following we present several ways to address this idea from using our *in silico* replicas of the colonies.

5.3.5.1 Experiment I: Crossing food conditions

One can compute the time it takes for the computational replicas to reach the food locations under crossed scenarios (so the replica adapted to random conditions is tested under D food conditions, and vice versa).

Again, we set the initial state of the spin-glass at $\mathbf{I} = 0$, which corresponds to all nodes empty, so there are no ants within the arena, except for the nest position. Then, the system

is stochastically allowed to evolve in time according to a Monte Carlo dynamics with the Metropolis algorithm and develop its characteristic patterns.

We assume that the food will be picked up as soon the colony reached there, so we will use as a measure of efficiency the foraging time T_f, which is defined as the number of Monte Carlo steps that the replica requires to reach both food pieces in the experiment.

According to the results found from this *in silico* experiment (figure 5.21), the replicas adapted to S conditions require the same time T_f to locate the food items independently of how they are placed in space (randomly or deterministically). On the contrary, the replicas D are much more efficient (one order of magnitude) when the resources are located in the deterministic region, which is the case to which they are adapted, and perform much worse under uncertain (S) conditions. The latter colony **exploits** the acquired knowledge and is almost unable to forage through unexplored regions of the structure to which it is not adapted

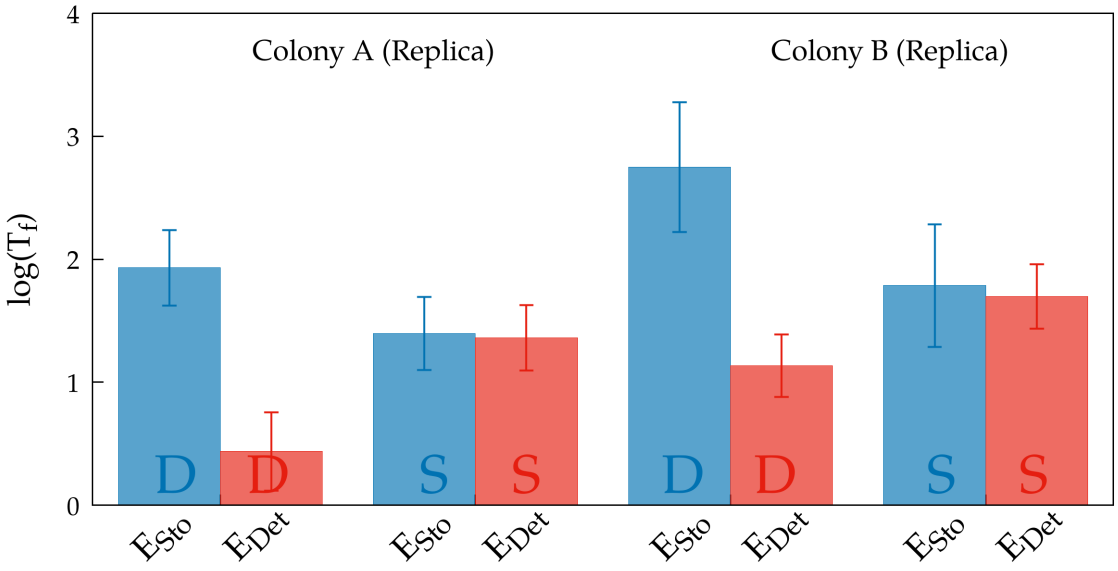

Figure 5.21: *Averaged number of MonteCarlo steps (T_f) the replica uses to find both worm pieces. The data is presented in a logarithmic format and the error bars correspond to the standard deviation. The color code corresponds to the experimental condition, being the blue color the experiment with the resources located randomly and the red color, the experiment with the resources in the hot spots. D corresponds to the replica trained with the data of the condition D, while S trained with the data of the condition S.*

5.3.5.2 Experiment II: Size of hot spots

How efficient the colonies adapted to one specific condition would be under more realistic scenarios (where the location of food resources is not purely stochastic or deterministic) represents another question of major interest. As a possible approximation to the answer, we consider new *in silico* experiments where we compare the efficiency of the different replicas under scenarios in which the resources are located in a circular region of radius R around the intersection of the deterministic locations for conditions D (see figure 5.22).

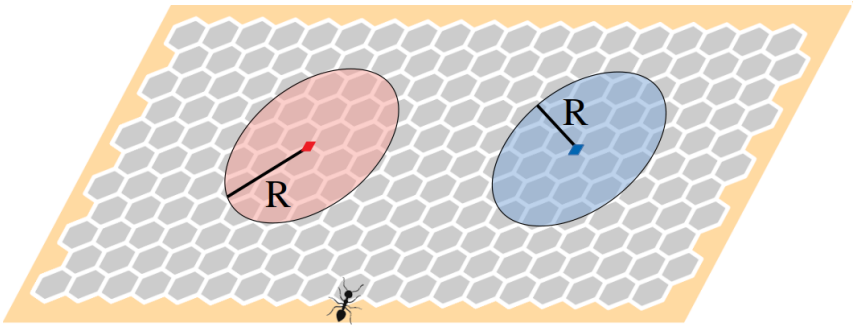

Figure 5.22: *Schematic representation of the scenario of the in silico experiment. The virtual worm pieces will be located in a random intersection of the region delimited by the circumferences of radius R around the hot spots of condition D.*

When $R = 0$ mm, the resource condition D is recovered. As long as R increases, the location region covers the entire structure and the resource condition S is approached. Though the lab experiments were conducted with two food (worm) pieces, the feasibility of *in silico* conditions allow us to explore now foraging in many other situations. We will show results for the cases when there are one, two or four worm pieces. According to the results

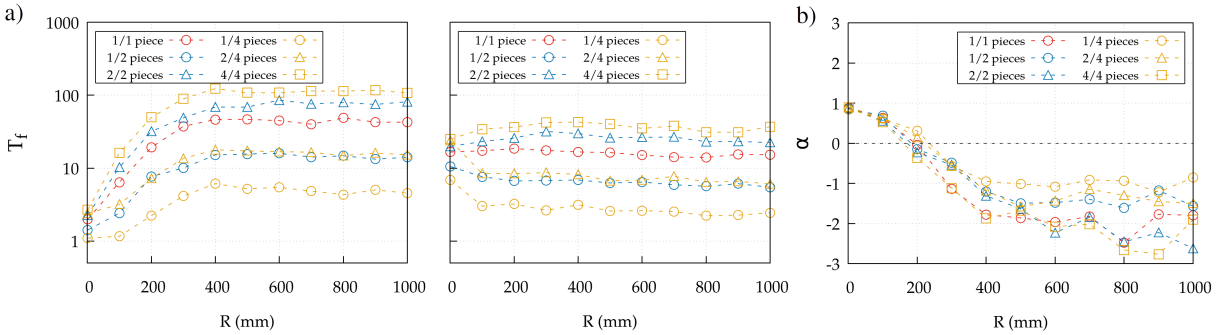

Figure 5.23: *a) Averaged number of MonteCarlo steps (T_f) the replica uses to find the worm pieces according to the size of the resource region R. Left panel corresponds to the replica trained with the data of the condition D and the right panel corresponds to the replica trained with the data of the condition S. b) Coverage time comparison for the case of* 4 *worm pieces. The y-axis value corresponds to the relative difference between the T_f of both replicas, and it is defined as* $\alpha = 1 - \frac{T_f^D}{T_f^S}$.

provided in figure 5.23, we find that relative performance of the different replicas changes as a function of the radius R. When the pieces are located around the deterministic locations (in particular, if $R < 200mm$), the replica adapted to D conditions is more efficient than the other one as the properties of the deterministic condition D still remain, approximately. However, when R is increased and further regions need to be explored, the replica adapted to the random (or S) conditions becomes more efficient. While the replica adapted to D requires to complete the task a time that can vary up to two orders of magnitude, the replica adapted to S exhibits a much more homogeneous behavior between the different realizations of the process. These features reveal again that the preconditioning of the colonies will largely affect its performance under unfamiliar scenarios. Interestingly, the number of food items does not seem to modify the convenience of one strategy over the other, as the point trade-off remains around $R = 200$ mm. The size of the regime in which exploration is more efficient may be a relevant factor to characterize the **trade-off** and to define a more optimal strategy under realistic (so complex) environments. For the sake

of simplicity, we presented here the experiments with the colony A replicas; the same experiments were conducted for the colony B, with similar conclusions.

5.3.5.3 Experiment III: Combining hot spots and randomness

Adding still a new level of detail on the previous scheme, realistic environments may combine the presence of fixed exploitable sources together with more unpredictable or random food sources. For those cases, again, it is far from clear which is the level of **randomness/uncertainty** at which one replica or the other will show a higher efficiency.

Following this idea, we propose a scenario in which the resources may be either located at the deterministic locations from conditions D, or randomly at any other place of the arena. In particular, every food item will be located with probability P_s according to the D conditions, or located randomly with probability $1 - P_s$. Then the situations so considered range from the random (S) condition for $P_s = 0$ to the deterministic (D) condition, when $P_s = 1$.

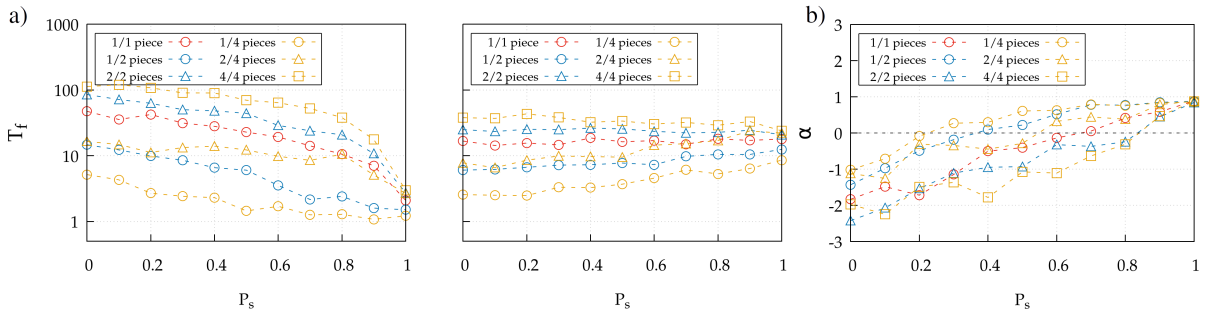

Figure 5.24: *a) Averaged number of MonteCarlo steps (T_f) the replica uses to find the worm pieces according to the probability P_s. Left panel corresponds to the replica trained with the data of the condition D and the right panel corresponds to the replica trained with the data of the condition S. b) Coverage time comparison for the case of 4 worm pieces. The y-axis value corresponds to the relative difference between the T_f of both replicas, and it is defined as* $\alpha = 1 - \frac{T_f^D}{T_f^S}$.

In agreement with the results for the experiment II, the most convenient strategy changes when the value of P_s is tuned, independently of the number of food items located in the structure (figure 5.24). When the daily location is mainly stochastic (small P_s), the exploration preconditioning (this is, the replica adapted to S conditions) is more effective. When the scenario tends to be mostly deterministic, the replica adapted to the D conditions reaches a higher efficiency (this is, it reaches food faster in average). While the replica adapted to D requires foraging times that could vary up to two orders of magnitude, the replica adapted to S finishes the process in times that are always of the same order. Nevertheless, in this case we observe a relevant effect on the number of food items present in the system on the value of P_s at which the switch occurs. When computing the time required for acquiring the first piece of food, the **turnaround** in the more efficient replica is produced around $P_s = 0.6$, $P_s = 0.3$ and $P_s = 0.2$ when there are 1, 2 or 4 pieces in the structure, respectively. In consequence, it can be stated that the optimal foraging

strategy is not just a consequence of the resource density and location but also of the colony requirements. For the sake of simplicity, we presented here the experiments with the colony A replicas; the same experiments were conducted for the colony B, with similar conclusions.

Concluding remarks

- The complexity of Spin-Glass frameworks (as an example of state-based description) allows to capture collective space use by biological populations or superorganisms.
- Producing *in silico* replicas using these frameworks opens the possibility to explore the behavior of those populations in a wide range of scenarios without a need for extensive field experiments.

6 Conclusions

This thesis has addressed the movement patterns of living with different levels of cognitive ability/complexity, both in isolated and collective situations, developing theoretical models rooted in statistical physics. Here, we summarize the main conclusions (•) and future perspectives (⋄) for each chapter.

In Chapter 1, we proposed the use of stochastic movement models to describe the organisms navigation. We started by presenting the ordinary Random Walk. From this, we incorporated multiple cognitive layers (self-avoidance, impairment and prospection) to the walker's dynamics, from which we draw the following:

- We propose two cognitive or memory mechanisms (bSAW and tSAW) as an alternative for the SAW. Both proposals avoid the presence of dead ends, representing then a more adequate description of living organism navigation.
- Impairment in the walker's cognitive memory has been revealed surprisingly beneficial for the bSAW in some particular situations. This is because it avoids the ordinary diffusive regime that appears when the energy landscape is homogeneous. However, when the energy landscape is kept heterogeneous (as in the tSAW case), this effect goes away.
- Prospection of non-local information has been shown to be beneficial just when the walker's process it accurately. In other cases, to focus on local information optimizes the coverage process.

⋄ In the future, alternative cognitive layers (including obstacles or alternatives objects, or multiple signals, for instance) can be introduced into the energy landscape. How these layers (and their interplay with the other ones) impact the walker's navigation would represent a interesting field of study to increase our comprehension of the cognitive mechanisms exhibited by living organisms.

In Chapter 2, we proposed an entropic mechanism to describe how organisms quantify when they have processed enough information to make a decision. We presented the most common accumulator mechanism (DDM) and we proposed an 'entropy refinement' mechanism to capture the way humans carry out decisions in certain particular navigation tasks. From this study, we conclude:

- When presented sequential-decision making tasks, humans explicitly use prospection of the future outcomes. While this is not surprising, we have found a way to confirm and quantify this property. Our random-walk algorithm reveals that the performance of subjects in the experimental navigation task used could not be explained in absence of such prospection mechanism.

- An entropic refinement mechanism seems compatible with the way humans estimate how reliable is to make a decision in a decision-tree context with a given amount of information. It is plausible, then, that they implicitly compute that magnitude during the prospection processes as a way to gain reliability on the options available. This conclusion is supported both from the examination of eye-tracking data revealing (i) the waiting time distributions between decisions shown by the subjects, and (ii) the fact that final values of the entropy shown at the moment of taking the decisions are approximately independent of the decision time.

◇ Explore the entropic mechanism and its validity in more complex scenarios through the design of new sequential decision making experiments (for example, by removing the fact that not all decisions were completely identical in the maze used in our experiment). The new experiments may help to clarify the origin of the characteristic power-law distributions ($P(t) \sim t^{-3}$) reported in our navigation task.

In Chapter 3, we extended the coverage efficiency analysis of the cognitive walker of Chapter 1 to the case where multiple walkers, sharing cognitive information in an indirect way (through their trajectories), are considered. The main conclusion is:

- The topology of the region to cover can produce a 'more is less' effect, where the coverage time gets increased as more walkers are added to the search process. That feature appears for one-dimensional searches of walkers with intense self-avoidance. However, as the dimension of the region gets increased the intuitive result of more walkers covering it faster is recovered.

◇ Explore the collective patterns and their impact over the search efficiency when direct interactions (such as repulsive/attractive potentials or hydrodynamic forces) between the walkers are considered.

Chapter 4 focuses on pedestrian dynamics. We explored how pedestrians can be described in physical terms and how collective patterns emerge from the interactions between them. We draw the following:

- One can propose effective forces to describe pedestrians interactions. The corresponding balance between avoiding collisions and individual preferences make collective patterns such as jamming or lane formation emerge.
- Multiple proposals of social force collapse to the same general behavior in the τ-space (of times-to-collision). The structure analysis within τ-space allows to discriminate if the crowd motion is disordered (which corresponds to an effective interaction $V(\tau) \sim \tau^{-2}$ between pedestrians) or organized in lanes (which corresponds to an effective interaction $V(\tau) \sim \tau^{-1}$)), which increases the flow of pedestrians.

◇ Generalize the bidirectional scenario to a multi-directional one and explore if the τ-space keeps yielding an effective description for those cases.

- ◇ Study if the τ-space can describe adequately the collective patterns exhibited by dense crowds in more complex scenarios, such as turbulence or stop-and-go waves.

In Chapter 5, we focus on how the Spin-Glass model can represent a convenient framework to describe social organization in the way how space is collectively occupied and/or explored by biological populations. More concretely, we use it to analyze the foraging patterns of ant colonies. From this, we conclude:

- A state-based approach can capture adequately the correlations that characterize the superorganism behavior of an ant colony. Trough the Spin-Glass model, we obtain a description of the ants space use not only in the stationary state but also at the level of the time evolution of the system.
- The Spin-Glass provides a virtual replica of the real system. With this replica, one can design new *in silico* experiments. We have explored this for the exploration-exploitation trade-off in ant colonies under different environmental conditions, which represents a very relevant aspect to understand animal foraging.

- ◇ Extend the analysis the exploration-exploitation trade-off through new *in silico* experiments to characterize the efficiency of the foraging strategies under variable circumstances.
- ◇ Explore the use of the Spin-Glass model to as a tool to characterize collective organization in living organisms or complex systems.

Globally, this thesis illustrates how cognitive mechanisms of living organisms can be gained by models based on statistical physics. Thus, it encourages to extend this approach with the aim of gaining a physical understanding of cognition and information processing. Thereby, perhaps, this direction of study can devise general physical principles of mental processing and its consequences in social organization.

Acronyms

The next list describes several acronyms that have been used during this thesis.

bSAW Binary Self-Avoiding Walk

DDM Drift Diffusion model

EEG Electroencephalography

IP Independent Pair approximation

MC Monte Carlo

MEP Maximal Entropy Principle

MFPT Mean First Passage Time

MSD Mean Square Displacement

PRW Persistent Random Walk

RW Random Walk

SAW Self-Avoiding Walk

SG Spin-Glass

SM Sassek-Monasson approximation

SPRT Sequential probability ratio test

tSAW True Self-Avoiding Walk

Bibliography

Here are the references in citation order.

[1] Louis de Broglie. 'XXXV. A tentative theory of light quanta'. In: *The London, Edinburgh, and Dublin Philosophical Magazine and Journal of Science* 47.278 (1924), pp. 446–458. DOI: 10.1080/14786442408634378 (cited on page 1).

[2] J. Bardeen, L. N. Cooper, and J. R. Schrieffer. 'Theory of Superconductivity'. In: *Phys. Rev.* 108.5 (Dec. 1957), pp. 1175–1204. DOI: 10.1103/PhysRev.108.1175 (cited on page 1).

[3] URL: https://www.nature.com/articles/d41586-018-06034-8 (cited on page 1).

[4] Christopher W. Lynn and Danielle S. Bassett. 'The physics of brain network structure, function and control'. In: *Nature Reviews Physics* 1.5 (May 2019), pp. 318–332. DOI: 10.1038/s42254-019-0040-8 (cited on page 2).

[5] Karl Friston, James Kilner, and Lee Harrison. 'A free energy principle for the brain'. In: *Journal of Physiology-Paris* 100.1 (2006). Theoretical and Computational Neuroscience: Understanding Brain Functions, pp. 70–87. DOI: https://doi.org/10.1016/j.jphysparis.2006.10.001 (cited on pages 2, 50).

[6] Mark Buchanan. 'What has econophysics ever done for us?' In: *Nature Physics* 9.6 (2013), p. 317. DOI: 10.1038/nphys2648 (cited on page 2).

[7] Christophe Schinckus. 'Introduction to econophysics: towards a new step in the evolution of physical sciences'. In: *Contemporary Physics* 54.1 (2013), pp. 17–32. DOI: 10.1080/00107514.2013.774528 (cited on page 2).

[8] Gandhimohan. M. Viswanathan et al. *The Physics of Foraging: An Introduction to Random Searches and Biological Encounters*. Cambridge University Press, 2011 (cited on pages 2, 15).

[9] N. Bohr. 'Light and Life'. In: *Nature* 131.1 (1933), pp. 421–423. DOI: 10.1038/131421a0 (cited on page 2).

[10] Erwin Schrödinger. *What is Life? The Physical Aspect of the Living Cell*. Cambridge University Press, 1944 (cited on page 2).

[11] Kim Sneppen and Giovanni Zocchi. 'Evolution'. In: *Physics in Molecular Biology*. Cambridge University Press, 2005, pp. 245–279. DOI: 10.1017/CBO9780511755699.011 (cited on page 2).

[12] Serge Galam, Yuval Gefen (Feigenblat), and Yonathan Shapir. 'Sociophysics: A new approach of sociological collective behaviour. I. mean-behaviour description of a strike'. In: *The Journal of Mathematical Sociology* 9.1 (1982), pp. 1–13. DOI: 10.1080/0022250X.1982.9989929 (cited on page 2).

[13] E.Roy John. 'The neurophysics of consciousness'. In: *Brain Research Reviews* 39.1 (2002), pp. 1–28. DOI: https://doi.org/10.1016/S0165-0173(02)00142-X (cited on page 2).

[14] Santo Motta and Francesco Pappalardo. 'Mathematical modeling of biological systems'. In: *Briefings in Bioinformatics* 14.4 (Oct. 2012), pp. 411–422. DOI: 10.1093/bib/bbs061 (cited on page 2).

[15] S. I. Rubinow. 'Introduction to Mathematical Biology'. In: 1975 (cited on page 2).

[16] Yuri I. Wolf, Mikhail I. Katsnelson, and Eugene V. Koonin. 'Physical foundations of biological complexity'. In: *Proceedings of the National Academy of Sciences* (2018). DOI: 10.1073/pnas.1807890115 (cited on page 2).

[17] Kyle Vining and David Mooney. 'Mechanical forces direct stem cell behaviour in development and regeneration'. In: *Nature Reviews Molecular Cell Biology* 18 (Nov. 2017). DOI: 10.1038/nrm.2017.108 (cited on page 2).

[18] Pere Roca-Cusachs, Vito Conte, and Xavier Trepat. 'Quantifying forces in cell biology'. In: *Nature cell biology* 19 (June 2017). DOI: 10.1038/ncb3564 (cited on page 2).

[19] Nicholas H. Barton and Harold Perez de Vladar. 'Statistical Mechanics and the Evolution of Quantitative Traits'. In: *Genetics* (2008). DOI: 10.1534/genetics.108.099309 (cited on page 2).

[20] Adam Prügel-Bennett and Jonathan L. Shapiro. 'Analysis of genetic algorithms using statistical mechanics'. In: *Phys. Rev. Lett.* 72.9 (Feb. 1994), pp. 1305–1309. DOI: 10.1103/PhysRevLett.72.1305 (cited on page 2).

[21] Nicholas A. Licata et al. 'Diffusion of Bacterial Cells in Porous Media'. In: *Biophysical Journal* 110.1 (2016), pp. 247–257. DOI: https://doi.org/10.1016/j.bpj.2015.09.035 (cited on page 3).

[22] G. Wadhams and J. Armitage. 'Making sense of it all: bacterial chemotaxis'. In: *Nature Reviews Molecular Cell Biology* 5 (2004), pp. 1024–1037 (cited on page 3).

[23] Mathieu Lihoreau et al. 'Collective selection of food patches in Drosophila'. In: *Journal of Experimental Biology* 219 (Jan. 2016). DOI: 10.1242/jeb.127431 (cited on page 3).

[24] Claire Detrain and Jean-Louis Deneubourg. 'Collective Decision-Making and Foraging Patterns in Ants and Honeybees'. In: ed. by S.J. Simpson. Vol. 35. Advances in Insect Physiology. Academic Press, 2008, pp. 123–173. DOI: https://doi.org/10.1016/S0065-2806(08)00002-7 (cited on page 3).

[25] Karin A. Jansen et al. 'A guide to mechanobiology: Where biology and physics meet'. In: *Biochimica et Biophysica Acta (BBA) - Molecular Cell Research* 1853.11, Part B (2015). Mechanobiology, pp. 3043–3052. DOI: https://doi.org/10.1016/j.bbamcr.2015.05.007 (cited on page 3).

[26] Leonid Perlovsky. 'Physics of the Mind'. In: *Frontiers in Systems Neuroscience* 10 (Nov. 2016). DOI: 10.3389/fnsys.2016.00084 (cited on page 3).

[27] Franziska Michor et al. 'What does physics have to do with cancer?' In: *Nature reviews. Cancer* 11 (Aug. 2011), pp. 657–70. DOI: 10.1038/nrc3092 (cited on page 3).

[28] D. Wirtz, K. Konstantopoulos, and P.C. Searson. 'The physics of cancer: The role of physical interactions and mechanical forces in metastasis'. In: *Nature Reviews Cancer* 11.7 (2011). cited By 687, pp. 512–522. DOI: 10.1038/nrc3080 (cited on page 3).

[29] Dirk Helbing and Peter Molnar. 'Social Force Model for Pedestrian Dynamics'. In: *Physical Review E* 51 (May 1998). DOI: 10.1103/PhysRevE.51.4282 (cited on page 3).

[30] John Urry. 'Small Worlds and the New 'Social Physics''. In: *Global Networks* 4.2 (2004), pp. 109–130. DOI: https://doi.org/10.1111/j.1471-0374.2004.00083.x (cited on page 3).

[31] Alessandro Vespignani et al. 'Modelling COVID-19'. In: *Nature Reviews Physics* 2 (May 2020). DOI: 10.1038/s42254-020-0178-4 (cited on page 3).

[32] Matjaž Perc et al. 'Forecasting COVID-19'. In: *Frontiers in Physics* 8 (2020), p. 127. DOI: 10.3389/fphy.2020.00127 (cited on page 3).

[33] Ran Nathan et al. 'A movement ecology paradigm for unifying organismal movement research'. In: *Proceedings of the National Academy of Sciences* 105.49 (2008), pp. 19052–19059. DOI: 10.1073/pnas.0800375105 (cited on page 5).

[34] H. Dingle. 'Migration: The Biology of Life on the Move'. In: 1996 (cited on page 5).

[35] H. Dingle, Ian Swingland, and P. Greenwood. 'The Ecology of Animal Movement'. In: *The Journal of Animal Ecology* 54 (Feb. 1985), p. 339. DOI: 10.2307/4647 (cited on page 5).

[36] Paul Racey. 'Ecology of Bat Reproduction'. In: *Ecology of bats* (Jan. 1982), pp. 57–104. DOI: 10.1007/978-1-4613-3421-7_2 (cited on page 5).

[37] Mark C. Mainwaring et al. 'The design and function of birds' nests'. In: *Ecology and Evolution* 4.20 (2014), pp. 3909–3928. DOI: https://doi.org/10.1002/ece3.1054 (cited on pages 5, 7).

[38] Graham H. Pyke. 'Optimal foraging: Movement patterns of bumblebees between inflorescences'. In: *Theoretical Population Biology* 13.1 (1978), pp. 72–98. DOI: https://doi.org/10.1016/0040-5809(78)90036-9 (cited on page 5).

[39] Simon Benhamou. 'Space use and foraging movements in the American red squirrel (Tamiasciurus hudsonicus)'. In: *Behavioural Processes* 37.2 (1996), pp. 89–102. DOI: https://doi.org/10.1016/0376-6357(95)00073-9 (cited on page 5).

[40] Mathieu Lihoreau et al. 'Collective selection of food patches in Drosophila'. In: *Journal of Experimental Biology* 219 (Jan. 2016). DOI: 10.1242/jeb.127431 (cited on page 5).

[41] Iain D. Couzin. 'Collective cognition in animal groups'. In: *Trends in Cognitive Sciences* 13.1 (2009), pp. 36–43. DOI: https://doi.org/10.1016/j.tics.2008.10.002 (cited on page 5).

[42] Colin W. Clark and Marc Mangel. 'Foraging and Flocking Strategies: Information in an Uncertain Environment'. In: *The American Naturalist* 123.5 (1984), pp. 626–641. DOI: 10.1086/284228 (cited on page 5).

[43] George W. Uetz. 'Foraging strategies of spiders'. In: *Trends in Ecology and Evolution* 7.5 (1992), pp. 155–159. DOI: https://doi.org/10.1016/0169-5347(92)90209-T (cited on page 5).

[44] URL: https://historia.nationalgeographic.com.es/a/stephen-hawking-y-origen-universo_16059 (cited on page 5).

[45] Robert J. Sternberg. *Adaptive Intelligence: Surviving and Thriving in Times of Uncertainty*. Cambridge University Press, 2021 (cited on page 5).

[46] Robert J. Sternberg. 'A Theory of Adaptive Intelligence and Its Relation to General Intelligence'. In: *Journal of Intelligence* 7.4 (2019) (cited on page 5).

[47] F. Vertosick. 'The genius within : discovering the intelligence of every living thing'. In: 2002 (cited on page 5).

[48] Klaas Hellingwerf. 'Bacterial observations: A rudimentary form of intelligence?' In: *Trends in microbiology* 13 (May 2005), pp. 152–8. DOI: 10.1016/j.tim.2005.02.001 (cited on page 5).

[49] T. Nakagaki, H. Yamada, and Á. Tóth. 'Intelligence: Maze-solving by an amoeboid organism'. In: *Nature* 407 (2000), pp. 470–470 (cited on page 5).

[50] T Nakagaki, H Yamada, and A Tóth. 'Maze-solving by an amoeboid organism'. In: *Nature* 407.6803 (Sept. 2000), p. 470. DOI: 10.1038/35035159 (cited on page 5).

[51] Julius Adler. 'Chemotaxis in Bacteria'. In: *Science* 153.3737 (1966), pp. 708–716. DOI: 10.1126/science.153.3737.708 (cited on pages 5, 18).

[52] HC Berg and DA Brown. 'Chemotaxis in Escherichia coli analysed by three-dimensional tracking'. In: *Nature* 239.5374 (Oct. 1972), pp. 500–504. DOI: 10.1038/239500a0 (cited on page 5).

[53] Diana Clausznitzer et al. 'Chemotactic Response and Adaptation Dynamics in Escherichia coli'. In: *PLOS Computational Biology* 6.5 (May 2010), pp. 1–11. DOI: 10.1371/journal.pcbi.1000784 (cited on pages 5, 18).

[54] G. Wadhams and J. Armitage. 'Making sense of it all: bacterial chemotaxis'. In: *Nature Reviews Molecular Cell Biology* 5 (2004), pp. 1024–1037 (cited on page 5).

[55] D. M. O'halloran and A. M. Burnell. 'An investigation of chemotaxis in the insect parasitic nematode Heterorhabditis bacteriophora'. In: *Parasitology* 127.4 (2003), pp. 375–385. DOI: 10.1017/S0031182003003688 (cited on page 5).

[56] Paulo Amorim. 'Modeling ant foraging: A chemotaxis approach with pheromones and trail formation'. In: *Journal of Theoretical Biology* 385 (Sept. 2014). DOI: 10.1016/j.jtbi.2015.08.026 (cited on page 5).

[57] F.G. Barth and A. Schmid. *Ecology of Sensing*. Ecology of Sensing. Springer Berlin Heidelberg, 2001 (cited on page 5).

[58] D Osorio, A Miklósi, and Zs Gonda. 'Visual ecology and perception of coloration patterns by domestic chicks'. In: *Evolutionary Ecology* 13.7 (1999), pp. 673–689 (cited on page 5).

[59] Quentin Gaudry, Katherine I Nagel, and Rachel I Wilson. 'Smelling on the fly: sensory cues and strategies for olfactory navigation in Drosophila'. In: *Current Opinion in Neurobiology* 22.2 (2012). Neuroethology, pp. 216–222. DOI: https://doi.org/10.1016/j.conb.2011.12.010 (cited on page 5).

[60] Julia Trommershäuser, Laurence T. Maloney, and Michael S. Landy. 'Decision making, movement planning and statistical decision theory'. In: *Trends in Cognitive Sciences* 12.8 (), pp. 291–297. DOI: 10.1016/j.tics.2008.04.010 (cited on page 5).

[61] Massimo Vergassola, Emmanuel Villermaux, and Boris Shraiman. ''Infotaxis' as a strategy for searching without gradients'. In: *Nature* 445 (Feb. 2007), pp. 406–9. DOI: 10.1038/nature05464 (cited on page 5).

[62] Andrew M. Wikenheiser, David W. Stephens, and A. David Redish. 'Subjective costs drive overly patient foraging strategies in rats on an intertemporal foraging task'. In: *Proceedings of the National Academy of Sciences* 110.20 (2013), pp. 8308–8313. DOI: 10.1073/pnas.1220738110 (cited on page 7).

[63] M. P. Hassell and T. R. E. Southwood. 'Foraging Strategies of Insects'. In: *Annual Review of Ecology and Systematics* 9.1 (1978), pp. 75–98. DOI: 10.1146/annurev.es.09.110178.000451 (cited on page 7).

[64] Dominic A. Edward. 'The description of mate choice'. In: *Behavioral Ecology* 26.2 (Aug. 2014), pp. 301–310. DOI: 10.1093/beheco/aru142 (cited on page 7).

[65] T. S. McCann. 'The Pinnipeds: Seals, Sea Lions, and Walruses. Marianne Riedman'. In: *The Quarterly Review of Biology* 65.4 (1990), pp. 519–520. DOI: 10.1086/417012 (cited on page 7).

[66] David Wiggins. 'Foraging Success and Aggression in Solitary and Group-Feeding Great Egrets (Casmerodius albus)'. In: *Colonial Waterbirds* 14 (Jan. 1991), p. 176. DOI: 10.2307/1521508 (cited on page 7).

[67] URL: https://www.turismodeobservacion.com/foto/de-pesca-gaviota-reidora-pescando-en-el-embalse-de-bellus/90445/ (cited on page 7).

[68] Curtis W. Marean. 'The transition to foraging for dense and predictable resources and its impact on the evolution of modern humans'. In: *Philosophical Transactions of the Royal Society B: Biological Sciences* 371.1698 (2016), p. 20150239. DOI: 10.1098/rstb.2015.0239 (cited on page 7).

[69] W. Oswalt. 'Habitat and technology;: The evolution of hunting'. In: 1972 (cited on page 7).

[70] Sara J Shettleworth. *Cognition, evolution, and behavior*. Oxford university press, 2009 (cited on page 7).

[71] Michael H Goldstein et al. 'General cognitive principles for learning structure in time and space'. In: *Trends in cognitive sciences* 14.6 (2010), pp. 249–258 (cited on page 7).

[72] Sushil Bikhchandani and Sunil Sharma. 'Optimal search with learning'. In: *Journal of Economic Dynamics and Control* 20.1 (1996), pp. 333–359. DOI: https://doi.org/10.1016/0165-1889(94)00854-7 (cited on page 7).

[73] Peter Morgan and Richard Manning. 'Optimal Search'. In: *Econometrica* 53.4 (1985), pp. 923–944 (cited on page 7).

[74] Thomas Kratzke, Lawrence Stone, and J.R. Frost. 'Search and Rescue Optimal Planning System'. In: Aug. 2010, pp. 1–8. DOI: 10.1109/ICIF.2010.5712114 (cited on page 8).

[75] Stefan Kurtz et al. 'Versatile and Open Software for Comparing Large Genomes'. In: *Genome biology* 5 (Feb. 2004), R12. DOI: 10.1186/gb-2004-5-2-r12 (cited on page 8).

[76] Wichor Bramer et al. 'Optimal database combinations for literature searches in systematic reviews: A prospective exploratory study'. In: *Systematic Reviews* 6 (Dec. 2017), p. 245. DOI: 10.1186/s13643-017-0644-y (cited on page 8).

[77] Karl Pearson. 'The problem of the random walk'. In: *Nature* 72.1867 (1905), pp. 342–342 (cited on pages 9, 10).

[78] Lord Rayleigh. 'The problem of the random walk'. In: *Nature* 72.1866 (1905), p. 318 (cited on page 9).

[79] M von Smoluchowski. 'Drei vortrage uber diffusion, brownsche bewegung und koagulation von kolloidteilchen'. In: *Zeitschrift fur Physik* 17 (1916), pp. 557–585 (cited on page 9).

[80] George E Uhlenbeck and Leonard S Ornstein. 'On the theory of the Brownian motion'. In: *Physical review* 36.5 (1930), p. 823 (cited on page 9).

[81] A. Einstein. 'Zur Theorie der Brownschen Bewegung'. In: *Annalen der Physik* 324.2 (1906), pp. 371–381. DOI: https://doi.org/10.1002/andp.19063240208 (cited on page 9).

[82] Yang Zhang et al. 'On continuum limits of Markov chains and network modeling'. In: *49th IEEE Conference on Decision and Control (CDC)*. 2010, pp. 6779–6784. DOI: 10.1109/CDC.2010.5716965 (cited on page 10).

[83] Sidney Redner. *A Guide to First-Passage Processes*. Cambridge University Press, 2001 (cited on page 13).

[84] G. Klein and Max Born. 'Mean first-passage times of Brownian motion and related problems'. In: *Proceedings of the Royal Society of London. Series A. Mathematical and Physical Sciences* 211.1106 (1952), pp. 431–443. DOI: 10.1098/rspa.1952.0051 (cited on page 13).

[85] Vicenç Mendez, Daniel Campos, and Frederic Bartumeus. *Stochastic foundations in movement ecology*. Springer, 2016 (cited on pages 14, 93).

[86] S. Condamin and O. Bénichou. 'Exact expressions of mean first-passage times and splitting probabilities for random walks in bounded rectangular domains'. In: *The Journal of Chemical Physics* 124.20 (2006), p. 206103. DOI: 10.1063/1.2192770 (cited on pages 14, 15).

[87] A. Berezhkovskii, Yurii Makhnovskii, and R.A. Suris. 'Wiener sausage volume moments'. In: *Journal of Statistical Physics* 57 (Oct. 1989), pp. 333–346. DOI: 10.1007/BF01023647 (cited on page 15).

[88] Amir Dembo et al. 'Cover Times for Brownian Motion and Random Walks in Two Dimensions'. In: *Annals of Mathematics* 160 (Aug. 2001). DOI: 10.4007/annals.2004.160.433 (cited on page 15).

[89] Carlos S.O. Yokoi, A. Hernández-Machado, and L. Ramírez-Piscina. 'Some exact results for the lattice covering time problem'. In: *Physics Letters A* 145.2 (1990), pp. 82–86. DOI: https://doi.org/10.1016/0375-9601(90)90196-U (cited on page 15).

[90] Adolfo M. Nemirovsky and Mauricio D. Coutinho-Filho. 'Lattice covering time in D dimensions: theory and mean field approximation'. In: *Physica A: Statistical Mechanics and its Applications* 177.1 (1991), pp. 233–240. DOI: https://doi.org/10.1016/0378-4371(91)90158-9 (cited on page 15).

[91] M.J.A.M. Brummelhuis and H.J. Hilhorst. 'How a random walk covers a finite lattice'. In: *Physica A: Statistical Mechanics and its Applications* 185.1 (1992), pp. 35–44. DOI: https://doi.org/10.1016/0378-4371(92)90435-S (cited on pages 15, 16).

[92] K. R. Coutinho et al. 'Partial and random lattice covering times in two dimensions'. In: *Phys. Rev. Lett.* 72.24 (June 1994), pp. 3745–3749. DOI: 10.1103/PhysRevLett.72.3745 (cited on page 15).

[93] M.J.A.M. Brummelhuis and H.J. Hilhorst. 'Covering of a finite lattice by a random walk'. In: *Physica A: Statistical Mechanics and its Applications* 176.3 (1991), pp. 387–408. DOI: https://doi.org/10.1016/0378-4371(91)90220-7 (cited on page 16).

[94] Peter Grassberger. 'How fast does a random walk cover a torus?' In: *Phys. Rev. E* 96.1 (July 2017), p. 012115. DOI: 10.1103/PhysRevE.96.012115 (cited on pages 16, 21, 28).

[95] Marie Chupeau, Olivier Bénichou, and Raphaël Voituriez. 'Cover times of random searches'. In: *Nature Physics* 11 (Aug. 2015). DOI: 10.1038/nphys3413 (cited on pages 16, 26).

[96] Jaume Masoliver, Katja Lindenberg, and George Weiss. 'A Continuous-Time Generalization of the Persistent Random Walk'. In: *Physica A: Statistical Mechanics and its Applications* 157 (June 1989), pp. 891–898. DOI: 10.1016/0378-4371(89)90071-X (cited on page 16).

[97] Hsin-i Wu et al. 'Modelling animal movement as a persistent random walk in two dimensions: expected magnitude of net displacement'. In: *Ecological Modelling* 132.1 (2000), pp. 115–124. DOI: https://doi.org/10.1016/S0304-3800(00)00309-4 (cited on page 16).

[98] URL: https://clisby.net/projects/saw_feature/ (cited on page 18).

[99] A. Patteson et al. 'Running and tumbling with E. coli in polymeric solutions'. In: *Scientific Reports* 5 (2015) (cited on page 18).

[100] Jens Elgeti and Gerhard Gompper. 'Run-and-tumble dynamics of self-propelled particles in confinement'. In: *EPL* 109.5 (2015), p. 58003. DOI: 10.1209/0295-5075/109/58003 (cited on page 18).

[101] J Murlis, J S Elkinton, and R T Cardé. 'Odor Plumes and How Insects Use Them'. In: *Annual Review of Entomology* 37.1 (1992), pp. 505–532. DOI: 10.1146/annurev.en.37.010192.002445 (cited on page 18).

[102] Hans G Wallraff. 'Avian olfactory navigation: its empirical foundation and conceptual state'. In: *Animal Behaviour* 67.2 (2004), pp. 189–204. DOI: https://doi.org/10.1016/j.anbehav.2003.06.007 (cited on page 18).

[103] U. Mugan and M. A. MacIver. 'Spatial planning with long visual range benefits escape from visual predators in complex naturalistic environments'. In: *Nature Communications* 11 (2020) (cited on page 18).

[104] Malcolm A. MacIver et al. 'Massive increase in visual range preceded the origin of terrestrial vertebrates'. In: *Proceedings of the National Academy of Sciences* 114.12 (2017), E2375–E2384. DOI: 10.1073/pnas.1615563114 (cited on page 18).

[105] Harry Kesten. 'On the Number of Self-Avoiding Walks'. In: *Journal of Mathematical Physics* 4.7 (1963), pp. 960–969. DOI: 10.1063/1.1704022 (cited on page 19).

[106] Cyril Domb. 'Self-Avoiding Walks on Lattices'. In: *Advances in Chemical Physics*. John Wiley and Sons, Ltd, 1969, pp. 229–259. DOI: https://doi.org/10.1002/9780470143605.ch13 (cited on page 19).

[107] Karl F. Freed. 'Polymers as Self-Avoiding Walks'. In: *The Annals of Probability* 9.4 (1981), pp. 537–554. DOI: 10.1214/aop/1176994359 (cited on page 19).

[108] P.J. Flory. *Principles of Polymer Chemistry*. Baker lectures 1948. Cornell University Press, 1953 (cited on page 19).

[109] Deepak Dhar. 'Self-avoiding random walks: Some exactly soluble cases'. In: *Journal of Mathematical Physics* 19 (Jan. 1978), pp. 5–11. DOI: 10.1063/1.523515 (cited on page 19).

[110] B. Duplantier and H. Saleur. 'Exact critical properties of two-dimensional dense self-avoiding walks'. In: *Nuclear Physics B* 290 (1987), pp. 291–326. DOI: https://doi.org/10.1016/0550-3213(87)90190-8 (cited on page 19).

[111] P. M. Lee. 'Random Walks and Random Environments: Volume 1: Random Walks'. In: 1995 (cited on page 19).

[112] N. Madras and G. Slade. *The Self-Avoiding Walk*. Probability and Its Applications. Birkhäuser Boston, 1996 (cited on page 20).

[113] Wei-Shih Yang and David Klein. 'A note on the critical dimension for weakly self-avoiding walks'. In: *Probability Theory and Related Fields* 79 (1988), pp. 99–114 (cited on pages 20, 21).

[114] Shlomo Havlin and Daniel ben-Avraham. 'Theoretical and numerical study of fractal dimensionality in self-avoiding walks'. In: *Phys. Rev. A* 26 (Sept. 1982). DOI: 10.1103/PhysRevA.26.1728 (cited on page 20).

[115] Sergio Caracciolo et al. ‘Correction-to-Scaling Exponents for Two-Dimensional Self-Avoiding Walks’. In: *Journal of Statistical Physics* 120 (Sept. 2005), pp. 1037–1100. DOI: 10.1007/s10955-005-7004-3 (cited on page 20).

[116] Yup Kim. ‘Renormalisation-group study of self-avoiding walks on the random lattice’. In: *Journal of Physics C: Solid State Physics* 16.8 (Mar. 1983), pp. 1345–1352. DOI: 10.1088/0022-3719/16/8/005 (cited on page 20).

[117] Daniel J. Amit, G. Parisi, and L. Peliti. ‘Asymptotic behavior of the "true" self-avoiding walk’. In: *Phys. Rev. B* 27.3 (Feb. 1983), pp. 1635–1645. DOI: 10.1103/PhysRevB.27.1635 (cited on pages 21, 26).

[118] Russell Epstein et al. ‘The cognitive map in humans: Spatial navigation and beyond’. In: *Nature Neuroscience* 20 (Oct. 2017), pp. 1504–1513. DOI: 10.1038/nn.4656 (cited on page 21).

[119] William Fagan et al. ‘Spatial memory and animal movement’. In: *Ecology letters* 16 (Aug. 2013), pp. 1316–1329. DOI: 10.1111/ele.12165 (cited on page 21).

[120] Thomas Collett and Matthew Collett. ‘Memory use in insect visual navigation’. In: *Nature reviews. Neuroscience* 3 (Aug. 2002), pp. 542–52. DOI: 10.1038/nrn872 (cited on page 21).

[121] E. T. Jaynes. ‘Information Theory and Statistical Mechanics’. In: *Phys. Rev.* 106.4 (May 1957), pp. 620–630. DOI: 10.1103/PhysRev.106.620 (cited on pages 22, 99, 114).

[122] E. Jaynes and R. Rosenkrantz. ‘E. T. Jaynes: Papers on Probability, Statistics and Statistical Physics’. In: 1983 (cited on pages 22, 99, 114).

[123] Zhi-Jie Tan et al. ‘“True” self-attracting walk’. In: *Physics Letters A* 289.4 (2001), pp. 251–254. DOI: https://doi.org/10.1016/S0375-9601(01)00559-X (cited on page 23).

[124] V. B. Sapozhnikov. ‘Self-attracting walk with nu 1/2’. In: *Journal of Physics A: Mathematical and General* 27.6 (Mar. 1994), pp. L151–L153. DOI: 10.1088/0305-4470/27/6/001 (cited on page 23).

[125] A. Ordemann et al. ‘Structural properties of self-attracting walks.’ In: *Physical review. E, Statistical, nonlinear, and soft matter physics* 64 4 Pt 2 (2001) (cited on page 23).

[126] Yup Kim, Seokjong Park, and Soon-Hyung Yook. ‘Network exploration using true self-avoiding walks’. In: *Phys. Rev. E* 94.4 (Oct. 2016), p. 042309. DOI: 10.1103/PhysRevE.94.042309 (cited on page 26).

[127] Fereydoon Family and M. Daoud. ‘Experimental realization of true self-avoiding walks’. In: *Phys. Rev. B* 29.3 (Feb. 1984), pp. 1506–1507. DOI: 10.1103/PhysRevB.29.1506 (cited on page 26).

[128] R Rammal, J C Angles dAuriac, and A Benott. ‘Statistics of the true self-avoiding walk in one dimension’. In: *Journal of Physics A: Mathematical and General* 17.1 (Jan. 1984), pp. L9–L14. DOI: 10.1088/0305-4470/17/1/003 (cited on page 26).

[129] David W. Sims et al. 'Hierarchical random walks in trace fossils and the origin of optimal search behavior'. In: *Proceedings of the National Academy of Sciences* 111.30 (2014), pp. 11073–11078. DOI: 10.1073/pnas.1405966111 (cited on page 26).

[130] Benno Liebchen and Hartmut Löwen. 'Synthetic Chemotaxis and Collective Behavior in Active Matter'. In: *Accounts of Chemical Research* 51.12 (2018), pp. 2982–2990. DOI: 10.1021/acs.accounts.8b00215 (cited on page 26).

[131] Víctor M. López Millán et al. 'A model of self-avoiding random walks for searching complex networks'. In: *Networks* 60.2 (2012), pp. 71–85. DOI: https://doi.org/10.1002/net.20461 (cited on page 26).

[132] Hiraku Oshima and Takashi Odagaki. 'Finite Memory Walk and Its Application to Small-World Network'. In: *Journal of the Physical Society of Japan* 81.7 (2012), p. 074004. DOI: 10.1143/JPSJ.81.074004 (cited on page 26).

[133] Johannes Nauta, Yara Khaluf, and Pieter Simoens. 'Hybrid foraging in patchy environments using spatial memory'. In: *Journal of The Royal Society Interface* 17.166 (2020), p. 20200026. DOI: 10.1098/rsif.2020.0026 (cited on page 29).

[134] Adam Bulley and Muireann Irish. 'The Functions of Prospection – Variations in Health and Disease'. In: *Frontiers in Psychology* 9 (2018), p. 2328. DOI: 10.3389/fpsyg.2018.02328 (cited on page 36).

[135] Karl K. Szpunar, R. Nathan Spreng, and Daniel L. Schacter. 'A taxonomy of prospection: Introducing an organizational framework for future-oriented cognition'. In: *Proceedings of the National Academy of Sciences* 111.52 (2014), pp. 18414–18421. DOI: 10.1073/pnas.1417144111 (cited on page 36).

[136] David Vernon, Michael Beetz, and Giulio Sandini. 'Prospection in Cognition: The Case for Joint Episodic-Procedural Memory in Cognitive Robotics'. In: *Frontiers in Robotics and AI* 2 (2015), p. 19. DOI: 10.3389/frobt.2015.00019 (cited on page 36).

[137] Thomas Ducourant et al. 'Timing and distance characteristics of interpersonal coordination during locomotion'. In: *Neuroscience Letters* 389.1 (2005), pp. 6–11. DOI: https://doi.org/10.1016/j.neulet.2005.06.052 (cited on page 36).

[138] Anders Johansson. 'Constant-net-time headway as a key mechanism behind pedestrian flow dynamics'. In: *Phys. Rev. E* 80.2 (Aug. 2009), p. 026120. DOI: 10.1103/PhysRevE.80.026120 (cited on page 36).

[139] Kerstin Gidlöf et al. 'Using Eye Tracking to Trace a Cognitive Process: Gaze Behaviour During Decision Making in a Natural Environment'. In: *Journal of Eye Movement Research* 6 (Jan. 2013). DOI: 10.16910/jemr.6.1.3 (cited on page 36).

[140] Sung-Hee Kim et al. 'Does an Eye Tracker Tell the Truth about Visualizations?: Findings while Investigating Visualizations for Decision Making'. In: *IEEE Transactions on Visualization and Computer Graphics* 18.12 (2012), pp. 2421–2430. DOI: 10.1109/TVCG.2012.215 (cited on page 36).

[141] Thomas Suddendorf. 'Behavioural evidence for mental time travel in non-human animals'. In: *Behavioural brain research* 215 (Dec. 2009), pp. 292–8. DOI: 10.1016/j.bbr.2009.11.044 (cited on page 36).

[142] William Roberts. 'Evidence for future cognition in animals'. In: *Learning and Motivation* 43 (Nov. 2012), pp. 169–180. DOI: 10.1016/j.lmot.2012.05.005 (cited on page 36).

[143] Brad E. Pfeiffer and David J. Foster. 'Hippocampal place cell sequences depict future paths to remembered goals'. In: *Nature* 497 (2013), pp. 74–79 (cited on page 36).

[144] Karline Janmaat et al. 'Wild chimpanzees plan their breakfast time, type, and location'. In: *Proceedings of the National Academy of Sciences* 111 (Oct. 2014). DOI: 10.1073/pnas.1407524111 (cited on page 36).

[145] Mathias Osvath and Helena Osvath. 'Chimpanzee (Pan troglodytes) and orangutan (Pongo abelii) forethought: Self-control and pre-experience in the face of future tool use'. In: *Animal cognition* 11 (July 2008), pp. 661–74. DOI: 10.1007/s10071-008-0157-0 (cited on page 36).

[146] A. D. Wissner-Gross and C. E. Freer. 'Causal Entropic Forces'. In: *Phys. Rev. Lett.* 110.16 (Apr. 2013), p. 168702. DOI: 10.1103/PhysRevLett.110.168702 (cited on pages 36, 37, 79).

[147] Nico Roos. 'Entropic forces in Brownian motion'. In: *American Journal of Physics* 82 (July 2013). DOI: 10.1119/1.4894381 (cited on page 36).

[148] Philip Taylor and Jason Tabachnik. 'Entropic forces - Making the connection between mechanics and thermodynamics in an exactly soluble model'. In: *European Journal of Physics* 34 (Apr. 2013), p. 729. DOI: 10.1088/0143-0807/34/3/729 (cited on page 36).

[149] L.M. Martyushev and V.D. Seleznev. 'Maximum entropy production principle in physics, chemistry and biology'. In: *Physics Reports* 426.1 (2006), pp. 1–45. DOI: https://doi.org/10.1016/j.physrep.2005.12.001 (cited on page 37).

[150] Axel Kleidon. 'Life, hierarchy, and the thermodynamic machinery of planet Earth'. In: *Physics of Life Reviews* 7.4 (2010), pp. 424–460. DOI: https://doi.org/10.1016/j.plrev.2010.10.002 (cited on page 37).

[151] Raphael Bousso et al. 'Predicting the cosmological constant from the causal entropic principle'. In: *Phys. Rev. D* 76.4 (Aug. 2007), p. 043513. DOI: 10.1103/PhysRevD.76.043513 (cited on page 37).

[152] Tim Shallice and Paul Burgess. 'Deficits in strategy application following frontal lobe damage in man'. In: *Brain : a journal of neurology* 114 (Pt 2) (May 1991), pp. 727–41. DOI: 10.1093/brain/114.2.727 (cited on page 41).

[153] Daniel Schacter, Brendan Gaesser, and Donna Addis. 'Remembering the Past and Imagining the Future in the Elderly'. In: *Gerontology* 59 (Sept. 2012). DOI: 10.1159/000342198 (cited on page 41).

[154] Jonathan Redshaw and Thomas Suddendorf. 'Children's and Apes' Preparatory Responses to Two Mutually Exclusive Possibilities'. In: *Current Biology* 26.13 (2016), pp. 1758–1762. DOI: https://doi.org/10.1016/j.cub.2016.04.062 (cited on page 41).

[155] Joshua I. Gold and Michael N. Shadlen. 'The Neural Basis of Decision Making'. In: *Annual Review of Neuroscience* 30.1 (2007). PMID: 17600525, pp. 535–574. DOI: 10.1146/annurev.neuro.29.051605.113038 (cited on page 46).

[156] Simon P. Kelly and Redmond G. O'Connell. 'The neural processes underlying perceptual decision making in humans: Recent progress and future directions'. In: *Journal of Physiology-Paris* 109.1 (2015). Neural Basis of Adaptive Control, pp. 27–37. DOI: https://doi.org/10.1016/j.jphysparis.2014.08.003 (cited on page 46).

[157] Sarah-Jayne Blakemore and Trevor Robbins. 'Decision-making in the adolescent brain'. In: *Nature neuroscience* 15 (Aug. 2012), pp. 1184–91. DOI: 10.1038/nn.3177 (cited on page 46).

[158] Benedetto Martino et al. 'Frames, Biases, and Rational Decision-Making in the Human Brain'. In: *Science (New York, N.Y.)* 313 (Sept. 2006), pp. 684–7. DOI: 10.1126/science.1128356 (cited on page 46).

[159] Daeyeol Lee. 'Game theory and neural basis of social decision making'. In: *Nature neuroscience* 11 (May 2008), pp. 404–9. DOI: 10.1038/nn2065 (cited on page 46).

[160] Daeyeol Lee et al. 'Reinforcement learning and decision making in monkeys during a competitive game'. In: *Brain research. Cognitive brain research* 22 (Jan. 2005), pp. 45–58. DOI: 10.1016/j.cogbrainres.2004.07.007 (cited on page 46).

[161] Iain Couzin et al. 'Effective leadership and decision-making in animal groups on the move'. In: *Nature* 433 (Mar. 2005), pp. 513–6. DOI: 10.1038/nature03236 (cited on page 46).

[162] Ashley Ward et al. 'Quorum decision-making facilitates information transfer in fish shoals'. In: *Proceedings of the National Academy of Sciences of the United States of America* 105 (June 2008), pp. 6948–53. DOI: 10.1073/pnas.0710344105 (cited on page 46).

[163] Gabriele Valentini, E. Ferrante, and M. Dorigo. 'The Best-of-n Problem in Robot Swarms: Formalization, State of the Art, and Novel Perspectives'. In: *Frontiers Robotics AI* 4 (2017), p. 9 (cited on page 46).

[164] Larissa Conradt and Christian List. 'Group decisions in humans and animals: A survey'. In: *Philosophical transactions of the Royal Society of London. Series B, Biological sciences* 364 (Mar. 2009), pp. 719–42. DOI: 10.1098/rstb.2008.0276 (cited on page 46).

[165] Sidney Redner. 'Reality-inspired voter models: A mini-review'. In: *Comptes Rendus Physique* 20 (June 2019). DOI: 10.1016/j.crhy.2019.05.004 (cited on pages 46, 76).

[166] Pedro Ortega and Daniel Braun. 'Thermodynamics as a theory of decision making with information processing costs'. In: *Royal Society of London Proceedings Series A* 469 (Apr. 2012). DOI: 10.1098/rspa.2012.0683 (cited on page 46).

[167] V. Yukalov and Didier Sornette. 'Self-organization in complex systems as decision making'. In: *Advances in Complex Systems* 17 (Aug. 2014). DOI: 10.1142/S0219525914500167 (cited on page 46).

[168] Philipp Schwartenbeck et al. 'Exploration, Novelty, Surprise and Free Energy Minimisation'. In: *Frontiers in psychology* 4 (Oct. 2013), p. 710. DOI: 10.3389/fpsyg.2013.00710 (cited on page 46).

[169] Édgar Roldán et al. 'Decision Making in the Arrow of Time'. In: *Phys. Rev. Lett.* 115.25 (Dec. 2015), p. 250602. DOI: 10.1103/PhysRevLett.115.250602 (cited on page 46).

[170] Maroussia Favre et al. 'Quantum Decision Theory in Simple Risky Choices'. In: *PLOS ONE* 11 (Feb. 2016). DOI: 10.1371/journal.pone.0168045 (cited on page 46).

[171] KH Britten et al. 'The analysis of visual motion: a comparison of neuronal and psychophysical performance'. In: *The Journal of neuroscience : the official journal of the Society for Neuroscience*. 1992 (cited on page 46).

[172] Jamie Roitman and Michael Shadlen. 'Response of neurons in the lateral intraparietal area during a combined visual discrimination reaction time task'. In: *The Journal of neuroscience : the official journal of the Society for Neuroscience* 22 (Dec. 2002), pp. 9475–89. DOI: 10.3410/f.1002839.152957 (cited on page 46).

[173] Mark Mazurek et al. 'A role for neural integrators in perceptual decision making'. In: *Cerebral cortex (New York, N.Y. : 1991)* 13 (Dec. 2003), pp. 1257–69 (cited on page 46).

[174] R. Ratcliff et al. 'Diffusion Decision Model: Current Issues and History'. In: *Trends in Cognitive Sciences* 20 (2016), pp. 260–281 (cited on page 46).

[175] Satohiro Tajima, Jan Drugowitsch, and Alexandre Pouget. 'Optimal policy for value-based decision-making'. In: *Nature Communications* 7 (Aug. 2016), p. 12400. DOI: 10.1038/ncomms12400 (cited on page 47).

[176] E. Fehr and A. Rangel. 'Neuroeconomic Foundations of Economic Choice—Recent Advances'. In: *Journal of Economic Perspectives* 25 (2011), pp. 3–30 (cited on page 48).

[177] D. Fudenberg, P. Strack, and Tomasz Strzalecki. 'Speed, Accuracy, and the Optimal Timing of Choices'. In: *The American Economic Review* 108 (2018), pp. 3651–3684 (cited on page 48).

[178] Milosavljevic Milica et al. 'The Drift Diffusion Model Can Account for the Accuracy and Reaction Time of Value-Based Choices Under High and Low Time Pressure'. In: *Judgment and Decision Making* 5 (Oct. 2010). DOI: 10.2139/ssrn.1901533 (cited on page 48).

[179] M. L. Pedersen, M. Frank, and G. Biele. 'The drift diffusion model as the choice rule in reinforcement learning'. In: *Psychonomic Bulletin Review* 24 (2017), pp. 1234–1251 (cited on page 48).

[180] Guy Hawkins et al. 'Revisiting the Evidence for Collapsing Boundaries and Urgency Signals in Perceptual Decision-Making'. In: *The Journal of neuroscience : the official journal of the Society for Neuroscience* 35 (Feb. 2015), pp. 2476–84. DOI: 10.1523/JNEUROSCI.2410-14.2015 (cited on page 48).

[181] Laura Fontanesi et al. 'A reinforcement learning diffusion decision model for value-based decisions'. In: *Psychonomic Bulletin and Review* 26 (Mar. 2019). DOI: 10.3758/s13423-018-1554-2 (cited on page 48).

[182] David Thura et al. 'Decision making by urgency gating: Theory and experimental support'. In: *Journal of neurophysiology* 108 (Sept. 2012). DOI: 10.1152/jn.01071.2011 (cited on page 48).

[183] Paul Cisek, Geneviève Aude Puskas, and Stephany El-Murr. 'Decisions in Changing Conditions: The Urgency-Gating Model'. In: *Journal of Neuroscience* 29.37 (2009), pp. 11560–11571. DOI: 10.1523/JNEUROSCI.1844-09.2009 (cited on page 48).

[184] Khai Chiong et al. 'Split-second Decision-Making in the Field: Response Times in Mobile Advertising'. In: *SSRN Electronic Journal* (Jan. 2018). DOI: 10.2139/ssrn.3289386 (cited on page 48).

[185] Ian Krajbich and Antonio Rangel. 'Multialternative drift-diffusion model predicts the relationship between visual fixations and choice in value-based decisions'. In: *Proceedings of the National Academy of Sciences* 108.33 (2011), pp. 13852–13857. DOI: 10.1073/pnas.1101328108 (cited on page 48).

[186] A. Wald. 'Sequential Tests of Statistical Hypotheses'. In: *The Annals of Mathematical Statistics* 16.2 (1945), pp. 117–186. DOI: 10.1214/aoms/1177731118 (cited on page 48).

[187] R. Bogacz et al. 'The physics of optimal decision making: a formal analysis of models of performance in two-alternative forced-choice tasks.' In: *Psychological review* 113 4 (2006), pp. 700–765 (cited on page 48).

[188] A. Wald and J. Wolfowitz. 'Optimum Character of the Sequential Probability Ratio Test'. In: *Annals of Mathematical Statistics* 19 (1948), pp. 326–339 (cited on page 48).

[189] Daniel Gilbert and Timothy Wilson. 'Prospection: Experiencing the Future'. In: *Science (New York, N.Y.)* 317 (Oct. 2007), pp. 1351–4. DOI: 10.1126/science.1144161 (cited on page 50).

[190] Thomas Suddendorf. 'The evolution of foresight: What is mental time travel, and is it unique to humans?' In: *The Behavioral and brain sciences* 30 (July 2007), 299–313, discussion 313. DOI: 10.1017/S0140525X07001975 (cited on page 50).

[191] Brad E. Pfeiffer and David J. Foster. 'Hippocampal place cell sequences depict future paths to remembered goals'. In: *Nature* 497 (2013), pp. 74–79 (cited on page 50).

[192] Elisa M. Tartaglia, Aaron M. Clarke, and Michael H. Herzog. 'What to Choose Next? A Paradigm for Testing Human Sequential Decision Making'. In: *Frontiers in Psychology* 8 (2017), p. 312. DOI: 10.3389/fpsyg.2017.00312 (cited on page 50).

[193] Dandan Zhang and Ruolei Gu. 'Behavioral preference in sequential decision-making and its association with anxiety'. In: *Human brain mapping* 39 (Feb. 2018). DOI: 10.1002/hbm.24016 (cited on page 50).

[194] Khanh P. Nguyen, Krešimir Josić, and Zachary P. Kilpatrick. 'Optimizing sequential decisions in the drift–diffusion model'. In: *Journal of Mathematical Psychology* 88 (2019), pp. 32–47. DOI: https://doi.org/10.1016/j.jmp.2018.11.001 (cited on page 50).

[195] Guillem Collell and Jordi Fauquet. 'Brain activity and cognition: a connection from thermodynamics and information theory'. In: *Frontiers in Psychology* 6 (2015), p. 818. DOI: 10.3389/fpsyg.2015.00818 (cited on page 50).

[196] Neil Stewart, Nick Chater, and Gordon D.A. Brown. 'Decision by sampling'. In: *Cognitive Psychology* 53.1 (2006), pp. 1–26. DOI: https://doi.org/10.1016/j.cogpsych.2005.10.003 (cited on page 50).

[197] Edward Vul et al. 'One and Done? Optimal Decisions From Very Few Samples'. In: *Cognitive Science* 38 (Jan. 2014). DOI: 10.1111/cogs.12101 (cited on page 50).

[198] Hildward Vandormael et al. 'Robust sampling of decision information during perceptual choice'. In: *Proceedings of the National Academy of Sciences* 114.10 (2017), pp. 2771–2776. DOI: 10.1073/pnas.1613950114 (cited on page 50).

[199] B. Forstmann, R. Ratcliff, and E. Wagenmakers. 'Sequential Sampling Models in Cognitive Neuroscience: Advantages, Applications, and Extensions.' In: *Annual review of psychology* 67 (2016), pp. 641–666 (cited on page 50).

[200] Andrew Caplin, Mark Dean, and Daniel Martin. 'Search and Satisficing'. In: *American Economic Review* 101.7 (Dec. 2011), pp. 2899–2922. DOI: 10.1257/aer.101.7.2899 (cited on page 50).

[201] Falk Lieder and Thomas L Griffiths. 'Resource-rational analysis: Understanding human cognition as the optimal use of limited computational resources'. In: *The Behavioral and brain sciences* 43 (Feb. 2019), e1. DOI: 10.1017/s0140525x1900061x (cited on page 50).

[202] URL: https://tobii.23video.com/tobii-pro-x2-eye-tracker-installation (cited on page 54).

[203] F. Hopf, Thomas Valone, and James Brown. 'Competition theory and the structure of ecological communities'. In: *Evolutionary Ecology* 7 (Mar. 1993), pp. 142–154. DOI: 10.1007/BF01239385 (cited on page 64).

[204] URL: https://commons.wikimedia.org/wiki/File:Murray_Gell-Mann_at_Lection.JPG (cited on page 64).

[205] Robert Beschta. 'Cottonwoods, elk, and wolves in the Lamar Valley of Yellowstone National Park'. In: *Ecological Applications - ECOL APPL* 13 (Oct. 2003), pp. 1295–1309. DOI: 10.1890/02-5175 (cited on page 64).

[206] Kim Berger, Eric Gese, and Joel Berger. 'Indirect effects and traditional trophic cascades: A test involving wolves, coyotes, and pronghorn'. In: *Ecology* 89 (Apr. 2008), pp. 818–28. DOI: 10.1890/07-0193.1 (cited on page 64).

[207] E. Mayr. 'Animal Species and Evolution'. In: 1963 (cited on page 64).

[208] David Pfennig and Karin Pfennig. 'Evolution's wedge: Competition and the origins of diversity'. In: *Evolution's Wedge: Competition and the Origins of Diversity* (Oct. 2012). DOI: 10.1525/california/9780520274181.001.0001 (cited on page 64).

[209] Iain D. Couzin. 'Collective cognition in animal groups'. In: *Trends in Cognitive Sciences* 13.1 (2009), pp. 36–43. DOI: https://doi.org/10.1016/j.tics.2008.10.002 (cited on page 64).

[210] Deborah M. Gordon. 'The Ecology of Collective Behavior'. In: *PLOS Biology* 12.3 (Mar. 2014), pp. 1–4. DOI: 10.1371/journal.pbio.1001805 (cited on page 64).

[211] Robert L. Goldstone and Todd M. Gureckis. 'Collective Behavior'. English (US). In: *Topics in Cognitive Science* 1.3 (July 2009). Copyright: Copyright 2011 Elsevier B.V., All rights reserved., pp. 412–438. DOI: 10.1111/j.1756-8765.2009.01038.x (cited on page 64).

[212] Jens Krause, Graeme D. Ruxton, and Stefan Krause. 'Swarm intelligence in animals and humans'. In: *Trends in Ecology and Evolution* 25.1 (2010), pp. 28–34. DOI: https://doi.org/10.1016/j.tree.2009.06.016 (cited on page 64).

[213] D. A. Mavridou et al. 'Bacteria Use Collective Behavior to Generate Diverse Combat Strategies'. In: *Current Biology* 28 (2018), 345–355.e4 (cited on page 64).

[214] Olaya Rendueles and J. Ghigo. 'Mechanisms of Competition in Biofilm Communities.' In: *Microbiology spectrum* 3 3 (2015) (cited on page 64).

[215] T Matsuyama and M Matsushita. 'Fractal morphogenesis by a bacterial cell population'. In: *Critical reviews in microbiology* 19.2 (1993), pp. 117–135. DOI: 10.3109/10408419309113526 (cited on page 64).

[216] M. Obert, P. Pfeifer, and M. Sernetz. 'Microbial growth patterns described by fractal geometry.' In: *Journal of bacteriology* 172 3 (1990), pp. 1180–1185 (cited on page 64).

[217] P. Friedl and D. Gilmour. 'Collective cell migration in morphogenesis, regeneration and cancer'. In: *Nature Reviews Molecular Cell Biology* 10 (2009), pp. 445–457 (cited on page 64).

[218] P. Rørth. 'Collective cell migration.' In: *Annual review of cell and developmental biology* 25 (2009), pp. 407–429 (cited on page 64).

[219] Deborah Gordon. 'From division of labor to the collective behavior of social insects'. In: *Behavioral Ecology and Sociobiology* 70 (July 2016). DOI: 10.1007/s00265-015-2045-3 (cited on page 65).

[220] Deborah M. Gordon. 'The Ecology of Collective Behavior in Ants'. In: *Annual Review of Entomology* 64.1 (2019). PMID: 30256667, pp. 35–50. DOI: 10.1146/annurev-ento-011118-111923 (cited on page 65).

[221] Matz Larsson. 'Why do fish school?' In: *Current Zoology* 58.1 (Feb. 2012), pp. 116–128. DOI: 10.1093/czoolo/58.1.116 (cited on page 65).

[222] Nils Olav Handegard et al. 'The Dynamics of Coordinated Group Hunting and Collective Information Transfer among Schooling Prey'. In: *Current Biology* 22.13 (2012), pp. 1213–1217. DOI: https://doi.org/10.1016/j.cub.2012.04.050 (cited on page 65).

[223] Evelyn Shaw. 'Schooling Fishes: The school, a truly egalitarian form of organization in which all members of the group are alike in influence, offers substantial benefits to its participants'. In: *American Scientist* 66.2 (1978), pp. 166–175 (cited on page 65).

[224] Michele Ballerini et al. 'Empirical investigation of starling flocks: a benchmark study in collective animal behaviour'. In: *Animal Behaviour* 76.1 (2008), pp. 201–215. DOI: https://doi.org/10.1016/j.anbehav.2008.02.004 (cited on page 65).

[225] 'Animal behaviour: Benefits of mixed flocks'. In: *Nature* 492 (2012), pp. 314–314 (cited on page 65).

[226] William H. Warren. 'Collective Motion in Human Crowds'. In: *Current Directions in Psychological Science* 27.4 (2018), pp. 232–240. DOI: 10.1177/0963721417746743 (cited on page 65).

[227] Jesse L. Silverberg et al. 'Collective Motion of Humans in Mosh and Circle Pits at Heavy Metal Concerts'. In: *Phys. Rev. Lett.* 110.22 (May 2013), p. 228701. DOI: 10.1103/PhysRevLett.110.228701 (cited on page 65).

[228] Dirk Helbing, Anders Johansson, and Habib Zein Al-Abideen. 'Dynamics of crowd disasters: An empirical study'. In: *Phys. Rev. E* 75.4 (Apr. 2007), p. 046109. DOI: 10.1103/PhysRevE.75.046109 (cited on page 65).

[229] J. V. Bavel et al. 'Using social and behavioural science to support COVID-19 pandemic response'. In: *Nature Human Behaviour* 4 (2020), pp. 460–471 (cited on page 65).

[230] Haibo Hu. 'Competing opinion diffusion on social networks'. In: *Royal Society Open Science* 4.11 (2017), p. 171160. DOI: 10.1098/rsos.171160 (cited on page 65).

[231] Robert Cialdini and Noah Goldstein. 'Social Influence: Compliance and Conformity'. In: *Annual review of psychology* 55 (Feb. 2004), pp. 591–621. DOI: 10.1146/annurev.psych.55.090902.142015 (cited on page 65).

[232] Adam D. I. Kramer, Jamie E. Guillory, and Jeffrey T. Hancock. 'Experimental evidence of massive-scale emotional contagion through social networks'. In: *Proceedings of the National Academy of Sciences* 111.24 (2014), pp. 8788–8790. DOI: 10.1073/pnas.1320040111 (cited on page 65).

[233] URL: https://www.immunology.org/culture-plate-1887 (cited on page 65).

[234] URL: https://mappingignorance.org/2015/12/16/building-bridges/ (cited on page 65).

[235] Yaniss Touahmi et al. 'Congestion Avoidance for Multiple Micro-Robots Using the Behaviour of Fish Schools'. In: *International Journal of Advanced Robotic Systems* 9 (Sept. 2012). DOI: 10.5772/51190 (cited on page 65).

[236] URL: Jan%20van%20der%20Greef/%20Buiten-beeld/Minden%20Pictures/Corbis (cited on page 65).

[237] N. Smelser. 'Theory Of Collective Behavior'. In: 1962 (cited on page 65).

[238] C. Dennis et al. 'The influence of collective behavior on the magnetic and heating properties of iron oxide nanoparticles'. In: *Journal of Applied Physics* 103 (2008) (cited on page 65).

[239] I. Groma. 'Link between the microscopic and mesoscopic length-scale description of the collective behavior of dislocations'. In: *Phys. Rev. B* 56.10 (Sept. 1997), pp. 5807–5813. DOI: 10.1103/PhysRevB.56.5807 (cited on page 65).

[240] Caterina Soldano, Ather Mahmood, and Erik Dujardin. 'Production, properties and potential of graphene'. In: *Carbon* 48.8 (2010), pp. 2127–2150. DOI: https://doi.org/10.1016/j.carbon.2010.01.058 (cited on page 65).

[241] Barry A. Cipra. 'An Introduction to the Ising Model'. In: *The American Mathematical Monthly* 94.10 (1987), pp. 937–959. DOI: 10.1080/00029890.1987.12000742 (cited on page 65).

[242] Xi Zhang et al. 'Water's phase diagram: From the notion of thermodynamics to hydrogen-bond cooperativity'. In: *Progress in Solid State Chemistry* 43.3 (2015), pp. 71–81. DOI: https://doi.org/10.1016/j.progsolidstchem.2015.03.001 (cited on page 66).

[243] Luc-Alain Giraldeau and Frédérique Dubois. 'Chapter 2 Social Foraging and the Study of Exploitative Behavior'. In: vol. 38. Advances in the Study of Behavior. Academic Press, 2008, pp. 59–104. DOI: https://doi.org/10.1016/S0065-3454(08)00002-8 (cited on page 67).

[244] Esteban Fernández-Juricic, Jonathan T. Erichsen, and Alex Kacelnik. 'Visual perception and social foraging in birds'. In: *Trends in Ecology and Evolution* 19.1 (2004), pp. 25–31. DOI: https://doi.org/10.1016/j.tree.2003.10.003 (cited on page 67).

[245] Oded Keynan, Amanda R. Ridley, and Arnon Lotem. 'Social foraging strategies and acquisition of novel foraging skills in cooperatively breeding Arabian babblers'. In: *Behavioral Ecology* 26.1 (Oct. 2014), pp. 207–214. DOI: 10.1093/beheco/aru181 (cited on page 67).

[246] Randolf Menzel et al. 'Honey bees navigate according to a map-like spatial memory'. In: *Proceedings of the National Academy of Sciences* 102.8 (2005), pp. 3040–3045. DOI: 10.1073/pnas.0408550102 (cited on page 67).

[247] Matthew Collett, Lars Chittka, and Thomas S. Collett. 'Spatial Memory in Insect Navigation'. In: *Current Biology* 23.17 (2013), R789–R800. DOI: https://doi.org/10.1016/j.cub.2013.07.020 (cited on page 67).

[248] Claudio Castellano, Santo Fortunato, and Vittorio Loreto. 'Statistical physics of social dynamics'. In: *Rev. Mod. Phys.* 81.2 (May 2009), pp. 591–646. DOI: 10.1103/RevModPhys.81.591 (cited on page 76).

[249] Romualdo Pastor-Satorras et al. 'Epidemic processes in complex networks'. In: *Rev. Mod. Phys.* 87.3 (Aug. 2015), pp. 925–979. DOI: 10.1103/RevModPhys.87.925 (cited on page 76).

[250] Anna Sieben, Jette Schumann, and Armin Seyfried. 'Collective phenomena in crowds—Where pedestrian dynamics need social psychology'. In: *PLOS ONE* 12.6 (June 2017), pp. 1–19. DOI: 10.1371/journal.pone.0177328 (cited on page 76).

[251] Alexander John et al. 'Collective effects in traffic on bi-directional ant trails'. In: *Journal of theoretical biology* 231.2 (2004), pp. 279–285 (cited on page 76).

[252] Iain D Couzin and Nigel R Franks. 'Self-organized lane formation and optimized traffic flow in army ants'. In: *Proceedings of the Royal Society of London. Series B: Biological Sciences* 270.1511 (2003), pp. 139–146 (cited on pages 76, 93).

[253] Dirk Helbing. 'Traffic and related self-driven many-particle systems'. In: *Reviews of modern physics* 73.4 (2001), p. 1067 (cited on page 77).

[254] Yaochen Zheng et al. 'Modeling of pedestrian evacuation based on the particle swarm optimization algorithm'. In: *Physica A: Statistical Mechanics and its Applications* 391.17 (2012), pp. 4225–4233 (cited on page 77).

[255] Ansgar Kirchner and Andreas Schadschneider. 'Simulation of evacuation processes using a bionics-inspired cellular automaton model for pedestrian dynamics'. In: *Physica A: statistical mechanics and its applications* 312.1-2 (2002), pp. 260–276 (cited on page 77).

[256] Pierre Degond et al. 'Vision-based macroscopic pedestrian models'. In: *arXiv preprint arXiv:1307.1953* (2013) (cited on page 77).

[257] Yalda Rahmati and Alireza Talebpour. 'Learning-based game theoretical framework for modeling pedestrian motion'. In: *Physical Review E* 98.3 (2018), p. 032312 (cited on page 77).

[258] Dirk Helbing, Illés J Farkas, and Tamás Vicsek. 'Freezing by heating in a driven mesoscopic system'. In: *Physical review letters* 84.6 (2000), p. 1240 (cited on page 77).

[259] Guillermo H Goldsztein. 'Crowd of individuals walking in opposite directions. A toy model to study the segregation of the group into lanes of individuals moving in the same direction'. In: *Physica A: Statistical Mechanics and its Applications* 479 (2017), pp. 162–173 (cited on page 77).

[260] Mohcine Chraibi, Armin Seyfried, and Andreas Schadschneider. 'Generalized Centrifugal Force Model for Pedestrian Dynamics'. In: *Physical review. E, Statistical, nonlinear, and soft matter physics* 82 (Oct. 2010), p. 046111. DOI: 10.1103/PhysRevE.82.046111 (cited on page 77).

[261] W. J. Yu et al. 'Centrifugal force model for pedestrian dynamics'. In: *Phys. Rev. E* 72.2 (Aug. 2005), p. 026112. DOI: 10.1103/PhysRevE.72.026112 (cited on page 77).

[262] Dirk Helbing and Péter Molnár. 'Social force model for pedestrian dynamics'. In: *Phys. Rev. E* 51.5 (May 1995), pp. 4282–4286. DOI: 10.1103/PhysRevE.51.4282 (cited on pages 77–79).

[263] Dirk Helbing, Illés Farkas, and Tamás Vicsek. 'Simulating Dynamic Features of Escape Panic'. In: *Nature* 407 (Sept. 2000), pp. 487–490. DOI: 10.1038/35035023 (cited on page 78).

[264] Stefania Bandini et al. 'A Cellular Automata Based Model for Pedestrian and Group Dynamics: Motivations and First Experiments'. In: *Parallel Computing Technologies*. Ed. by Victor Malyshkin. Berlin, Heidelberg: Springer Berlin Heidelberg, 2011, pp. 125–139 (cited on page 79).

[265] C Burstedde et al. 'Simulation of pedestrian dynamics using a two-dimensional cellular automaton'. In: *Physica A: Statistical Mechanics and its Applications* 295.3 (2001), pp. 507–525. DOI: https://doi.org/10.1016/S0378-4371(01)00141-8 (cited on page 79).

[266] Tamás Vicsek et al. 'Novel type of phase transition in a system of self-driven particles'. In: *Physical review letters* 75.6 (1995), p. 1226 (cited on page 79).

[267] Peijie Ma and Binghong Wang. 'The escape of pedestrians with view radius'. In: *Physica A: Statistical Mechanics and its Applications* 392.1 (2013), pp. 215–220 (cited on page 79).

[268] Masakuni Muramatsu, Tunemasa Irie, and Takashi Nagatani. 'Jamming transition in pedestrian counter flow'. In: *Physica A: Statistical Mechanics and its Applications* 267.3-4 (1999), pp. 487–498 (cited on page 79).

[269] Yushi Suma, Daichi Yanagisawa, and Katsuhiro Nishinari. 'Anticipation effect in pedestrian dynamics: Modeling and experiments'. In: *Physica A: Statistical Mechanics and its Applications* 391.1-2 (2012), pp. 248–263 (cited on page 79).

[270] Claudio Feliciani and Katsuhiro Nishinari. 'Empirical analysis of the lane formation process in bidirectional pedestrian flow'. In: *Physical Review E* 94.3 (2016), p. 032304 (cited on page 79).

[271] Aitor Martın-Gómez et al. 'Collective motion of active Brownian particles with polar alignment'. In: *Soft matter* 14.14 (2018), pp. 2610–2618 (cited on page 79).

[272] Ioannis Karamouzas, Brian Skinner, and Stephen J Guy. 'Universal power law governing pedestrian interactions'. In: *Physical review letters* 113.23 (2014), p. 238701 (cited on pages 79–81, 83, 86, 87, 91, 92).

[273] Richard P Mann and Roman Garnett. 'The entropic basis of collective behaviour'. In: *Journal of the Royal Society Interface* 12.106 (2015), p. 20150037 (cited on page 79).

[274] Dirk Helbing et al. 'Self-organized pedestrian crowd dynamics: Experiments, simulations, and design solutions'. In: *Transportation science* 39.1 (2005), pp. 1–24 (cited on page 80).

[275] Markus Huber et al. 'Adjustments of speed and path when avoiding collisions with another pedestrian'. In: *PloS one* 9.2 (2014), e89589 (cited on page 80).

[276] Mehdi Moussaıd, Dirk Helbing, and Guy Theraulaz. 'How simple rules determine pedestrian behavior and crowd disasters'. In: *Proceedings of the National Academy of Sciences* 108.17 (2011), pp. 6884–6888 (cited on pages 82–84, 92).

[277] H.E. Stanley. *Introduction to Phase Transitions and Critical Phenomena*. International series of monographs on physics. Oxford University Press, 1987 (cited on page 85).

[278] SV Savenko and Marjolein Dijkstra. 'Asymptotic decay of the pair correlation function in molecular fluids: Application to hard rods'. In: *Physical Review E* 72.2 (2005), p. 021202 (cited on page 86).

[279] D. Chandler and D. Wu. *Introduction to Modern Statistical Mechanics*. Oxford University Press, 1987 (cited on page 89).

[280] Douglas H. Kelley and N. Ouellette. 'Emergent dynamics of laboratory insect swarms'. In: *Scientific Reports* 3 (2013) (cited on page 93).

[281] J. Buhl et al. 'From Disorder to Order in Marching Locusts'. In: *Science* 312.5778 (2006), pp. 1402–1406. DOI: 10.1126/science.1125142 (cited on page 93).

[282] G. Sword, P. D. Lorch, and D. Gwynne. 'Insect behaviour: Migratory bands give crickets protection'. In: *Nature* 433 (2005), pp. 703–703 (cited on page 93).

[283] Mathieu Lihoreau et al. ‘Collective selection of food patches in Drosophila’. In: *Journal of Experimental Biology* 219 (Jan. 2016). DOI: 10.1242/jeb.127431 (cited on page 93).

[284] G. Theraulaz et al. ‘The formation of spatial patterns in social insects: from simple behaviours to complex structures’. In: *Philosophical Transactions of the Royal Society of London. Series A: Mathematical, Physical and Engineering Sciences* 361 (2003), pp. 1263–1282 (cited on page 93).

[285] Claire Detrain and Jean-Louis Deneubourg. ‘Collective Decision-Making and Foraging Patterns in Ants and Honeybees’. In: ed. by S.J. Simpson. Vol. 35. Advances in Insect Physiology. Academic Press, 2008, pp. 123–173. DOI: https://doi.org/10.1016/S0065-2806(08)00002-7 (cited on page 93).

[286] Dominic D.R. Burns, Ana B. Sendova-Franks, and Nigel R. Franks. ‘The effect of social information on the collective choices of ant colonies’. In: *Behavioral Ecology* 27.4 (Feb. 2016), pp. 1033–1040. DOI: 10.1093/beheco/arw005 (cited on page 93).

[287] K Jaffe and PE Howse. ‘The mass recruitment system of the leaf cutting ant, Atta cephalotes (L.)’ In: *Animal Behaviour* 27 (1979), pp. 930–939 (cited on page 93).

[288] Stamatios C Nicolis and Jean-Louis Deneubourg. ‘Emerging patterns and food recruitment in ants: an analytical study’. In: *Journal of theoretical biology* 198.4 (1999), pp. 575–592 (cited on page 93).

[289] Athula B Attygalle and E David Morgan. ‘Ant trail pheromones’. In: *Advances in insect physiology* 18 (1985), pp. 1–30 (cited on page 93).

[290] Vincent Fourcassié, Audrey Dussutour, and Jean-Louis Deneubourg. ‘Ant traffic rules’. In: *Journal of Experimental Biology* 213.14 (2010), pp. 2357–2363 (cited on page 93).

[291] Ofer Feinerman et al. ‘The physics of cooperative transport in groups of ants’. In: *Nature Physics* 14.7 (2018), pp. 683–693 (cited on page 93).

[292] Takao Sasaki and Stephen C Pratt. ‘The psychology of superorganisms: collective decision making by insect societies’. In: *Annual Review of Entomology* 63 (2018), pp. 259–275 (cited on page 93).

[293] Lars Straub et al. ‘Superorganism resilience: eusociality and susceptibility of ecosystem service providing insects to stressors’. In: *Current Opinion in Insect Science* 12 (2015), pp. 109–112 (cited on page 93).

[294] Iain D Couzin et al. ‘Effective leadership and decision-making in animal groups on the move’. In: *Nature* 433.7025 (2005), pp. 513–516 (cited on page 93).

[295] David J. T. Sumpter. *Collective Animal Behavior*. Princeton University Press, 2010 (cited on page 93).

[296] Volker Grimm et al. ‘A standard protocol for describing individual-based and agent-based models’. In: *Ecological Modelling* 198.1 (2006), pp. 115–126. DOI: https://doi.org/10.1016/j.ecolmodel.2006.04.023 (cited on page 94).

[297] Eric Bonabeau. 'Agent-based modeling: Methods and techniques for simulating human systems'. In: *Proceedings of the National Academy of Sciences* 99.suppl 3 (2002), pp. 7280–7287. DOI: 10.1073/pnas.082080899 (cited on page 94).

[298] Leif Gustafsson and Mikael Sternad. 'Consistent micro, macro and state-based population modelling'. In: *Mathematical Biosciences* 225.2 (2010), pp. 94–107. DOI: https://doi.org/10.1016/j.mbs.2010.02.003 (cited on page 94).

[299] Pablo Gómez-Mourelo. 'From individual-based models to partial differential equations: An application to the upstream movement of elvers'. In: *Ecological Modelling* 188.1 (2005). Special Issue on Theoretical Ecology and Mathematical Modelling: Problems and Methods, pp. 93–111. DOI: https://doi.org/10.1016/j.ecolmodel.2005.05.014 (cited on page 94).

[300] Van Parunak, Robert Savit, and Rick Riolo. 'Agent-Based Modeling vs. Equation-Based Modeling: A Case Study and Users' Guide'. In: July 2000. DOI: 10.1007/10692956_2 (cited on page 94).

[301] Stephen Omohundro. 'Modelling cellular automata with partial differential equations'. In: *Physica D: Nonlinear Phenomena* 10.1 (1984), pp. 128–134. DOI: https://doi.org/10.1016/0167-2789(84)90255-0 (cited on page 94).

[302] Ido Golding et al. 'Studies of bacterial branching growth using reaction–diffusion models for colonial development'. In: *Physica A: Statistical Mechanics and its Applications* 260.3 (1998), pp. 510–554. DOI: https://doi.org/10.1016/S0378-4371(98)00345-8 (cited on page 94).

[303] S. C. Maitra N. S. Goel and E. W. Montroll. 'On the Volterra and Other Nonlinear Models of Interacting Populations'. In: *Rev. Mod. Phys.* 43.2 (Apr. 1971), pp. 231–276. DOI: 10.1103/RevModPhys.43.231 (cited on page 94).

[304] A. Berryman. 'The Orgins and Evolution of Predator-Prey Theory'. In: *Ecology* 73 (1992), pp. 1530–1535 (cited on page 94).

[305] Julien Lefèvre and Jean-François Mangin. 'A Reaction-Diffusion Model of Human Brain Development'. In: *PLOS Computational Biology* 6.4 (Apr. 2010), pp. 1–10. DOI: 10.1371/journal.pcbi.1000749 (cited on page 94).

[306] Gašper Tkačik et al. 'Searching for Collective Behavior in a Large Network of Sensory Neurons'. In: *PLOS Computational Biology* 10.1 (Jan. 2014), pp. 1–23. DOI: 10.1371/journal.pcbi.1003408 (cited on pages 95, 98).

[307] Christopher W. Lynn et al. 'Surges of Collective Human Activity Emerge from Simple Pairwise Correlations'. In: *Phys. Rev. X* 9.1 (Feb. 2019), p. 011022. DOI: 10.1103/PhysRevX.9.011022 (cited on pages 95, 98).

[308] Javier Cristín et al. 'Occupancy patterns in superorganisms: a spin-glass approach to ant exploration'. In: *Royal Society Open Science* 7.12 (2020), p. 201250. DOI: 10.1098/rsos.201250 (cited on pages 95, 113).

[309] Jordi Bascompte. 'Disentangling the web of life'. In: *Science* 325.5939 (2009), pp. 416–419 (cited on page 96).

[310] Jens Krause, David Lusseau, and Richard James. 'Animal social networks: an introduction'. In: *Behavioral Ecology and Sociobiology* 63.7 (2009), pp. 967–973 (cited on page 96).

[311] Stefano Allesina and Mercedes Pascual. 'Network structure, predator–prey modules, and stability in large food webs'. In: *Theoretical Ecology* 1.1 (2008), pp. 55–64 (cited on page 96).

[312] Ricard V Sole and Ma Montoya. 'Complexity and fragility in ecological networks'. In: *Proceedings of the Royal Society of London. Series B: Biological Sciences* 268.1480 (2001), pp. 2039–2045 (cited on page 96).

[313] Noa Pinter-Wollman et al. 'The dynamics of animal social networks: analytical, conceptual, and theoretical advances'. In: *Behavioral Ecology* 25.2 (2014), pp. 242–255 (cited on page 96).

[314] Damien R Farine and Hal Whitehead. 'Constructing, conducting and interpreting animal social network analysis'. In: *Journal of animal ecology* 84.5 (2015), pp. 1144–1163 (cited on page 96).

[315] Erik Andersson and Örjan Bodin. 'Practical tool for landscape planning? An empirical investigation of network based models of habitat fragmentation'. In: *Ecography* 32.1 (2009), pp. 123–132 (cited on page 96).

[316] Ikka Hanski. 'Metapopulation dynamics'. In: *Nature* 396 (June 1998), pp. 41–49. DOI: 10.1038/23876 (cited on page 96).

[317] R. Levins. 'Some Demographic and Genetic Consequences of Environmental Heterogeneity for Biological Control'. In: *Bulletin of the Entomological Society of America* 15 (1969), pp. 237–240 (cited on page 96).

[318] Elva JH Robinson. 'Polydomy: the organisation and adaptive function of complex nest systems in ants'. In: *Current Opinion in Insect Science* 5 (2014). Social insects/-Global change biology, pp. 37–43. DOI: https://doi.org/10.1016/j.cois.2014.09.002 (cited on page 96).

[319] D.G. Green. 'Cellular automata models in biology'. In: *Mathematical and Computer Modelling* 13.6 (1990), pp. 69–74. DOI: https://doi.org/10.1016/0895-7177(90)90010-K (cited on page 96).

[320] Yuri I. Wolf, Mikhail I. Katsnelson, and Eugene V. Koonin. 'Physical foundations of biological complexity'. In: *Proceedings of the National Academy of Sciences* 115.37 (2018), E8678–E8687. DOI: 10.1073/pnas.1807890115 (cited on page 97).

[321] H. Chau Nguyen, Riccardo Zecchina, and Johannes Berg. 'Inverse statistical problems: from the inverse Ising problem to data science'. In: *Advances in Physics* 66.3 (2017), pp. 197–261. DOI: 10.1080/00018732.2017.1341604 (cited on pages 97, 114).

[322] William Bialek et al. 'Social interactions dominate speed control in poising natural flocks near criticality'. In: *Proceedings of the National Academy of Sciences* 111.20 (2014), pp. 7212–7217. DOI: 10.1073/pnas.1324045111 (cited on page 98).

[323] T. Bury. 'Market structure explained by pairwise interactions'. In: *Physica A-statistical Mechanics and Its Applications* 392 (2013), pp. 1375–1385 (cited on page 98).

[324] Stanislav Borysov, Yasser Roudi, and A. Balatsky. 'U.S. stock market interaction network as learned by the Boltzmann machine'. In: *The European Physical Journal B* 88 (Apr. 2015), p. 321. DOI: 10.1140/epjb/e2015-60282-3 (cited on page 98).

[325] S. Kullback and R. A. Leibler. 'On Information and Sufficiency'. In: *The Annals of Mathematical Statistics* 22.1 (1951), pp. 79–86. DOI: 10.1214/aoms/1177729694 (cited on page 98).

[326] Tamara Broderick et al. 'Faster solutions of the inverse pairwise Ising problem'. In: *arXiv: Quantitative Methods* (2008) (cited on page 99).

[327] Ulisse Ferrari. 'Learning maximum entropy models from finite-size data sets: A fast data-driven algorithm allows sampling from the posterior distribution'. In: *Phys. Rev. E* 94.2 (Aug. 2016), p. 023301. DOI: 10.1103/PhysRevE.94.023301 (cited on page 99).

[328] H. Kappen and Francisco de Borja Rodríguez Ortiz. 'Boltzmann Machine Learning Using Mean Field Theory and Linear Response Correction'. In: *NIPS*. 1997 (cited on page 99).

[329] Toshiyuki Tanaka. 'Mean-field theory of Boltzmann machine learning'. In: *Phys. Rev. E* 58.2 (Aug. 1998), pp. 2302–2310. DOI: 10.1103/PhysRevE.58.2302 (cited on page 99).

[330] T. Plefka. 'Convergence condition of the TAP equation for the infinite-ranged Ising spin glass model'. In: *Journal of Physics A* 15 (1982), pp. 1971–1978 (cited on page 99).

[331] A Georges and J S Yedidia. 'How to expand around mean-field theory using high-temperature expansions'. In: *Journal of Physics A: Mathematical and General* 24.9 (May 1991), pp. 2173–2192. DOI: 10.1088/0305-4470/24/9/024 (cited on page 99).

[332] V. Sessak and R. Monasson. 'Small-correlation expansions for the inverse Ising problem '. In: *Journal of Physics A* 42 (2009), p. 055001 (cited on pages 99, 114).

[333] Xim Cerdá et al. 'Individual and collective foraging decisions: A field study of worker recruitment in the gypsy ant Aphaenogaster senilis'. In: *Behavioral Ecology and Sociobiology* 63 (Feb. 2009), pp. 551–562. DOI: 10.1007/s00265-008-0690-5 (cited on page 100).

[334] Tanya Latty and Madeleine Beekman. 'Keeping track of changes: the performance of ant colonies in dynamic environments'. In: *Animal Behaviour* 85.3 (2013), pp. 637–643. DOI: https://doi.org/10.1016/j.anbehav.2012.12.027 (cited on page 111).

[335] Cleo Bertelsmeier et al. 'Discovery–dominance trade-off among widespread invasive ant species'. In: *Ecology and Evolution* in press (June 2015). DOI: 10.1002/ece3.1542 (cited on page 111).

[336] Katja Mehlhorn et al. *Unpacking the Exploration-Exploitation Tradeoff: A Synthesis of Human and Animal Literatures*. June 2018. DOI: 10.1184/R1/6571526.v1. URL: https://kilthub.cmu.edu/articles/journal_contribution/Unpacking_the_Exploration-Exploitation_Tradeoff_A_Synthesis_of_Human_and_Animal_Literatures/6571526/1 (cited on page 111).

[337] Zoe Cook, Daniel W. Franks, and Elva J.H. Robinson. 'Exploration versus exploitation in polydomous ant colonies'. In: *Journal of Theoretical Biology* 323 (2013), pp. 49–56. DOI: https://doi.org/10.1016/j.jtbi.2013.01.022 (cited on page 111).

[338] Thomas T. Hills et al. 'Exploration versus exploitation in space, mind, and society'. In: *Trends in Cognitive Sciences* 19.1 (2015), pp. 46–54. DOI: https://doi.org/10.1016/j.tics.2014.10.004 (cited on page 111).

[339] Daniel Campos et al. 'Variability in individual activity bursts improves ant foraging success'. In: *Journal of The Royal Society Interface* 13.125 (2016), p. 20160856. DOI: 10.1098/rsif.2016.0856 (cited on page 113).

[340] Daniel Campos et al. 'Reorientation patterns in central-place foraging: internal clocks and klinokinesis'. In: *Journal of The Royal Society Interface* 11.90 (2014), p. 20130859. DOI: 10.1098/rsif.2013.0859 (cited on page 113).